Design of a Few Backstepping Sliding Mode Based Robust Control Techniques for Robot Manipulators

Nabanita Adhikary

Design of a Few Backstepping Sliding Mode Based Robust Control Techniques for Robot Manipulators

A
Thesis Submitted
in Partial Fulfilment of the Requirements
for the Degree of

DOCTOR OF PHILOSOPHY

By
Nabanita Adhikary

Department of Electronics and Electrical Engineering
Indian Institute of Technology Guwahati
Guwahati - 781 039, INDIA.
November, 2017

Certificate

This is to certify that the thesis titled "**Design of a Few Backstepping Sliding Mode Based Robust Control Techniques for Robot Manipulators**", submitted by **Nabanita Adhikary** (11610206), a research scholar in the *Department of Electronics & Electrical Engineering, Indian Institute of Technology Guwahati*, for the award of the degree of **Doctor of Philosophy**, has been carried out by her under my supervision and guidance. The thesis has fulfilled all requirements as per the regulations of the institute and in my opinion has reached the standard needed for submission. The results embodied in this thesis have not been submitted to any other University or Institute for the award of any degree or diploma.

Dated:
Guwahati.

Prof. Chitralekha Mahanta
Dept. of Electronics & Electrical Engg.
Indian Institute of Technology Guwahati
Guwahati - 781039, Assam, India.

Acknowledgements

I am deeply grateful to my supervisor Prof. Chitralekha Mahanta for her encouragement, support and meticulous guidance throughout the entire duration of my research. With great patience and careful instructions, she has guided me step by step in my research and has inspired me to keep on learning and exploring the ever-evolving world of technology. I would also like to thank her immensely for always carrying out the tedious task of carefully inspecting and rectifying all my manuscripts. It has been a privilege to work under her tutelage.

I will be forever grateful to my doctoral committee members, Dr. Indrani Kar, Dr. Sisir Kumar Nayak and Dr. Srinivasan Krishnaswamy, for taking out the time from their busy schedule to evaluate my thesis work. Their valuable suggestions have been extremely helpful in setting the proper course of my research. I would also like to take this chance to appreciate all the faculty members of the department for their support and training during my academic studies. My special thanks to Mr. Sidananda Sonowal, Syed Samimul Mazid, Mr. Sanjib Das, Mr. Pranab Jyoti Goswami and all the members of the Control & Instrumentation Laboratory for providing the technical resources and help throughout my research.

I would like to thank Science and Engineering Research Board (SERB), Department of Science and Technology (DST), Govt. of India, for granting us the funding for purchasing various hardware, software, books and such other necessary items for carrying out the research without any hindrance. Their support has been invaluable to me. I am also thankful to IIT Guwahati and MHRD, India, for granting the scholarship for undertaking my research.

My sincere gratitude goes to my friends in IITG who have always been there for me. Their friendship, love, and support helped in every step of my research and my life. I thank all my friends in the Control & Instrumentation Laboratory for always helping me with their useful suggestions and for providing an excellent research environment.

Last but not the least, I would like to thank my family. My father and my sister are the rock of my life and their endless love and support have made it possible for me to forever keep on moving forward. My most sincere thanks to my dear husband and his family for their unconditional love and support.

(Nabanita Adhikary)

Abstract

To design a structurally simple controller for robot manipulators is a challenging task because these are highly coupled multi input multi output nonlinear dynamic systems. Quite often there happens to be a compromise between the controller structure and its performance. A strict performance requirement normally results in a complex controller design. This thesis focuses on designing a controller that yields satisfactory performance while maintaining its structural simplicity. The basic methodology used in the thesis is the backstepping based sliding mode controller. Since robustness against the mismatched uncertainty cannot be guaranteed by the conventional sliding mode controller (SMC), it is integrated with backstepping methodology that transforms the system states in such a way that it can tackle both matched and mismatched uncertainties. Another drawback of the SMC is the presence of high frequency chattering in the control input which is highly undesirable especially in the case of mechanical systems like robot manipulators. To find a solution to this problem, an integral backstepping based SMC (IBSMC) that augments an integrator block to the system is proposed so that the input to the manipulator is obtained as an integrated smooth signal. Although effective, this method leads to increased structural complexity of the controller due to the requirement of differentiation of manipulator dynamics causing explosion of terms. This complexity is minimized using a first order low pass filter instead of direct differentiation resulting in the integral adaptive dynamic surface control (IADSC). Chattering mitigation is also attempted by using an adaptively tuned controller gain which uses a lower input energy to produce similar tracking performance for the manipulator. Stability issues arising due to the presence of filters motivated to propose a proportional integral derivative (PID) type sliding surface for using in the adaptive backstepping SMC giving rise to the ABSMC-PID. This ABSMC-PID method is also used for impedance control of a robot manipulator when encountering highly stiff surfaces during trajectory tracking in the Cartesian space by the end-effector. A model free controller is developed next using the time delay estimation and the PID sliding surface in the backstepping SMC is replaced by a fast terminal sliding surface that can provide finite time convergence of the tracking error. This adaptive backstepping based fast terminal SMC (ABFTSMC) can be used effectively for higher DoF manipulators or in the cases where determining the manipulator model is not easy. Detailed Lyapunov based stability analysis is conducted for all the proposed controllers. Simulation studies are carried out to validate the proposed control methodologies against some existing control methods. Implementation of dynamic control on a position commanded servomotor actuating the robot manipulator is next attempted in this thesis. Experiments are conducted on a robot arm to investigate about the possibility of realizing the proposed dynamic control methods in real time applications.

Contents

List of Figures

List of Tables

List of Acronyms

ABSMC	Adaptive backstepping sliding mode controller
ABFTSMC	Adaptive backstepping based fast terminal sliding mode controller
CLF	Control Lyapunav function
CTA	Cartesian target acceleration
CTV	Cartesian target velocity
DC	Direct current
DoF	Degrees of freedom
DSC	Dynamic surface control
HIC	Hybrid impedance control
HJ	Hamilton Jacobi
IADSC	Integral adaptive dynamic surface controller
IBSMC	Integral backstepping sliding mode controller
MAE	Mean absolute error
MASSE	Mean absolute steady state error
MIMO	Multiple input multiple output
MRAC	Model reference adaptive control
NLMI	Nonlinear linear matrix inequality
NRIC	Nonlinear robust internal-loop compensator
PID	Proportional integral derivative
PPF	Parametric pure feedback
PSF	Parametric strict feedback
RMSE	Root mean square error
RFTSC	Robust finite time sliding mode control
SSF	Semi strict feedback
SMC	Sliding mode controller
TDC	Time delay control
TDE	Time delay estimation
TSM	Terminal sliding mode
TV	Total Variation

Mathematical Notations

$\alpha_1,\ \alpha_2,\ \alpha_\tau$	Virtual control laws of BSMC
α_f	Filtered signal of virtual control
a	Complex number frequency parameter of Laplace transform
β	User defined positive parameter of the nonsingular fast terminal sliding surface
B_m	Motor damping
$\boldsymbol{C(q,\dot{q})}$	Coriolis matrix of manipulator
$\boldsymbol{C_h}$	Coriolis matrix of combined manipulator and actuator dynamics
$\boldsymbol{c_1},\ \boldsymbol{c_2}$	Design parameters of backstepping in diagonal matrix form
$c_1,\ c_2$	Design parameters of backstepping in scalar form
$\mathcal{D}$	Boundary layer for smooth SMC
δ	User defined parameter of nonsingular fast terminal sliding surface where $1 < \delta < 2$
$\boldsymbol{\epsilon}$	Leakage term for adaptive law
e_{ss}	Steady state error
f_s	Static friction
$\boldsymbol{f(q,\dot{q},t)}$	Unknown disturbance in the manipulator joints
$\boldsymbol{F(q,\dot{q},\ddot{q},t)}$	Unknown disturbances for combined manipulator and actuator dynamics
$\boldsymbol{f_1}$	Upperbound of $\boldsymbol{f(q,\dot{q},t)}$
g	Gravitational constant $= 9.81 m/s^2$
$\boldsymbol{G(q)}$	Vector of gravitational torques in manipulator
$\boldsymbol{G_h}$	Gravitational torques for combined manipulator and actuator dynamics
$\boldsymbol{\Gamma}$	Adaptive gain
Γ_{ijk}	*Christoffel symbols* of robot manipulator
$\boldsymbol{I_n}$	$n \times n$ inertia matrix
J_g	Gearbox inertia
J_m	Motor inertia
$k,\ k_1,\ k_{2d}$	Constant gain of SMC
$\hat{k}, \hat{k}_1, \hat{k}_2$	Adaptively tuned constant gain of SMC
k_c	Coulomb friction coefficient
k_v	Viscous friction coefficient
$\frac{1}{k_g}$	Gear ratio
k_p	Proportional gain

$\lambda_{min}\{\bullet\}$	Minimum eigenvalue
$\lambda_{max}\{\bullet\}$	Maximum eigenvalue
$\lambda_{min}(A_1, \ldots, A_n)$	Minimum of the eigenvalues of $A_i, i = 1, \ldots, n$ where A_i is any real valued matrix
L	Motor armature inductance
M_o	Peak overshoot
M_u	Peak undershoot
$\boldsymbol{M(q)}$	Inertia matrix of the manipulator
$\boldsymbol{M_h}$	Inertia matrix of combined manipulator and actuator dynamics
$\mu_{min},\ \mu_{max}$	Minimum and maximum bounds of $\boldsymbol{M(q)}$
n	Number of DoF in the manipulator
q	Joint position
$\dot{q}$	Joint velocity
$\ddot{q}$	Joint acceleration
q_e	Tracking error
q_{cmd}	Position command sent to servo motor
q_d	Desired angular position
$\dot{q}_d$	Desired angular velocity
$\ddot{q}$	Desired angular acceleration
q_m	Angular position of motor shaft
$\dot{q}_m$	Angular velocity of motor shaft
$\ddot{q}_m$	Angular acceleration of motor shaft
R	Motor armature resistance
r	Gear reduction ratio
$\mathbb{R}^{n\times n}$	The $n \times n$ dimension of real numbers
$\mathbb{R}^n$	The $n \times 1$ dimension
$s,\ s_1, s_2$	Sliding surfaces
$sign(\bullet)$	Signum function
t	Time in seconds
t_r	Rise time
t_s	Settling time
t_p	Time of peak overshoot
t_u	Time of peak undershoot
τ	Actuating torque
τ_l	Disturbance torque
$T(q, \dot{q})$	Kinetic energy
T_e	Electrical time constant
T_f	Filter time constant
T_m	Mechanical time constant
T_r	Time taken by the states to reach the sliding surface (Reaching time)
T_s	Sampling time

u	Control input
$U(q)$	Potential energy
$V_1,\ V_2,\ V_k,\ V_s$	Lyapunov functions
$\boldsymbol{W},\ \boldsymbol{W_1},\ \boldsymbol{W_2}$	Proportional gain of SMC
$\boldsymbol{x}$	A real vector
$z_1,\ z_2,\ z_3$	Auxiliary variables of BSMC
$\|\| \bullet \|\|$	2-norm of the signal
$\boldsymbol{v_1} \circ \boldsymbol{v_2}$	Elementwise multiplication of two vectors $\boldsymbol{v_1}$ and $\boldsymbol{v_2}$

List of Publications

Journal Publications

1. Nabanita Adhikary and Chitralekha Mahanta, "Integral backstepping sliding mode control for underactuated systems: Swing-up and stabilization of the cartpendulum system ", *ISA Transactions, Elsevier*, vol. 52, no 6, pp. 870-880, 2013.

2. Nabanita Adhikary and Chitralekha Mahanta,"Inverse Dynamics based Robust Control Method for Position Commanded Servo Actuators in Robot Manipulators ", accepted in Control Engineering Practice, Elsevier

Conference Publications

1. Nabanita Adhikary and Chitralekha Mahanta, "Backstepping sliding mode controller for a co-ordinated links (cool) robot arm", *13th International Workshop on Variable Structure Systems (VSS),* IEEE, 29 June-02 July, 2014, pp.1-5, Nantes, France.

2. Nabanita Adhikary and Chitralekha Mahanta, "Adaptive backstepping sliding mode controller with PID sliding surface for a co-ordinated links (COOL) robotic arm ", *Proceedings of the 2015 Conference on Advances In Robotics (p. 4), ACM*, 02-04 July 2015, Goa, India.

3. Nabanita Adhikary and Chitralekha Mahanta, "Hybrid impedance control of robotic manipulator using adaptive backstepping sliding mode controller with PID sliding surface", *2017 Indian Control Conference (ICC)*, 04-06 Jan, 2017, pp. 391-396, Guwahati, India.

4. Nabanita Adhikary and Chitralekha Mahanta, "Kinematic control of a 6 DOF robotic manipulator using sliding mode", *2017 Indian Control Conference (ICC)*, 04-06 Jan, 2017, pp. 350-355, Guwahati, India.

1

Introduction

Contents

1.1 Robot manipulator

Only a few decades ago robots were an idea in the pages of science friction but now the technological advancement has made it a reality. In modern times robots are used in a wide variety of fields starting from industry, laboratory, space and underwater exploration tools to educational and assitive robotics where they actually interact with human beings. Such colossal advancements in robots, both in terms of structure and usability have developed robotics into an extensively researched topic for about more than half a century. A significant branch of robotics is humanoid robotics involving robot manipulators or robot arms having similar functions as the human arm which can operate as a single mechanism or part of a larger, more complex system. These humanlike robot manipulators have been extensively used in factories, laboratories, bio-hazardous areas like nuclear plants, toxic places, military application such as bomb diffusion and also in high precision tasks like laser cutting, microsurgery. Further, robots are successfully employed in inaccessible terrains like underground tunnels, underwater and are also functioning as assistive technology for specially abled persons in the form of replacement limbs.

Robot manipulators can be vastly classified into rigid and soft manipulators. The early robot manipulators were mainly developed for industrial use due to which their links were made with rigid body and hence they were called rigid manipulators. A more recent and bio-inspired approach to developing manipulators involves using soft, flexible and compliant materials to obtain more life like grasping and movements. The advantage of the rigid manipulators over soft manipulators is the high precision in trajectory tracking, whereas soft manipulators can provide a more compliant behaviour.

Rigid manipulators can have two types of joints, viz. revolute (R) and prismatic (P). As shown in Figure 1.1, (a) the prismatic joint produces a linear motion whereas (b) the revolute joint produces an angular motion with respect to a pivotal point. Other types of joints such as cylindrical, spherical and planar joints are results of combination of the revolute and the prismatic motions. Depending upon the kinematic arrangement of joints, manipulators are categorized as follows [10]:

(i) Articulated arm (RRR), also called Revolute or Anthropomorphic arm (due to the resemblance in structure with the human arm)

(ii) Spherical arm (RRP)

(iii) SCARA (Selective Compliant Articulated Robot for Assembly) arm (RRP)

(iv) Cylindrical arm (RPP)

(v) Cartesian arm (PPP).

Among the above mentioned configurations, the articulated arm (RRR) is the most dextrous one as it can provide more freedom in a constrained workspace as compared to the other configurations [11] and it has the best similarity with the human arm.

Robot manipulator control can be broadly classified into two areas – (I) Kinematic control and (II) Dynamic control [10]. The kinematic control involves solving the inverse kinematics to obtain the manipulator joint motions that produce the desired motion defined for the end-effector or the tool frame of the robot arm in the task space (Cartesian space). The dynamic controller calculates the

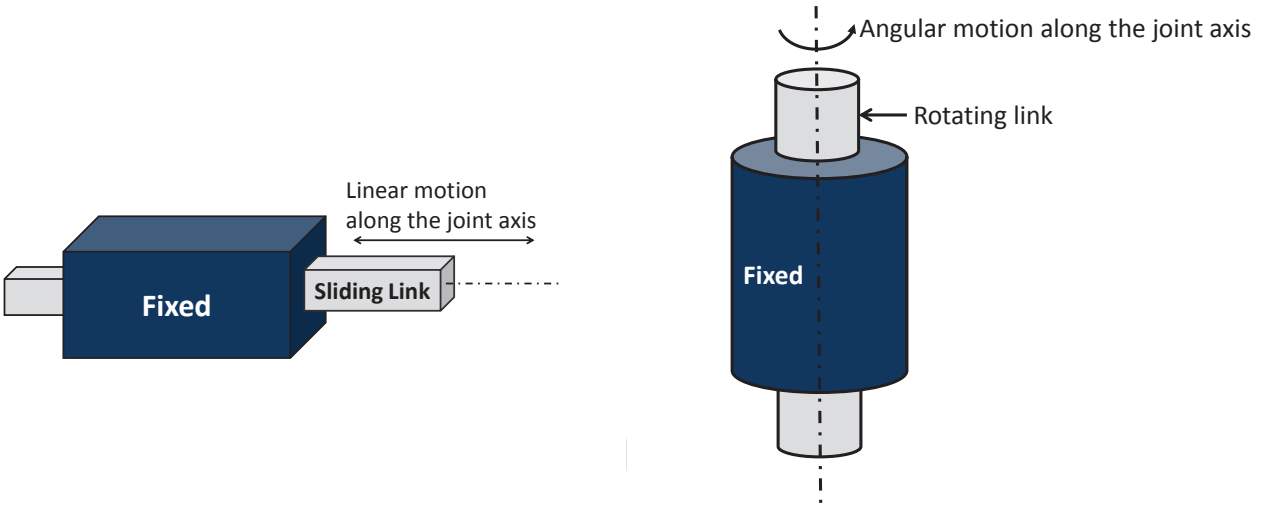

(a) Prismatic joint (b) Revolute joint

Figure 1.1: Manipulator joint types

commanding torque or force to act on the robot joints to achieve a desired motion defined in either the task space or the joint space. Although from the position control point of view the kinematic control is sufficient, however, following disadvantages are faced while implementing the kinematic control method:

(i) The load dynamics of the manipulator can affect the joint motion that might increase the steady state error if only kinematic control is implemented.

(ii) In practice, actuators in the manipulator joints have torque or force limits which are not considered by the kinematics.

(iii) Dynamic disturbances such as frictional force cones, center of pressure positions [11] are also not considered in the kinematics.

(iv) One very important aspect is the compliance of the manipulator, where, in addition to the manipulator position and orientation, the interaction forces and torques with the external environment also need to be controlled, which cannot be attained via kinematics.

The above mentioned shortcomings of the kinematic control are overcome in dynamic controllers. The dynamic controller uses the manipulator and the disturbance dynamics or their estimates to generate the input signal in terms of actuator torques and forces. The control law can be modified to reject any unwanted dynamic behaviour and tackle the various constraints mentioned above.

1.2 Literature review: Robust controllers for robot manipulators

Robot manipulators developed in early years were remotely controlled mechanical arms used in nuclear plants for handling radioactive material like the MSM-8 (Master Slave Manipulator Mk.8) developed for the Argonne National Laboratory by the Central Research Laboratories in the US. Meanwhile, George Devol in 1961 developed the Unimation Puma robot in a General Motors plant. The Puma robot was inspired by the high performance Computer Numerically Controlled (CNC) tools developed for accurate milling of aircraft parts. The Puma robot replaced the master manipulator in the master slave system. However, manually operating the master arm by a human operator was not always feasible owing to space constraints or the distant location of the remote site producing large transmission delays [12]. This drawback was addressed using two methods – (i) Direct control of the manipulator through a computer in a closed loop and (ii) Supervisory control where occasionally the desired sequence of subgoals was set by an operator. The supervisory control loop was closed through a human operator whereas the direct control was a fully automated system. The first automatic manipulator was developed by H.A. Ernst in Massachusetts institute of technology (MIT) [13] in 1968. The idea of automatic manipulation gained much popularity since it did not have to deal with the communication delays of the master-slave manipulators and could be indefinitely operated for a preset trajectory. A few mentionable works in the early period for automatic manipulator control are [14–17]. With the evolution of the automated manipulator, the significance of torque control was closely noticed. Previously operated manipulators were mainly position commanded where the position or velocity command was produced based on the manipulator kinematics and the desired trajectory to be followed. Since in the master-slave manipulators, the force exerted by the arm on the external objects was controlled by the human operator, the force control or the compliance control was not an issue. However, with the automated manipulators, controlling the interacting force with the environment was also necessary which led to the evolution of compliance controllers. The joint torque control method provided more scope in the interaction force control than the position command and inspired further research into the inverse dynamics control of the manipulator. A comparative analysis of the computed torque method and the positional servoing of manipulators can be found in the report by Markiewicz [18] where he has mentioned that both the methods have their own merits and demerits and can be selected depending upon the area of application. In the technical report of NASA by A.K. Bejcky [16], a detailed report on the dynamics and control of robot manipulators is provided. A few other early works on the dynamic control of manipulators are by Raibert and Horn [19], Yuan [20].

Dynamic controllers for robot manipulators can be broadly classified into (i) Robust controllers and (ii) Intelligent controllers. Robust controllers [21] rely on the system modeling to construct a proper control law in order to perform a desired task, whereas intelligent control methods [22] do not rely on the system model and use the available system behaviour to heuristically construct the controller. A brief yet comprehensive survey of the robust control methods developed for robot manipulators can be found in [21] and [23] whereas [22] provides an overview of the main intelligent control methods like neural networks, fuzzy logic, genetic algorithm and hybrid intelligent controller for humanoid robots. Although intelligent controllers are appealing because of their model free nature, heuristic design and lesser design effort, but for complex systems, the computational burden, possibility of over-estimation

and deviation from normal behaviour may severely affect their performance. Moreover, intelligent control methods can at best guarantee asymptotic tracking whereas with some advanced robust control methods, finite time convergence can be achieved [24]. Therefore, if the system model is available, it is preferable to use a robust control method for achieving reliable performance. Model estimation methods like time delay estimation (TDE) [25] have made it possible to implement classical robust control methods even when exact model of the system is not available.

Sage *et al.* [21] have categorized robust controllers designed for robot manipulators into the following classes:

(i) Linear controllers

  (a) Proportional Derivative (PD) and Proportional Integral Derivative (PID) controllers

  (b) Linear H_∞ Controllers

(ii) Nonlinear controllers

  (a) Passivity Based Controllers

  (b) Lyapunov Based Controllers

  (c) Sliding Mode Controllers (SMCs)

  (d) Nonlinear H_∞ Controllers

  (e) Robust Adaptive Controllers

A brief overview of the above robust control methods is given below:

(i) Linear controllers

(a) Proportional Derivative (PD) and Proportional Integral Derivative (PID) controllers

Simple structure and ease of implementation made PD and PID controllers quite popular. The PD controller was originally designed for linear systems and in case of robot manipulators the controller was designed for a linearized robot model. Therefore, the global asymptotic stability could be guaranteed only for point to point motion with high velocity gain and gravity term compensation [26–28], whereas for trajectory tracking, only local or semiglobal stability was assured [29]. Despite these limitations, PD and PID controllers are still widely used in industrial manipulators mainly because of their simple structure. However, for precise trajectory tracking tasks, these controllers fail to provide global stability and hence they are often combined with other nonlinear methods giving rise to nonlinear PID controllers. For example, Tomei [27] proposed an adaptive PD controller where the gravity terms were compensated through an adaptive law and the controller was implemented for regulation as well as trajectory tracking control. In [30], Vega *et al.* proposed a PID controller for a decentralized system. Their method combined a PID controller with a sliding mode without the reaching phase and terminal attractors to obtain global asymptotic stability in manipulator trajectory tracking. Su *et al.* [31, 32] proposed a nonlinear

PID controller for trajectory tracking of robot manipulators using nonlinear differentiators for noisy signals. The PID controller has also been combined with fuzzy control methods as can be found in Meza *et al.* [33]. Dumlu and Erenturk [34] proposed a fractional order PID controller for trajectory tracking of a parallel robot manipulator.

Although the PD and PID controllers are easy choices for application to the linearized and decentralized model of a robot manipulator, in practical situations PD or PID controllers alone cannot tackle the possible nonlinear disturbances and guarantee a stable operation.

(b) Linear H_∞ controllers

The H_∞ control is an attractive robust control methodology due to the following properties [35]:

- It is a multivariable technique
- The performance and the robustness both can be addressed
- The uncertainty can be directly handled.

Initial attempts of H_∞ control of robot manipulator involved linearisation of the manipulator dynamics using a feedback control law [35] and then applying the H_∞ control in the inner loop for the linearized system. Sage *et al.* [36] derived a controller having an outer velocity loop controlled by PI/PD controller and the inner linear position control loop controlled via linear H_∞ control.

The H_∞ controller was developed either by solving Riccatti equation or linear matrix inequality. However, implementation of the controller was not easy due to solvability issue of the Hamilton Jacobi (HJ) inequality. Moreover, because of using the linearized model, the unmodeled nonlinearity and gear backlash could not be accounted for, leading to degradation of performance of the H_∞ controller.

(ii) Nonlinear controllers

(a) Passivity based controllers

Robot manipulators are passive systems and the early use of passivity in manipulator control can be found in [37] by Arimoto and Takegaki where they used a simple PD controller with gravity compensation in order to obtain global stability for set point regulation. Use of passivity made it possible to design adaptive controllers without the knowledge of acceleration of the manipulator. As such, various passivity based adaptive controllers can be found in the literature including Ortega and Spong [38], Leal and De Wit [39], Tang and Arteaga [40], Villani *et al.* [41], Hsu *et al.* [42]. Passivity can also be used to control the manipulator directly where the natural energy of the robot is reshaped. The controller is designed based on an energy function of the closed loop system and then damping is added via velocity feedback for asymptotic stability [43–46].

(b) Lyapunov based controllers

Lyapunov based controllers are designed based on the stability of the system. A positive definite control Lyapunov function (CLF) representing the generalized energy is defined for

the controlled system and following Lyapunov's second theorem, a control law is derived to bound the system error within an arbitrarily small region. Lyapunov method is more of a tool for stability analysis of nonlinear systems. The pioneering works by Leitmann [47] and Corless and Leitmann [48] inspired the design of Lyapunov based controllers. Following the methodology of [48], these controllers for robot manipulators were developed based on the knowledge of the uncertainty bound. High gain saturation type functions were used here to tackle uncertainties [49–51]. Based on the works of Slotine and Li [52], Johansson [53] developed a Lyapunov based adaptive controller for robot manipulators. Backstepping [54, 55], introduced in 90's was another Lyapunov based design where a sequence of virtual subsystems of relative degree one were designed and based on a CLF defined for each subsystem, a virtual control law was derived. The actual control was obtained in the final step of the algorithm as a function of the previously derived virtual controllers. The unknown functions and uncertainties at each step were tuned using an adaptive law. Due to the systematic design methodology and the ease of stability analysis, backstepping has been extensively used in manipulator control [56–62]. For the Lyapunov based controller, existence of the CLF is a necessary and sufficient condition for ensuring stability of the controlled system. But in this method, only stability is established, whereas performance cannot be always guaranteed.

(c) Sliding mode controllers (SMCs)

Sliding mode control (SMC) [63,64] is a variable structure control method where a switching controller is designed based on a predefined sliding surface. The originally proposed SMC had a first order linear sliding surface that was used as the switching function for the controller. The controller operates in two stages: *reaching phase* where the control input brings the system states to the sliding surface in finite time and the *sliding phase* when the system states are on the sliding surface and approaches equilibrium asymptotically. During the sliding phase the states are no longer affected by the system dynamics but are governed by the sliding surface dynamics thus making the system robust to disturbances.

Robustness and structural simplicity are two main features of the SMC due to which this control method has been widely used in controlling nonlinear systems. Some early works on robot manipulator control using the SMC are reported in [65–69] . Despite the robustness of the SMC, it suffers from the unwanted *chattering* phenomenon which can prove harmful to mechanical joints and actuators. The chattering occurs due to the switching function present in the control input. The initial efforts to minimize the chattering were to replace the discontinuous switching law by a continuous function or using a boundary layer approximation [68, 70–73]. But such actions led to compromising in the tracking performance and the stability margins. Another drawback of the SMC is that its robustness can be guaranteed only when the system states are on the sliding surface but in the reaching phase it is not immune to the uncertainty. Utkin and Shi [74] proposed the integral sliding mode controller where the sliding surface had the same dimension as that of the controlled system and thus the robustness could be guaranteed during the whole state motion. The dynamical

SMC proposed in [75,76] was an attempt to mitigate chattering in the control input. Based on the terminal attractors introduced by Zak [77], the terminal sliding mode control [78,79] was derived which, in addition to finite reaching time, also provided finite time convergence of the system states to the equilibrium. Unlike the traditional SMC, controller gain in the terminal SMC was significantly reduced but it suffered from the singularity problem and degradation of convergence performance when the error states were far from the equilibrium. The non-singular terminal SMC [80] and the fast terminal SMC were [24] developed as a solution to these problems. Another important class of the SMC are the second and higher order SMCs proposed by A. Levant [81] that can provide a smooth control law while maintaining its robustness and performance. Considerable work has been done on designing higher order SMCs for robot manipulators [82–87].

(d) Nonlinear H_∞ controllers

Yim and Park [88] proposed nonlinear H_∞ control, where the robot dynamics were transformed to an affine nonlinear system about the state and input and the associated HJ inequality was derived in the form of nonlinear matrix inequality (NLMI). In [89], Kim *et al.* proposed a nonlinear robust internal loop compensator (NRIC) using H_∞ optimization, which had the similar structure as that of model reference adaptive control (MRAC). However, the H_∞ compensation in [89] attenuated the deviations from the nominal behaviour instead of adjusting the controller/modeling parameters like the MRAC. Rigatos *et al.* [90] proposed local linearisation of robot dynamics about the equilibrium in order to apply H_∞ control theory. The controller was designed by solving the Riccatti equation. However, like most of the H_∞ control methods [90] also suffers from the drawback of linearisation, especially when the number of DoFs are high making it difficult to analytically obtain the linearized model.

(e) Robust adaptive controllers

The early works on the adaptive control of robot manipulators [91–93] were mainly passivity based adaptive control schemes. Based on the adaptive controller proposed by Slotine and Li [91], many variants were proposed [94, 95]. The overestimation issue of the adaptive law was tackled by introducing the leakage term as proposed by Ioannou and Tsakalis in [96] which ensured that the signals in the adaptive loop were bounded with only a small residual tracking error. The robust adaptive controller obtained likewise has been successfully implemented in the dynamic control of robot manipulators [97–102]. One constraint of the robust adaptive controller was that knowledge about the joint acceleration was essential. Middletone and Goodwin [103] proposed a linear estimation technique with computed torque which did not require the acceleration measurement. Hsu [104] proposed a prediction error based estimation that allowed adaptive control of manipulators without the joint acceleration measurement. Other control methods like neural and fuzzy controllers and disturbance observers were also combined with the robust adaptive controller to improve its performance while eliminating its drawbacks [105–111].

1.3 Motivation

1.3.1 Controller design

As discussed, researchers have attempted to build control strategies by integrating multiple control methodologies with an aim to improve system performance without compromising too much on the system robustness and vice versa. However, other two factors that has to be considered in controller design is the controller structure and the information demand. Simple structure and a low information demand are the major features to be looked into while considering its practical application in robot manipulators. This is the reason for the PD/PI/PID being the most widely used controller for commercial robot manipulators till date. Simple structure and ease in implementation are the reasons for popularity of the PID controller although its performance may not be the best. Moreover, the PID controller can be implemented even without any detailed knowledge about the system model and the number of its parameters to be tuned is also small.

The same is not true for the H∞, the passivity and Lyapunov based control or adaptive control methods. These controllers, although showing superior performance, cannot offer the same simplicity in design and structure as the PID controller. However, the conventional SMC has a simple structure that can be easily implemented on linear or nonlinear systems and it has better robustness and performance characteristics than the PID controller possesses. But the presence of mismatched uncertainty in the manipulator and the high frequency chattering imposes a restriction on the use of the conventional SMC in the robot manipulator. The higher order SMC (HOSMC) can eliminate the chattering phenomenon while retaining robustness of the controller and offering satisfactory transient and steady state performances. However, the HOSMC requires knowledge of the higher derivatives of the sliding surface. Due to this increased information demand, simplicity in structure of the conventional SMC is lost.

Backstepping is a Lyapunov based method that uses smaller subsystems to design synthetic control laws until the actual control input is realized finally. For a relative degree 2 system like the robot manipulator, use of backstepping is fairly simple as it will require only two steps to derive the control law. In terms of the synthetic control laws, backstepping renders each subsystem into having reduced relative degree and using the SMC in the steps of backstepping can make the SMC immune to mismatched uncertainties [112, 113]. This is an elegant and effective solution to the robustness issue of the SMC involving mismatched uncertainties and additionally, a methodical analysis of the system stability can be attained through the control Lyapunov function (CLF) designed for backstepping. However, most of the controllers using the backstepping based sliding mode methodology utilize neural networks, fuzzy logic, optimal design or disturbance observers for improved performance. Although such combinations improve the controller performance, they also increase the number of controller parameters to be tuned. Backstepping sliding mode control (BSMC) techniques not using these methods incorporate compensation schemes to reduce the effects of uncertainty and chattering [114,115] which, however, results in increased information demand on the system or rise in parameters to be tuned.

Thus, it can be observed that a host of robust and intelligent control methods have evolved for robot manipulators to enhance their performance. However, for applying these control schemes in real

world, the following major criteria need to be considered:

- The first and foremost criterion is always guaranteed robustness of the controller, coupled by stability and satisfactory system performance.
- The second important criterion is the structural simplicity of the controller and minimal information demand. A controller having complex structure and high information demand can loose its portability despite its robustness and acceptable performance. Since most of the controllers implemented in the modern time are digital, having a complex structure of the controller means requirement of more memory space and faster processors. Increased information demand requires more sensors and all of these combined ultimately raises the implementation cost.
- The third criterion is the ease of design. Too many controller parameters and optimizing technique can yield very good performance, but it may not be appealing for a real time application. Robot manipulators are nonlinear system and tuning parameters for nonlinear systems is a tedious task for which standard procedures are difficult to find. Too many parameters to be tuned can make the controller difficult for realization.

Keeping in mind the above mentioned basic requirements, this thesis aims to design suitable robust controllers based on the backstepping sliding mode control (BSMC) methodology. The BSMC is chosen primarily for the reason that it does not require linearisation of the system model and nonlinearities in the system can be retained without any loss to their inherent characteristics. Effort of the research work is on achieving a structurally simple control method, without having to resort to any intelligent methods, optimization process or disturbance observers. Although the controller simplicity may not match that of the PID controller, the controller design will be focused on reducing the structural complexity of the controller without having to compromise too much on the stability and performance. Various BSMC based control schemes proposed in the thesis will attempt to address issues pertinent to implementation in robot manipulator.

1.3.2 Dynamic torque control of position commanded robot manipulators

Most of the low cost robotic manipulators normally have servo motors as the joint actuators and these servos have internal microcontrollers for position and speed control. This makes the robots position commanded, meaning that only the joint position can be sent as the input to the actuators. The main disadvantages of this arrangement are as follows:

- The controllers inside the servos are designed for single motor operation only. When the servos are linked and operated as a whole arm, the dynamics of the entire arm affects each servo motor. Since the servo controllers are proportional integral derivative (PID) or its variants, they are not very effective when affects of such load dynamics are high during arm motions. As such, the steady state error tends to increase with increasing load.
- While interacting with the external environment or working with humans, position control of the arm alone may not be sufficient since the forces and torques also need to be taken care of.

Therefore, to achieve a compliant motion, relying solely on the internal position controllers will not be adequate.

- Standard position control does not consider the constraints affecting the humanoid manipulators like torque limits, frictional force cones, center of pressure positions [11], which is otherwise possible with inverse dynamics control.

Khatib et al. [116] proposed a torque to position transformer based on the actuator transfer function which was identified using higher order polynomials without relying on the direct measurement of joint torques. This strategy has been successfully implemented on the humanoid robot Asimo arm [116]. In [117], a three part torque control law, which required estimation of the joint torques based on the end-effector torque sensor data and the robot model, was formulated. Both the studies showed that the position command to the digital servos could be manipulated to obtain the dynamic controller effects. Inspired by [116], this thesis attempts to devise a transformation method that enables implementation of a torque controller on a position commanded motor.

1.4 Contributions of the thesis

This thesis is aimed at developing a simple SMC based chattering free control method for application to robot manipulators. The primary contributions of the thesis are listed below:

(i) **Integral backstepping sliding mode controller (IBSMC)**
A simple control method is developed for robot manipulators combining integral backstepping [54] and the sliding mode control [118]. The controller design is based on the works by Ramirez and Santiago [119], Boliver *et al.* [120], Liu and Zinober [121], Quing-xuan *et al.* [122]. The proposed controller produces a smooth control law which ensures satisfactory performance in position control tasks. The proposed IBSMC can also be used for stabilisation of underactuated systems.

(ii) **Integral adaptive dynamic surface controller (IADSC)**
The inherent "*explosion of terms*" encountered in backstepping tends to increase the number of terms in the controller due to the successive differentiation, thus increasing the structural complexity. The dynamic surface [123, 124] is used to develop an IADSC that uses simple first order low pass filters instead of differentiation. In the proposed control method, the filter is used only in the final step of the integral backstepping controller unlike the DSC [123]. This is done to avoid differentiating the manipulator dynamics. The controller gain is tuned adaptively and hence knowledge about the uncertainty bounds is not a prerequisite for designing the controller. Also, now the controller gain is not unduly high and so chattering is reduced.

(iii) **Adaptive backstepping sliding mode controller with PID sliding surface (ABSMC-PID)**
Inclusion of low pass filters in the IADSC somehow limits the bandwidth of the controller application as the filter dynamics can affect the controller stability. In case of digital implementation

of the controller, the varying sampling time and possible delays will require redesigning of the filter to avoid unstable operations. Therefore, the integrator block in the backstepping method is replaced by a PID type of sliding surface. This eliminated the requirement of the low pass filter. The proportional, integral and derivative gains of the sliding surface are derived via backstepping. This way, tuning of the PID sliding surface is totally eliminated. Moreover, as the backstepping is a Lyapunov based design, a stable sliding surface is always guaranteed. The proposed ABSMC-PID method is also used for impedance controller design of robot manipulators. Unlike the existing impedance control methods, the ABSMC-PID uses backstepping to arrive at the desired manipulator impedance defined in terms of the sliding surface.

(iv) **Adaptive backstepping based fast terminal sliding mode controller (ABFTSM) with time delay estimation**
The structure of the manipulator dynamics becomes more complex as the number of DoF increases. To avoid this problem, a model free controller is designed using the time delay estimation (TDE) method [25]. The TDE is implemented to estimate the soft nonlinearities of the manipulator dynamics which include the centrifugal and Coriolis force and the gravitational effects. The inertia matrix of the manipulator is replaced with an estimated constant diagonal matrix. The proposed controller uses backstepping to derive a fast terminal sliding surface that has finite time convergence properties. The controller gains are tuned adaptively in order to compensate for the unknown disturbances and the modeling error encountered due to the TDE.

(v) **Torque to position conversion**
Most of the digital servos used as actuators for the low cost commercially available manipulators are position commanded and hence implementing dynamic torque control for them is quite difficult. Motivated by the works of Khatib *et al.* [116], a simplified torque to position conversion method is proposed where the servos have only proportional control as their built in internal control. Through simulation and experimentation, the proposed method is validated and is used for implementing the control methods proposed in this thesis. The results confirm that inclusion of an outer dynamic control loop in the position commanded actuators can actually improve the performance of the controlled system.

1.5 Organization of the thesis

This thesis is divided into six chapters. The organization of the thesis is as follows:

- **Chapter 2:** In the first part of this chapter the integral backstepping sliding mode controller (IBSMC) for robot manipulators is derived. A detailed stability analysis and comparison of simulation results with already existing control methods are provided. Moreover, simulation results obtained by implementing the controller for stabilizing the underactuated inverted cart pendulum system is also presented. In the second part of the chapter, the design, stability analysis and simulation results for the integral adaptive dynamic surface controller (IADSC)

are provided. The proposed IADSC is compared with the IBSMC and some other controllers existing in literature.

- **Chapter 3:** The adaptive backstepping sliding mode controller with PID sliding surface (ABSMC-PID) is designed in this chapter. The first part of the chapter includes the controller design, stability analysis and simulation results for joint trajectory tracking of the robot manipulator. In the second part of the chapter, the ABSMC-PID is designed for impedance control of robot manipulators while interacting with the external environment. The system compliance has showed improvement during collision with stiff surfaces while performing trajectory tracking tasks.

- **Chapter 4:** The model free adaptive backstepping based fast terminal sliding mode controller (ABFTSMC) with time delay estimation is presented in this chapter. The detailed stability analysis and the simulation results are presented to confirm the controller performance.

- **Chapter 5:** The description of the experimental setup and a detailed derivation of the torque to position conversion for position commanded digital servomotor is presented in this chapter along with simulation and experimental validation. Experimental validation of the proposed conversion methods as well as the proposed control laws, ABSMC-PID and ABFTSMC, are also presented in this chapter.

- **Chapter 6:** Conclusions are drawn and scope for future research are presented in this chapter.

2

Integral Backstepping Sliding Mode Controller

Contents

2.1 Motivation

The characteristic robustness against matched uncertainties and the order reduction in the sliding mode control (SMC) have rendered it an attractive domain in the field of controller design. In case of robot manipulators, application of the SMC has been highly researched for joint tracking, task space tracking as well as compliant control tasks. Guaranteed transient performance and final tracking accuracy in presence of both parametric uncertainty and unknown nonlinear functions satisfying the matching conditions have made the SMC a popular choice for controlling nonlinear systems. However, the strong robustness of the SMC is achieved at the cost of high controller gain which may lead to actuator saturation and high cost of the controller. Moreover, the inherent high frequency chattering in the control input of the SMC is undesirable as it may cause damage to the system actuators. Also, robustness of the SMC is guaranteed against uncertainties satisfying the matching conditions only [64], whereas in presence of mismatched uncertainties the system stability cannot be assured.

A well known control algorithm providing global stabilization is backstepping [54, 125]. It is a recursive procedure for designing an adaptive nonlinear feedback control, where a step by step coordinate transformation occurs with a Lyapunov based synthetic control developed at each stage and an adaptive tuning function estimating the unknown functions. The actual control is obtained in the last step. In order to design a backstepping controller the system is initially represented in parametric pure feedback (PPF), parametric strict feedback (PSF) or semi strict feedback (SSF) form and then the whole system is divided into small subsystems [54].

The attractive qualities of backstepping method are (i) *asymptotic global stability against parametric uncertainty*, (ii) *guaranteed transient performance and methodical analysis ability due to the control Lyapunov functions* and (iii) *Retention of system nonlinearities*. In order to utilize the benefits of both backstepping and sliding mode control, these have been combined to develop the backstepping sliding mode controller [126, 127]. The integral backstepping is a method which is applied for lower order systems to obtain a strict feedback form [54, 128]. The integral backstepping has been modified and combined with the sliding mode control to achieve a continuous control signal, thus eliminating chattering from the control input [129].

The IBSMC can combine the main advantages of both the controllers namely, *asymptotic stability against both the matched and mismatched parametric uncertainties* offered by backstepping method and *guaranteed transient performance and final tracking accuracy* offered by the SMC. Moreover, due to backstepping, the resultant controller will have a methodically defined Lyapunov function for stability analysis and more flexibility in terms of design parameters.

The merger of integral backstepping and sliding mode control methods mainly offers the benefits of both the controllers while at the same time compensating the drawbacks of each other. For systems like robot manipulators which are extremely prone to both structured and unstructured uncertainties, it is necessary for the torque controller to have robustness and adaptiveness against both. Most importantly, such a controller is well suited for the dynamic structure of the robot manipulator to produce a feedback control law that ultimately linearizes the system.

A few among the pioneering works on integral backstepping sliding mode control are [119–121]. The use of backstepping for robot manipulators was initially somewhat limited owing to its multi

input multi output (MIMO) nature and high coupling of the input matrix, which was however later overcome using the semi-strict feedback form of the MIMO system as can be found in [130]. Some recent literature on controlling robot manipulators using backstepping sliding mode controller are [112–115, 122, 131, 132], where backstepping sliding mode is combined with other algorithms such as optimal control, neural networks and time delay control to get satisfactory performance corresponding to the control objectives.

In this chapter an integral backstepping sliding mode controller (IBSMC) is proposed for the dynamic control of nonlinear robot manipulator systems and the block diagram of the proposed IBSMC is shown in Fig. 2.1. In Fig. 2.1, $u(t)$ is the control input to the system, $q, \dot{q}$ are the states and y is the output of the system and y_d is the reference signal. Two design approaches, namely integral back-

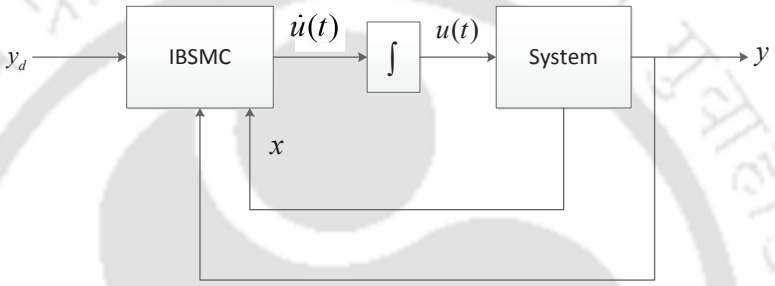

Figure 2.1: Block diagram: Integral Backstepping Sliding Mode Control

stepping sliding mode controller (IBSMC) and integral adaptive dynamic surface controller (IADSC) are proposed. The IBSMC derives a sliding surface based on the integral backstepping method and finally produces a discontinuous function as the derivative of the control input. As the control input is obtained at the output of an integrator, it is free from chattering and due to backstepping the controller can handle both matched and mismatched uncertainties. However, the analysis and the simulations showed that the IBSMC had certain disadvantages, mainly *explosion of terms and necessity of the knowledge about the uncertainty bounds*. In order to eliminate these drawbacks, the dynamic surface control (DSC) [123] methodology is adopted along with the adaptive tuning of the sliding mode controller gain [133].

The outline of the chapter is as follows. Section 2.2 includes the design and stability analysis of the IBSMC. Simulation results obtained by applying the IBSMC for an under-actuated cart-pendulum system are firstly presented in this chapter. Then, simulation studies of the proposed IBSMC for stabilizing a robot manipulator are conducted. The design process of the IADSC for a robot manipulator and its stability analysis are discussed in Section 2.3. The effectiveness of the proposed IADSC method is validated by comparing it with some existing robust control methods. In Section 2.4 a brief summary of the proposed controllers is presented.

2.2 IBSMC design for robot manipulators

2.2.1 System Description

In order to derive an IBSMC for a robot manipulator, the following generalized dynamics for a n-DoF robot manipulator is considered [11]:

$$\boldsymbol{M(q)\ddot{q} + C(q,\dot{q})\dot{q} + G(q) = \tau + f(q,\dot{q},t)} \tag{2.1}$$

where the $n \times 1$ vectors $\boldsymbol{q},\ \boldsymbol{\dot{q}},\ \boldsymbol{\ddot{q}}\ \in \mathbb{R}$ are respectively the joint angle position, angular velocity and angular acceleration of the manipulator, $\boldsymbol{M(q)} \in \mathbb{R}^{n\times n}$ is the inertia matrix, $\boldsymbol{C(q,\dot{q})} \in \mathbb{R}^{n\times n}$ is the centripetal and Coriolis force matrix and $\boldsymbol{G(q)} \in \mathbb{R}^n$ is the gravitational force vector. The input torques acting on each of the joints are represented by the vector $\boldsymbol{\tau} \in \mathbb{R}^n$. The vector $\boldsymbol{f(q,\dot{q},t)} \in \mathbb{R}^n$ represents the frictional torque acting on the joints and is considered as an unknown disturbance torque. The derivation of the manipulator dynamics is given in Appendix A.1.

Considering revolute joint manipulators, the properties of the manipulator dynamics [11] are as follows:

Property 1. *The inertia matrix $\boldsymbol{M(q)}$ is bounded, symmetric and positive definite which means,*

$$\mu_{min}||\boldsymbol{x}||^2 \leq \boldsymbol{x}^T\boldsymbol{M(q)x} \leq \mu_{max}||\boldsymbol{x}||^2 \tag{2.2}$$

where $\boldsymbol{x} \in \mathbb{R}$ is any real valued vector with $||x||$ as its Euclidian norm and $0 < \mu_{min} < \mu_{max}$ represents the bounds of $\boldsymbol{M(q)}$.

Property 2. *The robotic manipulator is a passive system which means*

$$\boldsymbol{x}^T\left(\frac{1}{2}\dot{\boldsymbol{M}}(\boldsymbol{q}) - \boldsymbol{C(q,\dot{q})}\right)\boldsymbol{x} = 0, \quad \forall \boldsymbol{x} \neq 0. \tag{2.3}$$

The following assumptions are made for the robot manipulator:

Assumption 1. *All the joints of the robotic manipulator are revolute. This assumption makes Property 1 valid.*

Assumption 2. *The reference trajectory, defined as $\boldsymbol{q_d(t)} \in \mathbb{R}^n$, as well as its time derivatives $\boldsymbol{\dot{q}_d(t)},\ \boldsymbol{\ddot{q}_d(t)}$ and $\dddot{\boldsymbol{q}}_{\boldsymbol{d}}\boldsymbol{(t)}$ are continuous and bounded.*

Assumption 3. *The vector $\boldsymbol{f(q,\dot{q},t)}$ containing the frictional uncertainties satisfies the following:*

$$|\boldsymbol{f(q,\dot{q},t)}| \leq \boldsymbol{f_1} \tag{2.4}$$

where $\boldsymbol{f_1 > 0}$ is a constant.

Following the integral backstepping algorithm [125], where an integrator block is augmented with

the main system to increase its relative degree, (2.1) can be rewritten as follows:

$$\begin{aligned}\ddot{\boldsymbol{q}} =& \boldsymbol{M(q)}^{-1}\left(\boldsymbol{\tau} - \boldsymbol{C(q,\dot{q})\dot{q}} - \boldsymbol{G(q)}\right)\\ \dot{\boldsymbol{\tau}} =& \boldsymbol{u}.\end{aligned} \tag{2.5}$$

The unmodeled forces are not considered in (2.5) for ease of design and will be later treated during stability analysis of the closed loop system.

2.2.2 Design Process

The controller design process involves arriving at a stable sliding surface using the backstepping method and finally deriving the switching control law for the converted system (2.5). The augmented integrator block will then integrate this discontinuous signal to produce a smooth control law for the actual plant as shown in Fig. 2.1. The design process can be divided into the following steps:

Step I:

The first regulatory variable is defined in this step which is generally the tracking error (in case of trajectory tracking controller) or the joint locations (in case of stabilizing controller). Here the tracking error is considered as the first regulatory variable ($\boldsymbol{z_1}$) defined as follows:

$$\begin{aligned}\boldsymbol{z_1} &= \boldsymbol{q} - \boldsymbol{q_d}\\ \dot{\boldsymbol{z}}_{\boldsymbol{1}} &= \dot{\boldsymbol{q}} - \dot{\boldsymbol{q}}_{\boldsymbol{d}}.\end{aligned} \tag{2.6}$$

The joint velocity $\dot{\boldsymbol{q}}$ is now considered as the control variable for the subsystem (2.6). A control Lyapunov function (CLF) is now defined for (2.6) as follows:

$$\begin{aligned}V_1 =& \frac{1}{2}\boldsymbol{z_1^T z_1}\\ \dot{V}_1 =& \boldsymbol{z_1^T \dot{z}_1} = \boldsymbol{z_1^T(\dot{q} - \dot{q}_d)}.\end{aligned} \tag{2.7}$$

Based on the CLF an artificial control $\boldsymbol{\alpha_1}$ will be formed so that when $\dot{\boldsymbol{q}} = \boldsymbol{\alpha_1}$, (2.6) will be stabilized. Following $\boldsymbol{\alpha_1}$ is used that will render $\dot{V}_1$ negative definite,

$$\boldsymbol{\alpha_1} = -\boldsymbol{c_1 z_1} + \dot{\boldsymbol{q}}_{\boldsymbol{d}} \tag{2.8}$$

where $\boldsymbol{c_1} = diag(c_{1i})$, $c_{1i} > 0, i = 1, \ldots, n$ is a user defined constant matrix. This selection of $\boldsymbol{\alpha_1}$ will convert (2.6) to the following stable form

$$\dot{\boldsymbol{z}}_{\boldsymbol{1}} = -\boldsymbol{c_1 z_1}. \tag{2.9}$$

Step II:

The error between the artificial control $\boldsymbol{\alpha_1}$ and the velocity $\dot{\boldsymbol{q}}$ forms the second regulatory variable $\boldsymbol{z_2}$

as follows:

$$\begin{aligned}\boldsymbol{z_2} =&\dot{\boldsymbol{q}} - \boldsymbol{\alpha_1} = \dot{\boldsymbol{q}} - \dot{\boldsymbol{q}}_{\boldsymbol{d}} + \boldsymbol{c_1 z_1}\\ \dot{\boldsymbol{z}}_{\boldsymbol{2}} =&\ddot{\boldsymbol{q}} - \ddot{\boldsymbol{q}}_{\boldsymbol{d}} + \boldsymbol{c_1}\dot{\boldsymbol{z}}_{\boldsymbol{1}} = \boldsymbol{M(q)^{-1}(\tau - C(q,\dot{q})\dot{q} - G(q)) - \ddot{q}_d + c_1\dot{z}_1}.\end{aligned} \tag{2.10}$$

Introduction of $\boldsymbol{z_2}$ along with $\boldsymbol{\alpha}_1$ changes (2.6) to the following form:

$$\dot{\boldsymbol{z}}_{\boldsymbol{1}} = -\boldsymbol{c_1 z_1} + \boldsymbol{z_2}. \tag{2.11}$$

With $\boldsymbol{\tau}$ as the control variable, following CLF V_2 is defined for (2.10), which is positive definite for all $\boldsymbol{z_1},\ \boldsymbol{z_2} \neq \boldsymbol{0}$.

$$\begin{aligned}V_2 =&V_1 + \frac{1}{2}\boldsymbol{z_2^T z_2}\\ \dot{V}_2 =&-\boldsymbol{z_1^T c_1 z_1} + \boldsymbol{z_1^T z_2} + \boldsymbol{z_2^T(M(q)^{-1}(\tau - C(q,\dot{q})\dot{q} - G(q)) - \ddot{q}_d + c_1\dot{z}_1)}.\end{aligned} \tag{2.12}$$

Based on the CLF V_2, the following artificial control law $\boldsymbol{\alpha_2}$ is defined.

$$\boldsymbol{\alpha_2} = \boldsymbol{C(q,\dot{q})\dot{q} + G(q) + M(q)\left(\ddot{q}_d - c_2 z_2 - c_1\dot{z}_1\right)} \tag{2.13}$$

where $\boldsymbol{c_2} = diag(c_{2i}),\ c_{2i} > 0, i = 1, \ldots, n$ is a user defined constant matrix.

Application of the synthetic control $\boldsymbol{\alpha_2}$ on (2.12) yields the following:

$$\begin{aligned}\dot{V}_2 =&-\boldsymbol{z_1^T c_1 z_1} - \boldsymbol{z_2^T c_2 z_2} + \boldsymbol{z_1^T z_2}\\ =&-\begin{bmatrix}\boldsymbol{z_1}^T & \boldsymbol{z_2}^T\end{bmatrix}\begin{bmatrix}\boldsymbol{c_1} & -\frac{1}{2}\boldsymbol{I}_n\\ -\frac{1}{2}\boldsymbol{I}_n & \boldsymbol{c_2}\end{bmatrix}\begin{bmatrix}\boldsymbol{z_1}\\ \boldsymbol{z_2}\end{bmatrix}\end{aligned} \tag{2.14}$$

which will be negative definite $\forall \boldsymbol{z_1},\ \boldsymbol{z_2} \neq 0$, if the symmetric matrix $\begin{bmatrix}\boldsymbol{c_1} & -\frac{1}{2}\boldsymbol{I}_n\\ -\frac{1}{2}\boldsymbol{I}_n & \boldsymbol{c_2}\end{bmatrix}$ is positive definite and this can be ensured if the following condition holds:

$$\boldsymbol{c_1} > \frac{1}{4}\boldsymbol{c_2^{-1}}. \tag{2.15}$$

Step III:

The last regulatory variable $\boldsymbol{z_3}$ is now defined as the difference between $\boldsymbol{\tau}$ and the artificial control $\boldsymbol{\alpha}_2$ as follows:

$$\begin{aligned}\boldsymbol{z_3} =&\boldsymbol{\tau - \alpha_2} = \boldsymbol{\tau - C(q,\dot{q})\dot{q} - G(q) - M(q)\left(\ddot{q}_d - c_2 z_2 - c_1\dot{z}_1\right)}\\ \dot{\boldsymbol{z}}_{\boldsymbol{3}} =&\boldsymbol{u - \eta(q,\dot{q},\tau)}\end{aligned} \tag{2.16}$$

where

$$\boldsymbol{u} = \dot{\boldsymbol{\tau}}$$

$$\begin{aligned}\boldsymbol{\eta(q,\dot{q},\tau)} =& \boldsymbol{\dot{C}(q,\dot{q})\dot{q} + C(q,\dot{q})\ddot{q} + \dot{G}(q) + M(q)(\dddot{q}_d - c_2\ddot{z}_2 - c_1\dddot{z}_1)} \\ &+ \boldsymbol{\dot{M}(q)\left(\ddot{q}_d - c_2 z_2 - c_1\dot{z}_1\right)}. \end{aligned} \tag{2.17}$$

Introduction of the variable $\boldsymbol{z_3}$ will cause the time derivative $\dot{V}_2$ to have the following form,

$$\dot{V}_2 = -z_1^T c_1 z_1 - z_2^T c_2 z_2 + z_1^T z_2 + z_2^T z_3. \tag{2.18}$$

The following sliding variable ($\boldsymbol{s}$) is now defined as the function of the regulatory variables obtained through backstepping:

$$\boldsymbol{s} = \sigma_1 z_1 + \sigma_2 z_2 + z_3 \tag{2.19}$$

$$\begin{aligned}\dot{\boldsymbol{s}} =& \sigma_1\dot{z}_1 + \sigma_2\dot{z}_2 + \dot{z}_3 \\ =& \sigma_1\dot{z}_1 + \sigma_2\dot{z}_2 + u - \eta(q,\dot{q},\tau)\end{aligned} \tag{2.20}$$

where, $\boldsymbol{\sigma_1,\ \sigma_2}$ are chosen to be positive such that the polynomial $\boldsymbol{s = \sigma_1 z_1 + \sigma_2 z_2 + z_3}$ is Hurwitz stable.

Now, the control law $\boldsymbol{u}$ will be derived in two parts: (i) the equivalent control, $\boldsymbol{u_{eq}}$ obtained by using $\dot{s} = 0$ and (ii) the switching control $\boldsymbol{u_{sw}}$ derived based on the reaching law approach [134]. Accordingly, the equivalent control law $\boldsymbol{u_{eq}}$ is found to be

$$\boldsymbol{u_{eq} = \eta(q,\dot{q},\tau) - \sigma_1\dot{z}_1 - \sigma_2\dot{z}_2}$$

and the switching control $\boldsymbol{u_{sw}}$ is found to be

$$\boldsymbol{u_{sw} = -k \circ sign(s) - Ws}. \tag{2.21}$$

where $\boldsymbol{k > 0,\ W > 0}$ are design parameters and '$\circ$' represents elementwise multiplication of two vectors. Thus the net control $\boldsymbol{u}$ is obtained as

$$\boldsymbol{u = u_{eq} + u_{sw} = \eta(q,\dot{q},\tau) - \sigma_1\dot{z}_1 - \sigma_2\dot{z}_2 - k \circ sign(s) - Ws}. \tag{2.22}$$

With $\boldsymbol{u}$ being the control input to the augmented system (2.5), the input $\boldsymbol{\tau}$ to the manipulator is obtained as follows:

$$\boldsymbol{\tau} = \int_0^t \boldsymbol{u(\theta)}d\boldsymbol{\theta}. \tag{2.23}$$

Thus any discontinuity in $\boldsymbol{u}$ will be removed in the input torque $\boldsymbol{\tau}$ due to the above integral operation, producing a chattering free, smooth control input for the manipulator system.

2.2.3 Stability Analysis

The sliding surface is already chosen to be Hurwitz stable. Therefore, stability concerns are with the reaching phase when the system is still vulnerable to the uncertainties. Moreover, analysis of the

overall stability of the controlled system is also important to establish robustness and applicability of the proposed IBSMC. Stability of the sliding surface reaching phase as well as the overall system can be analyzed in the form of the following Lemmas:

Lemma 1. *The sliding surface reaching phase will be stable provided the controller gain* $\boldsymbol{k}$ *satisfies the following condition:*

$$\boldsymbol{k} \geq \boldsymbol{h}^* > \boldsymbol{0} \tag{2.24}$$

where $\boldsymbol{h}^* \geq |\boldsymbol{h}(\boldsymbol{q}, \dot{\boldsymbol{q}})|$ *and* $\boldsymbol{h}(\boldsymbol{q}, \dot{\boldsymbol{q}})$ *is the vector of uncertainties effecting the system 2.20.*

Proof. In order to prove stability of the sliding surface reaching phase in presence of uncertainty, Lyapunov function V_s is used which is positive definite for all $\boldsymbol{s} \neq \boldsymbol{0}$.

$$\begin{aligned}
V_s =& \frac{1}{2}\boldsymbol{s}^T\boldsymbol{s} \\
\dot{V}_s =& \boldsymbol{s}^T\dot{\boldsymbol{s}} = \boldsymbol{s}^T(\boldsymbol{\sigma}_1\dot{\boldsymbol{z}}_{\boldsymbol{1}} + \boldsymbol{\sigma}_2\dot{\boldsymbol{z}}_2 + \dot{\boldsymbol{z}}_3) \\
=& \boldsymbol{s}^T(\boldsymbol{\sigma}_1\dot{\boldsymbol{z}}_1 + \boldsymbol{\sigma}_2\dot{\boldsymbol{z}}_2 + \boldsymbol{u} - \boldsymbol{\eta}(\boldsymbol{q}, \dot{\boldsymbol{q}}, \boldsymbol{\tau}) + \boldsymbol{h}(\boldsymbol{q}, \dot{\boldsymbol{q}})) \\
=& \boldsymbol{s}^T(\boldsymbol{\sigma}_1\dot{\boldsymbol{z}}_1 + \boldsymbol{\sigma}_2\dot{\boldsymbol{z}}_2 + \boldsymbol{\eta}(\boldsymbol{q}, \dot{\boldsymbol{q}}, \boldsymbol{\tau}) - \boldsymbol{\sigma}_1\dot{\boldsymbol{z}}_1 - \boldsymbol{\sigma}_2\dot{\boldsymbol{z}}_2 - \boldsymbol{k} \circ sign(\boldsymbol{s}) - \boldsymbol{W}\boldsymbol{s} - \boldsymbol{\eta}(\boldsymbol{q}, \dot{\boldsymbol{q}}, \boldsymbol{\tau}) + \boldsymbol{h}(\boldsymbol{q}, \dot{\boldsymbol{q}})) \\
=& \boldsymbol{s}^T(-\boldsymbol{k} \circ sign(\boldsymbol{s}) - \boldsymbol{W}\boldsymbol{s} + \boldsymbol{h}(\boldsymbol{q}, \dot{\boldsymbol{q}})) \\
\leq& -|\boldsymbol{s}|^T\boldsymbol{k} - \boldsymbol{s}^T\boldsymbol{W}\boldsymbol{s} + |\boldsymbol{s}|^T|\boldsymbol{h}(\boldsymbol{q}, \dot{\boldsymbol{q}})| \\
\leq& -|\boldsymbol{s}|^T(\boldsymbol{k} - |\boldsymbol{h}(\boldsymbol{q}, \dot{\boldsymbol{q}})|) - \boldsymbol{s}^T\boldsymbol{W}\boldsymbol{s}.
\end{aligned} \tag{2.25}$$

From the control algorithm it is evident that due to the recursive nature of the backstepping method all the uncertainties in the system are carried to the final subsystem of the process, hence they can all be accumulated as the single term $\boldsymbol{h}(\boldsymbol{q}, \dot{\boldsymbol{q}})$. This way sliding mode will be able to reject both matched and mismatched uncertainties of the system. When the uncertainty bounds are known and the switching gain $\boldsymbol{k}$ is such that $\boldsymbol{k} \geq \boldsymbol{h}^* > |\boldsymbol{h}(\boldsymbol{q}, \dot{\boldsymbol{q}})|$, the time derivative $\dot{V}_s$ can be written as follows:

$$\dot{V}_s \leq -\boldsymbol{s}^T\boldsymbol{W}\boldsymbol{s} < 0, \forall \boldsymbol{s} \neq 0. \tag{2.26}$$

Since $\forall \boldsymbol{s} \neq 0$, $\boldsymbol{s}^T\boldsymbol{W}\boldsymbol{s}$ is positive definite and $\lim_{t\to\infty} \boldsymbol{s}^T\boldsymbol{W}\boldsymbol{s} = \boldsymbol{0}$, it can be concluded that the sliding surface converges to the equilibrium asymptotically. □

Remark 2. *As can be found in [134], the finite time* T_r *required by the system error states to reach from initial condition to the sliding surface can be derived from (2.21) as*

$$T_r = W^{-1}\ln\left(\frac{W|s(0)| + k}{k}\right). \tag{2.27}$$

Lemma 3. *Provided the reaching phase is stable, the overall controlled system will be stable if the matrix* $\boldsymbol{Q} = \begin{bmatrix} \boldsymbol{c}_1 & -\frac{1}{2}(\boldsymbol{I}_n - \boldsymbol{\sigma}_1) & \boldsymbol{0} \\ -\frac{1}{2}(\boldsymbol{I}_n - \boldsymbol{\sigma}_1) & \boldsymbol{c}_2 + \boldsymbol{\sigma}_2 & -\frac{1}{2}\boldsymbol{I}_n \\ \boldsymbol{0} & -\frac{1}{2}\boldsymbol{I}_n & \boldsymbol{W} \end{bmatrix}$ *is positive definite, where* $\boldsymbol{I}_n$ *is an* $n \times n$ *identity matrix.*

Proof. The lemma can be proved using the following Lyapunov function V:

$$\begin{aligned}
V =& \frac{1}{2}(\boldsymbol{z_1^T z_1 + z_2^T z_2 + s^T s}) \\
\dot{V} =& \boldsymbol{z_1^T \dot{z}_1 + z_2^T \dot{z}_2 + s^T \dot{s}} \\
=& -\boldsymbol{z_1^T c_1 z_1 - z_2^T c_2 z_2 + z_1^T z_2 + z_2^T z_3 - |s|^T k - s^T W s + s^T h(q,\dot{q})} \\
=& -\boldsymbol{z_1^T c_1 z_1 - z_2^T c_2 z_2 - s^T W s + z_1^T z_2 + z_2^T (s - \sigma_1 z_1 - \sigma_2 z_2)} \\
& -\boldsymbol{|s|^T k + s^T h(q,\dot{q})}\,, \qquad (from (2.19)) \\
\leq& -\begin{bmatrix} z_1^T & z_2^T & s^T \end{bmatrix} \begin{bmatrix} \boldsymbol{c_1} & -\frac{1}{2}(\boldsymbol{I_n - \sigma_1}) & \boldsymbol{0} \\ -\frac{1}{2}(\boldsymbol{I_n - \sigma_1}) & \boldsymbol{c_2 + \sigma_2} & -\frac{1}{2}\boldsymbol{I_n} \\ 0 & -\frac{1}{2}\boldsymbol{I_n} & \boldsymbol{W} \end{bmatrix} \begin{bmatrix} z_1 \\ z_2 \\ s \end{bmatrix} - \boldsymbol{|s|^T k + |s|^T |h(q,\dot{q})|} \\
\leq& -\begin{bmatrix} z_1^T & z_2^T & s^T \end{bmatrix} \boldsymbol{Q} \begin{bmatrix} \boldsymbol{z_1} \\ \boldsymbol{z_2} \\ \boldsymbol{s} \end{bmatrix} - \boldsymbol{|s|^T k + |s|^T |h(q,\dot{q})|} \qquad (2.28)
\end{aligned}$$

where $\boldsymbol{Q} = \begin{bmatrix} \boldsymbol{c_1} & -\frac{1}{2}(\boldsymbol{I_n - \sigma_1}) & \boldsymbol{0} \\ -\frac{1}{2}(\boldsymbol{I_n - \sigma_1}) & \boldsymbol{c_2 + \sigma_2} & -\frac{1}{2}\boldsymbol{I_n} \\ \boldsymbol{0} & -\frac{1}{2}\boldsymbol{I_n} & \boldsymbol{W} \end{bmatrix}$. For a positive definite matrix $\boldsymbol{Q}$ and $\boldsymbol{k} > |\boldsymbol{h(q,\dot{q})}|$, $\dot{V}$ will be negative definite and the system will be asymptotically stable. Using Schur's complement for symmetric block matrix [135] (Appendix A.2), the matrix $\boldsymbol{Q}$ will be positive definite provided $\boldsymbol{c_1}$, $\boldsymbol{c_2}$, $\boldsymbol{\sigma_1}$, $\boldsymbol{\sigma_2}$, $\boldsymbol{k}$ and $\boldsymbol{W}$ are positive definite and they satisfy the following condition:

$$\boldsymbol{c_2 + \sigma_2} > \frac{1}{4}\boldsymbol{W^{-1}} \qquad (2.29)$$

$$\boldsymbol{c_1} > \frac{1}{4}(\boldsymbol{I_n - \sigma_1})(\boldsymbol{c_2 + \sigma_2} - \frac{1}{4}\boldsymbol{W^{-1}})^{-1}(\boldsymbol{I_n - \sigma_1}). \qquad (2.30)$$

□

2.2.4 Simulation Results

The IBSMC derived above is tested via simulations performed in Matlab/Simulink environment. The proposed IBSMC is first applied to an underactuated system by properly selecting the backstepping variables. The cart-pendulum, being a benchmark under-actuated system, is controlled through the proposed IBSMC method and the results are shown in Section 2.2.4.1. The second set of simulations show the controller performance on a 2 DoF robot manipulator.

2.2.4.1 IBSM Control of an Underactuated Cart-Pendulum System

The proposed IBSMC is applied for swing-up and stabilization of an underactuated cart-pendulum system [1]. Fig. 2.2 shows the cart-pendulum system whose dynamic model is represented as

$$\boldsymbol{M(q)\ddot{q} + C(q,\dot{q})\dot{q} + G(q) = F + F_d} \qquad (2.31)$$

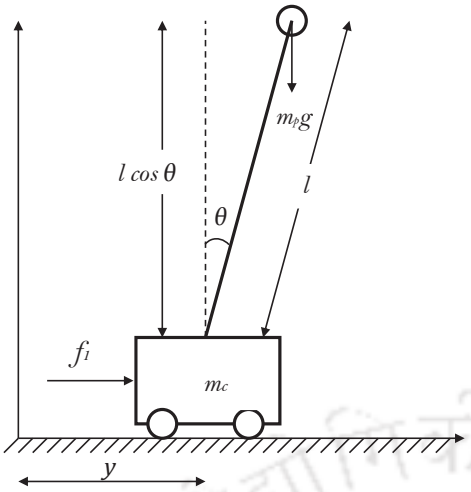

Figure 2.2: Cart-pendulum system

Table 2.1: Parameters of the Cart-Pendulum System

Unit	m_c (kg)	m_p (kg)	l (m)	J $(kg \cdot m^2)$
Value	1.12	0.11	0.1407	0.0038

where $\boldsymbol{q}$, $\dot{\boldsymbol{q}}$ and $\ddot{\boldsymbol{q}}$ represent the position, velocity and acceleration of the system, $\boldsymbol{M(q)}$ is the inertia matrix, $\boldsymbol{C(q,\dot{q})}$ is the centripetal and Coriolis force matrix and $\boldsymbol{G(q)}$ is the gravitational force vector. Furthermore, $\boldsymbol{F}$ represents the applied force and $\boldsymbol{F_d}$ corresponds to the disturbance force caused by uncertainties. In Figure 2.2, y and θ are the linear displacement of the cart and the angular displacement of the pendulum respectively and $\boldsymbol{q} = [y,\ \theta]^T$.

For the cart-pendulum system shown in Figure 2.2, the dynamics (2.31) is described in details in Appendix A.3. The parameters of the cart-pendulum system are given in Table 2.1.

The derivation of the IBSM controller for the inverted pendulum system is given in detail in Appendix A.4. The proposed IBSMC method is compared with the coupled SMC method designed by Park and Chwa [1] which is elaborated in Appendix A.5. A matched disturbance $f_{d_1} = 0.1\sin 2t$ is applied to the cart-pendulum system and the performances of the two controllers, IBSMC and SMC [1] are compared. The simulation results are shown in Figure 2.3 and performances of these controllers are summarized in Table 2.2 and Table 2.3. The performance indices used in the tables are: rise time (t_r), peak overshoot (M_p), peak time (t_p), settling time (t_s), the steady-state root mean square error ($RMSE_{ss}$), 2-norm of the control input ($||u||$) and the total variation (TV) of the control input (2.32) indicating the amount of chattering content. The total variation (TV) is computed by using the following formula (assuming a discrete signal obtained through software implementation or sampling of the continuous signal) [136]

$$TV = \sum_{i=1}^{p-1} |u_{i+1} - u_i| \tag{2.32}$$

where p is the total number of sample points.

In addition to the applied matched disturbance $f_{d_1} = 0.1\sin 2t$, a change in pendulum mass is

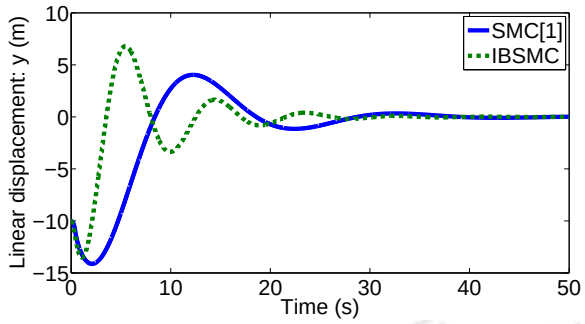

(a) Linear Displacement of the cart

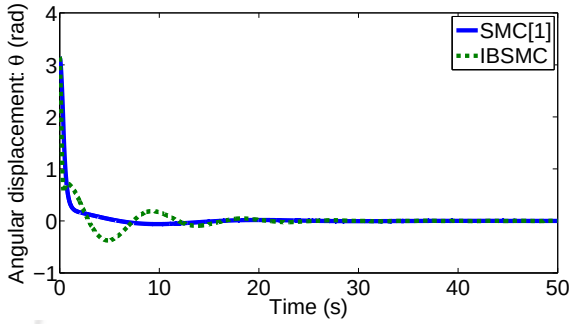

(b) Angular Displacement of the pendulum from vertically upward position

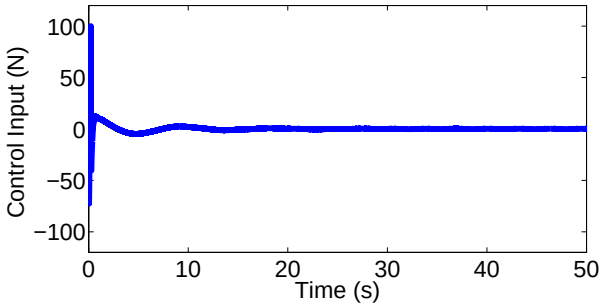

(c) Control Input with IBSMC

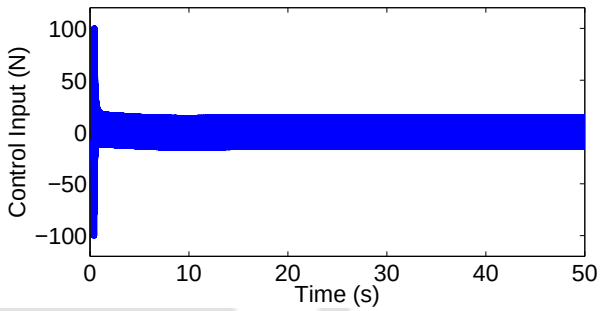

(d) Control Input with SMC [1]

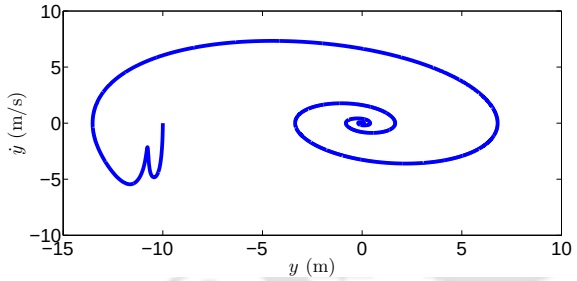

(e) Phase plot for $\dot{y}$ vs. y(with IBSMC)

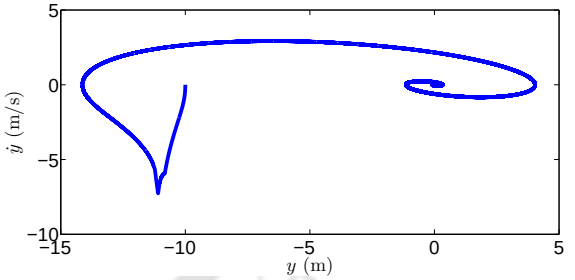

(f) Phase plot for $\dot{y}$ vs. y(with SMC [1])

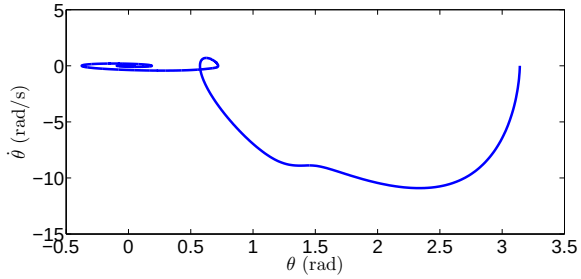

(g) Phase plot for $\dot{\theta}$ vs. θ(with IBSMC)

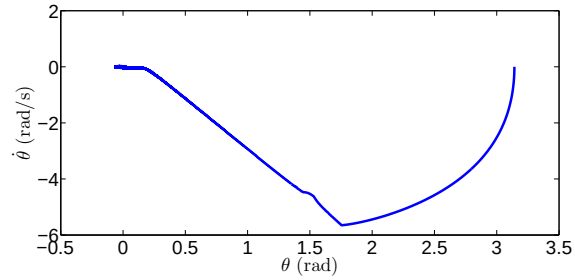

(h) Phase plot for $\dot{\theta}$ vs. θ(with SMC [1])

Figure 2.3: Simulation results of IBSMC and SMC [1] for swing-up and stabilization of cart-pendulum system with matched uncertainty

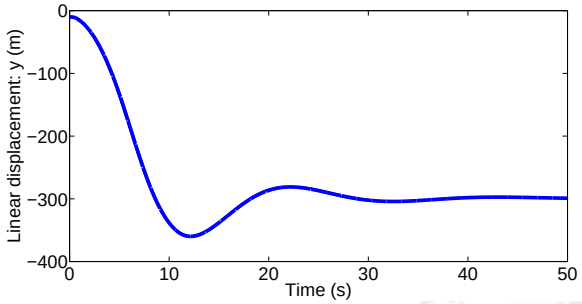

(a) Linear Displacement of the cart with SMC [1]

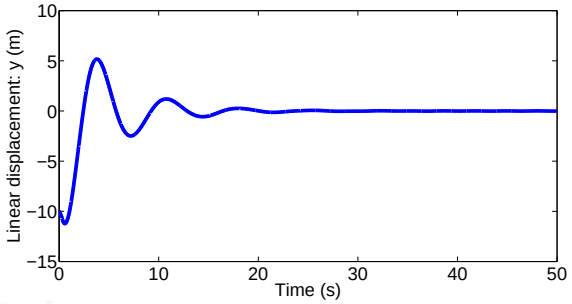

(b) Linear Displacement of the cart with IBSMC

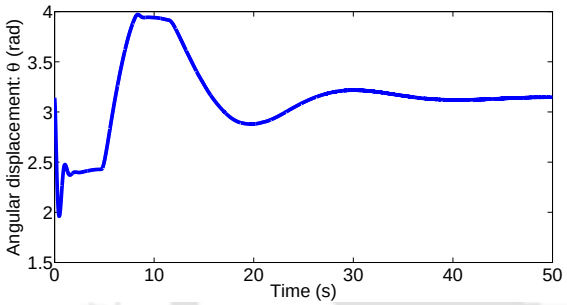

(c) Angular Displacement of the pendulum with SMC [1]

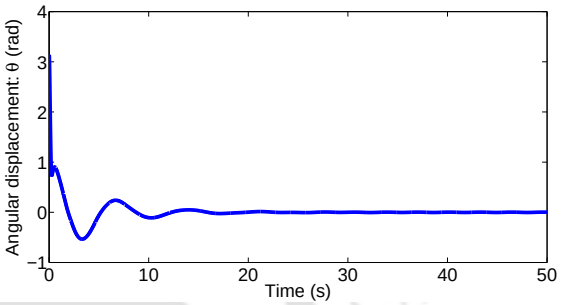

(d) Angular Displacement of the pendulum with IBSMC

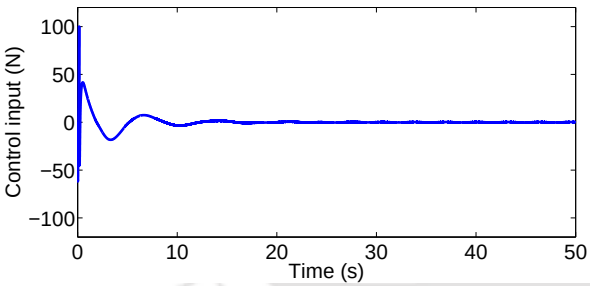

(e) Control Input with IBSMC

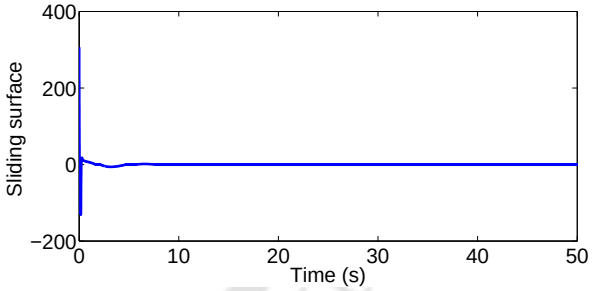

(f) Sliding Surface with IBSMC

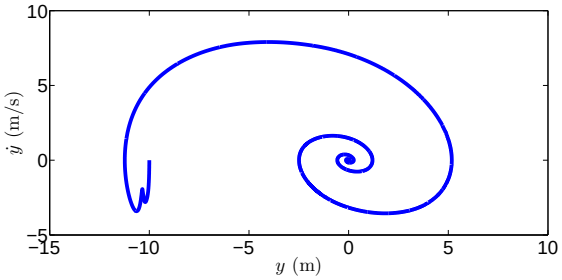

(g) Phase plot for $\dot{y}$ vs. y(with IBSMC)

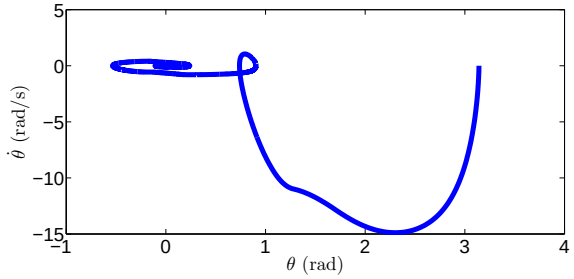

(h) Phase plot for $\dot{\theta}$ vs. θ(with IBSMC)

Figure 2.4: Simulation results of IBSMC and SMC [1] for swing-up and stabilization of cart-pendulum system with matched and mismatched uncertainties

Table 2.2: Stabilizing cart-pendulum system with matched uncertainty for linear displacement

Controller	t_r (s)	M_p (m)	t_p (s)	t_s (s)	$RMSE_{ss}$(m)	$\|\|u\|\|$ (N)	TV (N)
IBSMC	3.5390	6.7969	5.4490	24.7360	0.0776	916.8659	1.242134×10^3
SMC [1]	8.4030	4.0398	12.2600	34.4358	0.1018	3.3868×10^3	1.419360×10^6

Table 2.3: Stabilizing cart-pendulum system with matched uncertainty for angular displacement

Controller	t_r (s)	M_p (rad)	t_p (s)	t_s (s)	$RMSE_{ss}$(rad)
IBSMC	2.918	-0.3757	4.8450	15.0183	0.0153
SMC [1]	0.9191	0	–	4.3141	0.0218

Table 2.4: Stabilizing cart-pendulum system with matched and mismatched uncertainties using IBSMC

	t_r (s)	M_p	t_p (s)	t_s (s)	$RMSE_{ss}$	$\|\|u\|\|$ (N)	TV (N)
y	2.429	5.175m	3.788	18.6251	0.0463m	1.54×10^3	1.24×10^3
θ	1.912	-0.5354rad	3.3160	11.3685	0.0137rad	–	–

now considered which will produce a mismatched disturbance in the system. A change of mass from $m_p = 0.11kg$ to $m_p = 2kg$ is carried out for examining the effects on both of the controllers. The simulation results are plotted in Figure 2.4 and summarized in Table 2.4. The performance indices used in the table are the same as described above for Table 2.2 and 2.3. It is observed from Figure 2.4 that the SMC [1] fails in the presence of mismatched uncertainty in the system. On the other hand, the IBSMC remains immune to mismatched uncertainty and is able to successfully swing-up the cart-pendulum system to the equilibrium point and stabilize it.

2.2.4.2 IBSM control of a 2 DoF Robot Manipulator: Stabilization of Joint Positions

The proposed IBSMC method is now applied for stabilizing control of a 2DoF robot manipulator shown in Figure 2.5. The obtained results are compared with a conventional first order sliding mode controller (SMC). The parameters used for the proposed IBSMC (2.22) are:

$$\boldsymbol{c}_1 = 20\boldsymbol{I}_n,\ \boldsymbol{c}_2 = 30\boldsymbol{I}_n,\ \boldsymbol{\sigma}_1 = \boldsymbol{\sigma}_2 = 10\boldsymbol{I}_n, \boldsymbol{k} = [8,8,8]^T,\ W = 100\boldsymbol{I}_n \tag{2.33}$$

where I_n is an $n \times n$ identity matrix.

The conventional first order SMC is given by

$$\boldsymbol{\tau_s} = \boldsymbol{C(q,\dot{q})\dot{q} + G(q) + M(q)^{-1}(\ddot{q}_d - k \circ sign(s) - Ws)} \tag{2.34}$$

where $\boldsymbol{k} = 8\boldsymbol{I}_n,\ \boldsymbol{W} = 100\boldsymbol{I}_n$. The sliding variable $\boldsymbol{s}$ is formed as

$$\boldsymbol{s} = \dot{q} + \Lambda \boldsymbol{q} \tag{2.35}$$

where $\Lambda = 10$. The rest of the terms in the SMC (2.34) represent the same quantities as described in the previous sections.

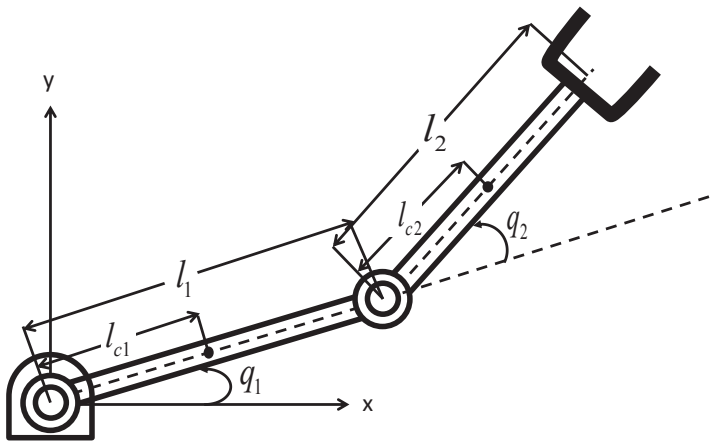

Figure 2.5: 2DoF manipulator schematics used for simulation

The dynamics of the manipulator model shown in Figure 2.5 is given below:

$$\begin{bmatrix} m_{11} & m_{12} \\ m_{21} & m_{22} \end{bmatrix} \begin{bmatrix} \ddot{q}_1 \\ \ddot{q}_2 \end{bmatrix} + \begin{bmatrix} c_{11} & c_{12} \\ c_{21} & c_{22} \end{bmatrix} \begin{bmatrix} \dot{q}_1 \\ \dot{q}_2 \end{bmatrix} + \begin{bmatrix} G_1 \\ G_2 \end{bmatrix} = \begin{bmatrix} \tau_1 \\ \tau_2 \end{bmatrix} \tag{2.36}$$

where $m_{11} = (m_1 + m_2)l_1^2 + m_2 l_2^2 + 2m_2 l_1 l_2 \cos(q_2) + J_1;\ m_{12} = m_{21} = m_1 l_2^2 + m_2 l_1 l_2 \cos(q_2);\ m_{22} = m_2 l_2^2 + J_2;\ c_{11} = -b\dot{q}_1;\ c_{12} = -2b\dot{q}_1;\ c_{21} = 0; c_{22} = b\dot{q}_2;\ b = m_2 l_1 l_2 \sin(q_2);\ G_1 = (m_1 + m_2)l_1 g \cos(q_2) + m_2 l_2 \cos(q_1 + q_2);\ G_2 = g m_2 l_2 \cos(q_1 + q_2)$. The manipulator parameter values are:
$m_1 = 0.5kg,\ m_2 = 1.5kg,\ l_1 = 1m,\ l_2 = 0.8m,\ g = 9.81m/s^s$.

To induce structured uncertainty, the link masses m_1 and m_2 are perturbed by 40% and 20% respectively. Simulation is performed for the regulation task where the controller objective is to bring and regulate both the joints from initial 0 rad position to the final 1 rad. The position stabilization for joints 1 and 2 (q_1 and q_2) are shown in Figure 2.6. The control torques for the joints q_1 and q_2 are shown in Figure 2.7, which clearly show that a smooth control law can be obtained via IBSMC as opposed to the SMC input which contains high chattering. But the tracking accuracy of the SMC is slightly superior than the proposed IBSMC. However, the cost of reduction in accuracy is lower compared to the smoothness gained in the control input of the IBSMC. Table 2.5 compares important output performance indices like rise time (t_r), peak overshoot (M_p), peak time (t_p), settling time (t_s), steady state error (e_{ss}) and input performance indices like 2 norm of the control input ($||\tau||$) indicating energy spent and the total variation (TV) [136] showing smoothness.

From Table 2.5, it is observed that the proposed IBSMC method and the conventional SMC have comparable transient performance in terms of the speed of convergence and overshoot. However, he proposed IBSMC has greater steady state error compared to the SMC. But chattering in the control input obtained through IBSMC is significantly lower than in the case of the SMC as clearly visible in Figure 2.7(a) and Figure 2.7(b). Therefore, except for a slight loss in tracking accuracy, the proposed IBSMC yields a chattering free smooth control signal with satisfactory transient performance.

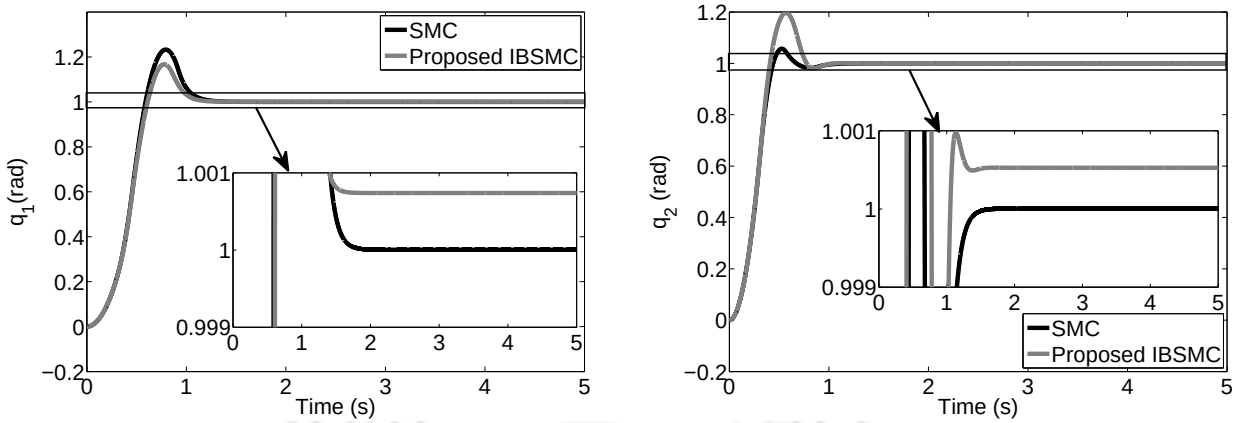

(a) Angular position of joint 1 (b) Angular position of joint 2

Figure 2.6: Simulation results of joint angular positions for joint angle regulation of 2DoF robot manipulator using IBSMC and SMC

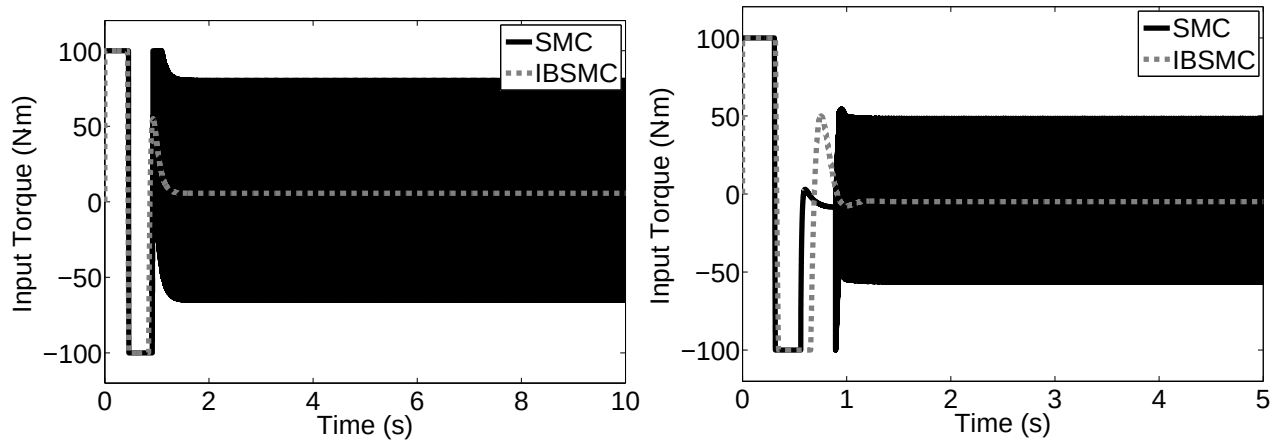

(a) Control torque for joint 1 (b) Control torque for joint 2

Figure 2.7: Simulation results of control torques for joint angle regulation of 2DoF robot manipulator using IBSMC and SMC

Table 2.5: Performance comparison for stabilizing task of 2 DoF manipulator

Joint	Controller	t_r (s)	M_p (rad)	t_p (s)	t_s (s)	e_{ss}(rad)	$\|\|\tau\|\|$ (N·m)	TV (N·m)
q_1	IBSMC	0.6086	1.1780	0.7802	1.0568	5.7365×10^{-4}	9.5963×10^{3}	5.174007×10^{2}
	SMC	0.5907	1.2327	0.7929	1.1137	3.5786×10^{-6}	2.2411×10^{4}	1.166980×10^{7}
q_2	IBSMC	0.4071	1.2018	0.5693	0.7533	3.2526×10^{-4}	8.4625×10^{3}	5.359030×10^{2}
	SMC	0.4399	1.0571	0.5265	0.6171	4.8393×10^{-6}	1.5928×10^{4}	8.241659×10^{6}

2.2.5 Discussion

The simulation studies conducted on both the cart-pendulum and 2DoF manipulator show that the proposed method of combining integral backstepping with the SMC has the advantage of chattering removal. Moreover, the control law can tackle both matched and mismatched uncertainties as opposed to only SMC which fails in the presence of mismatched uncertainty as evident in the simulation example of the cart-pendulum control. However, despite having these two major advantages, the following demerits are observed in the IBSMC:

(i) The smoothness in the control law is achieved at the cost of tracking accuracy as observed in the 2DoF manipulator control. Since the switching nature of the SMC is the key feature making it robust and imparting high accuracy, losing discontinuity in the control signal by making it continuous will evidently lead to a loss in accuracy.

(ii) The *"explosion of terms"* problem inherent in conventional backstepping has given rise to a complex structure of the control law. This problem is the result of taking the time derivative of the synthetic input at each step of backstepping. In the proposed method the explosion of terms can be clearly observed in the definition of $\eta(q, \dot{q}, \tau)$ in (2.17) obtained after differentiating the nonlinear system matrices. Clearly $\eta(q, \dot{q}, \tau)$ has a very complex structure, thereby complicating the control law structure. Moreover, higher order manipulators will have more nonlinearities with larger matrices which will result in a more complex structured control law rendering it impractical for real time uses.

(iii) The switching controller gain $\boldsymbol{k}$ is determined based on the assumption that the uncertainty bounds are known so that choosing $\boldsymbol{k} > |\boldsymbol{h}(\boldsymbol{q}, \dot{\boldsymbol{q}})|$ will make the controller robust and stable. But the knowledge of the uncertainty bound is not always easily available. Moreover, some uncertainty might also go unnoticed. Although choosing a very high value for k might work, it is not a practical solution since this will unnecessarily increase the use of input energy.

(iv) Computation of the IBSM control law requires upto third time derivative of the desired trajectory which puts additional constraint on the controller design process.

2.3 Integral Adaptive Dynamic Surface Controller

2.3.1 Motivation

Efforts have been made to eliminate the explosion of terms occurring in backstepping by using first and second order filters or command filter to obtain the derivative of the virtual control laws [123, 124, 137–139]. Here the time derivative of the virtual control was considered as an uncertainty to be compensated for which sliding mode control [140] and robust second order filter [141] were utilized. The dynamic surface control (DSC) method proposed by Swaroop *et al.* [123,124] has gained considerable popularity as an alternative to the integral backstepping control. The DSC algorithm uses a first order filter to obtain the time derivatives of the virtual controls and then uses the difference between the actual and the filtered signal as a sliding surface. The algorithm is easy to implement

as it uses first order filters and moreover, the filtering error is accounted for due to multiple sliding surfaces.

Adaptive tuning of the controller gain for the SMC [142–145] has proved to be a good alternative to the fixed gain for dealing with unknown bounds of uncertainties as well as chattering suppression. The adaptive law tunes the controller gain based on the sliding surface which is generally a function of the system errors. Thus occurrence of any unknown uncertainty that results in rise in system error will cause the tuning law to adjust the controller gain accordingly. Further, on reaching the steady state when the error tends to zero, the controller gain will be very low, thus lowering chattering and preventing unnecessary use of the control energy.

The dynamic surface control algorithm is adopted to contain the explosion of terms in backstepping controller developed in this research work. However, instead of using the filter at every stage of backstepping, it is introduced only in the final step so that a much simpler structure of the controller is obtained as compared to the IBSMC. The gain of the switching part of the control law in the last stage is derived using an adaptive tuning law. A leakage term [146] is added to the adaptive gain tuning law in order to prevent overestimation or unbounded value of the tuned gain. The resultant control method is named as integral adaptive dynamic surface control (IADSC).

2.3.2 Controller Design

In this section, the IADSC will be designed for the robot manipulator system augmented with an integrator block as represented by (2.5).

Step I:

The trajectory tracking error $\boldsymbol{z_1}$ is defined as [147]

$$\begin{aligned} \boldsymbol{z_1} &= \boldsymbol{q} - \boldsymbol{q_d} \\ \dot{\boldsymbol{z}}_{\boldsymbol{1}} &= \dot{\boldsymbol{q}} - \dot{\boldsymbol{q}}_{\boldsymbol{d}}. \end{aligned} \tag{2.37}$$

A CLF V_1 for the system is defined as follows:

$$\begin{aligned} V_1 =& \frac{1}{2}\boldsymbol{z_1^T z_1} \\ \dot{V}_1 =& \boldsymbol{z_1^T \dot{z}_1 = -z_1^T c_1 z_1 + z_1^T z_2}. \end{aligned} \tag{2.38}$$

Now (2.37) is stabilized if $\dot{V}_2 < 0$ and considering $\dot{\boldsymbol{q}}$ to be the control input, the following can be derived:

$$\dot{\boldsymbol{q}} = -\boldsymbol{c_1 z_1} + \dot{\boldsymbol{q}}_{\boldsymbol{d}} \tag{2.39}$$

where $\boldsymbol{c_1} = diag(c_{1i}), c_{1i} > 0, i = 1, \ldots, n$ is a design parameter. The value of $\boldsymbol{c_1}$ determines the rate of convergence of the tracking errors.

Step II:

However, the relation (2.39) is not true yet. Hence considering $\boldsymbol{\alpha_q} = -\boldsymbol{c_1 z_1} + \dot{\boldsymbol{q}}_{\boldsymbol{d}}$ as the virtual control

input for this stage, the next variable $\boldsymbol{z_2}$ is defined as

$$\begin{aligned} \boldsymbol{z_2} =& \dot{\boldsymbol{q}} - \boldsymbol{\alpha_q} \\ \Rightarrow \boldsymbol{z_2} =& \dot{\boldsymbol{q}} + \boldsymbol{c_1 z_1} - \dot{\boldsymbol{q}}_{\boldsymbol{d}}. \end{aligned} \tag{2.40}$$

Substituting (2.40) in (2.37) yields

$$\dot{\boldsymbol{z}}_{\boldsymbol{1}} = -\boldsymbol{c_1 z_1} + \boldsymbol{z_2}. \tag{2.41}$$

A sliding variable $\boldsymbol{s_1}$ is defined as

$$\boldsymbol{s_1} = \boldsymbol{z_2} = \boldsymbol{c_1 z_1} + \dot{\boldsymbol{z}}_{\boldsymbol{1}}. \tag{2.42}$$

Now taking time derivative of (2.42) and using (2.5), (2.37) yields

$$\dot{\boldsymbol{s}}_{\boldsymbol{1}} = \boldsymbol{c_1}\dot{\boldsymbol{z}}_{\boldsymbol{1}} + \boldsymbol{M(q)^{-1}}\left[\boldsymbol{\tau} - \boldsymbol{C(q,\dot{q})\dot{q}} - \boldsymbol{G} - \boldsymbol{f(\dot{q})}\right] - \ddot{\boldsymbol{q}}_{\boldsymbol{d}}. \tag{2.43}$$

The next Lyapunov function V_2 is now defined as

$$\begin{aligned} V_2 =& \frac{1}{2}\boldsymbol{s_1^T s_1} \\ \Rightarrow \dot{V}_2 =& \boldsymbol{s_1^T}\dot{\boldsymbol{s}}_{\boldsymbol{1}}. \end{aligned} \tag{2.44}$$

A constant plus proportional reaching law [134]

$$\dot{\boldsymbol{s}}_{\boldsymbol{1}} = -\boldsymbol{k_1} \circ \boldsymbol{sign}(\boldsymbol{s_1}) - \boldsymbol{W_1 s_1} \tag{2.45}$$

is used where $\boldsymbol{k_1 > 0}$ is the constant gain and $\boldsymbol{W_1 > 0}$ is the proportional gain so that

$$\dot{V}_2 = -|\boldsymbol{s_1}|^{\boldsymbol{T}}\boldsymbol{k_1} - \boldsymbol{s_1^T W_1 s_1} \tag{2.46}$$

is guaranteed. For achieving this objective, a virtual control $\boldsymbol{\alpha_\tau}$ is defined at this stage as

$$\boldsymbol{\alpha_\tau} = \boldsymbol{C(q,\dot{q})\dot{q}} + \boldsymbol{G} - \boldsymbol{M(q)}(\boldsymbol{c_1}\dot{\boldsymbol{z}}_{\boldsymbol{1}} - \ddot{\boldsymbol{q}}_{\boldsymbol{d}} + \boldsymbol{k_1} \circ \boldsymbol{sign}(\boldsymbol{s_1}) + \boldsymbol{W_1 s_1}). \tag{2.47}$$

Step III:

When $\boldsymbol{\tau = \alpha_\tau}$, (2.44) takes the following form:

$$\begin{aligned} \dot{V}_2 &= -|\boldsymbol{s_1}|^{\boldsymbol{T}}\boldsymbol{k_1} - \boldsymbol{s_1^T W_1 s_1} + \boldsymbol{s_1^T M(q)^{-1} f(\dot{q})} \\ &\leq -|\boldsymbol{s_1}|^{\boldsymbol{T}}\boldsymbol{k_1} - \boldsymbol{s_1^T W_1 s_1} + \boldsymbol{s_1^T M(q)^{-1} f_1} \\ &\leq -|\boldsymbol{s_1}|^{\boldsymbol{T}}[\boldsymbol{k_1} - \boldsymbol{M(q)^{-1} f_1}] - \boldsymbol{s_1^T W_1 s_1}. \end{aligned} \tag{2.48}$$

Since the relative degree of the system is increased by one as given in (2.5), the actual control input is now $\boldsymbol{u = \dot{\tau}}$. Now the dynamic surface control method [124] is used where the virtual control $\boldsymbol{\alpha_\tau}$ is passed through a first order low pass filter to obtain the filtered signal $\boldsymbol{\alpha_f}$ as

$$\begin{aligned} \boldsymbol{\alpha_\tau} =& \boldsymbol{\alpha_f + T_f \dot{\alpha}_f} \\ \Rightarrow \boldsymbol{\dot{\alpha}_f} =& \frac{1}{T_f}(\boldsymbol{\alpha_\tau - \alpha_f}) \end{aligned} \tag{2.49}$$

where T_f is the time constant of the filter. The filter error is defined as

$$\boldsymbol{y} = \boldsymbol{\alpha_f - \alpha_\tau = -T_f \dot{\alpha}_f} \tag{2.50}$$

$$|\boldsymbol{y}| = \bar{\boldsymbol{y}} \tag{2.51}$$

where $\boldsymbol{\bar{y} > 0}$ is the bound of the error signal $\boldsymbol{y}$.
The error between $\boldsymbol{\tau}$ and $\boldsymbol{\alpha_f}$ is defined as the next sliding variable $\boldsymbol{s_2}$ where

$$\boldsymbol{s_2} = \boldsymbol{\tau - \alpha_f} \tag{2.52}$$

$$\Rightarrow \boldsymbol{\dot{s}_2} = \boldsymbol{\dot{\tau} - \dot{\alpha}_f = u} - \frac{1}{T_f}(\boldsymbol{\alpha_\tau - \alpha_f}). \tag{2.53}$$

From (2.52) the control torque is obtained as

$$\boldsymbol{\tau} = \boldsymbol{s_2 + \alpha_f = s_2 + \alpha_\tau - T_f \dot{\alpha}_f = s_2 + \alpha_\tau + y}. \tag{2.54}$$

Replacing (2.54) in (2.43) and using (2.52) yields

$$\boldsymbol{\dot{s}_1 = -k_1 \circ sign(s_1) - W_1 s_1 + M(q)^{-1}(s_2 + y + f(\dot{q}))}. \tag{2.55}$$

Now using (2.55) in (2.44) and applying (2.2), (2.4) and (2.47) yields

$$\begin{aligned} \dot{V}_2 =& -|\boldsymbol{s_1}|^T \boldsymbol{k_1} - \boldsymbol{s_1^T W_1 s_1} + \boldsymbol{s_1^T M(q)^{-1}(s_2 + y + f(\dot{q}))} \\ \Rightarrow \dot{V}_2 \leq& -|\boldsymbol{s_1}|^T [\boldsymbol{k_1 - \mu_{min}^{-1}(\bar{y} + f_1)}] - \boldsymbol{s_1^T W_1 s_1 + \mu_{min}^{-1} s_1^T s_2}. \end{aligned} \tag{2.56}$$

The next control law should be so designed such that the sliding surface $\boldsymbol{s_2}$ converges to zero. The control input $\boldsymbol{u}$ is designed to achieve the constant plus proportional reaching law

$$\boldsymbol{\dot{s}_2 = -k_2 \circ sign(s_2) - W_2 s_2} \tag{2.57}$$

where $\boldsymbol{k_2 > 0}$ is the constant gain and $\boldsymbol{W_2 > 0}$ is the proportional gain. The system (2.1) may have time varying uncertainty, so instead of selecting a constant gain $\boldsymbol{k_2}$, an adaptively tuned gain $\boldsymbol{\hat{k}_2}$ is used [143]. The gain $\boldsymbol{\hat{k}_2}$ is determined by using the following adaptive law:

$$\boldsymbol{\dot{\hat{k}}_2 = \Gamma(|s_2| - \epsilon \hat{k}_2)} \tag{2.58}$$

where $\boldsymbol{\Gamma} > \mathbf{0}$ is the adaptive gain matrix and $\boldsymbol{\epsilon} > \mathbf{0}$ is the leakage parameter [146] that will keep $\hat{\boldsymbol{k}}_{\boldsymbol{2}}$ bounded. Replacing $\hat{\boldsymbol{k}}_{\boldsymbol{2}}$ in (2.57) and using (2.53), the control signal $\boldsymbol{u}$ is now obtained as

$$\boldsymbol{u} = \frac{\mathbf{1}}{\boldsymbol{T_f}}(\boldsymbol{\alpha_\tau} - \boldsymbol{\alpha_f}) - \hat{\boldsymbol{k}}_{\boldsymbol{2}} \circ \boldsymbol{sign}(\boldsymbol{s_2}) - \boldsymbol{W_2 s_2} \tag{2.59}$$

which is a discontinuous signal. Following (2.5), the actual control input $\boldsymbol{\tau}$ is obtained as

$$\boldsymbol{\tau} = \int_0^t \boldsymbol{u}(\theta) d\theta. \tag{2.60}$$

From (2.47) and (2.60) it can be observed that the expression of $\boldsymbol{u}$ contains $\dot{\boldsymbol{\alpha}}_{\boldsymbol{\tau}}$, which after integration will leave $\boldsymbol{\alpha_\tau}$ in the expression of the actual control $\boldsymbol{\tau}$. Since $\boldsymbol{\alpha_\tau}$ contains a switching function $sign(\boldsymbol{s_1})$, this will produce chattering in the input; however, elimination of $sign(\boldsymbol{s_1})$ will cause loss in accuracy. Therefore, as a trade-off measure, $sign(\boldsymbol{s_1})$ is replaced with a boundary layer [118] approximation $(\frac{\boldsymbol{s_1}}{|\boldsymbol{s_1}|+\mathcal{D}})$, where $0 < \mathcal{D} < 1$ and $\boldsymbol{\alpha_\tau}$ is obtained as

$$\boldsymbol{\alpha_\tau} = \boldsymbol{C(q,\dot{q})\dot{q} + G - M(q)(c_1 \dot{z}_1 - \ddot{q}_d + k_1 \circ \frac{s_1}{|s_1| + \mathcal{D}} + W_1 s_1)}. \tag{2.61}$$

The IADSC obtained above clearly has a simpler structure as compared to the IBSMC method designed in the previous section. The IADSC does not require differentiation of the system matrices which has reduced the computational burden on the controller.

2.3.3 Stability Analysis

The overall system stability is now investigated using Lyapunov method. A positive definite function V is defined in terms of the tracking error and the sliding surfaces obtained in each step of the design procedure as given below,

$$\begin{aligned} V =& \frac{1}{2}(\boldsymbol{z_1^T z_1 + s_1^T s_1 + s_2^T s_2 + \tilde{k}_2^T \Gamma^{-1} \tilde{k}_2}) \\ V =& \frac{1}{2}\boldsymbol{Z^T P Z} \end{aligned} \tag{2.62}$$

where

$$\boldsymbol{\tilde{k}_2 = \hat{k}_2 - k_{2d}} \tag{2.63}$$

and $\boldsymbol{k_{2d} > 0}$ is an arbitrary gain value. Further, $\boldsymbol{Z^T} = \begin{bmatrix} \boldsymbol{z_1^T} & \boldsymbol{s_1^T} & \boldsymbol{s_2^T} & \boldsymbol{\tilde{k}^T} \end{bmatrix}$, $\boldsymbol{Z} = \begin{bmatrix} \boldsymbol{z_1} & \boldsymbol{s_1} & \boldsymbol{s_2} & \boldsymbol{\tilde{k}} \end{bmatrix}^T$ and $\boldsymbol{P} = diag\{\boldsymbol{I_n},\ \boldsymbol{I_n},\ \boldsymbol{I_n},\ \boldsymbol{\Gamma^{-1}}\} \in \mathbb{R}^{4n \times 4n}$ is a positive definite block diagonal matrix. Taking time derivative of V and using (2.38), (2.56), (2.57) and (2.58) yields

$$\begin{aligned} \dot{V} =& \boldsymbol{z_1^T \dot{z}_1 + s_1^T \dot{s}_1 + s_2^T \dot{s}_2 + \tilde{k}_2^T \Gamma^{-1} \dot{\hat{k}}_2} \\ \leq& \boldsymbol{-z_1^T c_1 z_1 + z_1^T s_1 - |s_1|^T k_1 - s_1^T W_1 s_1 + \mu_{min}^{-1} s_1^T (s_2 + \bar{y} + f_1) - |s_2|^T \hat{k}_2} \\ & \boldsymbol{- s_2^T W_2 s_2 + \tilde{k}_2^T \Gamma^{-1} \left[\Gamma(|s_2| - \epsilon \hat{k}_2)\right]} \end{aligned}$$

$$\leq -\boldsymbol{z_1^T c_1 z_1} - \boldsymbol{s_1^T W_1 s_1} - \boldsymbol{s_2^T W_2 s_2} - |\boldsymbol{s_1}|^T \boldsymbol{k_1} + \boldsymbol{\mu_{min}^{-1}} |\boldsymbol{s_1}|^T (\bar{\boldsymbol{y}} + \boldsymbol{f_1}) + \boldsymbol{z_1^T s_1} + \boldsymbol{\mu_{min}^{-1}} \boldsymbol{s_1^T s_2} - |\boldsymbol{s_2}|^T (\hat{\boldsymbol{k}}_2 - \tilde{\boldsymbol{k}}_2) - \tilde{\boldsymbol{k}}_2^T \boldsymbol{\epsilon} \hat{\boldsymbol{k}}_2. \tag{2.64}$$

Now from (2.63)

$$\tilde{\boldsymbol{k}}_2 = \hat{\boldsymbol{k}}_2 - \boldsymbol{k_{2d}} \Rightarrow \boldsymbol{\epsilon k_{2d}} = \boldsymbol{\epsilon}(\hat{\boldsymbol{k}}_2 - \tilde{\boldsymbol{k}}_2)$$
$$\boldsymbol{k_{2d}^T \epsilon k_{2d}} = (\hat{\boldsymbol{k}}_2 - \tilde{\boldsymbol{k}}_2)^T \boldsymbol{\epsilon} (\hat{\boldsymbol{k}}_2 - \tilde{\boldsymbol{k}}_2). \tag{2.65}$$

Lemma 4. *For real vectors* $\tilde{\boldsymbol{k}}_2,\ \hat{\boldsymbol{k}}_2,\ \boldsymbol{k_{2d}} > \boldsymbol{0}$ *and positive definite diagonal matrix* $\boldsymbol{\epsilon} \in \mathbb{R}^{n \times n}$*, if* $\tilde{\boldsymbol{k}}_2 = \hat{\boldsymbol{k}}_2 - \boldsymbol{k_{2d}}$*, then* $\tilde{\boldsymbol{k}}_2^T \boldsymbol{\epsilon} \hat{\boldsymbol{k}}_2 \geq \frac{1}{2}(\tilde{\boldsymbol{k}}_2^T \boldsymbol{\epsilon} \tilde{\boldsymbol{k}}_2 - \boldsymbol{k_{2d}^T \epsilon k_{2d}})$.

Proof. Proof is given in Appendix A.6. □

As proved in Appendix A.6 for a diagonal matrix $\boldsymbol{\epsilon}$, the following relation can be obtained:

$$\tilde{\boldsymbol{k}}_2^T \boldsymbol{\epsilon} \hat{\boldsymbol{k}}_2 \geq \frac{1}{2}(\tilde{\boldsymbol{k}}_2^T \boldsymbol{\epsilon} \tilde{\boldsymbol{k}}_2 - \boldsymbol{k_{2d}^T \epsilon k_{2d}}). \tag{2.66}$$

Using (2.66), $\dot{V}$ can be rewritten as

$$\dot{V} \leq -\boldsymbol{z_1^T c_1 z_1} - \boldsymbol{s_1^T W_1 s_1} - \boldsymbol{s_2^T W_2 s_2} - \frac{\boldsymbol{1}}{\boldsymbol{2}} \tilde{\boldsymbol{k}}_2^T \boldsymbol{\epsilon} \tilde{\boldsymbol{k}}_2 + \frac{\boldsymbol{1}}{\boldsymbol{2}} \boldsymbol{k_{2d}^T \epsilon k_{2d}} - |\boldsymbol{s_1}|^T \left[\boldsymbol{k_1} - \boldsymbol{\mu_{min}^{-1}} (\boldsymbol{f_1} + \bar{\boldsymbol{y}} + |\boldsymbol{z_1}|) \right] - |\boldsymbol{s_2}|^T \left(\boldsymbol{k_{2d}} - \boldsymbol{\mu_{min}^{-1}} |\boldsymbol{s_1}| \right). \tag{2.67}$$

To ensure that $\dot{V}$ is negative definite, $\boldsymbol{k_{2d}} > 0$ and $\boldsymbol{k_1} > 0$ should satisfy the following

$$\left(\boldsymbol{k_{2d}} - \boldsymbol{\mu_{min}^{-1}} |\boldsymbol{s_1}| \right) > \boldsymbol{0} \tag{2.68}$$
$$\left[\boldsymbol{k_1} - \boldsymbol{\mu_{min}^{-1}} (\boldsymbol{f_1} + \bar{\boldsymbol{y}}) - |\boldsymbol{z_1}| \right] > \boldsymbol{0}. \tag{2.69}$$

Remark 5. *The controller gain* k_{2d} *is tuned adaptively (see equation (2.58)) and thus can take any arbitrary positive value. On the other hand the gain* $\boldsymbol{k_1}$ *is a constant parameter that determines the controller robustness. Assuming the upper limits of* $\boldsymbol{f_1}$ *and* $\bar{\boldsymbol{y}}$ *are known,* $\boldsymbol{k_1}$ *can be selected as* $\boldsymbol{k_1} > \mu_{min}^{-1}(max(|\boldsymbol{f_1}|) + max(\bar{\boldsymbol{y}})) + max(|\boldsymbol{q}|) + max(|\boldsymbol{q_d}|)$*, where* $max(\bullet)$ *indicates the saturation limit of the signal. Generally, during the simulations a small positive value of* $\boldsymbol{k_1}$ *is chosen and then increased gradually according to the performance requirements. Although higher values of* $\boldsymbol{k_1}$ *considerably reduces the bound of the tracking error, it cannot be made arbitrarily large owing to hardware limitations [114], as high value of* $\boldsymbol{k_1}$ *leads to increased amount of input energy.*

Now, with $\boldsymbol{k_{2d}}$ and $\boldsymbol{k_1}$ satisfying (2.69) and (2.69), $\dot{V}$ can be rewritten as

$$\dot{V} \leq -\boldsymbol{z_1^T c_1 z_1} - \boldsymbol{s_1^T W_1 s_1} - \boldsymbol{s_2^T W_2 s_2} - \frac{\boldsymbol{1}}{\boldsymbol{2}} \tilde{\boldsymbol{k}}_2^T \boldsymbol{\epsilon} \tilde{\boldsymbol{k}}_2 + \frac{\boldsymbol{1}}{\boldsymbol{2}} \boldsymbol{k_{2d}^T \epsilon k_{2d}}$$
$$\dot{V} \leq -\boldsymbol{Z^T Q Z} + \frac{\boldsymbol{1}}{\boldsymbol{2}} \boldsymbol{k_{2d}^T \epsilon k_{2d}}$$
$$\dot{V} \leq -2\psi V + \rho \tag{2.70}$$

where $\boldsymbol{Q} = \begin{bmatrix} \boldsymbol{c_1} & 0 & \boldsymbol{0} & \boldsymbol{0} \\ 0 & \boldsymbol{W_1} & 0 & \boldsymbol{0} \\ \boldsymbol{0} & 0 & \boldsymbol{W_2} & \boldsymbol{0} \\ \boldsymbol{0} & \boldsymbol{0} & \boldsymbol{0} & \frac{1}{2}\boldsymbol{\epsilon} \end{bmatrix} \in \mathbb{R}^{4n \times 4n}$ is a block diagonal matrix. The scalar ψ represents the smallest eigenvalue of $\boldsymbol{P^{-1}Q}$. In order to obtain a stable closed loop system, $\boldsymbol{Q}$ should be a positive definite matrix. Using the properties of positive definite block matrices (Appendix A.2), the following conditions can be obtained for the controller parameters:

$$\frac{1}{2}\boldsymbol{\Gamma\epsilon} > 0 \tag{2.71}$$

$$\boldsymbol{c_1, W_1, W_2 > 0} \tag{2.72}$$

$$\tag{2.73}$$

From (2.70), the following is derived:

$$V(t) \leq \left(V(0) - \frac{\rho}{2\psi}\right) e^{-2\psi t} + \frac{\rho}{2\psi}. \tag{2.74}$$

Therefore, for $V(0) > \frac{\rho}{2\psi}$ and $\frac{\rho}{2\psi} < 1$, $V(t)$ will be a decreasing function indicating the convergence of the system errors to the equilibrium. From (2.62) and (2.74), the following can be obtained:

$$\frac{1}{2}\boldsymbol{z_1^T z_1} \leq V(t) \leq \left(V(0) - \frac{\rho}{2\psi}\right) e^{-2\psi t} + \frac{\rho}{2\psi}. \tag{2.75}$$

Hence from (2.75), it can be concluded that as $t \to \infty$, the tracking error $\boldsymbol{z_1}$ is bounded by the following condition,

$$|\boldsymbol{z_1}| \leq \sqrt{\frac{\rho}{\psi}}. \tag{2.76}$$

Therefore, by proper selection of the design parameters, the tracking error can be made sufficiently small.

2.3.4 Simulation Results

The proposed IADSC method is applied for joint torque control of the 2 DoF manipulator shown in Figure 2.5 whose dynamics are given by (2.36). Next the proposed IADSC method is tested for joint torque control of a 3DoF coordinated links (COOL) robot arm described in Appendix A.9. The results obtained by using the proposed IADSC for the 2 DoF manipulator are compared with the results obtained by using the SMC (2.34) and the proposed IBSMC (2.22- 2.23).

2.3.4.1 Simulation results for stabilization of a 2DoF manipulator

The manipulator model and parameters are the same as described in (2.36). The design parameters used for the IBSMC (2.22 - 2.23) are $\boldsymbol{c}_1 = 20\boldsymbol{I}_n$, $\boldsymbol{c}_2 = 30\boldsymbol{I}_n$, $\boldsymbol{\sigma}_1 = \boldsymbol{\sigma}_2 = 10\boldsymbol{I}_n$, $\boldsymbol{k} = [8, 8, 8]^T$, $\boldsymbol{W} = 100\boldsymbol{I}_n$. The design parameters for the SMC (2.34) are $\boldsymbol{k} = 8\boldsymbol{I}_n$, $\boldsymbol{W} = 100\boldsymbol{I}_n$, $\Lambda = 10$. The design

parameters chosen for the proposed IADSC controller are as follows:

$$\boldsymbol{c_1} = 5\boldsymbol{I}_2,\ \boldsymbol{\epsilon} = 0.1\boldsymbol{I}_2,\ \boldsymbol{\Gamma} = 100\boldsymbol{I}_2,\ \boldsymbol{k}_1 = [30,\ 30]^T,$$
$$\boldsymbol{W}_1 = 10\boldsymbol{I}_2,\ \boldsymbol{W}_2 = 100\boldsymbol{I}_2,\ \mathcal{D} = 0.001,\ T_f = 0.029.$$

The controller objective is to bring both the joint positions from their initial position at 0 rad to 1 rad. The system is induced with modeling error by perturbing the link masses m_1 and m_2 by 40% and 20% respectively.

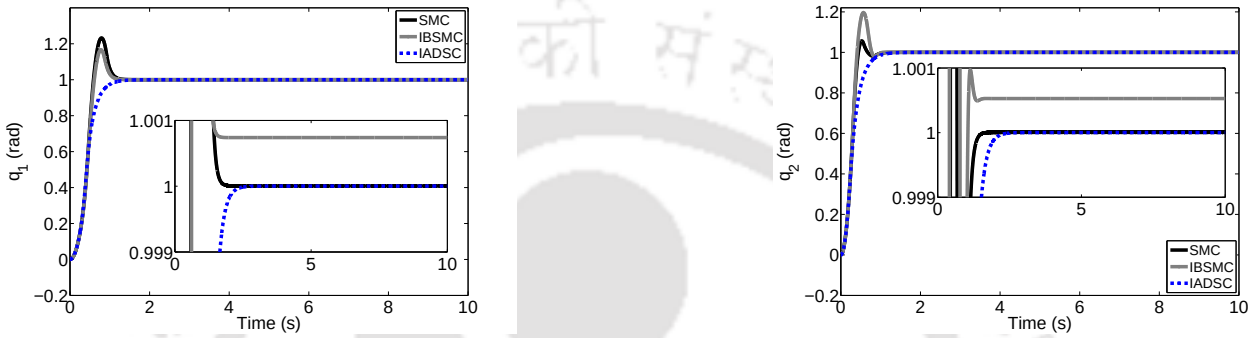

(a) Angular position of joint 1 (b) Angular position of joint 2

Figure 2.8: Simulation results for joint angle regulation of a 2DoF manipulator: Joint angular positions

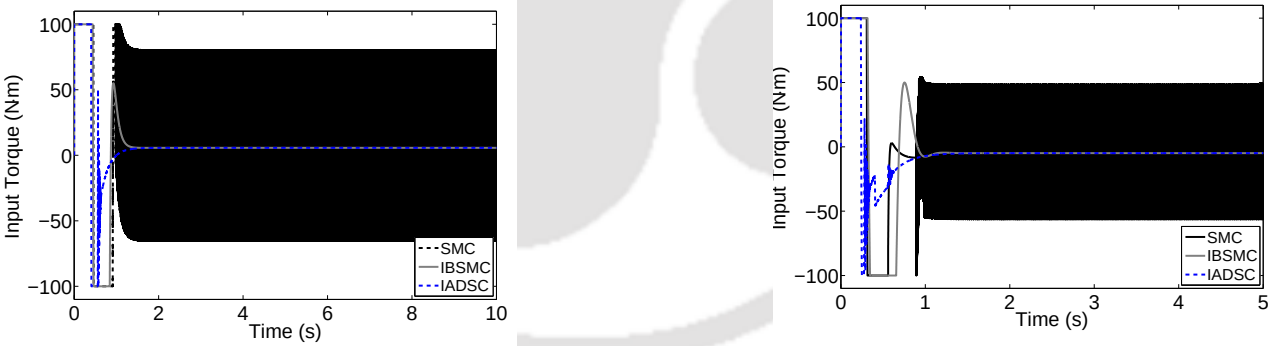

(a) Control torque for joint 1 (b) Control torque for joint 2

Figure 2.9: Simulation results for joint angle regulation of a 2DoF manipulator: Control torques

The regulations of the joint positions q_1 and q_2 are shown in Figure 2.8 and the input torques are shown in Figure 2.9. The performances of the controllers in terms of the rise time (t_r), peak overshoot (M_p), peak time (t_p), settling time (t_s), steady state error (e_{ss}), 2-norm of the control input ($||u||$) and the total variation (TV) [136] of the control input (2.32) are compared in Table 2.6. The simulation results show that the IADSC produces transient and steady state performances better or at par with the other two controllers but at the cost of much lower control energy.

Table 2.6: Performance comparison for stabilizing task of 2 DoF manipulator

Joint	Controller	t_r (s)	M_p (rad)	t_p (s)	t_s (s)	e_{ss}(rad)	$\|\|u\|\|$ (N·m)	TV (N·m)
q_1	IADSC	0.5221	0	–	1.0520	-1.3996×10^{-6}	2.4630×10^{3}	1.3976×10^{3}
	IBSMC	0.6086	1.1780	0.7802	1.0568	5.7365×10^{-4}	9.5963×10^{3}	5.174007×10^{2}
	SMC	0.5907	1.2327	0.7929	1.1137	3.5786×10^{-6}	2.2411×10^{4}	1.16698×10^{7}
q_2	IADSC	0.4790	0	–	0.9231	-1.1046×10^{-6}	1.8371×10^{3}	1.2885×10^{3}
	IBSMC	0.4071	1.2018	0.5693	0.7533	3.2526×10^{-4}	8.4625×10^{3}	5.359030×10^{2}
	SMC	0.4399	1.0571	0.5265	0.6171	4.8393×10^{-6}	1.5928×10^{4}	8.241659×10^{6}

2.3.4.2 Simulation results for trajectory tracking of a 2DoF manipulator

In this section the proposed IADSC will be tested through simulation for trajectory tracking in presence of uncertainties. The controller performance is compared with Yang *et al.* 's [2] decentralized adaptive robust control method using disturbance observers whose description is given in Appendix A.8. The same manipulator model used in [2] is used in this simulation study for ensuring fair comparison. The manipulator model and the added uncertainties are described in Appendix A.7. The tracking performance of the controller will be investigated using the following time varying reference trajectories:

$$\begin{aligned} q_{d1}(t) &= 0.2 + 2\sin(2t)\ rad \\ q_{d2}(t) &= -1.7 + 1.8\cos(2t)\ rad \end{aligned} \tag{2.77}$$

with the initial conditions for the tracking errors as

$$z_1(0) = [0.2,\ -0.2]\ rad, \quad \dot{z}_1(0) = [-0.25,\ 0.2]\ rad/s.$$

Simulations are performed using a step size of 0.0005s in the Matlab Simulink environment. The design parameters chosen for the proposed IADSC given by (2.59 - 2.61) are as follows:

$$\begin{aligned} &\boldsymbol{c}_1 = 25\boldsymbol{I}_{2\times2},\ \boldsymbol{k}_1 = [10,\ 10]^T,\ \boldsymbol{W}_1 = 200\boldsymbol{I}_{2\times2}, \boldsymbol{W}_2 = 500\boldsymbol{I}_{2\times2}, \\ &\boldsymbol{\epsilon} = 0.1\boldsymbol{I}_{2\times2},\ \boldsymbol{\Gamma} = 100\boldsymbol{I}_{2\times2}, \mathcal{D} = 0.001, T_f = 0.001. \end{aligned} \tag{2.78}$$

The tracking errors for both the joints are shown in Figure 2.10 which clearly shows that the proposed controller has faster transient response as well as lower steady state error as compared to [2]. The control torques are plotted in Figure 2.11 which show that the proposed IADSC uses much lesser control energy than the controller proposed by Yang *et al.* [2]. The simulation results are summarized in Table 2.7 for better comparison listing the performance indices like rise time (t_r), settling time (t_s), root mean square error (RMSE), the 2-norm of the control input ($||u||$) and the total variation (TV) of the control input (2.32).

The controller proposed by Yang *et al.* [2] uses a disturbance observer that compensates for any unmodeled and unknown uncertainties entering the system and utilizes an adaptively tuned controller. However, the proposed IADSC relies simply on the adaptively tuned gain and the robustness of the

backstepping sliding mode control. From Table 2.7 it can be clearly observed that the proposed IADSC yields superior transient and steady-state performances using lower amount of input energy as compared to the controller proposed by Yang *et al.* [2]. Moreover, the control input produced by the proposed IADSC is smoother than that of [2]. It should be noted that both the controllers are operated under the same conditions using the same amount of output information from the plant.

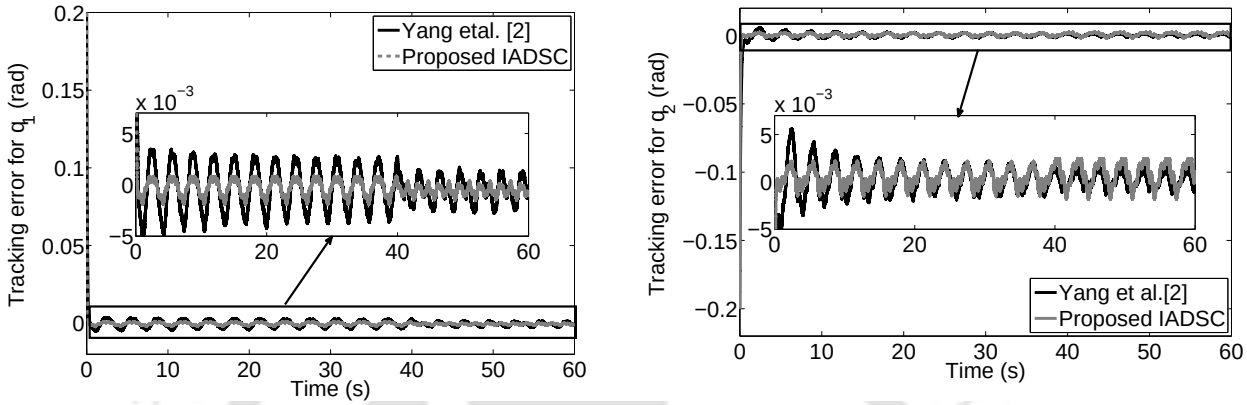

(a) Tracking error of joint 1 (b) Tracking error of joint 2

Figure 2.10: Simulation results: Comparison of tracking errors for the 2DoF manipulator

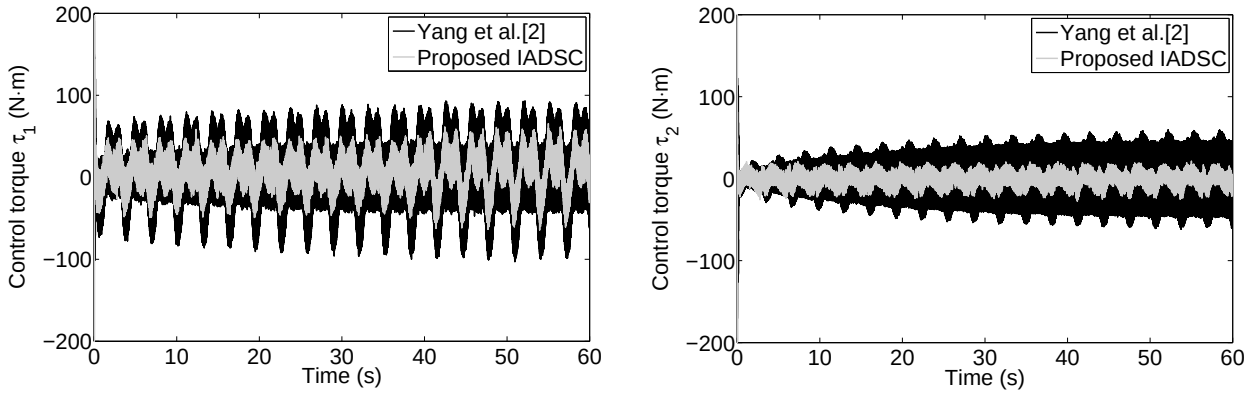

(a) Input torque of joint 1 (b) Input torque of joint 2

Figure 2.11: Simulation results: Comparison of control torques for the 2DoF manipulator

Table 2.7: Performance comparison for joint tracking control of the 2DoF manipulator

Joint	Controller	t_r (s)	t_s (s)	RMSE (rad)	$\|\|u\|\|$ (N·m)	TV (N·m)
q_1	IADSC	0.0935	0.1755	0.0073	6.4766×10^{3}	1.0255×10^{6}
	Yang *et al.* [2]	0.1620	0.4811	0.0081	1.5881×10^{4}	5.9904×10^{6}
q_2	IADSC	0.0938	0.1863	0.0074	3.0180×10^{3}	5.3422×10^{5}
	Yang *et al.* [2]	0.2687	0.4805	0.0084	1.2605×10^{4}	4.6765×10^{6}

2.3.4.3 Simulation results for trajectory tracking of a 3DoF manipulator

The proposed IADSC is now applied for a Coordinated Links (COOL) dual robot arm system as in Figure 2.12. The mass, inertia and link lengths of the COOL robot arm are given in Table 2.8. The center of mass for each link is considered to be its middle point. In Figure 2.12 and Table 2.8, L and R represent the left and right arms of the robot.

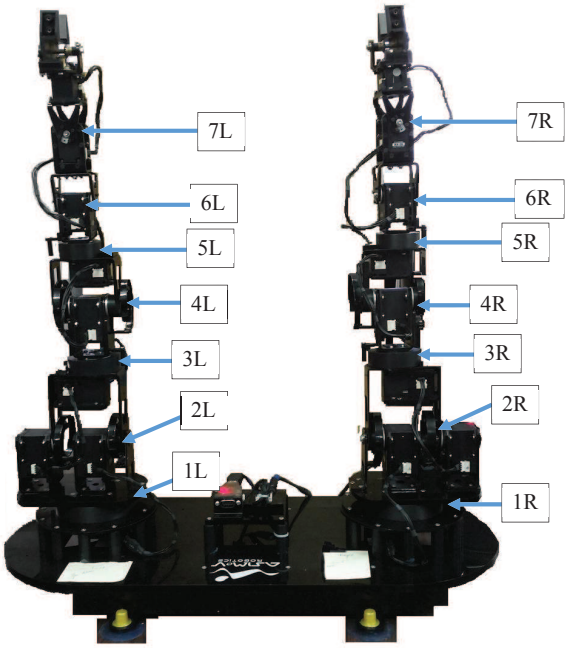

Figure 2.12: The Coordinated Links (COOL) robot arm

Table 2.8: Parameters of the COOL Robot Arm

Joint No.	Link Mass (kg)	Link Length (m)
1L/1R	0.6	0.025
2L/2R	0.32	0.110
3L/3R	0.23	0.060
4L/4R	0.23	0.080
5L/5R	0.13	0.070
6L/6R	0.13	0.082
7L/7R	0.18	0.081

For simulation purpose, only 3 joints of the right arm, i.e., joint number 1R, 4R and 7R are considered and the other joints are kept locked in the positions of 0rad. The mathematical model of the resulting 3 DoF robot arm is given in Appendix A.9. The control task is to bring each joint from the initial position of -0.1 rad to final 1 rad position. A uniform random noise having limits $\pm 0.0001 rad$ is added to the measurements of positions. Speeds of the joints are obtained through pseudodifferentiation of the joint positions using $\frac{a}{0.001a+1}$ [2], where a is the complex number frequency parameter for representation of the differentiator in the Laplace domain. An additional load of 0.5 kg is added to the end-effector to induce uncertainty. The proposed controller performance is studied when the robotic arm is affected by these uncertainties. The following reference trajectory is used for each of the joints to examine the controller performance:

$$q_d = 2\sin(2t) rad \tag{2.79}$$

with the initial conditions for the position and velocity of all the joints at $q(0)$=-0.1 rad and $\dot{q}(0)$=0 rad/s. Simulation results of the proposed IADSC are compared with those of a conventional sliding

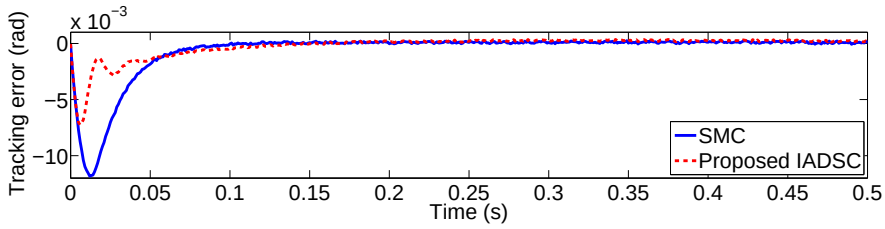

(a) Tracking error of joint 1

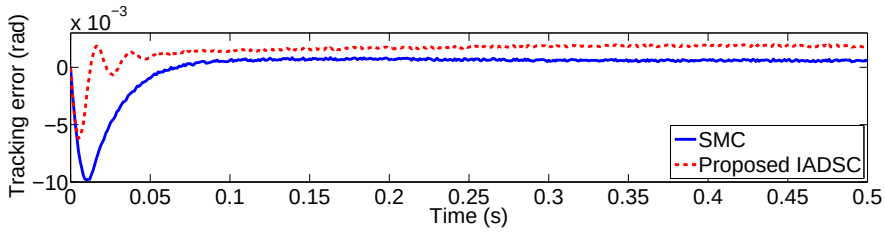

(b) Tracking error of joint 2

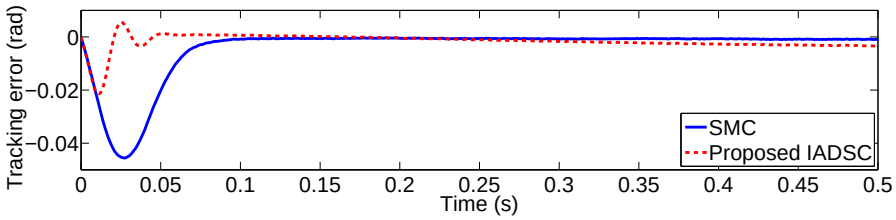

(c) Tracking error of joint 3

Figure 2.13: Simulation results: Comparison of tracking errors for 3DoF manipulator

mode controller (SMC) having the following structure:

$$\boldsymbol{\tau} = \boldsymbol{C}(\boldsymbol{q}, \dot{\boldsymbol{q}}) + \boldsymbol{G}(\boldsymbol{q}) + \boldsymbol{M}(\boldsymbol{q})(\ddot{\boldsymbol{q}}_{\boldsymbol{d}} - \boldsymbol{k} \circ \boldsymbol{sign}(\boldsymbol{s}) - \boldsymbol{W}\boldsymbol{s}) \tag{2.80}$$

where $\boldsymbol{s} = \dot{\boldsymbol{e}} + \boldsymbol{\phi}\boldsymbol{e}$, $\boldsymbol{e} = \boldsymbol{q} - \boldsymbol{q}_{\boldsymbol{d}}$, $\dot{\boldsymbol{e}} = \dot{\boldsymbol{q}} - \dot{\boldsymbol{q}}_{\boldsymbol{d}}$ and $\phi = 50$, $k = 200$, $W = 100$ are constant parameters. The design parameters used in the proposed IADSC are:

$$\boldsymbol{c}_1 = 25\boldsymbol{I}_{3\times3},\ \boldsymbol{\epsilon} = 0.1\boldsymbol{I}_{3\times3},\ \boldsymbol{\Gamma} = 100\boldsymbol{I}_{3\times3},\ \boldsymbol{k}_1 = [30,\ 30,\ 30]^T,$$
$$\boldsymbol{W}_1 = 1000\boldsymbol{I}_{3\times3},\ \boldsymbol{W}_2 = 200\boldsymbol{I}_{3\times3}, \mathcal{D} = 0.001,\ T_f = 0.001.$$

The trajectory tracking results for each joint are shown in Figure 2.13 and the input torques are plotted in Figure 2.14. From Figure 2.13, it can be observed that SMC has no overshoot and IADSC shows small overshoot in the tracking of the joints 2 and 3, whereas the undershoot with IADSC is much lower than that of SMC. Inspection of the input torques in Figure 2.14 clearly shows that the IADSC produces a smoother control signal as opposed to the highly oscillatory input generated by the SMC. For a clearer comparison, the performances of both the controllers are listed in Table 2.9. The performance indices compared in Table 2.9 are rise time (t_r), peak undershoot (M_u), peak time

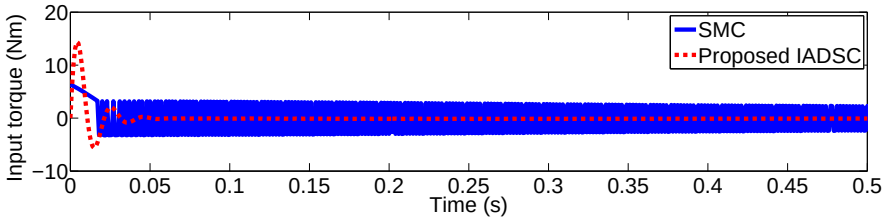

(a) Input torque in joint 1

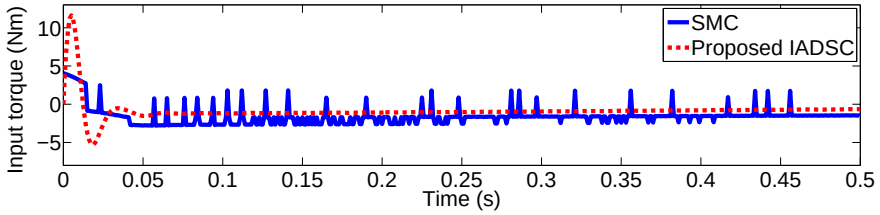

(b) Input torque in joint 2

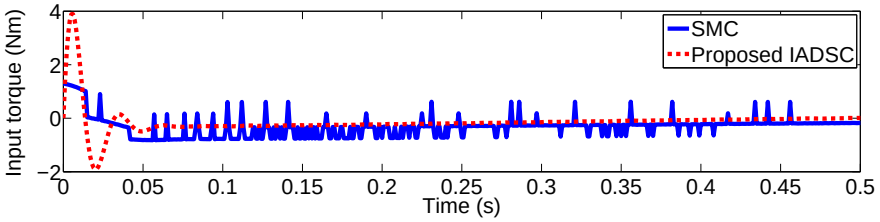

(c) Input torque in joint 3

Figure 2.14: Simulation results: Comparison of input torques for 3DoF manipulator

Table 2.9: Performance comparison for joint trajectory tracking of 3DoF manipulator

Joint	Controller	t_r (s)	M_u (rad)	t_p (s)	t_s (s)	RMSE (rad)	$\|\|u\|\|$ (N·m)	TV (N·m)
q_1	IADSC	0.1058	-0.007	0.006	0.1878	2.1865×10^{-4}	68.7318	244.9105
	SMC	0.0406	-0.01	0.014	0.0852	1.8168×10^{-4}	264.3090	4.8334×10^{4}
q_2	IADSC	0.0375	-0.006	0.006	0.082	0.0017	133.4563	366.5995
	SMC	0.0305	-0.009	0.012	0.0554	6.8450×10^{-4}	184.3059	5.2317×10^{3}
q_3	IADSC	0.0079	-0.021	0.012	0.052	0.0029	41.1756	167.8220
	SMC	0.0305	-0.045	0.028	0.159	0.0025	44.3870	1.4347×10^{3}

(t_p), settling time (t_s), root mean square error (RMSE), the 2-norm of control input ($||u||$) and the total variation (TV) (2.32).

2.3.5 Discussion

The proposed IADSC method utilizes the dynamic surface control methodology to simplify the backstepping controller structure by eliminating the differentiation of the synthetic control. Thus the proposed IADSC avoids the explosion of terms encountered in regular backstepping method. Simulation results show the suitability of the proposed IADSC in trajectory tracking tasks of robot

manipulators. The controller is free from chattering and has the capability to tackle uncertainties without having to resort to observers. The adaptively tuned controller gain helps in maintaining the controller robustness against unknown and varying uncertainties and also aids in reducing the unnecessary use of input energy during the steady state. Despite the advantages of the proposed IADSC method, it has certain drawbacks. Following are the difficulties that may arise while designing the controller:

(i) The design of the controller gain is an issue since it is generally done heuristically, normally selecting a very high gain value. Moreover, the filter time constant and the gain values are related and there is no analytical method to select the design constants except trial and error through numerical simulation.

(ii) The most challenging part of the IADSC design process is the filter time constant T_f. Generally the value of T_f is chosen as small as possible. But this is only possible in case of numerical simulations. When hardware application is concerned, this value cannot be made arbitrarily small owing to the hardware performance limitations such as the sampling frequency in real time and communication delay. Any change in the sampling time requires a modification in the filter time constant and in such cases stability cannot always be guaranteed. In [123], Swaroop *et al.* demonstrated that the DSC was very sensitive to the filter constant perturbations and became unstable for higher values of T_f.

(iii) The sliding surface gains cannot be made arbitrarily large since they may result in input saturation even to relatively small surface errors caused by uncertainties and disturbances.

2.4 Summary

In this chapter a robot manipulator controller is designed using integral backstepping based sliding mode control (IBSMC) methodology with the primary focus being chattering mitigation and efficient trajectory tracking in presence of uncertainties and external disturbances. The simulation studies for regulation of a 2DoF manipulator show that the proposed IBSMC is robust towards both matched and mismatched uncertainties and it can produce a smooth control input with satisfactory performance as compared to the conventional sliding mode controller. The proposed IBSMC is also applied to an underactuated cart-pendulum system and the simulation results are compared with the SMC proposed by Park *et al.* [1]. The simulations show that the proposed IBSMC can provide faster transient response and better steady state tracking while delivering a chattering free smooth control law. Although the IBSMC provided smoother control and robustness against both matched and mismatched uncertainties, yet it has a few disadvantages mainly, (i) *the controller accuracy is somewhat compromised for obtaining a smooth control law*, (ii) *the* "explosion of terms" *inherent in backstepping is encountered that causes a very complex structure of the controller* and (iii) *designing the controller gain* $\boldsymbol{k}$ *becomes difficult if the uncertainty bounds are not known apriori.* In the second part of the chapter the integral adaptive dynamic surface controller (IADSC) is proposed to overcome the above mentioned shortcomings of the IBSMC. The IADSC uses the dynamic surface control methodology

in the final step of the controller design process to obtain the filtered derivative of the last synthetic control of backstepping. Thereby it prevents the explosion of terms and a controller with a simpler structure than IBSMC is obtained. Moreover, the controller gain is now adaptively tuned to handle the uncertainties with unknown bounds. The proposed IADSC is simulated for joint angle regulation of a 2DoF manipulator and the results are compared with both the IBSMC and the SMC. The comparison shows that the IADSC provides a chattering free smooth input signal with better tracking performance than the IBSMC. The IADSC uses much lower control energy compared to the SMC and has a simpler structure than the IBSMC. The IADSC is also compared with the disturbance observer based robust controller proposed by Yang *et al.* [2] for trajectory tracking of a 2DoF manipulator. The proposed IADSC is able to utilize lower control energy while providing good tracking performance. Results are verified by applying the proposed IADSC on a 3DoF robot manipulator also.

3

Adaptive Backstepping Sliding Mode Controller with PID Sliding Surface

Contents

3.1 Motivation

Higher order sliding mode controllers first introduced by Levant [81] and especially the second order sliding mode control have been extensively used for controlling robot manipulator systems [82–87]. However, apart from the super twisting algorithm [148–150] all other higher order sliding mode methods require information regarding the derivative of the sliding surface, thus demanding more information and increasing the structural complexity of the control law. The primary goal of this chapter is to obtain a smooth control law without adding an integrator block or using higher order sliding mode control so that a computationally simple, easily comprehensible and applicable control law can be obtained. The flexibility offered by the SMC to modify the dynamics of the system allows the use of any form of stable sliding surface with suitable parameters. A proportional-integral-derivative (PID) type sliding surface [151–153] has faster response with lesser steady state error as compared to PD surfaces [154]. In this chapter a first order sliding controller will be designed with an adaptively tuned controller gain. Unlike the existing methods of SMC design with a predefined PID surface, here backstepping is used, which helps in obtaining a step by step analysis of the controller structure and thus provides a more flexible way of choosing the controller and the sliding surface parameters. The proposed adaptive backstepping sliding mode controller with the PID sliding surface (ABSMC-PID) will be used for designing impedance control of robot manipulators. This is a new approach for designing an impedance controller as well as hybrid impedance and hybrid force/position controller and is another highlight of this chapter.

The notable benefit of deriving a hybrid impedance controller (HIC) using the proposed method is the design flexibility and methodical analysis offered by the backstepping method and the robustness induced due to the sliding mode controller. As the main aim of the impedance control method is to maintain a compliant behavior during interaction of the robot manipulator with the external environment, it tries to maintain a predefined virtual impedance between the robot arm tool and the environment. In the proposed ABSMC-PID control method, the PID sliding surface will be imparted the dynamics of the desired impedance and the system will be maintained on the sliding surface equilibrium through the proposed ABSMC controller. Simply introducing the desired interaction force to the ABSMC-PID task space controller converts it to an impedance controller and the introduction of the task space selection matrix to the ABSMC-PID impedance controller can convert it to a hybrid force/position controller. Simplicity, portability, flexibility in design as well as robustness against noise and structural uncertainty are the main advantages of the proposed ABSMC-PID.

The organization of the chapter is as follows. The design procedure for the proposed ABSMC-PID controller and its stability analysis are presented in Section 3.2 which also includes simulation studies on robot manipulators. The proposed ABSMC-PID is then used for impedance control of a robot manipulator in Section 3.3 where detailed stability analysis and simulation results are presented. A brief summary of the chapter is provided in Section 3.4.

3.2 Adaptive Backstepping Sliding Mode Controller with PID Sliding Surface

In this section the detailed design procedure and stability analysis of the adaptive backstepping sliding mode controller with a PID sliding surface (ABSMC-PID) are presented. Prior to controller design, the manipulator described in (2.1) is remodeled by adding the joint actuator dynamics and this combined manipulator-motor dynamics will be considered throughout the chapter.

3.2.1 System Description

An n-DoF robot manipulator is represented by the following generalized dynamics:

$$\boldsymbol{M(q)\ddot{q} + C(q,\dot{q})\dot{q} + G(q) = \tau} + f(q,\dot{q},t) \tag{3.1}$$

whose detailed description is already presented in Section 2.2 of Chapter 2. For real time implementation of the control algorithm on manipulators, the actuator dynamics need to be included in the manipulator dynamics [155]. When the joints of the manipulator are driven by DC servo motors, the following motor dynamics are to be considered:

$$\boldsymbol{J\ddot{q}_m + B\dot{q}_m = \tau_m - r\tau} \tag{3.2}$$

where $\boldsymbol{q_m} \in \mathbb{R}^n$, $\boldsymbol{\dot{q}_m} \in \mathbb{R}^n$ and $\boldsymbol{\ddot{q}_m} \in \mathbb{R}^n$ respectively represent the angular position, the angular velocity and the angular acceleration of the motor shaft, $\boldsymbol{J} = diag\{J_1, J_2, \ldots J_n\}$ is the moment of inertia matrix of the motor combined with the gearbox inertia, $\boldsymbol{B} = diag\{B_1, B_2, \ldots, B_n\}$ represents the viscous friction matrix of the motor shaft, $r = \frac{q}{q_m}$ is the gear reduction ratio and $\boldsymbol{\tau_m} \in \mathbb{R}^n$ is the motor torque. Using (3.1) in (3.2) yields

$$\boldsymbol{M_h\ddot{q} + C_h\dot{q} + G_h + F(q,\dot{q},\ddot{q},t) = \tau_m} \tag{3.3}$$

where $\boldsymbol{M_h = rM(q) + r^{-1}J}$, $\boldsymbol{C_h = rC(q,\dot{q}) + r^{-1}B}$ and $\boldsymbol{G_h = rG(q)}$. The uncertainties and the disturbances in the system are included in the vector $\boldsymbol{F(q,\dot{q},\ddot{q},t)} \in \mathbb{R}^n$.

The combined manipulator-motor dynamics have the same properties as the manipulator dynamics [156] mentioned below:

Property 3. *The inertia matrix $\boldsymbol{M_h}$ is bounded, symmetric and positive definite which means,*

$$m_{min}||\boldsymbol{x}||^2 \leq \boldsymbol{x^T M_h x} \leq m_{max}||\boldsymbol{x}||^2 \tag{3.4}$$

where $\boldsymbol{x} \in \mathbb{R}$ is a real valued vector and $||\boldsymbol{x}||$ is its Euclidian norm.

Property 4. *The robotic manipulator is a passive system which means*

$$\boldsymbol{x}^T(\frac{1}{2}\dot{\boldsymbol{M}}_{\boldsymbol{h}} - \boldsymbol{C_h})\boldsymbol{x} = 0, \quad \forall \boldsymbol{x} \neq 0. \tag{3.5}$$

The assumptions made while designing the controller are the following:

Assumption 4. *All the joints of the robotic manipulator are revolute.*

Assumption 5. *The desired trajectory for each joint* $\boldsymbol{q_d} \in \mathbb{R}^n$ *is smooth and continuous, meaning that the time derivatives* $\dot{\boldsymbol{q}}_{\boldsymbol{d}}$ *and* $\ddot{\boldsymbol{q}}_{\boldsymbol{d}}$ *exist for all time and are continuous and bounded.*

Assumption 6. *The vector* $\boldsymbol{F}(\boldsymbol{q}, \dot{\boldsymbol{q}}, \ddot{\boldsymbol{q}}, \boldsymbol{t})$ *representing the uncertainties and disturbances occurring in the system is bounded and its partial derivatives are continuous and locally uniformly bounded meaning*

$$|\boldsymbol{F}(\boldsymbol{q}, \dot{\boldsymbol{q}}, \ddot{\boldsymbol{q}}, \boldsymbol{t})| \leq \bar{\boldsymbol{F}} < \infty \tag{3.6}$$

where, $0 \leq \bar{\boldsymbol{F}} < \infty$ *is the unknown upper bound of the system uncertainties.*

The objective is to design a stable controller so that for a given desired trajectory $\boldsymbol{q_d}$, the tracking error $\boldsymbol{q_e} = \boldsymbol{q} - \boldsymbol{q_d}$ converges to zero.

3.2.2 Controller Design

Unlike the existing design methods of sliding mode controller with a PID sliding surface [157], the proposed controller defines a PID sliding surface systematically using backstepping. The Lyapunov based backstepping process is used to arrive at a stable PID sliding surface and thereafter the control law is derived using the sliding mode with an adaptively tuned controller gain. A step by step illustration of the controller design process is presented below:

Step I:
The first step involves defining a regulatory variable $\boldsymbol{z_1}$ following the backstepping method [54]. The integral of the error is considered as the first variable and is given as

$$\boldsymbol{z_1} = \int \boldsymbol{q_e} dt = \int (\boldsymbol{q} - \boldsymbol{q_d}) dt \tag{3.7}$$

$$\dot{\boldsymbol{z}}_{\boldsymbol{1}} = \boldsymbol{q} - \boldsymbol{q_d}. \tag{3.8}$$

The control Lyapunov function (CLF) for the above system is considered as

$$V_1 = \frac{1}{2} \boldsymbol{z_1^T z_1} \tag{3.9}$$

$$\dot{V}_1 = \boldsymbol{z_1^T \dot{z}_1} = \boldsymbol{z_1^T} \left(\boldsymbol{q} - \boldsymbol{q_d} \right). \tag{3.10}$$

The angular position $\boldsymbol{q}$ is considered as the controller for the subsystem (3.8) and the following synthetic control law $\boldsymbol{\alpha}_1$ is used for stabilizing (3.8):

$$\boldsymbol{\alpha_1} = -\boldsymbol{c_1 z_1} + \boldsymbol{q_d} \tag{3.11}$$

where $\boldsymbol{c_1} = diag(c_{1i}), i = 1 \dots n$, is a user defined diagonal matrix with $c_{1i} > 0, i = 1 \dots n$, and when $\boldsymbol{q = \alpha_1}$, $\dot{V}_1$ will be negative definite, meaning that

$$\dot{V}_1 = -\boldsymbol{z_1^T c_1 z_1} \leq 0. \tag{3.12}$$

Step II:

However, as the actual control law is yet to be defined, the next regulatory variable is defined as

$$\boldsymbol{z_2} = \boldsymbol{q - \alpha_1 = q + c_1 z_1 - q_d} \tag{3.13}$$

$$\boldsymbol{\dot{z}_2} = \boldsymbol{\dot{q} - \dot{q}_d + c_1 \dot{z}_1}. \tag{3.14}$$

With the introduction of $\boldsymbol{z_2}$, derivative of V_1 becomes

$$\dot{V}_1 = -\boldsymbol{z_1^T c_1 z_1 + z_1^T z_2}. \tag{3.15}$$

The CLF for the subsystem (3.14) is now defined as

$$V_2 = V_1 + \frac{1}{2}\boldsymbol{z_2^T z_2} \tag{3.16}$$

$$\begin{aligned} \dot{V}_2 &= -\boldsymbol{z_1^T c_1 z_1 + z_1^T z_2 + z_2^T \dot{z}_2} \\ &= -\boldsymbol{z_1^T c_1 z_1 + z_1^T z_2 + z_2^T (\dot{q} - \dot{q}_d + c_1 \dot{z}_1)}. \end{aligned} \tag{3.17}$$

Taking $\boldsymbol{\dot{q}}$ as the controlling term for (3.14), the synthetic control $\boldsymbol{\alpha_2}$ will now be defined so that $\boldsymbol{\dot{q}} = \boldsymbol{\alpha}_2$ makes $\dot{V}_2$ negative semidefinite, making (3.14) stable.

$$\boldsymbol{\alpha}_2 = -\boldsymbol{c_2 z_2 - c_1 \dot{z}_1 + \dot{q}_d} \tag{3.18}$$

where $\boldsymbol{c_2} = diag(c_{2i}),\ c_{2i} > 0,\ i = 1 \dots n$, is a user defined diagonal matrix.

Replacing (3.18) in (3.17), the derivative of the CLF $\dot{V}_2$ is re-evaluated as follows:

$$\begin{aligned} \dot{V}_2 &= -\boldsymbol{z_1^T c_1 z_1 + z 1^T z_2 + z_2^T (-c_2 z_2)} \\ &= -\boldsymbol{z_1^T c_1 z_1 - z_2^T c_2 z_2 + z_1^T z_2} \\ &= -\begin{bmatrix} \boldsymbol{z_1^T} & \boldsymbol{z_2^T} \end{bmatrix} \begin{bmatrix} \boldsymbol{c_1} & -\frac{1}{2}\boldsymbol{I}_n \\ -\frac{1}{2}\boldsymbol{I}_n & \boldsymbol{c_2} \end{bmatrix} \begin{bmatrix} \boldsymbol{z_1} \\ \boldsymbol{z_2} \end{bmatrix} \end{aligned} \tag{3.19}$$

If in (3.19) the matrix $\begin{bmatrix} \boldsymbol{c_1} & -\frac{1}{2}\boldsymbol{I_n} \\ -\frac{1}{2}\boldsymbol{I_n} & \boldsymbol{c_2} \end{bmatrix}$ is positive definite, then $\dot{V}_2$ will be negative definite.

Step III:

After obtaining $\boldsymbol{\alpha_2}$, the sliding variable $\boldsymbol{s}$ is now defined as the difference between $\boldsymbol{\dot{q}}$ and $\boldsymbol{\alpha_2}$ as follows:

$$\begin{aligned} \boldsymbol{s} &= \boldsymbol{\dot{q} - \alpha_2} \\ &= \boldsymbol{\dot{q} - (-c_2 z_2 - c_1 \dot{z}_1 + \dot{q}_d)} \end{aligned}$$

$$\begin{aligned}&=(\dot{\boldsymbol{q}}-\dot{\boldsymbol{q}}_{\boldsymbol{d}})+(\boldsymbol{c_1}+\boldsymbol{c_2})\boldsymbol{q_e}+\boldsymbol{c_1c_2}\int \boldsymbol{q_e}\boldsymbol{dt}\\&=\dot{\boldsymbol{q}}_{\boldsymbol{e}}+(\boldsymbol{c_1}+\boldsymbol{c_2})\,\boldsymbol{q_e}+\boldsymbol{c_1c_2}\int \boldsymbol{q_e}\boldsymbol{dt}.\end{aligned} \tag{3.20}$$

As can be observed from (3.20), $\boldsymbol{s}$ has a PID structure.

Now, $\boldsymbol{s}=\boldsymbol{0}$ is the sliding surface for the system and introduction of the sliding variable $\boldsymbol{s}$ changes (3.19) into the following:

$$\dot{V}_2=-\boldsymbol{z_1^T c_1 z_1}-\boldsymbol{z_2^T c_2 z_2}+\boldsymbol{z_1^T z_2}+\boldsymbol{z_2^T s}. \tag{3.21}$$

The time derivative of the sliding variable $\boldsymbol{s}$ is now derived as

$$\dot{\boldsymbol{s}}=\ddot{\boldsymbol{q}}-\ddot{\boldsymbol{q}}_{\boldsymbol{d}}+(\boldsymbol{c_1}+\boldsymbol{c_2})\,\dot{\boldsymbol{q}}_{\boldsymbol{e}}+\boldsymbol{c_1c_2q_e}. \tag{3.22}$$

Deriving $\ddot{\boldsymbol{q}}$ from (3.3) and replacing in (3.22) yields

$$\dot{\boldsymbol{s}}=\boldsymbol{M_h^{-1}}(\boldsymbol{\tau_m}-\boldsymbol{C_h}\dot{\boldsymbol{q}}-\boldsymbol{G_h})-\ddot{\boldsymbol{q}}_{\boldsymbol{d}}+(\boldsymbol{c_1}+\boldsymbol{c_2})\dot{\boldsymbol{q}}_{\boldsymbol{e}}+\boldsymbol{c_1c_2q_e}. \tag{3.23}$$

The Lyapunov function for this stage is defined as

$$V_3=V_2+\frac{1}{2}\boldsymbol{s^T s}. \tag{3.24}$$

The time derivative of V_3 is further expanded using (3.21) and (3.23) resulting in the following relation:

$$\begin{aligned}\dot{V}_3=&-\boldsymbol{z_1^T c_1 z_1}-\boldsymbol{z_2^T c_2 z_2}+\boldsymbol{z_1^T z_2}+\boldsymbol{z_2^T s}+\boldsymbol{s^T}(\boldsymbol{M_h^{-1}}(\boldsymbol{\tau_m}-\boldsymbol{C_h}\dot{\boldsymbol{q}}-\boldsymbol{G_h})-\ddot{\boldsymbol{q}}_{\boldsymbol{d}}\\&+(\boldsymbol{c_1}+\boldsymbol{c_2})\dot{\boldsymbol{q}}_{\boldsymbol{e}}+\boldsymbol{c_1c_2q_e}).\end{aligned} \tag{3.25}$$

Step IV:

In order to find a control law with reduced chattering, the reaching law approach [158] is followed. A constant plus proportional reaching law is used and an adaptive switching gain, which is a function of the sliding variable $\boldsymbol{s}$, is introduced. The purpose is to retain the controller robustness with a shorter reaching time, a good tracking performance and reduced chattering. The reaching law is given by

$$\dot{\boldsymbol{s}}=-\hat{\boldsymbol{k}}\circ\boldsymbol{sign}(\boldsymbol{s})-\boldsymbol{W}\boldsymbol{s} \tag{3.26}$$

where $\boldsymbol{W}=diag(w_i), w_i>0, i=1\ldots n$, is a designer defined diagonal matrix of constant elements and $\hat{\boldsymbol{k}}==[\hat{k}_i]_{n\times 1}, i=1\ldots n$, is the adaptively tuned parameter vector given by

$$\dot{\hat{\boldsymbol{k}}}=\boldsymbol{\Gamma}(|\boldsymbol{s}|-\boldsymbol{\epsilon}\hat{\boldsymbol{k}}). \tag{3.27}$$

Here $\boldsymbol{\Gamma}=diag(\gamma_i), \gamma_i>0, i=1\ldots n$, is the adaptive gain matrix that will determine the rate at which $\hat{\boldsymbol{k}}$ will converge to its final value $\boldsymbol{k}=[k_i]_{n\times 1}, i=1\ldots n,$. Further, $\boldsymbol{\epsilon}=diag(\epsilon_i), \epsilon_i>0, i=1\ldots n$, is the leakage parameter matrix [146] that will keep (3.27) from overestimating $\hat{\boldsymbol{k}}$, thus keeping it bounded.

The control law is now derived in two parts, (a) the equivalent control $\boldsymbol{u_{eq}}$ and (b) the switching control $\boldsymbol{u_{sw}}$. The equivalent control $\boldsymbol{\tau_{eq}}$ is obtained from (3.23) and (3.25) as follows:

$$\boldsymbol{\tau_{eq}} = \boldsymbol{C_h\dot{q} + G_h + M_h\left(\ddot{q}_d - (c_1 + c_2)\,\dot{q}_e - c_1c_2q_e\right)}. \tag{3.28}$$

The switching control $\boldsymbol{\tau_{sw}}$ is derived from (3.26) as follows:

$$\boldsymbol{\tau_{sw} = -M_h(\hat{k} \circ sign(s) + Ws)}. \tag{3.29}$$

The control law $\boldsymbol{u}$ to be applied to the manipulator is now obtained by combining (3.28) and (3.29) resulting in

$$\boldsymbol{\tau = \tau_{eq} + \tau_{sw}}. \tag{3.30}$$

3.2.3 Stability Analysis

(i) Stability of the adaptive law

First of all the stability of the adaptive law will be examined using the following Lyapunov function:

$$\begin{aligned} V_k =& \frac{1}{2}(\boldsymbol{s^T s + \tilde{k}^T\Gamma^{-1}\tilde{k}}) \\ \Rightarrow \dot{V}_k =& \boldsymbol{s^T\dot{s} + \tilde{k}^T\Gamma^{-1}\dot{\hat{k}}} \end{aligned} \tag{3.31}$$

where $\boldsymbol{\tilde{k} = \hat{k} - k}$ and $\boldsymbol{k}$ is a vector of positive arbitrary scalar values. Now, considering the presence of the system uncertainties $\boldsymbol{F(q, \dot{q}, \ddot{q}, t)}$ and using (3.27) and (3.30), the time derivative $\dot{V}_k$ can be rewritten as follows:

$$\begin{aligned} \dot{V}_k =& \boldsymbol{s^T\left(-\hat{k} \circ sign(s) - Ws + M_h^{-1}F(q, \dot{q}, \ddot{q}, t)\right)} + \boldsymbol{\tilde{k}^T}(|\boldsymbol{s}| - \boldsymbol{\epsilon\hat{k}}) \\ \leq& -|\boldsymbol{s}|^T\left(\boldsymbol{k} - |\boldsymbol{M_h^{-1}F(q, \dot{q}, \ddot{q}, t)}|\right) - \boldsymbol{s^TWs - \tilde{k}^T\epsilon\hat{k}}. \end{aligned} \tag{3.32}$$

From Lemma 4 for the positive diagonal matrix $\boldsymbol{\epsilon}$ and positive vector $\boldsymbol{k}$, the following relation is obtained:

$$\boldsymbol{\tilde{k}^T\epsilon\hat{k} \geq \frac{1}{2}(\tilde{k}^T\epsilon\tilde{k} - k^T\epsilon k)}. \tag{3.33}$$

Using (3.33) and the assumption (3.6), $\dot{V}_k$ can be rewritten as follows:

$$\dot{V}_k \leq -|\boldsymbol{s}|^T(\boldsymbol{k} - |\boldsymbol{M_h^{-1}}|\boldsymbol{\bar{F}}) - \boldsymbol{s^TWs} - \frac{1}{2}\boldsymbol{\tilde{k}^T\epsilon\tilde{k}} + \frac{1}{2}\boldsymbol{k^T\epsilon k} \tag{3.34}$$

Since $\boldsymbol{k}$ is an arbitrary positive gain, the condition $\boldsymbol{k} > m_{min}\boldsymbol{\bar{F}}$ can always be satisfied. Therefore, $\dot{V}_k$

can now be written as

$$\dot{V}_k \leq -\boldsymbol{s^T W s} - \frac{1}{2}\tilde{\boldsymbol{k}}^T\boldsymbol{\epsilon}\tilde{\boldsymbol{k}} + \frac{1}{2}\boldsymbol{k}^T\boldsymbol{\epsilon k} \tag{3.35}$$

Now choosing $\kappa_1 = \lambda_{min} diag\{\frac{1}{2}\boldsymbol{\epsilon\Gamma}, \boldsymbol{W}\}$ as the minimum of the eigenvalue of the block diagonal matrix $diag\{\boldsymbol{\epsilon\Gamma}, 2\boldsymbol{W}\}$, the following can be written:

$$\begin{aligned}\dot{V}_k &\leq -2\kappa_1 V_k + \rho \\ V_k &\leq \left(V_k(0) - \frac{\rho_1}{2\kappa_1}\right) e^{-2\kappa_1 t} + \frac{\rho_1}{2\kappa_1}.\end{aligned} \tag{3.36}$$

where, $\rho = \frac{1}{2}\boldsymbol{k}^T\boldsymbol{\epsilon k}$. Therefore, from (3.36), for $V_k(0) > \frac{\rho}{2\kappa_1}$, $\dot{V}_k \leq 0$ and the system errors will converge to a very small region bounded by a radius r around the origin, such that $V_k(r) < \frac{\rho_1}{2\kappa_1}$, asymptotically as $t \to \infty$

(ii) Stability of the overall system

The previously defined Lyapunov functions V_2 and V_k encompass all the variables defined throughout the design process and accordingly the following Lyapunov function can be used to inspect the stability of the overall system:

$$V = (V_2 + V_k) = \frac{1}{2}(\boldsymbol{z_1^T z_1} + \boldsymbol{z_2^T z_2} + \boldsymbol{s^T s} + \tilde{\boldsymbol{k}}^{\boldsymbol{T}}\boldsymbol{\Gamma^{-1}}\tilde{\boldsymbol{k}})$$

$$V = \frac{1}{2}\boldsymbol{Z^T P Z} \tag{3.37}$$

$$\Rightarrow \dot{V} = \dot{V}_2 + \dot{V}_k \tag{3.38}$$

where $\boldsymbol{Z^T} = [\boldsymbol{z_1^T}\ \ \boldsymbol{z_2^T}\ \ \boldsymbol{s^T}\ \ \tilde{\boldsymbol{k}}^{\boldsymbol{T}}]$, $\boldsymbol{Z} = [\boldsymbol{z_1}\ \ \boldsymbol{z_2}\ \ \boldsymbol{s}\ \ \tilde{\boldsymbol{k}}]^{\boldsymbol{T}}$ and $\boldsymbol{P} = diag\{\boldsymbol{I_n}, \boldsymbol{I_n}, \boldsymbol{I_n}, \boldsymbol{\Gamma^{-1}}\} \in \mathbb{R}^{4n\times 4n}$ is a positive definite block diagonal matrix. Using (3.21) and (3.34), $\dot{V}$ in (3.38) can be written as:

$$\begin{aligned}\dot{V} \leq &-\boldsymbol{z_1^T c_1 z_1} - \boldsymbol{z_2^T c_2 z_2} + \boldsymbol{z_1^T z_2} + \boldsymbol{z_2^T s} - |\boldsymbol{s}|^{\boldsymbol{T}}(\boldsymbol{k} - |\boldsymbol{M_h^{-1}}|\bar{\boldsymbol{F}}) \\ &- \boldsymbol{s^T W s} - \frac{\boldsymbol{1}}{\boldsymbol{2}}\tilde{\boldsymbol{k}}^{\boldsymbol{T}}\boldsymbol{\epsilon}\tilde{\boldsymbol{k}} + \frac{\boldsymbol{1}}{\boldsymbol{2}}\boldsymbol{k^T\epsilon k}.\end{aligned} \tag{3.39}$$

As mentioned earlier, the arbitrary constant vector $\boldsymbol{k}$ can satisfy $\boldsymbol{k} > |\boldsymbol{M_h^{-1}}|\bar{\boldsymbol{F}}$ which leads to the following form of $\dot{V}$:

$$\begin{aligned}\dot{V} &\leq -\boldsymbol{z_1^T c_1 z_1} + \boldsymbol{z_1^T z_2} - \boldsymbol{z_2^T c_2 z_2} + \boldsymbol{z_2^T s} - \boldsymbol{s^T W s} - \frac{\boldsymbol{1}}{\boldsymbol{2}}\tilde{\boldsymbol{k}}^{\boldsymbol{T}}\boldsymbol{\epsilon}\tilde{\boldsymbol{k}} + \frac{\boldsymbol{1}}{\boldsymbol{2}}\boldsymbol{k^T\epsilon k} \\ &\leq -\boldsymbol{Z^T Q Z} + \rho\end{aligned} \tag{3.40}$$

where

$$\boldsymbol{Q} = \begin{bmatrix} \boldsymbol{c_1} & -\frac{1}{2}\boldsymbol{I_n} & \boldsymbol{0} & \boldsymbol{0} \\ -\frac{1}{2}\boldsymbol{I_n} & \boldsymbol{c_2} & -\frac{1}{2}\boldsymbol{I_n} & \boldsymbol{0} \\ \boldsymbol{0} & -\frac{1}{2}\boldsymbol{I_n} & \boldsymbol{W} & \boldsymbol{0} \\ \boldsymbol{0} & \boldsymbol{0} & \boldsymbol{0} & \frac{1}{2}\boldsymbol{\epsilon} \end{bmatrix}_{4n\times 4n} \quad and \quad \rho = \frac{1}{2}\boldsymbol{k^T\epsilon k}$$

When the design parameters are chosen such that $\boldsymbol{Q} \in \mathbb{R}^{4n\times 4n}$ is positive definite, $\dot{V}$ can be written as follows:

$$\begin{aligned}\dot{V} &\leq -2\kappa_2 V(t) + \rho_2 \\ V(t) &\leq \left(V(0) - \frac{\rho}{2\kappa_2}\right) e^{-2\kappa_2 t} + \frac{\rho}{2\kappa_2}\end{aligned} \tag{3.41}$$

where $\kappa_2 = \lambda_{min}(\boldsymbol{P^{-1}Q}) > 0$ ($\lambda_{min}(\bullet)$ is the minimum eigenvalue). Therefore, for $V(0) > \frac{\rho}{2\kappa_2}$ and $\frac{\rho}{2\kappa_2} < 1$, $V(t)$ will be a decreasing function indicating the convergence of the system errors to equilibrium.

3.2.4 Simulation Results: Joint Space Trajectory Tracking of a 2DoF Manipulator

The performance of the proposed adaptive backstepping sliding mode control with the PID sliding surface (ABSMC-PID) is compared with the disturbance observer based decentralized adaptive robust control proposed by Yang *et al.* [2] and the IADSC (2.59-2.60) proposed in Chapter 2 through simulation in Matlab/Simulink environment. The dynamics of the 2DoF manipulator from Yang *et al.* [2] is used in the simulation and the mathematical model along with the structural uncertainty added as disturbance is described in Appendix A.7. The details of the controller proposed by Yang *et al.* [2] are described in Appendix A.8.

The parameters used in the ABSMC-PID are as follows:

$$\boldsymbol{c_1} = 20\boldsymbol{I_n},\ \boldsymbol{c_2} = 0.1\boldsymbol{I_n},\ \boldsymbol{W} = 60\boldsymbol{I_n}, \boldsymbol{\Gamma} = 10\boldsymbol{I_n},\ \boldsymbol{\epsilon} = 0.001\boldsymbol{I_2}, \mathcal{D} = 0.001 \tag{3.42}$$

where $\boldsymbol{I_n}$ is a $n \times n$ identity matrix.

In the simulations it is assumed that only the joint position information is available with an added uniform noise with bounds ± 0.0001rad. The joint velocity is derived through pseudo-differentiation using $\frac{a}{0.01a+1}$ (a is the complex number frequency parameter for representation of the differentiator in the Laplace domain). The selection of the pseudo-differentiator is different from the one used in the previous section (i.e., $\frac{a}{0.001a+1}$), since increasing the time constant offered some filtering of the measurement noise. At $t = 10s$ the link masses m_1 and m_2 are perturbed by 40% and 20% respectively. The following reference trajectories are defined for each of the joints:

$$\begin{aligned}q_{d1} &= 0.2 + 2\sin(2t)\ rad \\ q_{d2} &= -1.7 + 1.8\cos(2t)\ rad.\end{aligned} \tag{3.43}$$

The simulation results for tracking (3.43) are shown in Figure 3.1 and the control torques in the joints are shown in Figure 3.2. The transient and steady state behaviors along with the overall tracking error for each joint are shown in Figure 3.1. From Figure 3.1 it can be observed that the proposed ABSMC-PID has faster convergence than the disturbance observer based controller by Yang *et al.* [2] and in terms of the settling time and overshoot in the error, the response with the ABSMC-PID is better than the previously proposed IADSC. However, the improved performance of ABSMC-PID is

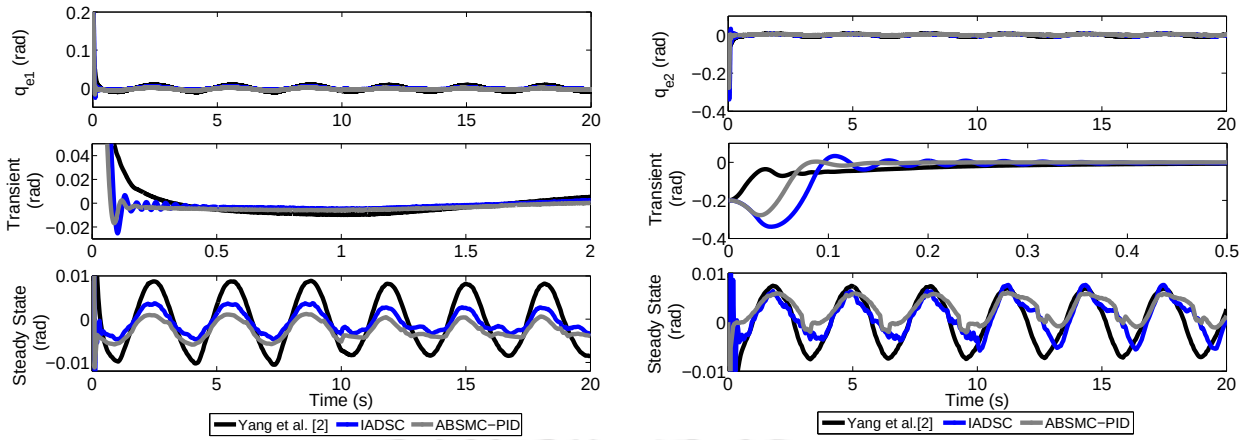

(a) Tracking error of joint 1

(b) Tracking error of joint 2

Figure 3.1: Simulation results: Tracking errors for 2DoF manipulator with Yang *et al.* 's controller [2], IADSC and the proposed ABSMC-PID in presence of measurement noise

achieved with the compromise of using slightly higher amount of input torque as compared to the disturbance observer based controller by Yang *et al.* [2] as can be observed in Figure 3.2.

For clarity of analysis the simulation results are tabulated in terms of the following output and input performance indices: rise time (t_r), settling time (t_s), peak overshoot (M_p), peak undershoot (M_u), peak overshoot time (t_p), peak undershoot time (t_u), the mean absolute steady state error (MASSE), 2-norm of the control input ($||u||$) and its total variation (TV) (2.32). The tracking performance indices are listed in Table 3.1 and the input torques are compared in Table 3.2. Due to the oscillatory nature of the tracking error in steady state, the MASSE is computed and listed in Table 3.1. The simulation results demonstrate that the proposed ABSMC-PID produces better transient and steady state responses than both Yang *et al.* 's [2] controller and the previously proposed IADSC at the expense of comparable control energy.

Table 3.1: Performance comparison for trajectory tracking of the 2DoF manipulator

Joint	Controller	t_r(s)	t_s(s)	Overshoot		Undershoot		MASSE(rad)
				M_p(rad)	t_p(s)	M_u(rad)	t_u(s)	
Joint 1	Yang *et al.* [2]	0.162	0.481	-	-	-	-	0.0062
	IADSC	0.093	0.175	-0.024	0.099	-	-	0.0029
	ABSMC-PID	0.071	0.153	-0.015	0.084	-	-	0.0032
Joint 2	Yang *et al.* [2]	0.268	0.6	-	-	-	-	0.0051
	IADSC	0.089	0.4	0.033	0.107	-0.338	0.043	0.0044
	ABSMC-PID	0.074	0.18	-	-	-0.277	0.032	0.0036

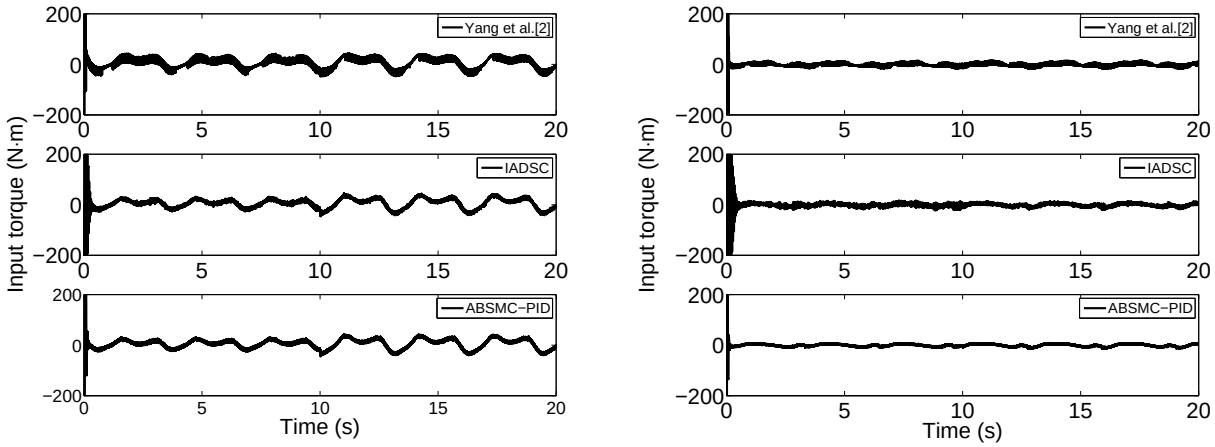

(a) Input torque of joint 1

(b) Input torque of joint 2

Figure 3.2: Simulation results: The input torques for 2DoF manipulator with Yang *et al.* 's controller [2], IADSC and the proposed ABSMC-PID in presence of measurement noise

Table 3.2: Performance comparison for input torques of the 2DoF manipulator

Joint	Controller	$\|\|u\|\|$(N·m)	TV (N·m)
Joint 1	Yang *et al.* [2]	5×10^3	2.9×10^5
	IADSC	5×10^3	0.47×10^5
	ABSMC-PID	4.6×10^3	4.04×10^5
Joint 2	Yang *et al.* [2]	2.7×10^3	1.59×10^5
	IADSC	2.1×10^3	0.25×10^5
	ABSMC-PID	3.04×10^3	1.9×10^5

3.3 ABSMC-PID for hybrid impedance control of robot manipulators

For real time implementation of a robotic manipulator, defining the desired trajectory in the task space instead of the joint space is more relevant. While designing a controller for tracking task space trajectories, the following two approaches can be followed:

- The task space trajectories can be converted to the joint space coordinates using inverse kinematics and then the obtained discrete joint coordinates are converted to time dependent trajectories via interpolation. This process is offline and the joint trajectories are then fed to the controller as the reference signal.

- The second approach is online, where the controller is designed for the task space only with the Cartesian force and torque coordinates as the controlling inputs. Then using the manipulator Jacobian the Cartesian inputs are converted to joint torques to be sent to the manipulator joint actuators.

Between the above two approaches, the online method of designing manipulator controller in the task space is more practical since it offers the freedom of changing the reference even during

the operation. The offline method offers a reliable and stable operation since prior to feeding in the trajectories the singularity can be avoided. However, this method is twofold and a change in reference trajectory means having to again calculate the inverse kinematics to obtain the desired joint trajectories and then changing the reference to the main controller.

While maintaining the motion of a robot manipulator in the task space, it is also vital to monitor and control the manipulator interaction with the environment it is contained in. For tasks which do not involve direct contact between manipulator end-effector and the external environment like in welding and spray painting, only position control is sufficient for satisfactory operation. However, for tasks involving interaction with the external environment such as polishing, writing, holding various objects as well as interacting with humans, it is very important to control the applied force and torques along with the position to achieve the desired goal and also to avoid any unwanted accidents. Therefore the force/position [159, 160] control and impedance control [161–163] of manipulators are extensively studied fields.

The manipulator dynamics during contact motion gets highly affected by the dynamics of the environment which can cause performance degradation and instability in impedance control. Considering a variable impedance that changes according to the manipulator interaction can help in achieving a better compliance. Early works in variable impedance control involved defining two different desired impedance behaviors depending upon the velocity of the operation where mostly the damping was adjusted [164]. Ikeura *et al.* [165] proposed a damping factor which varied optimally in accordance with a minimized cost function. In [166], Dubey *et al.* proposed damping and stiffness as continuously varying functions of the sensed force and velocity. Tsumugiwa *et al.* [167] proposed a variable stiffness for the human-robot cooperative task that was based on the estimated stiffness of the tip of the human arm. The human arm behavior was used in [168, 169] for interaction tasks. Buchli *et al.* [170] proposed a reinforcement learning PI^2 (Policy Improvement with Path Integrals) for gain scheduling of the variable impedance control. Learning based variable impedance control is reported in [168, 169, 171]. Variation of both the damping and stiffness of the impedance characteristics was suggested by Bae *et al.* [172]. Ficuciello *et al.* [163] proposed varying impedance control by changing the equivalent inertia during contact using the feedback of the exchanged force. The detailed stability issue and a generalized Lyapunov function for stability analysis of the variable impedance control (variable damping and stiffness) are discussed in [173].

Most of the existing impedance controller design using the variable structure method involves defining a dynamic compensator based on which the switching function is designed. Although these methods provide robustness and good tracking results, the number of design parameters are high due to the introduction of the dynamic compensator. In this section the proposed adaptive backstepping sliding mode controller with a PID sliding surface (ABSMC-PID) will be used for impedance control of robot manipulators. Unlike the existing methods of robust impedance control using sliding mode [174–176], in the proposed method the parameters of the backstepping are designed according to the desired impedance and finally the variables obtained via backstepping are used to define a PID sliding surface. When the equilibrium is reached, sliding mode will induce the desired impedance behavior to the system. In the proposed ABSMC-PID the backstepping is used to provide a varying design

parameter as a function of the system error. This varying parameter will ultimately induce variable damping and stiffness to the defined impedance so that the transition between no contact and contact with the external environment is obtained smoothly. The controller design along with the simulation results are given in detail in the following sections.

3.3.1 Control Objective

Considering no interaction with the environment, the robot dynamics in the task space can be written as

$$\boldsymbol{M_T(q)\ddot{x} + C_T(q,\dot{q})\dot{x} + G_T(q) + F_e = F_c + \tilde{F}} \tag{3.44}$$

where

$$\begin{aligned}
\boldsymbol{M_T(q)} &= \boldsymbol{J^{-T}(q)M(q)J^{-1}(q)} \\
\boldsymbol{C_T(q,\dot{q})} &= \boldsymbol{J^{-T}(q)C(q,\dot{q})J^{-1}(q) - J^{-T}(q)M(q)J^{-1}(q)\dot{J}(q)J^{-1}(q)} \\
\boldsymbol{G_T(q)} &= \boldsymbol{J^{-T}G},\ \boldsymbol{\tilde{F}(q,\dot{q}) = J^{-T}(q)f(q,\dot{q})},\ \boldsymbol{F_c = J^{-T}(q)\tau} \\
\boldsymbol{J^{-1}(q)} &= \boldsymbol{J(q)^T(J(q)J(q)^T + \lambda I)^{-1}},\ \boldsymbol{J^{-T}(q) = (J^{-1})^T}
\end{aligned}$$

and $\boldsymbol{x} \in \mathbb{R}^p$ is the position of the end-effector in the cartesian task space having dimension p, $\boldsymbol{J(q) = \frac{\delta x}{\delta q}}$ is the corresponding Jacobian matrix and $\boldsymbol{F_e}$ represents the interaction forces/moment exerted by the manipulator on the environment.

The properties of the manipulator in the joint space [156] also hold in the task space after the transformation and are mentioned below for the system (3.44):

Property 5. *The inertia matrix M_T is symmetric and positive definite meaning that $\boldsymbol{M_T = M_T^T}$ and $\boldsymbol{M_T > 0}$ and it is upper and lower bounded, which implies,*

$$\bar{\mu}_{min}\boldsymbol{I}_{p\times p} \leq \boldsymbol{M_T} \leq \bar{\mu}_{max}\boldsymbol{I}_{p\times p} \tag{3.45}$$

where $0 < \bar{\mu}_{min} < \bar{\mu}_{max}$ and $\boldsymbol{I}_{p\times p}$ is a $p \times p$ identity matrix.

Property 6. *The robot manipulator (3.44) is a passive system, which implies that*

$$\boldsymbol{x^T}\left[\frac{\boldsymbol{1}}{\boldsymbol{2}}\boldsymbol{\dot{M}_T - C_T}\right]\boldsymbol{x = 0} \quad \forall \boldsymbol{x \neq 0}. \tag{3.46}$$

The assumptions made for deriving a task space controller for the combined manipulator and actuator dynamics are given below:

Assumption 7. *All the joints of the robotic manipulator are revolute.*

Assumption 8. *The reference trajectory defined as $\boldsymbol{p_d(t)} \in \mathbb{R}^n$ and its time derivatives $\boldsymbol{\dot{p}_d(t)}$ and $\boldsymbol{\ddot{p}_d(t)}$ are continuous and bounded.*

Assumption 9. *The unknown force vector* $\tilde{\boldsymbol{F}}(\boldsymbol{q}, \dot{\boldsymbol{q}}, \boldsymbol{t})$ *satisfies*

$$|\tilde{\boldsymbol{F}}(\boldsymbol{q}, \dot{\boldsymbol{q}}, \boldsymbol{t})| \leq \bar{\boldsymbol{F}} \tag{3.47}$$

where $\bar{\boldsymbol{F}} > \boldsymbol{0}$ *is the unknown upper bound of the uncertainty.*

The aim of the control scheme is to employ impedance control for a manipulator subjected to constraint motion due to interaction with the external environment. The manipulator motion can be divided as (i) *the free motion control,* where only position control is required as there is no contact with the external environment and (ii) *the impedance control,* which will be active as soon as the robot arm end-effector comes in contact with the environment. The impedance controller design will be aimed towards avoiding large forces during contact as well as matching the manipulator impedance with the dynamics of the environment.

The desired impedance characteristics for the manipulator end-effector can be defined as follows:

$$\boldsymbol{M_d}(\ddot{\boldsymbol{x}} - \ddot{\boldsymbol{x}}_{\boldsymbol{d}}) + \boldsymbol{B_d}(\dot{\boldsymbol{x}} - \dot{\boldsymbol{x}}_{\boldsymbol{d}}) + \boldsymbol{K_d}(\boldsymbol{x} - \boldsymbol{d_d}) = -\boldsymbol{F_e} \tag{3.48}$$

where positive definite diagonal matrices $\boldsymbol{M_d}$, $\boldsymbol{B_d}$, $\boldsymbol{K_d}$ denote the desired inertia, damping and stiffness constants respectively, $\boldsymbol{F_e}$ is the interaction force and $\boldsymbol{x_d}$ is the desired motion trajectory in the task space of the manipulator. From (3.48), a Cartesian target acceleration (CTA) trajectory $\ddot{\boldsymbol{x}}_{\boldsymbol{t}}$ is defined as:

$$\ddot{\boldsymbol{x}}_{\boldsymbol{t}} = \ddot{\boldsymbol{x}}_{\boldsymbol{d}} - \boldsymbol{M_d^{-1}}\left(\boldsymbol{B_d}(\dot{\boldsymbol{x}} - \dot{\boldsymbol{x}}_{\boldsymbol{d}}) - \boldsymbol{K_d}(\boldsymbol{x} - \boldsymbol{x_d}) - \boldsymbol{F_e}\right) \tag{3.49}$$

such that when $\ddot{\boldsymbol{x}} = \ddot{\boldsymbol{x}}_{\boldsymbol{t}}$, the manipulator motion will follow the desired impedance characteristics defined in (3.48). Also, from (3.49), a Cartesian target velocity (CTV) profile $\dot{\boldsymbol{x}}_{\boldsymbol{t}}$ is generated as follows:

$$\dot{\boldsymbol{x}}_{\boldsymbol{t}} = \dot{\boldsymbol{x}}_{\boldsymbol{d}} - \boldsymbol{M_d^{-1}}\left(\boldsymbol{B_d}(\boldsymbol{x} - \boldsymbol{x_d}) - \boldsymbol{K_d}\int_0^t (\boldsymbol{x} - \boldsymbol{x_d})d\boldsymbol{\theta} - \int_0^t \boldsymbol{F_e} d\boldsymbol{\theta}\right). \tag{3.50}$$

Based on the desired impedance and the CTA profile developed, the design of the control law $\boldsymbol{F_c}$ should be such that

$$\ddot{\boldsymbol{x}} = \ddot{\boldsymbol{x}}_{\boldsymbol{t}} \tag{3.51}$$

so that the manipulator will follow the desired impedance dynamics.

3.3.2 Controller Design and Stability Analysis

3.3.2.1 Controller Design

In this subsection the controller design process is described. The backstepping method is used to design a sliding surface ($\boldsymbol{s} = \boldsymbol{0}$) in terms of the tracking errors. A salient feature of the SMC is that on the sliding surface the system states follow the surface dynamics. Using this property, the sliding

surface will be designed in such a way that $\boldsymbol{s = 0}$ will resemble the Cartesian target velocity, and at the equilibrium, where $\boldsymbol{s = \dot{s} = 0}$, the impedance dynamics will be achieved.

Step I:

In order to design a hybrid impedance control method using backstepping sliding mode methodology, the error $\boldsymbol{e_x}$ is defined in the task space as

$$\boldsymbol{e_x = x - x_d}.$$

The integral of this error is defined as the first regulatory variable $\boldsymbol{z_1}$ as

$$\boldsymbol{z_1} = \int \boldsymbol{e_x dt} \tag{3.52}$$

$$\boldsymbol{\dot{z}_1 = x - x_d}. \tag{3.53}$$

The control Lyapunov function (CLF) V_1 is defined for this subsystem as

$$V_1 = \frac{1}{2}\boldsymbol{z_1^T z_1}$$

$$\dot{V}_1 = \boldsymbol{z_1^T \dot{z}_1 = z_1^T (x - x_d)}. \tag{3.54}$$

Considering $\boldsymbol{x}$ to be the controlling quantity in this subsystem, a virtual control $\boldsymbol{\alpha_1}$ is defined such that when $\boldsymbol{x = \alpha_1}$ (3.53) is stable and is given by

$$\boldsymbol{\alpha_1 = -c_1 z_1 + x_d} \tag{3.55}$$

where $\boldsymbol{c_1} = diag(c_{1i}), i = 1 \ldots p, c_{1i} > 0$, is a user defined constant.

Substituting (3.55) into (3.54) yields

$$\dot{V}_1 = \boldsymbol{-z_1^T c_1 z_1 \leq 0}.$$

Step II:

The next regulatory variable $\boldsymbol{z_2}$ will now represent the error between $\boldsymbol{x}$ and $\boldsymbol{\alpha_1}$ as

$$\boldsymbol{z_2 = x - \alpha_1 = x - x_d + c_1 z_1} \tag{3.56}$$

$$\boldsymbol{\dot{z}_2 = \dot{x} - \dot{x}_d + c_1 \dot{z}_1}. \tag{3.57}$$

Substituting $\boldsymbol{x}$ from (3.56) into (3.54) yields

$$\dot{V}_1 = \boldsymbol{-z_1^T c_1 z_1 + z_1^T z_2}. \tag{3.58}$$

The CLF for the subsystem (3.57) defined by V_2 is given as

$$\begin{aligned} V_2 =& V_1 + \frac{1}{2}\boldsymbol{z_2^T z_2} \qquad (3.59)\\ \dot{V}_2 =& \dot{V}_1 + \boldsymbol{z_2^T \dot{z}_2}\\ =& \dot{V}_1 + \boldsymbol{z_2^T(\dot{x} - \dot{x}_d + c_1\dot{z}_1)}\\ \leq& -\boldsymbol{z_1^T c_1 z_1 + z_1^T z_2 + z_2^T(\dot{x} - \dot{x}_d + c_1\dot{z}_1)}\\ \leq& -\boldsymbol{z_1^T c_1 z_1 + z_2^T(\dot{x} - \dot{x}_d + c_1\dot{z}_1)}. \qquad (3.60) \end{aligned}$$

Based on $\dot{V}_2$ (3.60), the virtual control input $\boldsymbol{\alpha_2}$ to stabilize the subsystem (3.57) is derived as

$$\boldsymbol{\alpha_2 = -c_2 z_2 - c_1\dot{z}_1 + \dot{x}_d} \qquad (3.61)$$

where $\mathbf{c_2} = diag(c_{2i}), i = 1 \ldots p, c_{2i} > 0$, is a user defined constant. This leads to the following dynamic subsystem:

$$\begin{aligned} \boldsymbol{\dot{z}_2} &= \boldsymbol{-c_2 z_2}\\ \Rightarrow \boldsymbol{\dot{e}_x} &= \boldsymbol{-(c_1 + c_2)e_x - c_1 c_2}\int_0^t \boldsymbol{e_x d\theta}. \qquad (3.62) \end{aligned}$$

Replacing $\boldsymbol{\dot{x} = \alpha_2}$ in (3.60), the time derivative of the CLF V_2 is obtained as follows:

$$\dot{V}_2 \leq -\boldsymbol{z_1^T c_1 z_1 - z_2^T c_2 z_2 + z_1^T z_2}. \qquad (3.63)$$

Step III:

In this step the sliding variable $\boldsymbol{s}$ is defined by adding the term $\boldsymbol{k_f}\int \boldsymbol{e_f dt}$ to the next backstepping error $(\boldsymbol{\dot{x} - \alpha_2})$, so that at the equilibrium $\boldsymbol{\dot{s} = 0}$, the closed loop system dynamics resembles the desired impedance dynamics. For the impedance control $\boldsymbol{e_f = F_e}$ and $k_f = 1$. The sliding variable $\boldsymbol{s}$ is defined as follows:

$$\begin{aligned} \boldsymbol{s} =& \boldsymbol{\dot{x} - \alpha_2 + k_f}\int \boldsymbol{e_f dt}\\ \Rightarrow \boldsymbol{s} =& \boldsymbol{\dot{x} - \dot{x}_d + c_2 z_2 + c_1\dot{z}_1 + k_f}\int \boldsymbol{e_f dt}\\ =& \boldsymbol{\dot{e}_x + (c_1 + c_2)e_x + c_1 c_2}\int \boldsymbol{e_x dt + k_f}\int \boldsymbol{e_f dt}\\ \Rightarrow \boldsymbol{\dot{s}} =& \boldsymbol{\ddot{x} - \ddot{x}_d + (c_1 + c_2)(\dot{x} - \dot{x}_d) + c_1 c_2(x - x_d) + k_f e_f}. \qquad (3.64) \end{aligned}$$

Comparing (3.49) with the sliding surface equilibrium $\boldsymbol{\dot{s} = 0}$ ($\boldsymbol{\dot{s}}$ given by 3.64), the desired impedance parameters are obtained in terms of the controller parameters as follows

$$\boldsymbol{M_d^{-1} B_d(t) = c_1 + c_2}, \quad \boldsymbol{M_d^{-1} K_d(t) = c_1 c_2}. \qquad (3.65)$$

Now, comparing (3.49) and (3.50) with (3.64), the following can be written for the sliding surface

$$\boldsymbol{s} = \dot{\boldsymbol{x}} - \dot{\boldsymbol{x}}_{\boldsymbol{t}} \tag{3.66}$$

$$\ddot{\boldsymbol{s}} = \ddot{\boldsymbol{x}} - \ddot{\boldsymbol{x}}_{\boldsymbol{t}} \tag{3.67}$$

where the CTA and CTV in terms of the backstepping variables can be written as

$$\ddot{\boldsymbol{x}}_{\boldsymbol{t}} = \ddot{\boldsymbol{x}}_{\boldsymbol{d}} - \boldsymbol{c_1}\ddot{\boldsymbol{z}}_{\boldsymbol{1}} - \boldsymbol{c_2}\dot{\boldsymbol{z}}_{\boldsymbol{2}} - \boldsymbol{k_f}\boldsymbol{e_f} \tag{3.68}$$

$$\dot{\boldsymbol{x}}_{\boldsymbol{t}} = \dot{\boldsymbol{x}}_{\boldsymbol{d}} - \boldsymbol{c_1}\dot{\boldsymbol{z}}_{\boldsymbol{1}} - \boldsymbol{c_2}\boldsymbol{z_2} - \boldsymbol{k_f}\int \boldsymbol{e_f}\boldsymbol{dt} \tag{3.69}$$

Step IV:

The control law will be defined in such a way that the system states reach the sliding surface $\boldsymbol{s} = \boldsymbol{0}$ in finite time and then they converge to the equilibrium $\dot{\boldsymbol{s}} = \boldsymbol{0}$ asymptotically. In order to derive the control law the following Lyapunov function is defined

$$\begin{aligned} V_s =& \frac{1}{2}\boldsymbol{s^T M_T s} \\ \dot{V}_s =& \boldsymbol{s^T M_T \dot{s}} + \frac{1}{2}\boldsymbol{s^T \dot{M}_T s} \end{aligned} \tag{3.70}$$

Now, using *Property* 6 in (3.70) and then applying (3.66), (3.67) as well as the nominal system dynamics (3.44), $\dot{V}_s$ can be rewritten as

$$\begin{aligned} \dot{V}_s =& \boldsymbol{s^T M_T \dot{s}} + \boldsymbol{s^T C s} \\ =& \boldsymbol{s^T}(\boldsymbol{M_T}(\ddot{\boldsymbol{x}} - \ddot{\boldsymbol{x}}_{\boldsymbol{t}}) + \boldsymbol{C_T}(\dot{\boldsymbol{x}} - \dot{\boldsymbol{x}}_{\boldsymbol{t}})) \\ =& \boldsymbol{s^T}(\boldsymbol{F_c} - \boldsymbol{G_T} - \boldsymbol{F_e} - \boldsymbol{M_T}\ddot{\boldsymbol{x}}_{\boldsymbol{t}} - \boldsymbol{C_T}\dot{\boldsymbol{x}}_{\boldsymbol{t}}) \end{aligned} \tag{3.71}$$

Therefore, from (3.71), the equivalent part of the controller is derived as

$$(\boldsymbol{F_c})_{\boldsymbol{eq}} = \boldsymbol{M_T}\ddot{\boldsymbol{x}}_{\boldsymbol{t}} + \boldsymbol{C_T}\dot{\boldsymbol{x}}_{\boldsymbol{t}} + \boldsymbol{G_T} + \boldsymbol{F_e}. \tag{3.72}$$

The reaching law approach is used to design the switching part of the controller where a constant plus proportional reaching law [158] is used as follows,

$$\dot{\boldsymbol{s}} = -\hat{\boldsymbol{k}} \circ \boldsymbol{sign}(\boldsymbol{s}) - \boldsymbol{W}\boldsymbol{s} \tag{3.73}$$

where $\boldsymbol{W_{p\times p}} > 0$ is a user defined constant diagonal matrix with positive elements and $\hat{\boldsymbol{k}} > 0$ is an adaptively tuned gain given by the adaptive law [146]

$$\dot{\hat{\boldsymbol{k}}} = \boldsymbol{\Gamma}(|\boldsymbol{s}| - \boldsymbol{\epsilon}\hat{\boldsymbol{k}}) \tag{3.74}$$

where $\boldsymbol{\Gamma_{p\times p}} = diag(\Gamma_i),\ i = 1 \ldots p$ is the adaptive gain matrix with user defined gain parameters $\Gamma_i > 0$ and $\boldsymbol{\epsilon}_{p\times p} = diag(\epsilon_i),\ i = 1 \ldots p, \epsilon_i > 0$ is the leakage parameter [146] that prevents overestimation

by the adaptive law and ensures that $\hat{\boldsymbol{k}}$ converges to an arbitrary finite value $\boldsymbol{k}$. Thus, the switching part of the control derived based on (3.73) and (3.71) is

$$(\boldsymbol{F_c})_{sw} = -\hat{\boldsymbol{k}} \circ \boldsymbol{sign(s)} - \boldsymbol{Ws}. \tag{3.75}$$

The total control law $\boldsymbol{F_c}$ is defined as

$$\boldsymbol{F_c} = \boldsymbol{C_T}\dot{\boldsymbol{x}}_{\boldsymbol{t}} + \boldsymbol{G_T} + \boldsymbol{F_e} + \boldsymbol{M_T}\left(\ddot{\boldsymbol{x}}_{\boldsymbol{d}} - \boldsymbol{c_2}\dot{\boldsymbol{z}}_{\boldsymbol{2}} - \boldsymbol{c1}\ddot{\boldsymbol{z}}_{\boldsymbol{1}} - \boldsymbol{k_f e_f}\right) - \hat{\boldsymbol{k}} \circ \boldsymbol{sign(s)} - \boldsymbol{Ws}. \tag{3.76}$$

The above control law ensures that through sliding mode, the manipulator acceleration follows the CTA trajectory, i.e., $\ddot{\boldsymbol{x}} = \ddot{\boldsymbol{x}}_{\boldsymbol{t}}$, which will make the manipulator track the desired dynamics faithfully.

In order to achieve variable damping and stiffness values, the design parameter $\boldsymbol{c_2}$ is changed to the following variable function

$$\boldsymbol{c_2} = diag\{c_{2i} - (1 - \Sigma_i)(c_{2i} exp(-\eta z_{2i}^2))\}, \quad i = 1, \ldots, n \tag{3.77}$$

where Σ_i is the diagonal element of an $n \times n$ diagonal selection matrix $\boldsymbol{\Sigma}$ having entries 0 and 1 for contact and free motion respectively and η is a positive scalar. The selection of $\boldsymbol{c_2}$ as shown in (3.77) ensures that whenever the manipulator encounters contact in any direction, the element of $\boldsymbol{c_2}$ along that direction will change accordingly so that the stiffness of the desired impedance along that direction reduces during impact and thereby minimizing the possible high impact force especially in case of stiff environments.

3.3.2.2 Stability Analysis

Stability of the Sliding Surface and Adaptive Law

The following Lyapunov function $\mathbf{V_k}$ is chosen for the stability analysis of the sliding surface and the adaptive law,

$$V_k = \frac{1}{2}\boldsymbol{s^T M_T s} + \tilde{\boldsymbol{k}}^{\boldsymbol{T}} \boldsymbol{\Gamma^{-1}} \tilde{\boldsymbol{k}} \tag{3.78}$$

where $\tilde{\boldsymbol{k}} = \hat{\boldsymbol{k}} - \boldsymbol{k}$ with $\boldsymbol{k}$ being an arbitrary positive gain vector. Taking the time derivative of $\mathbf{V_k}$ yields

$$\dot{V}_k = \boldsymbol{s^T M_T}\dot{\boldsymbol{s}} + \frac{1}{2}\boldsymbol{s^T}\dot{\boldsymbol{M}}_{\boldsymbol{T}}\boldsymbol{s} + \tilde{\boldsymbol{k}}^{\boldsymbol{T}}\boldsymbol{\Gamma^{-1}}\dot{\tilde{\boldsymbol{k}}}.$$

Therefore, using (3.71) and including the disturbance forces, $\dot{V}_k$ can be rewritten as

$$\dot{V}_k = \boldsymbol{s^T}(\boldsymbol{F_c} - \boldsymbol{G_T} + \boldsymbol{F_e} + \tilde{\boldsymbol{F}} - \boldsymbol{M_T}\ddot{\boldsymbol{x}}_{\boldsymbol{t}} - \boldsymbol{C_T}\dot{\boldsymbol{x}}_{\boldsymbol{t}}) + \tilde{\boldsymbol{k}}^{\boldsymbol{T}}\boldsymbol{\Gamma^{-1}}\dot{\tilde{\boldsymbol{k}}}. \tag{3.79}$$

Substituting the control law (3.76) into (3.79) and using (3.74), the following can be obtained,

$$\dot{V}_k = \boldsymbol{s^T}(-\hat{\boldsymbol{k}} \circ \boldsymbol{sign(s)} - \boldsymbol{Ws} + \tilde{\boldsymbol{F}}) + \tilde{\boldsymbol{k}}^{\boldsymbol{T}}|s| - \tilde{\boldsymbol{k}}^{\boldsymbol{T}}\boldsymbol{\epsilon}\hat{\boldsymbol{k}}$$

$$\leq - |\boldsymbol{s}|^{\boldsymbol{T}}\boldsymbol{k} + |\boldsymbol{s}|^{\boldsymbol{T}}\tilde{\boldsymbol{F}} - \boldsymbol{s}^{\boldsymbol{T}}\boldsymbol{W}\boldsymbol{s} - \tilde{\boldsymbol{k}}^{\boldsymbol{T}}\boldsymbol{\epsilon}\hat{\boldsymbol{k}}. \tag{3.80}$$

From Lemma 4, for $\tilde{\boldsymbol{k}} = \hat{\boldsymbol{k}} - \boldsymbol{k}$ and a positive definite diagonal matrix $\boldsymbol{\epsilon}$, the following can be written:

$$\tilde{\boldsymbol{k}}^{\boldsymbol{T}}\boldsymbol{\epsilon}\hat{\boldsymbol{k}} \leq \frac{1}{2}(\tilde{\boldsymbol{k}}^{\boldsymbol{T}}\boldsymbol{\epsilon}\tilde{\boldsymbol{k}} - \boldsymbol{k}^{\boldsymbol{T}}\boldsymbol{\epsilon}\boldsymbol{k}). \tag{3.81}$$

From (3.80) and (3.81), the following inequality can be derived:

$$\dot{V}_k \leq -|\boldsymbol{s}|^{\boldsymbol{T}}(\boldsymbol{k} - \tilde{\boldsymbol{F}}) - \boldsymbol{s}^{\boldsymbol{T}}\boldsymbol{W}\boldsymbol{s} - \frac{\mathbf{1}}{\mathbf{2}}\tilde{\boldsymbol{k}}^{\boldsymbol{\epsilon}}\tilde{\boldsymbol{k}} + \frac{\mathbf{1}}{\mathbf{2}}\boldsymbol{k}^{\boldsymbol{T}}\boldsymbol{\epsilon}\boldsymbol{k}. \tag{3.82}$$

For the arbitrary positive parameter $\boldsymbol{k}$ satisfying $\boldsymbol{k} \geq \tilde{\boldsymbol{F}}$, $\dot{V}_k$ can be written as

$$\begin{aligned}\dot{V}_k \leq& - \boldsymbol{s}^{\boldsymbol{T}}\boldsymbol{W}\boldsymbol{s} - \frac{\mathbf{1}}{\mathbf{2}}\tilde{\boldsymbol{k}}^{\boldsymbol{\epsilon}}\tilde{\boldsymbol{k}} + \frac{\mathbf{1}}{\mathbf{2}}\boldsymbol{k}^{\boldsymbol{T}}\boldsymbol{\epsilon}\boldsymbol{k} \\ \leq& - 2\kappa V_k + \rho.\end{aligned} \tag{3.83}$$

where $\kappa = \lambda_{min}\left(diag\{\boldsymbol{W}, \frac{1}{2}\boldsymbol{\Gamma\epsilon}\}\right)$ and $\rho = \frac{1}{2}\boldsymbol{k}^{\boldsymbol{T}}\boldsymbol{\epsilon}\boldsymbol{k}$. Therefore, when $V_k(0) \geq \frac{\rho}{2\kappa}$ and $\frac{\rho}{2\kappa} < 1$, $\dot{V}_k < 0$ indicating the asymptotic stability of the sliding surface and the adaptive law .

(ii) Stability of the Desired Impedance

Following the stability analysis method provided in [173] the following Lyapunov function is chosen for the desired impedance characteristics:

$$V = \frac{1}{2}\dot{\boldsymbol{z}}_{\mathbf{2}}^{\boldsymbol{T}}\boldsymbol{M}_{\boldsymbol{d}}\dot{\boldsymbol{z}}_{\mathbf{2}} + \frac{1}{2}\boldsymbol{e}_{\boldsymbol{x}}^{\boldsymbol{T}}\boldsymbol{\beta}(\boldsymbol{t})\boldsymbol{e}_{\boldsymbol{x}} \tag{3.84}$$

where $\boldsymbol{\beta}(t)$ is a function of the variable damping and stiffness coefficients of the desired impedance and is a symmetric, positive definite and continuously differentiable diagonal matrix. The stability of the desired impedance characteristics can be examined using the following theorem.

Theorem 6. *If $\boldsymbol{M_d}$ is a constant, symmetric, positive definite diagonal matrix and $\boldsymbol{B_d}(t)$ and $\boldsymbol{K_d}(t)$ are symmetric, positive definite, continuously differentiable, varying damping and stiffness matrices, then with zero external force in (3.48), i.e., $\boldsymbol{F_e} = \mathbf{0}$ and a positive definite $\boldsymbol{c_1}$, the impedance characteristics will be asymptotically stable for $\forall t$ if the following conditions are satisfied:*

(i) $\boldsymbol{B_d(t) - c_1 M_d}$ *is a positive definite matrix,*

(ii) $\boldsymbol{c_1 K_d(t) - \frac{1}{2}\dot{K}_d(t) - \frac{1}{2}c_1\dot{B}_d(t)}$ *is positive definite.*

Proof. The proof can be found in Appendix A.10. □

From (3.65)b and (3.77), the damping and the stiffness parameters are obtained in the proposed controller as follows:

$$\boldsymbol{B_d}(t) = \boldsymbol{M_d(c_1 + c_2)} = \boldsymbol{M_d}\left(\boldsymbol{c_1} + diag\{c_{2i}\} + (\boldsymbol{I} - \boldsymbol{\Sigma})diag\{-c_{2i}exp(-\eta {z_{2i}}^2)\}\right) \tag{3.85}$$

$$\boldsymbol{K_d}(t) = \boldsymbol{M_d c_1 c_2} = \boldsymbol{M_d c_1}\left(diag\{c_{2i}\} + (\boldsymbol{I} - \boldsymbol{\Sigma})diag\{-c_{2i}exp(-\eta {z_{2i}}^2)\}\right). \tag{3.86}$$

Since the matrices $\boldsymbol{B_d}(t)$ and $\boldsymbol{K_d}(t)$ are diagonal, the following scalar equations can represent each entry of the respective matrices:

$$b_d = m_d \left[c_1 + c_2 \left(1 - exp(-\eta z_2^2)\right)\right] \tag{3.87}$$

$$k_d = m_d c_1 c_2 \left[1 - exp(-\eta z_2^2)\right] \tag{3.88}$$

where $m_d,\ b_d,\ k_d$ represent the diagonal elements of the matrices $\boldsymbol{M_d},\ \boldsymbol{B_d},\ \boldsymbol{K_d}$ respectively. Further, $c_1,\ c_2$ represent the diagonal elements of the matrices $\boldsymbol{c_1},\ \boldsymbol{c_2}$ respectively and z_2 represents the elements of the vector $\boldsymbol{z_2}$. Using the first condition of Theorem 6 and (3.87-3.88), the following can be derived:

$$c_2 \left(1 - exp(-\eta z_2^2)\right) > 0 \tag{3.89}$$

which is true since already by design $c_2 > 0$ and $\left(1 - exp(-\eta z_2^2)\right)$ is a positive semi-definite function. Using (3.87-3.88) and the second condition of Theorem 6, the following relation is obtained:

$$c_1 \left(1 - exp(-\eta z_2^2)\right) > 2\eta z_2 \dot{z}_2 exp(-\eta z_2^2). \tag{3.90}$$

Now, the desired impedance is obtained at the equilibrium of the sliding surface i.e., when $\boldsymbol{s = \dot{s} = 0}$. Since the derived control law decentralizes and stabilizes all the subsystems defined in backstepping, the following conditions hold when the sliding surface is reached:

$$\begin{cases} \dot{\boldsymbol{z}}_1 = & -\boldsymbol{c_1 z_1} \\ \dot{\boldsymbol{z}}_2 = & -\boldsymbol{c_2 z_2} \\ \dot{\boldsymbol{x}} = & -\boldsymbol{c_2 z_2 - c_1 \dot{z}_1 + \dot{x}_d}. \end{cases} \tag{3.91}$$

With the controlled system, the following Lyapunov function is considered and (3.91) is used in its time derivative.

$$\begin{aligned} V_{z_2} &= \frac{1}{2} \boldsymbol{z_2^T z_2} \\ \dot{V}_{z_2} &= \boldsymbol{z_2^T (\dot{z}_2)}. \end{aligned} \tag{3.92}$$

From (3.91) and (3.92), the following can be obtained:

$$\dot{V}_{z_2} = -\boldsymbol{z_2^T c_2 z_2} < 0, \quad \forall z_2 \neq 0. \tag{3.93}$$

Therefore, on the sliding surface $\boldsymbol{z_2^T \dot{z}_2} \leq 0$ and hence the inequality (3.90) will be satisfied for all nonzero $\boldsymbol{z_2}$ values. This shows that the impedance defined with the variable damping and stiffness through the backstepping design parameters is stable.

3.3.3 Simulation Results

The impedance controller designed using the proposed ABSMC-PID method is simulated for 3DoF operation of the 14DoF Coordinated Links (COOL) robot arm shown in Figure 2.12 of Chapter 2. The joints 1R, 4R and 7R are used for the simulation and the details of the 3DoF manipulator dynamics are given in Appendix A.9. It is assumed that only the position and the interaction force measurements are available and hence, the manipulator joint velocities are derived through pseudodifferentiation of the joint positions as mentioned in [2]. As a structural uncertainty, a load of 0.5kg is added to the manipulator end-effector and a position measurement noise bounded between ± 0.0001 rad is added as the unstructured uncertainty.

In the simulations the task space impedance control is considered. The following desired trajectory is defined for the x, y and z coordinates:

$$\boldsymbol{x_d} = [0.1\cos(t) + 0.2,\ 0.1\cos(t) + 0.2,\ 0.3]^T m. \tag{3.94}$$

with all the joints of the arm initially at 0 rad, thus making the initial location of the end-effector $\boldsymbol{x_0} = [0, 0, 0.56]^T$ m. In order to examine the interaction dynamics a solid horizontal wall is located at $pz_e = 0.33$m and a vertical wall is located at $px_e = 0.15$m that will work as constraints for the end-effector motion. The contact model is considered as a high stiffness spring system [177] as follows

$$\boldsymbol{F_e} = \boldsymbol{K_e}(\boldsymbol{x} - \boldsymbol{x_e}) \tag{3.95}$$

where $\boldsymbol{x_e} = [px_e, py_e, pz_e] = [0.15,\ 0,\ 0.33]m$ and $\boldsymbol{K_e} = diag\{K_x, K_y, K_z\}$ is the stiffness parameter of the environment. For x-direction $K_x = 2000$N/m and for z-direction $K_z = 10,000$N/m. There is no interaction along y-direction and hence $K_y = 0$. The interaction force will be zero when there is no contact of the end-effector with the external environment.

The parameters of the desired impedance used in the controller are as follows:

$$\boldsymbol{M_d} = \begin{bmatrix} 0.2 & 0 & 0 \\ 0 & 0.2 & 0 \\ 0 & 0 & 0.2 \end{bmatrix}, \quad \boldsymbol{B_d} = \begin{bmatrix} 10 & 0 & 0 \\ 0 & 16 & 0 \\ 0 & 0 & 8 \end{bmatrix}, \quad \boldsymbol{K_d} = \begin{bmatrix} 120 & 0 & 0 \\ 0 & 320 & 0 \\ 0 & 0 & 80 \end{bmatrix}.$$

The corresponding parameters $\boldsymbol{c_1}, \boldsymbol{c_2}$ of the ABSMC-PID are:

$$\boldsymbol{c_1} = \begin{bmatrix} 30 & 0 & 0 \\ 0 & 40 & 0 \\ 0 & 0 & 20 \end{bmatrix}, \quad \boldsymbol{c_2} = \begin{bmatrix} 20 & 0 & 0 \\ 0 & 40 & 0 \\ 0 & 0 & 20 \end{bmatrix}.$$

In order to induce variable damping and stiffness along the directions where the manipulator end-effector comes in contact with the external environment (i.e. x and z-directions), $\boldsymbol{c_2}$ is replaced with the following:

$$\boldsymbol{c_2} = (diag\{20,\ 40,\ 20\}) - (diag\{20,\ 40,\ 20\})\,(\boldsymbol{I} - \boldsymbol{\Sigma})\left(diag\{exp(-\eta_i z_{2i}^2)\}\right), \quad i = 1, 2, 3 \tag{3.96}$$

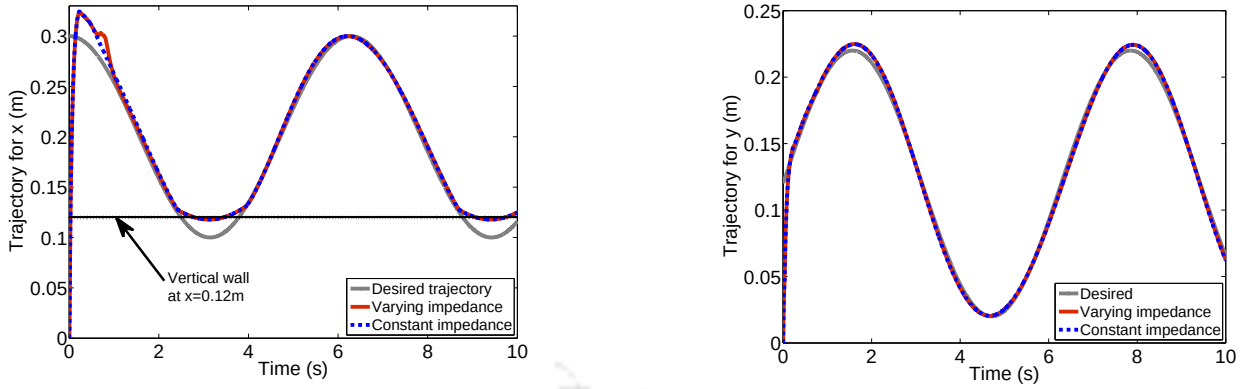

(a) Trajectory tracking along x-axis

(b) Trajectory tracking along y-axis

Figure 3.3: Tracking results with varying and constant impedance

where for the selection matrix $\Sigma_i = 1$ for free motion and $\Sigma_i = 0$ for contact motion and $\eta_i \in \boldsymbol{\eta} = diag\{100, 1, 1\}$. For the example under consideration, $\boldsymbol{c_2}$ has the following form:

$$\boldsymbol{c_2} = \begin{bmatrix} 20\left[1 - exp\left(-100 z_{21}^2\right)\right] & 0 & 0 \\ 0 & 40 & 0 \\ 0 & 0 & 20\left[1 - exp\left(-z_{23}^2\right)\right] \end{bmatrix}.$$

The parameters in the adaptive law are:

$$\Gamma = 100\boldsymbol{I}, \quad \boldsymbol{\epsilon} = 0.1\boldsymbol{I}. \tag{3.97}$$

The proportional constant of the sliding mode controller is $\boldsymbol{W} = 10\boldsymbol{I}$. The inertia matrix $\boldsymbol{M_T}$ of the manipulator is replaced with the estimated diagonal matrix $\bar{\boldsymbol{M}}_{\boldsymbol{b}} = diag\{2.5, 2.5, 10\}$. In order to test the influence of $\boldsymbol{c_2}$, the performances of the controller with both variable and constant values of $\boldsymbol{c_2}$ are compared.

The simulations results for trajectory tracking along the x and y axes are shown in Figure 3.3 and the interaction forces when the external obstacle is encountered are shown in Figure 3.4 with both the variable and constant values of controller gain $\boldsymbol{c_2}$. The torques produced by the controller for the three actuated joints are shown in Figure 3.5. The motion of the end-effector in the three dimensional Cartesian space is shown in Figure 3.6 along with the motion as observed in the x-y and y-z planes. As can be observed from Figure 3.3, in terms of tracking results during free motion both the constant and variable values of $\boldsymbol{c_2}$ offer almost the same performance. Notable improvement with the variable $\boldsymbol{c_2}$ is observed in the case of interaction force along the z-axis shown in Figure 3.4. As soon as the end-effector comes in contact with the wall, the maximum impact force with the variable c_2 is 26 N, whereas with the constant c_2 it is almost double, reaching up to 52 N. The input torques generated in both the cases are almost the same as can be observed in Figure 3.5. The motion of the end-effector in the x-y plane and the y-z plane are shown in Figure 3.6 for both varying and constant $\boldsymbol{c_2}$ values.

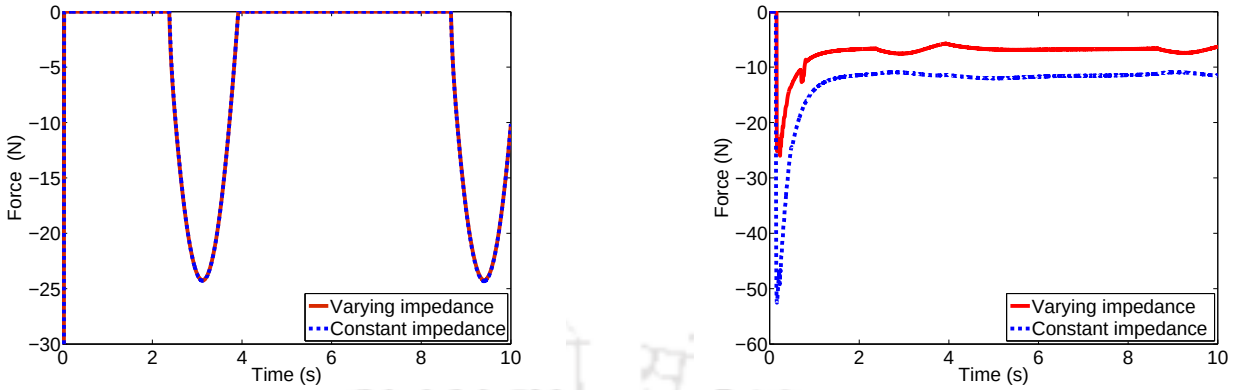

(a) Interaction force along x-axis

(b) Interaction force along z-axis

Figure 3.4: Interaction forces with varying and constant impedance

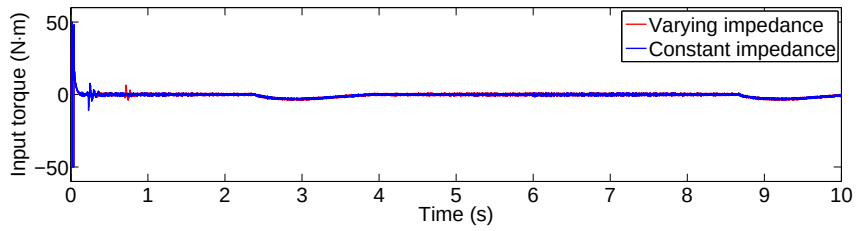

(a) Input torque for joint 1

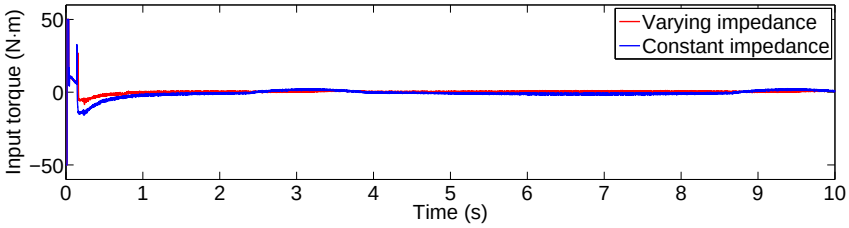

(b) Input torque for joint 2

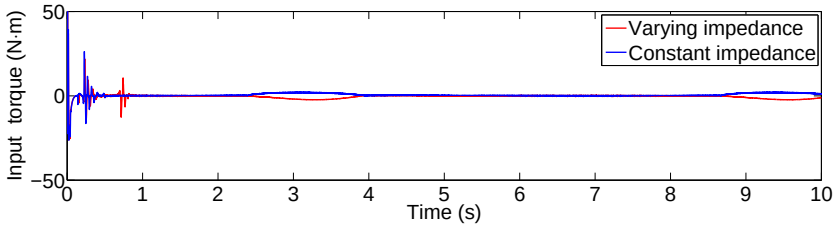

(c) Input torque for joint 3

Figure 3.5: Input torques for the manipulator joints with varying and constant impedance

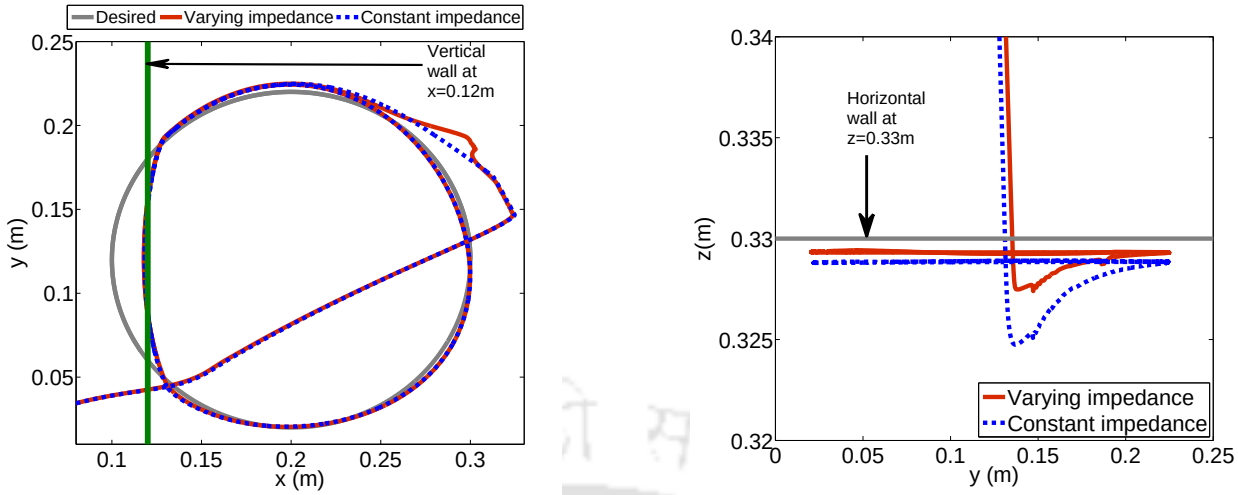

(a) Motion of the end-effector in x-y plane

(b) Motion of the end-effector in y-z plane

Figure 3.6: Motion of the end-effector in the Cartesian space

The norms of the input torques ($||u||$) for each joint and their total variations (TV) are listed in Table 3.3 and it is observed that these are comparable for both varying and constant $\boldsymbol{c_2}$ values.

Table 3.3: Performance indices for the input torques

	x-axis	y-axis	z-axis
$\|\|u_v\|\|$ (N·m)	316.59	341.32	230.78
$\|\|u_c\|\|$ (N·m)	322.63	407.32	233.77
TV_v (N·m)	6.47×10^3	4.01×10^3	1.62×10^3
TV_c (N·m)	5.46×10^3	4.56×10^3	1.31×10^3

$||u_v||, ||TV_v||$- Input norm and TV with varying c_2
$||u_c||, ||TV_c||$- Input norm and TV with constant c_2

3.4 Summary

The ABSMC-PID method proposed in this chapter provides a much simpler design strategy as well as simpler controller structure as compared to the IBSMC and the IADSC methods with minimal compromise in terms of the controller performance. The PID type sliding surface aids in achieving a faster transient response and yields a low steady state error. Use of the adaptive law to estimate the sliding mode controller gain and the constant plus proportional reaching law help in mitigating the chattering in the input. The comparison with other control methods based on disturbance observers showed that the proposed ABSMC-PID could improve the performance. The backstepping method used in the proposed controller enabled methodical building of an asymptotically stable control law. The same controller design algorithm was used for impedance control of the manipulator. The non-linear damping and stiffness induced by the variable parameter of the backstepping method helped in

lowering the impact force when the end-effector encounterd any surface with high stiffness.

However, the above controller design is based on the dynamical model of the manipulator. With increased DoF, the structural complexity of the manipulator dynamics increases. This complexity issue becomes severe especially if the manipulator wrist is not spherical. Using such complex manipulator model in the control law will unnecessarily complicate the controller structure and additionally require more memory space and compilation time for software implementation. As a solution, a time delay based estimation of the manipulator model is proposed in the next chapter that will lead to a model free controller design.

4

Adaptive Backstepping based Fast Terminal Sliding Mode Controller

Contents

4.1 Introduction

The backstepping sliding mode controllers proposed so far rely on the system model to form the control law. As mentioned in the previous chapter, for a highly coupled and nonlinear system like the robot manipulator, relying on a model based controller may lead to a structurally complex control law which is undesirable. Moreover, the manipulator model may not be available and often the derived dynamic model is prone to errors. Therefore, instead of relying on the exact manipulator model it may be estimated which will highly simplify the inverse dynamic control.

The time delay control (TDC) was first proposed by Youcef-Toumi and Ito [25] for systems having unknown or highly varying parameters. The method involves estimating the unknown system model based on the input and state values of the previous sampling instant assuming that the inputs and states are smooth. The method has proved effective not only in case of unknown system parameters but also in case of the systems with highly complex nonlinear model. The estimation of nonlinearities used in the TDC method is called time delay estimation (TDE) that can be useful in designing model free control laws for the robot manipulators. Some examples of applications of TDC in robotics are found in [178–181]. The most attractive quality of the TDE is that it does not require any prior knowledge of system parameters and involves no parameter that might need tuning. For applying TDE to robot manipulators the only additional information required is the joint acceleration data which can be easily derived from the available joint position information using robust differentiation method [182].

In [178] Jin *et al.* proposed the time delay controller (TDC) [25, 183] producing a terminal sliding surface of error dynamics for the manipulator control. The terminal sliding surface was introduced for enhancing the system performance which was degraded due to the time delay estimation error. The terminal attractors initially proposed by Zak [77] have been used as sliding surface to design a terminal sliding mode (TSM) control [79]. But the main disadvantages of the TSM are the singularity problem and the degradation of convergence performance when the error states are far from the equilibrium. To avoid the singularity problem, the non-singular terminal sliding mode was proposed in [80] and for consistent convergence performance, the fast terminal sliding mode (FTSM) control was suggested in [24]. Combination of these two have resulted in non-singular fast terminal sliding mode control, which has been effectively used for various nonlinear systems [184–186].

In this chapter TDE is used to compensate for the soft nonlinearities like the Coriolis, centrifugal, viscous and Coulomb friction, gravitational torques and thereby simplifying the system model. The model free controller uses the backstepping sliding mode method [129] with a non-singular fast terminal sliding surface. The resulting controller structure has reduced complexity and is suitable for practical implementation.

The organization of the chapter is as follows. The controller design methodology is explained in Section 4.2. Simulation results are presented in Section 4.3. A brief summary of the chapter is provided in Section 4.4.

4.2 Controller Design

The controller will be designed for the combined manipulator-actuator dynamics for an n-DoF manipulator as described in Section 3.2.1 of Chapter 3 and represented by the following differential equation:

$$\boldsymbol{M_h\ddot{q} + C_h\dot{q} + G_h + \tau_f = \tau_m}. \tag{4.1}$$

In (4.1), $\boldsymbol{M_h} \in \mathbb{R}^{n\times n}$ denotes the inertia matrix, $\boldsymbol{C_h} \in \mathbb{R}^{n\times n}$ is the Coriolis matrix, $\boldsymbol{G_h} \in \mathbb{R}^n$ represents the gravitational terms and $\boldsymbol{\tau_m} \in \mathbb{R}^n$ is the actuator torque vector for the manipulator joints. The vector $\boldsymbol{\tau_f} \in \mathbb{R}^n$ includes all the structured and unstructured uncertainties present in the system. Assuming $\boldsymbol{\tau_f}$ to be unknown and bounded, at first the controller will be designed for the following nominal system:

$$\boldsymbol{M_h\ddot{q} + C_h\dot{q} + G_h = \tau_m}. \tag{4.2}$$

Initially backstepping is used in the controller to derive a suitable nonsingular terminal sliding surface [24] based on the error variables. In the final step of backstepping, the final control law is derived using the time delay estimation (TDE) [25] to estimate the soft nonlinearities of the system model. The controller design process can be divided into three steps described as follows.

Step I:
For the backstepping method, tracking error is chosen as the first regulatory variable defined as:

$$\begin{aligned} \boldsymbol{z_1} &= \boldsymbol{q - q_d} \\ \boldsymbol{\dot{z}_1} &= \boldsymbol{\dot{q} - \dot{q}_d}. \end{aligned} \tag{4.3}$$

A control Lyapunov function (CLF) V_1 is defined as

$$\begin{aligned} V_1 &= \frac{\mathbf{1}}{\mathbf{2}}\boldsymbol{z_1^T z_1} \\ \dot{V}_1 &= \boldsymbol{z_1^T \dot{z}_1 = z_1^T(\dot{q} - \dot{q}_d)}. \end{aligned} \tag{4.4}$$

Assuming $\boldsymbol{\dot{q}}$ to be the controlling term in (4.3), a synthetic control $\boldsymbol{\alpha_1}$ is chosen such that $\boldsymbol{\dot{q} = \alpha_1}$ to stabilize the subsystem. Using the CLF, $\boldsymbol{\alpha_1}$ is derived as

$$\boldsymbol{\alpha_1 = -c_1 z_1 + \dot{q}_d} \tag{4.5}$$

where $\boldsymbol{c_1} = diag(c_{1i}),\ i = 1 \ldots n$ and $c_{1i} > 0$, is a user defined constant diagonal matrix.

Step II:
The next regulatory variable $\boldsymbol{z_2}$ is defined as the difference between $\boldsymbol{\alpha}_1$ and $\boldsymbol{\dot{q}}$ since the actual control

is not applied yet and hence these two terms will not be equal. So, $\boldsymbol{z_2}$ is given by

$$\begin{aligned}\boldsymbol{z_2} =& \dot{\boldsymbol{q}} - \boldsymbol{\alpha_1} = \dot{\boldsymbol{q}} + \boldsymbol{c_1 z_1} - \dot{\boldsymbol{q}}_{\boldsymbol{d}} \\ \dot{\boldsymbol{z}}_{\boldsymbol{2}} =& \ddot{\boldsymbol{q}} - \ddot{\boldsymbol{q}}_{\boldsymbol{d}} + \boldsymbol{c_1}\dot{\boldsymbol{z}}_{\boldsymbol{1}}.\end{aligned} \tag{4.6}$$

A nonsingular fast terminal sliding (NFTS) surface [184] is now chosen as

$$\boldsymbol{s} = \boldsymbol{z_1} + \beta \boldsymbol{z_2^{\delta}} = \boldsymbol{0} \tag{4.7}$$

where $|\boldsymbol{z_2}|^{\delta} \triangleq \left[|z_{21}|^{\delta},\ |z_{22}|^{\delta}, \ldots, |z_{2n}|^{\delta}\right]^T$ and $\beta > 0$, $1 < \delta < 2$ are user defined design parameters. Using (4.3) and (4.6) in (4.7) the following can be derived:

$$\boldsymbol{q_e} + \beta(\dot{\boldsymbol{q}}_{\boldsymbol{e}} + \boldsymbol{c_1 q_e})^{\delta} = \boldsymbol{0} \tag{4.8}$$

where $\boldsymbol{q_e} = \boldsymbol{q} - \boldsymbol{q_d}$ is the tracking error. The surface proposed in (4.8) has the same structure as the NFTS surface proposed in [184].

From (4.8), it is observed that when the error is far away from the equilibrium, a fast convergence rate is achieved; whereas closer to 0, the terminal attractor becomes the dominating dynamics driving the states to zero in finite time.

In order to avoid the complex value problem, the sliding surface is modified as [187]

$$\boldsymbol{s} = \boldsymbol{z_1} + \beta |\boldsymbol{z_2}|^{\delta} \circ sign(\boldsymbol{z_2}) = \boldsymbol{0}. \tag{4.9}$$

Remark 7. *The sliding variable $\boldsymbol{s}$ is a continuous and differentiable function and its derivative $\dot{\boldsymbol{s}}$ is also continuous as shown in Appendix A.11.*

Remark 8. *The time $\boldsymbol{T_{re}}$ required to reach from $\boldsymbol{q_e} = \boldsymbol{q_{e0}}$ (initial value of the error when the sliding surface is reached) to $\boldsymbol{q_e} = \boldsymbol{0}$ using the fast terminal sliding surface as shown in [184] is given by:*

$$\boldsymbol{T_{re}} = \frac{\boldsymbol{c_1^{-1}}}{(1-a)} \left[\ln\left(b + \boldsymbol{c}_1 |\boldsymbol{q}_{e0}|^{1-a}\right) - \ln(b)\right]. \tag{4.10}$$

where $b = (\frac{1}{\beta})^d$, $d = \frac{1}{\delta}$.

The subsystem (4.6) is rewritten as follows:

$$\dot{\boldsymbol{z}}_{\boldsymbol{2}} = \boldsymbol{M_h^{-1}}(\boldsymbol{\tau_m} - \boldsymbol{C_h}\dot{\boldsymbol{q}} - \boldsymbol{G_h}) - \ddot{\boldsymbol{q}}_{\boldsymbol{d}} + \boldsymbol{c_1}\dot{\boldsymbol{z}}_{\boldsymbol{1}}. \tag{4.11}$$

The control law $\boldsymbol{\tau_m}$ will now be derived in two parts as

$$\boldsymbol{\tau_m} = \boldsymbol{\tau_{tde}} + \boldsymbol{\tau_{sm}} \tag{4.12}$$

where $\boldsymbol{\tau_{tde}}$ denotes the control action designed using the time delay estimation of the system nonlinearities and uncertainties and $\boldsymbol{\tau_{sm}}$ is the control input derived from the sliding mode.

Step III:
In this step the control law is derived based on the sliding mode methodology and time delay control. In order to design $\boldsymbol{\tau_{sm}}$, the reaching law approach [158] is followed. A power rate reaching law combined with the proportional reaching term is used for obtaining a fast convergence rate for the reaching phase as

$$\dot{\boldsymbol{s}} = -\boldsymbol{k} \circ |\boldsymbol{s}|^{\rho} \circ sign(\boldsymbol{s}) - \boldsymbol{W}\boldsymbol{s} \tag{4.13}$$

where $0 < \rho < 1$, $\boldsymbol{k} = [k_1, k_2, \dots k_n]^T > 0;\ i = 1, \dots, n$ and $\boldsymbol{W} = diag(W_i),\ W_i > 0;\ i = 1, \dots, n$ are the user defined controller parameters with $|\boldsymbol{s}|^{\rho} \triangleq \left[|s_1|^{\rho},\ |s_2|^{\rho}, \dots,\ |s_n|^{\rho}\right]^T$.

The controller gain $\boldsymbol{k}$ determines the system robustness against uncertainties. In case of known bounds of the uncertainty, the value of $\boldsymbol{k} > \boldsymbol{0}$ is set higher than the uncertainty bound; however, it is always not possible to know the upper bound of the uncertainty affecting the system. In such cases $\boldsymbol{k}$ is adaptively tuned based on the system error. Moreover, the amount of control energy used and chattering in the control input are proportional to the value of $\boldsymbol{k}$. Since adaptive tuning will vary $\boldsymbol{k}$ according to system error, its value will be low when error is nearer to zero which leads to reduced control energy and chattering. The tuning law used here is given by

$$\dot{\hat{\boldsymbol{k}}} = \boldsymbol{\Gamma}(|\boldsymbol{s}|^{\rho+1} - \boldsymbol{\epsilon}\hat{\boldsymbol{k}}) \tag{4.14}$$

where $\boldsymbol{\Gamma} = diag(\Gamma_i),\ \Gamma_i > 0;\ i = 1, \dots, n$ is the adaptive gain that determines the speed of adaptation and $\boldsymbol{\epsilon} = diag(\epsilon_i),\ \epsilon_i > 0; i = 1, \dots, n$ is the leakage parameter [188]. The leakage term $-\boldsymbol{\Gamma\epsilon}\hat{\boldsymbol{k}}$ prevents over-adaptation of $\hat{k}$.

Remark 9. *As can be found in [24] the combination of the power rate and exponential reaching law yields a reaching time T_r as*

$$T_r = \frac{W^{-1}}{(1-\rho)}\left[\ln\left(\hat{k} + W|s_0|^{1-\rho}\right) - \ln(\hat{k})\right] \tag{4.15}$$

where $\boldsymbol{s_0}$ is the initial value of $\boldsymbol{s}$.

Using (4.9) and (4.11) gives

$$\begin{aligned}\dot{\boldsymbol{s}} =& \dot{\boldsymbol{z}}_{\boldsymbol{1}} + \beta\delta|\boldsymbol{z_2}|^{\delta-1} \circ \dot{\boldsymbol{z}}_{\boldsymbol{2}} \\ =& \dot{\boldsymbol{z}}_{\boldsymbol{1}} + \beta\delta|\boldsymbol{z_2}|^{\delta-1} \circ \left(\boldsymbol{M_h^{-1}}(\boldsymbol{\tau_m} - \boldsymbol{C_h}\dot{\boldsymbol{q}} - \boldsymbol{G_h}) - \ddot{\boldsymbol{q}}_{\boldsymbol{d}} + \boldsymbol{c_1}\dot{\boldsymbol{z}}_{\boldsymbol{1}}\right).\end{aligned} \tag{4.16}$$

Detailed derivation of $\dot{\boldsymbol{s}}$ is shown in Appendix A.12.

From (4.13) and (4.16), $\boldsymbol{\tau_{sm}}$ is derived as follows:

$$\boldsymbol{\tau_{sm}} = \boldsymbol{C_h}\dot{\boldsymbol{q}} + \boldsymbol{G_h} + \boldsymbol{M_h}(\ddot{\boldsymbol{q}}_{\boldsymbol{d}} - \boldsymbol{c_1}\dot{\boldsymbol{z}}_{\boldsymbol{1}}) - \frac{1}{\delta\beta}|\boldsymbol{z_2}|^{1-\delta} \circ \boldsymbol{M_h}\left(\dot{\boldsymbol{z}}_{\boldsymbol{1}} + \hat{\boldsymbol{k}} \circ |\boldsymbol{s}|^{\rho} \circ sign(\boldsymbol{s}) + \boldsymbol{W}\boldsymbol{s}\right). \tag{4.17}$$

The model of the robot manipulator contains the soft nonlinearities (centripetal, centrifugal and gravitational terms i.e., $\boldsymbol{C_h(q, \dot{q})\dot{q} + G_h(q)}$ and any other frictional and external torques) which are

estimated through the time delay estimation (TDE) method [178]. From the dynamics of the robot manipulator (4.1), the following can be found:

$$\boldsymbol{C_h\dot{q} + G_h + \tau_f = \tau_m - M_h\ddot{q}} \tag{4.18}$$

which can be equivalently expressed as

$$\boldsymbol{H = \tau_m - M_h\ddot{q}} \tag{4.19}$$

where $\boldsymbol{H = C_h\dot{q} + G_h + \tau_f}$ is the term containing the nonlinearities of the system associated with the frictional and the gravitational torques of the manipulator. The estimate of $\boldsymbol{H}$, denoted by $\boldsymbol{\hat{H}}$ is considered as the TDE input to the system as

$$\boldsymbol{\tau_{tde} \triangleq \hat{H}}. \tag{4.20}$$

At time instant t, $\boldsymbol{H}$ is obtained as

$$\boldsymbol{H}(t) = \boldsymbol{\tau_m}(t) - \boldsymbol{M_h}(t)\ddot{\boldsymbol{q}}(t) \tag{4.21}$$

where $\bullet(t)$ indicates the values of the respective terms at time instant t. Considering a very small time delay L (for example, in case of software application L will be the sampling time) and assuming $\boldsymbol{H}(t)$ to be a smooth continuous function, the delayed term $\boldsymbol{H}(t-L)$ is used as an estimate of $\boldsymbol{H}(t)$, meaning

$$\boldsymbol{\hat{H}}(t) \triangleq \boldsymbol{H}(t-L). \tag{4.22}$$

Therefore, assuming the joint acceleration is measurable, the TDE input to the system is derived as

$$\boldsymbol{\tau_{tde} = \hat{H} = \tau_m}(t-L) - \boldsymbol{M_h}(t-L)\ddot{\boldsymbol{q}}(t-L). \tag{4.23}$$

Using (4.23) in (4.17), the TDE based sliding mode control law for the robot manipulator is obtained as

$$\boldsymbol{\tau_m} = \boldsymbol{\hat{H} + M_h(\ddot{q}_d - c_1\dot{z}_1)} - (\delta\beta)^{-1}|\boldsymbol{z_2}|^{1-\delta} \circ \boldsymbol{M_h}\left(\boldsymbol{\dot{z}_1 + \hat{k} \circ |s|^{\rho} \circ sign(s) + W s}\right). \tag{4.24}$$

Considering the actuator saturation, the designed control law is modified as $\boldsymbol{\tau_{m\_mod}}$ given by

$$\boldsymbol{\tau_{m\_mod}} = sat_{|\boldsymbol{\tau_L}|}(\boldsymbol{\tau_m}) \tag{4.25}$$

where

$$sat_{|\boldsymbol{\tau_L}|}(\boldsymbol{\tau_m}) = \begin{cases} |\boldsymbol{\tau_L}|sign(\boldsymbol{\tau_m}), & |\boldsymbol{\tau_m}| > |\boldsymbol{\tau_L}| \\ \boldsymbol{\tau_m}, & |\boldsymbol{\tau_m}| \leq |\boldsymbol{\tau_L}| \end{cases}$$

with $\boldsymbol{\tau_L}$ denoting the limit of the allowable torque.

4.2.1 Stability Analysis

The Lyapunov based stability of the controlled system and the adaptive law are analyzed in this section. In order to prove the controlled system's stability, the boundedness of the time delay estimation error is ascertained at first. The TDE error can be represented as

$$\begin{aligned}\boldsymbol{\Delta H} =& \hat{\boldsymbol{H}} - \boldsymbol{H} \\ =& \big[\boldsymbol{C_h}(\boldsymbol{t-L})\dot{\boldsymbol{q}}(\boldsymbol{t-L}) - \boldsymbol{C_h}(\boldsymbol{t})\dot{\boldsymbol{q}}(\boldsymbol{t})\big] + \big[\boldsymbol{G_h}(\boldsymbol{t-L}) - \boldsymbol{G_h}(\boldsymbol{t})\big] + \big[\boldsymbol{\tau_f}(\boldsymbol{t-L}) - \boldsymbol{\tau_f}(\boldsymbol{t})\big]. \end{aligned} \tag{4.26}$$

Now, being a part of manipulator dynamics, both the functions $\boldsymbol{C}_h(\bullet)$ and $\boldsymbol{G}_h(\bullet)$ are smooth and hence for a sufficiently small time delay, the differences $\boldsymbol{C}_h(t-L)\dot{\boldsymbol{q}}(t-L) - \boldsymbol{C}_h(t)\dot{\boldsymbol{q}}(t)$ and $\boldsymbol{G_h}(t-L) - \boldsymbol{G_h}(t)$ will be bounded. Moreover, $\boldsymbol{\tau}_f$ includes the gear backlash, frictional force and other such unaccounted disturbances which are always bounded for the robot manipulator. Thus the TDE error will be bounded.

Replacing the control law (4.24) in (4.16), the time derivative of the sliding variable is obtained as follows:

$$\begin{aligned}\dot{\boldsymbol{s}} =& -\hat{\boldsymbol{k}} \circ |\boldsymbol{s}|^{\rho} \circ sign(\boldsymbol{s}) - \boldsymbol{W}\boldsymbol{s} + \beta\delta|\boldsymbol{z_2}|^{\delta-1} \circ \boldsymbol{M_h^{-1}}(\hat{\boldsymbol{H}} - \boldsymbol{H}) \\ =& -\hat{\boldsymbol{k}} \circ |\boldsymbol{s}|^{\rho} \circ sign(\boldsymbol{s}) - \boldsymbol{W}\boldsymbol{s} + \beta\delta|\boldsymbol{z_2}|^{\delta-1} \circ \boldsymbol{M_h^{-1}}\boldsymbol{\Delta H}. \end{aligned} \tag{4.27}$$

4.2.1.1 Stability of the Adaptive Law

The stability of the adaptive law is analyzed using the following Lyapunov function,

$$V_k = \frac{1}{2}(\boldsymbol{s^T s} + \tilde{\boldsymbol{k}}^{\boldsymbol{T}}\boldsymbol{\Gamma^{-1}}\tilde{\boldsymbol{k}}) \tag{4.28}$$

where

$$\tilde{\boldsymbol{k}} = \hat{\boldsymbol{k}} - \boldsymbol{k} \tag{4.29}$$

is the difference between the adapted value $\hat{\boldsymbol{k}}$ and the arbitrary value $\boldsymbol{k} > 0$ to which $\hat{\boldsymbol{k}}$ converges. Using (4.14), the time derivative of V_k is obtained as

$$\dot{V}_k = \boldsymbol{s^T}\dot{\boldsymbol{s}} + \tilde{\boldsymbol{k}}^{\boldsymbol{T}}(|\boldsymbol{s}|^{\rho+1} - \boldsymbol{\epsilon}\hat{\boldsymbol{k}}). \tag{4.30}$$

From (4.29), the following can be derived using Lemma 4,

$$\tilde{\boldsymbol{k}}^{\boldsymbol{T}}\boldsymbol{\epsilon}\hat{\boldsymbol{k}} \geq \frac{\boldsymbol{1}}{\boldsymbol{2}}(\tilde{\boldsymbol{k}}^{\boldsymbol{T}}\boldsymbol{\epsilon}\tilde{\boldsymbol{k}} - \boldsymbol{k}^{\boldsymbol{T}}\boldsymbol{\epsilon}\boldsymbol{k}). \tag{4.31}$$

Using (4.27) and (4.31) in (4.30) yields

$$\begin{aligned}\dot{V}_k \leq & -\boldsymbol{k^T}|\boldsymbol{s}|^{\rho+1} - \boldsymbol{s^T W s} + \beta\delta \boldsymbol{s^T}|\boldsymbol{z_2}|^{\delta-1} \circ \boldsymbol{M_h^{-1}\Delta H} - \frac{\mathbf{1}}{\mathbf{2}}\tilde{\boldsymbol{k}}^{\boldsymbol{T}}\boldsymbol{\epsilon}\tilde{\boldsymbol{k}} + \frac{\mathbf{1}}{\mathbf{2}}\boldsymbol{k^T\epsilon k} \\ \leq & -\boldsymbol{s^T W s} - \frac{\mathbf{1}}{\mathbf{2}}\tilde{\boldsymbol{k}}^{\boldsymbol{T}}\boldsymbol{\epsilon}\tilde{\boldsymbol{k}} - \left[\boldsymbol{k} - \beta\delta|\boldsymbol{s}|^{-\rho} \circ |\boldsymbol{z_2}|^{\delta-1} \circ |\boldsymbol{M_h^{-1}}||\boldsymbol{\Delta H}|\right]^T |\boldsymbol{s}|^{\rho+1} + \frac{1}{2}\boldsymbol{k^T\epsilon k}. \end{aligned} \tag{4.32}$$

The TDE error $\boldsymbol{\Delta H}$ has been considered to be bounded for small sampling time. Moreover, using Property 3, the inertia matrix $\boldsymbol{M_h}$ of the manipulator has been found to be bounded. Since $\boldsymbol{k}$ is an arbitrary value, it may be made to satisfy the condition

$$\boldsymbol{k} > \beta\delta|\boldsymbol{s}|^{-\rho} \circ |\boldsymbol{z_2}|^{\delta-1} \circ |\boldsymbol{M_h^{-1}}||\boldsymbol{\Delta H}|. \tag{4.33}$$

Hence it follows that

$$\begin{aligned}\dot{V}_k \leq & -\boldsymbol{s^T W s} - \frac{\mathbf{1}}{\mathbf{2}}\tilde{\boldsymbol{k}}^{\boldsymbol{T}}\boldsymbol{\epsilon}\tilde{\boldsymbol{k}} + \frac{1}{2}\boldsymbol{k}^T\boldsymbol{\epsilon k} \\ \leq & -2\psi V_k + \rho \end{aligned} \tag{4.34}$$

where, $\psi = \lambda_{min}\boldsymbol{Q}$, $\boldsymbol{Q} = (diag\{\boldsymbol{W}, 0.5\boldsymbol{\Gamma\epsilon}\})$ and $\rho = \frac{1}{2}\boldsymbol{k}^T\boldsymbol{\epsilon k}$. Thus, for $V_k(0) > \frac{\rho}{2\psi}$ and $\frac{\rho}{2\psi} < 1$, (4.34) will be negative definite and $V_k(t)$ will converge to a ball of very small radius given by $\frac{\rho}{2\psi}$.

4.2.1.2 Stability of the Sliding Surface

Lemma 10. *The sliding surface will be finite time stable provided the adaptive law is stable and (4.33) is satisfied.*

Proof. For the sliding surface $\boldsymbol{s} = \mathbf{0}$, Lyapunov function V_s is chosen as follows,

$$V_s = \frac{1}{2}\boldsymbol{s}^T\boldsymbol{s}. \tag{4.35}$$

Using (4.16), the time derivative of V_s is derived as

$$\dot{V}_s = \boldsymbol{s}^T\dot{\boldsymbol{s}} = \boldsymbol{s}^T\left[\dot{\boldsymbol{z}}_{\mathbf{1}} + \beta\delta|\boldsymbol{z_2}|^{\delta-1} \circ \left(\boldsymbol{M_h^{-1}}(\boldsymbol{\tau} - \boldsymbol{C_h}\dot{\boldsymbol{q}} - \boldsymbol{G_h}) - \ddot{\boldsymbol{q}}_{\boldsymbol{d}} + \boldsymbol{c_1}\dot{\boldsymbol{z}}_{\mathbf{1}}\right)\right] \tag{4.36}$$

Using (4.24) yields

$$\begin{aligned}\dot{V}_s = & -\hat{\boldsymbol{k}}^T|\boldsymbol{s}|^{\rho+1} - \boldsymbol{s}^T\boldsymbol{W s} + \beta\delta\boldsymbol{s}^T|\boldsymbol{z_2}|^{\delta-1} \circ \boldsymbol{M_h^{-1}\Delta H} \\ \leq & -\hat{\boldsymbol{k}}^T|\boldsymbol{s}|^{\rho+1} - \boldsymbol{s}^T\boldsymbol{W s} + \beta\delta\boldsymbol{s}^T|\boldsymbol{z_2}|^{\delta-1} \circ \boldsymbol{M_h^{-1}}|\boldsymbol{\Delta H}| \\ \leq & -(\tilde{\boldsymbol{k}} + \boldsymbol{k})^T|\boldsymbol{s}|^{\rho+1} - \boldsymbol{s}^T\boldsymbol{W s} + \beta\delta\boldsymbol{s}^T|\boldsymbol{z_2}|^{\delta-1} \circ \boldsymbol{M_h^{-1}}|\boldsymbol{\Delta H}| \\ \leq & -\tilde{\boldsymbol{k}}^T|\boldsymbol{s}|^{\rho+1} - \boldsymbol{s}^T\boldsymbol{W s} - \boldsymbol{k}^T|\boldsymbol{s}|^{\rho+1} + \beta\delta\boldsymbol{s}^T|\boldsymbol{z_2}|^{\delta-1} \circ \boldsymbol{M_h^{-1}}|\boldsymbol{\Delta H}| \\ \leq & -(|\boldsymbol{s}|^{\frac{\rho+1}{2}})^T\tilde{\boldsymbol{K}}|\boldsymbol{s}|^{\frac{\rho+1}{2}} - \boldsymbol{s}^T\boldsymbol{W s} - \left(\boldsymbol{k} - \beta\delta|\boldsymbol{s}|^{-\rho} \circ |\boldsymbol{z_2}|^{\delta-1} \circ \boldsymbol{M_h^{-1}}|\boldsymbol{\Delta H}|\right)^T |s|^{\rho+1} \end{aligned} \tag{4.37}$$

where $\tilde{\boldsymbol{K}} = diag(\tilde{k}_i)$ and $\boldsymbol{K} = diag(k_i)$ are the diagonal matrices with entries from $\tilde{\boldsymbol{k}}$ and $\boldsymbol{k}$ vectors.

Since the elements of $\boldsymbol{k}$ are arbitrary constant values, it may be made to satisfy the following:

$$\boldsymbol{k} \geq \beta\delta|\boldsymbol{s}|^{-\rho}|\circ \boldsymbol{z_2}|^{\delta-1} \circ \boldsymbol{M_h^{-1}}|\boldsymbol{\Delta H}|. \tag{4.38}$$

Therefore, (4.37) can be rewritten as follows:

$$\begin{aligned}\dot{V}_s \leq & -\boldsymbol{s}^T\boldsymbol{W}\boldsymbol{s} - (|\boldsymbol{s}|^{\frac{\rho+1}{2}})^T\tilde{\boldsymbol{K}}|\boldsymbol{s}|^{\frac{\rho+1}{2}} \\ \leq & -\eta_1 V_s - \eta_2 V_s^{\frac{\rho+1}{2}}.\end{aligned} \tag{4.39}$$

As shown in Lemma 1 in [189], for $\eta_1 > 0, \eta_2 > 0$ and $0 < \rho < 1$, with initial time t_0, V_s will converge to zero in a finite time t_s where

$$t_s \leq t_0 + \frac{2}{\eta_1(1-\rho)} \ln \frac{\eta_1 V_s^{\frac{1-\rho}{2}}(t_0) + \eta_2}{\eta_2}. \tag{4.40}$$

The above indicates that the sliding surface also converges to the equilibrium ($\boldsymbol{s} = 0,\ \dot{\boldsymbol{s}} = 0$) in a finite time and hence $\boldsymbol{s = 0}$ is a stable surface.

□

4.3 Simulation Results

The proposed adaptive backstepping based fast terminal sliding mode controller (ABFTSMC) is applied to a 2 DoF robotic manipulator used in [3] through MATLAB Simulink simulations with a sampling time of $L = 1ms$. The performance of the proposed controller is compared with the robust finite time stability control (RFTSC) proposed by Zhao *et al.* [3]. The details of the mathematical model of the manipulator are given in Appendix A.13.

The parameters of the manipulator are considered as: $m_1 = 0.5kg$, $m_2 = 1.5kg$, $l_1 = 1m$, $l_2 = 0.8m$, $J_1 = 5kgm^2$ and $J_2 = 5kgm^2$. In the controller, the manipulator link masses m_1 and m_2 are considered with 20% error as $\hat{m}_1 = 0.4$ kg and $\hat{m}_2 = 1.2$ kg respectively.

The parameters of the proposed controller (4.24) are: $\beta = 1.5$, $\delta = 5/7$, $\boldsymbol{c_1} = diag\{3, 3\}$, $\boldsymbol{W} = diag\{1, 1\}$, $\boldsymbol{\Gamma} = diag\{10, 10\}$, $\boldsymbol{\epsilon} = diag\{0.1, 0.1\}$ and $\rho = 0.3$. The limits for the actuator torques are taken as ± 70 Nm and in the control law, the manipulator inertia matrix $\boldsymbol{M_h}$ is replaced with a constant diagonal matrix $\boldsymbol{M_{ho}} = [0.5\ \ 0;\ 0\ \ 0.1]$ in order to further simplify the controller structure.

The details of the RFTSC based controller and the parameter values proposed by Zhao *et al.* [3] are given in Appendix A.14.

4.3.1 Case 1

The RFTSC proposed in [3] is used on the robot manipulator described in Appendix A.13 with a high frequency disturbance of $10\sin(100t)$ in the joint measurement occurring between $3.5\ s \leq t < 5\ s$. In order to observe the coupling effects, $q_{d1} = 1\ rad$ was commanded at $t = 0$ and then at $t = 1\ s$ $q_{d2} = 1\ rad$ was commanded.

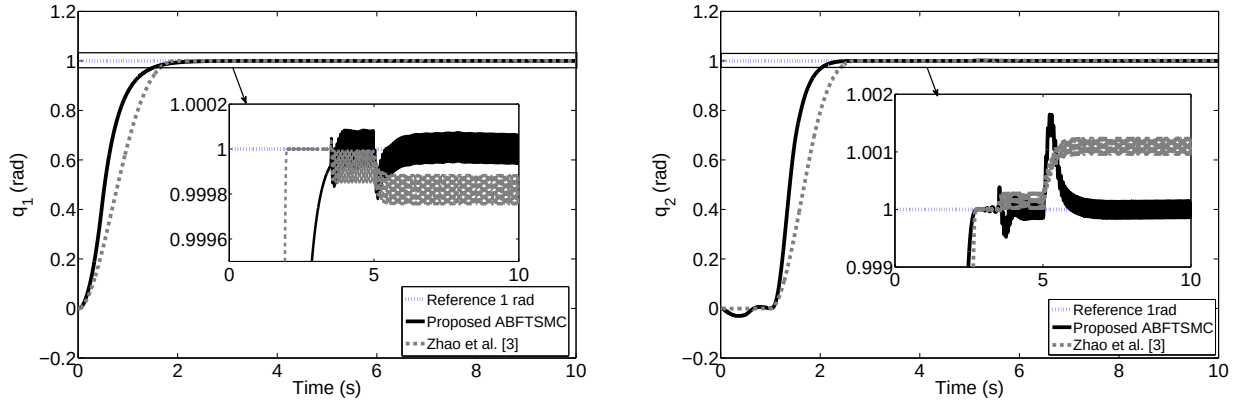

(a) Tracking Response of joint 1 (b) Tracking Response of joint 2

Figure 4.1: Tracking response with the proposed controller and RFTSC proposed by Zhao *et al.* [3] for Case 1

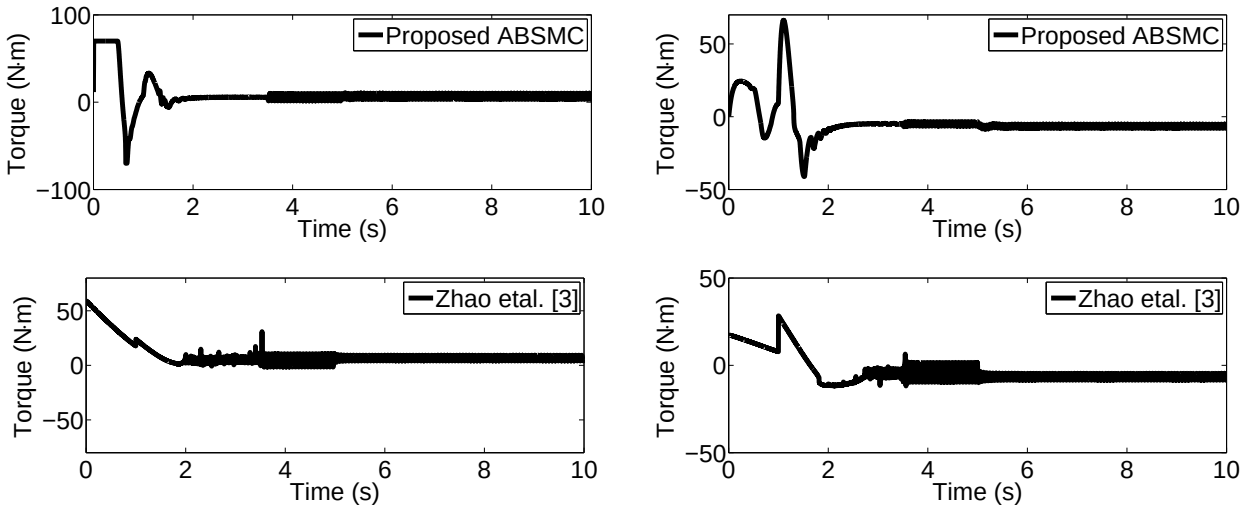

(a) Input torque of joint 1 (b) Input torque of joint 2

Figure 4.2: Input torques with the proposed controller and RFTSC proposed by Zhao *et al.* [3] for Case 1

Simulation results for position tracking are shown in Figure 4.1 and the control torques are shown in Figure 4.2. As it is clearly observed in Figure 4.1, the proposed control method yields a faster response than the RFTSC controller by Zhao *et al.* [3]. Moreover, the control input produced by the proposed method has much lower chattering than the RFTSC by Zhao *et al.* [3], as is evident in Figure 4.2.

4.3.2 Case 2

The performance of the proposed controller is next investigated for a continuous time trajectory and the results are compared with the RFTSC controller by Zhao *et al.* [3]. All the parameters for both the controllers are kept the same. The following reference trajectories are considered for the simulation study:

$$\begin{cases} q_{d1} = & 1.25 - \frac{7}{5}e^{-t} + \frac{7}{20}e^{-4t}\ rad \\ q_{d2} = & 1.25 + e^{-t} - \frac{1}{4}e^{-4t}\ rad. \end{cases} \tag{4.41}$$

The initial conditions for the joint angles in (4.41) are considered as $q_{10} = 1$ rad and $q_{20} = 1.5$ rad. The disturbance and the manipulator nominal parameters are kept the same as in Case 1.

The simulation results obtained for tracking (4.41) are shown in Figure 4.3 and Figure 4.4. From Figure 4.3(a) and Figure 4.3(b) it can be observed that with the proposed backstepping based adaptive FTSMC, both overshoot and undershoot in the system response are lesser than the controller of Zhao *et al.* [3]. The inset figures show that the error settles to the final value within a finite time in case of the proposed controller. The proposed controller uses almost the same amount of control energy as the controller by Zhao *et al.* [3], as observed from Figure 4.4(a) and Figure 4.4(b). However, the control input in the case of RFTSC contains excessive chattering, whereas the proposed controller produces smoother control signals.

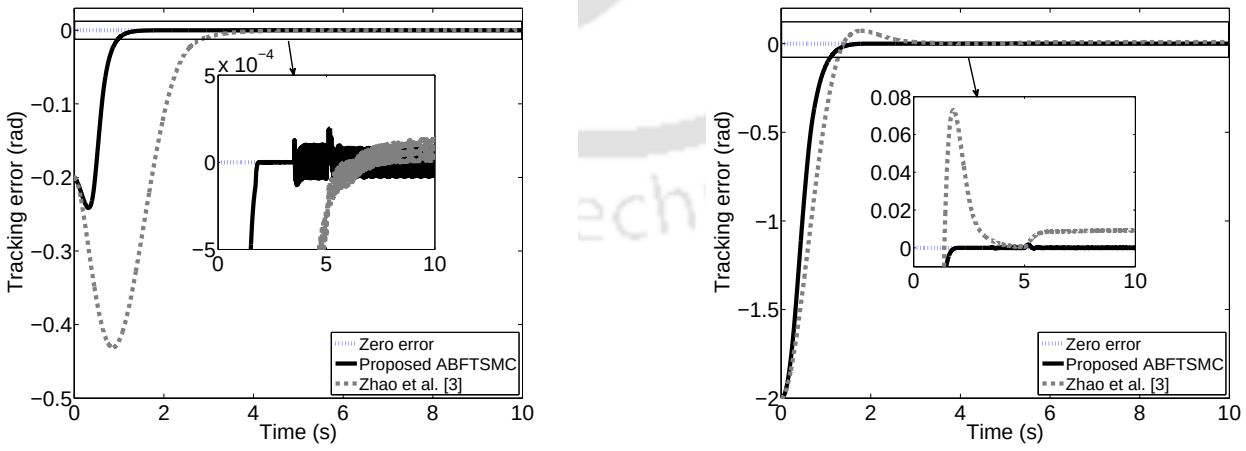

(a) Tracking error for joint 1

(b) Tracking error for joint 2

Figure 4.3: Tracking error by the proposed controller and RFTSC proposed by Zhao *et al.* [3] for Case 2

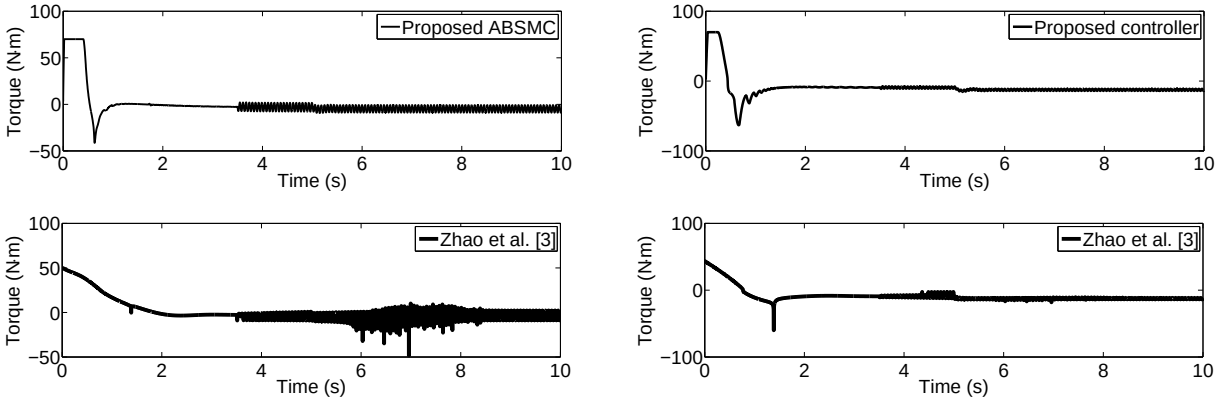

(a) Control input for joint 1 (b) Control input for joint 2

Figure 4.4: Input torques with the proposed controller and RFTSC proposed by Zhao *et al.* [3] for Case 2

Table 4.1: Simulation results of the proposed controller with the RFTSC proposed by Zhao *et al.* [3]

	Case 1		Case 2	
	Proposed	Zhao *et al.* [3]	Proposed	Zhao *et al.* [3]
$\|\|u_1\|\|_2$(N·m)	1.7039×10^3	1.4342×10^3	1.5658×10^3	1.2889×10^3
$\|\|u_2\|\|_2$(N·m)	1.2573×10^3	0.87×10^3	1.8224×10^3	1.3475×10^3
TV_{u_1}(N·m)	1.8234×10^3	3.4391×10^3	2.0039×10^3	3.2811×10^3
TV_{u_2}(N·m)	0.916×10^3	2.0747×10^3	948.6482	951.4276
tr_{e1}(s)	0.8349	1.1028	0.3932	0.8431
tr_{e2}(s)	0.5913	0.9228	0.6802	0.8979
tr_{s1}(s)	1.0812	1.6900	1.1287	3.0067
tr_{s2}(s)	1.0874	1.4439	1.2298	2.3018
M_{p1} (rad)	0	0	0.0002	0
M_{p2} (rad)	1.001	0	0	0.072
t_{p1} (s)	–	–	5.162	–
t_{p2} (s)	5.362	–	–	1.796
M_{u1} (rad)	0	0	-0.24	-0.43
M_{u2} (rad)	-0.03	0	0	0
t_{u1} (s)	–	–	0.351	0.932
t_{u2} (s)	0.395	–	–	–
e_{ss1}(rad)	6.3701×10^{-5}	-21.812×10^{-5}	8.1092×10^{-5}	13.527×10^{-5}
e_{ss2}(rad)	1.2964×10^{-4}	120×10^{-4}	0.6802	0.8979

$||u_i||_2$: 2 norm and TV_{ui}: Total variation of control input, tr_{ei}: rise time and ts_{ei}: settling time, M_{pi}: Peak overshoot, t_{pi}: peak overshoot time, M_{ui}: peak undershoot, t_{ui}: undershoot time ,e_{ssi}: steady state error for $i = 1, 2$

For better clarity, the simulation results are summarized in Table 4.1 where input and output performances of the controllers under study are compared. Input performance of the controller is evaluated by computing the control energy in terms of its 2nd norm and the total variation (TV) (2.32). Output performance of the controller is indicated by rise time, settling time and steady state error of the tracking response.

Table 4.1 shows that for two different types of trajectories the proposed backstepping based adap-

tive FTSMC attains consistent satisfactory robustness properties despite using time delay estimation of the nonlinearities and a non-varying estimate of the manipulator inertia matrix as opposed to the controller by Zhao *et al.* [3], where except for the difference in link masses, the exact nominal model of the manipulator is used. The proposed controller uses a little more energy than Zhao *et al.* 's controller [3]. However, the total variation (TV) measures of both the controllers in Table 4.1 show that the proposed ABSMC has lower chattering than that of the RFTSC.

The tracking results in Table 4.1 clearly show that the proposed controller is able to maintain a good tracking performance whereas Zhao *et al.* 's RFTSC [3] has higher overshoot and undershoot, higher steady state error, slower response and higher settling time meaning deterioration of performance with structural uncertainty caused by the change in link mass. The fast terminal sliding mode combined with backstepping and adaptively tuned controller gain imparts robustness to the controlled system despite probable modeling estimation error due to TDE. Therefore, this partially model free controller can be explored further for application in high DoF manipulators having structurally complex model.

4.4 Summary

In this chapter a backstepping based adaptive fast terminal SMC is proposed. A fast terminal sliding mode is combined with the backstepping method and an adaptive gain tuning law is used for the controller. The proposed controller has a simple structure as it does not depend on the exact manipulator model. Using only the joint acceleration information all the soft-nonlinearities of the manipulator are estimated using time delay estimation (TDE). The proposed controller is robust and chattering free. Simulation results on a robotic manipulator show that the proposed controller is able to produce superior tracking performance than some existing controller.

5

Torque Control of a Position Commanded Robot Manipulator: An Experimental Investigation

Contents

5.1 Introduction

Industrial robots are constructed with an aim to having a high value of stiffness to enable precise position tracking. Hence, affect of collision is very serious in position tracking. This is why in industries, the robot arm and human hardly interact since collision with the heavy rigid manipulator might prove very dangerous, even fatal. However, with the evolution and progress of advanced robotics technology, safe merging of human and robot workspace is increasingly attempted, like in medical robots [190, 191] and assistive technology [192, 193], which demand simultaneous control of motion and force. The inverse dynamics control [117] provides integration of motion and force controlled frameworks which is not possible in the case where position and kinematic controls are used.

Robot manipulators with direct torque controlled joints are generally expensive as this requires very low friction and no backlash in the gear box. As a result, most of the industrial manipulators and the commercially available modular manipulators are equipped with servos in the joints that have individual built-in position controllers. The modular robots have low price and low weight and can be reconfigured according to the desired task and additionally, any defective module can easily be replaced. Such arms are generally fitted with smart servos that have built-in position controllers whose input and feedback quantities are positions and because of these servos, such manipulators can be operated via position command only. These manipulators can be termed as position controlled manipulators. Such robot arms are rendered suitable only for the kinematic control. Since a lot of commercially available arms are inherently position controlled, changing their servos for torque controlled motors will not be very cost effective. Therefore, attempts have been made to incorporate dynamical control in such manipulators [116, 117, 194].

As can be found in [116, 117, 194, 195] and the references therein, as the position controller is present only in the individual motors in the joints, it imposes limitations on the performance and the precision of the overall system. The physical attributes of the manipulator joints like the acceleration limit, the torque limit along with the effects due to the load and the coupling forces are overlooked while performing only kinematic control using the joint position control. Neglecting the acceleration and torque limits can cause failure of actuators and may result in impractical motion. As the position controlled manipulators are easily available and hence are widely used, it is important to devise control plans beyond the kinematic control, that will enable the robot manipulator to perform well within acceptable limits, notwithstanding due considerations being given to the physical limitations and the additional forces and torques acting on it. In [196] Flacco and De Luca presented a velocity controller while considering the acceleration and the torque limits of the manipulator joints. On the other hand in [195], Shao *et al.* used a decentralized model of the manipulator where dynamics of each joint was controlled by using the information of the built-in position controller of the servo and then using the commanded position as the control input to obtain the torque for controlling the robot arm. Khatib *et al.* [116] and Prete *et al.* [117] proposed different methods of transforming the calculated torque command to the position command using the motor, joint and the built-in controller dynamics to facilitate implementation of the torque controller on the position commanded manipulator.

Keeping in view the necessity of implementation of dynamic control and the lack of cheap manipulators having direct torque control, the focus on the position controlled robot manipulator is

growing. This research work endeavors to realize robust control algorithms on a position controlled robot manipulator. For experimental studies, a coordinated links (COOL) dual arm manipulator having Dynamixel smart servos as the joint actuators is used. These servos have built-in position controllers and hence the manipulator becomes position controlled.

Motivated by the methods of Khatib [116] and Shao *et al.* [195], a simple torque to position conversion is proposed in this chapter. Khatib [116] proposed a transformation based on the information of the servo controller and the closed loop frequency response of the joint. Shao *et al.* [195] proposed a joint level controller for a decentralized manipulator system that contained Dynamixel AX series servo and designed the controller considering proportional (P) action in the internal control of the servo. Based on these works, a simplified torque to position conversion method is developed in this chapter using the ideal motor parameters. Adopting a simplification strategy and use of only nominal motor parameters, however, cannot mitigate structured and unstructured uncertainties present in the system and affecting the motor dynamics. Inaccuracies in system parameters and payload variation are the main sources of structured uncertainties. Unstructured uncertainties are caused by external disturbances, friction and saturation nonlinearities. All such uncertainties that are not dealt with by the internal controller in the servo motors will be tackled by the dynamic controllers proposed in the previous chapters, mainly the ABSMC-PID and the ABFTSMC.

The chapter is organized as follows: in Section 5.2 the coordinated links (COOL) robot arm and its parameters are described. The joint actuators and their technical specifications are presented in Section 5.3. The torque to position conversion method is derived in Section 5.4. Experimental results by using the ABSMC-PID and the ABFTSMC proposed in the thesis are prsented in Section 5.5 and Section 5.6 to validate the proposed torque to position converter as well as to study the effects of including the dynamics controller in the loop for a position commanded robot manipulator. A brief summary of the chapter is given in Section 5.7.

5.2 Position controlled manipulator: The Coordinated Links (COOL) robot arm

The hardware used as the experimental test-bed is a Coordinated Links (COOL) 14 degrees of freedom (DoF) dual robot arm, with each arm having 7 joints as shown in Fig. 2.12. All the joints in the manipulator are revolute joints and are serially connected to form an open chain manipulator. The details of the link mass and lengths are provided in Table 2.8.

In Fig. 2.12 and Table 2.8, the terms 'L' and 'R' are used to indicate the left and the right arm. All the manipulator joints can be operated together or in different combinations by keeping the non operating joints locked at one position. This allows each of the arms to be operated with any number of DoFs between 1 to 7 and also allows the arm to have different configurations depending upon the values of the angles the joints are fixed at.

The joints of the robot arm are equipped with Dynamixel RX-28 and Rx-64 series servos as shown in Fig. 5.1. The motors are connected serially via daisy chaining and each motor is given a unique ID and can be controlled using Packet communication.

The laboratory set-up used for conducting experiments on the COOL robot arm is shown in Fig. 5.2. The robot arm motion is programmed using an Intel(R) Core 2 Quad CPU Q6700 2.66 GHz processor desktop PC with 4GB RAM on Windows 7 platform. Communication between the PC and the robot arm is performed via the communication device called the USB2Dynamixel [197] which is connected to the USB port of the PC. Further, 3P and 4P connectors are installed in the USB2Dynamixel to connect the Dynamixel motors. The control algorithm and the communication between the PC and the arm are executed using Python.

5.3 Joint actuators

Each of the Dynamixel RX-28 and the RX-64 type servos has the following components:

- A brushed D.C. motor
- Gearbox
- Processing unit
- Sensor elements
- A communication interface
- Servo motor driver
- Signal light

The RX-28 type servo uses the RE-max 17 214897 maxon motor and the RX-64 type servo uses the RE-max 21 250003 maxon motor. The parameters of the RX-28 and RX-64 servos are listed in Table 5.1 and Table 5.2 respectively and the technical details of the maxon motors RE-max 17 214897 and RE-max 21 250003 are given in Table 5.3 and Table 5.4 respectively. Each servo is equipped with an AVR Atmega 8 microcontroller that comes with an installed command-line bootloader that can

(a) Dynamixel RX-28 (b) Dynamixel RX-64

Figure 5.1: Dynamixel servos RX-28 and RX-64 [4]

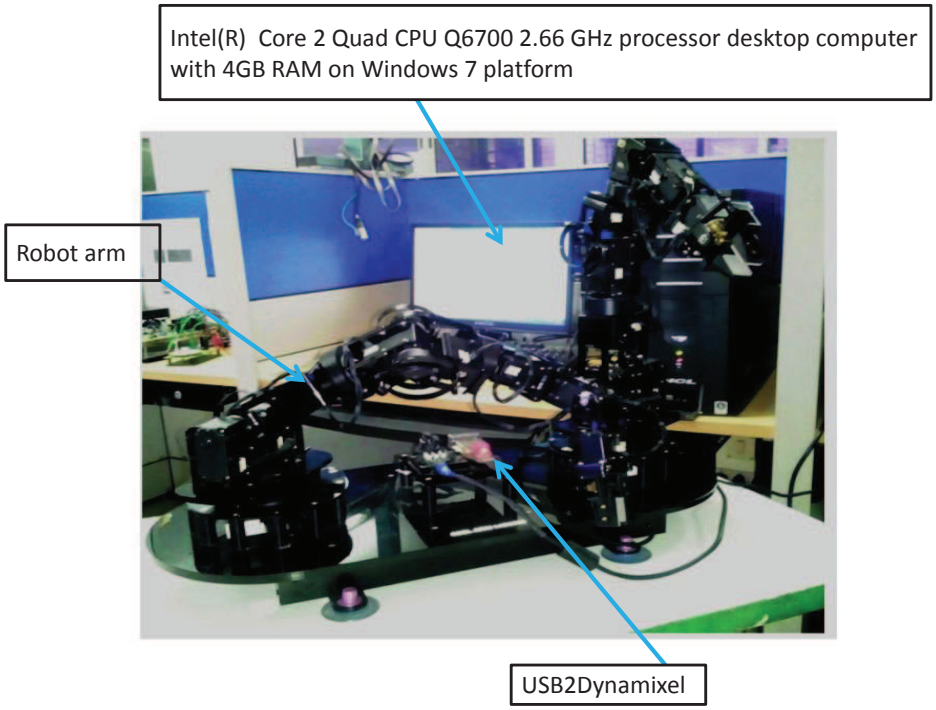

Figure 5.2: The experimental set-up for the robot arm

be used to change the firmware of the actuator. A linear potentiometer mechanically linked to the output shaft of the gearbox serves as the position sensor. The position data is used for the motor control and in addition, a voltage and a temperature sensor are also present in the servo for overload protection. An asynchronous half-duplex serial interface based on the EIA-485 bus standard is used as the communication interface. The magnitude and the polarity of the motor armature voltage control the angular speed and direction of the servo. Both the servo actuators are equipped with a full bridge motor driver with four double-diffused metaloxide semiconductor field-effect transistors (DMOSFET) and integrated protective diodes for powering the servo motor. The signal light indicates the operational status of the servo. A more detailed description of the Dynamixel RX-28 and RX-64 type servo can be found in [5].

Table 5.1: Parameters of the RX-28 servo [6]

Supply voltage range	12.0 V-18.5 V
Angular position range	± 2.6 rad
Angular speed limit	6.24 rad/s
Torque limit	3.6 N·m
Armature current limit	1.9 A
Gearbox ratio ($\frac{1}{k_g}$)	193
Gearbox Inertia (J_g)	79.6×10^{-6} kg·m^2

Table 5.2: Parameters of the RX-64 servo [7]

Supply voltage range	12.0 V-18.5 V
Angular position range	± 2.6 rad
Angular speed limit	6.24 rad/s
Torque limit	5.1 N·m
Armature current limit	2.6 A
Gearbox ratio ($\frac{1}{k_g}$)	200
Gearbox Inertia (J_g)	154.9×10^{-6} kg·m^2

Table 5.3: Technical specifications of RE-max 17 214897 [8]

Rated armature voltage	12.0 V
Motor speed constant	100.7 rad/Vs
Motor torque constant	10.7×10^{-3} N·m/A
Terminal resistance	8.3 Ω
Terminal inductance	0.206 mH
Mechanical time constant (T_m)	6.25 ms
Motor inertia (J_m)	86.4×10^{-9} kg·m^2

Table 5.4: Technical specifications of RE-max 21 250003 [9]

Rated armature voltage	15.0 V
Motor speed constant	74.9 rad/Vs
Motor torque constant	13.4×10^{-3} N·m/A
Terminal resistance	6.3 Ω
Terminal inductance	0.206 mH
Mechanical time constant (T_m)	6.72ms
Motor inertia (J_m)	217.0×10^{-9} kg·m^2

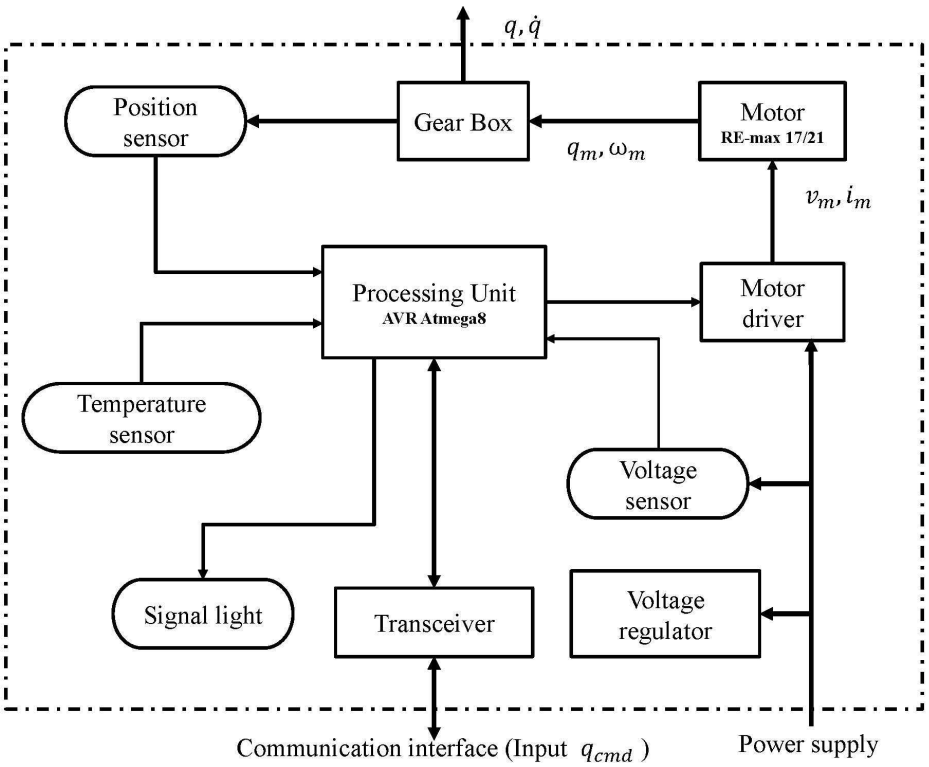

Figure 5.3: Set-up of the Dynamixel RX-28/64 servo [5]

The block diagram representation of the Dynamixel RX-28 and RX-64 servos [5] is shown in Figure 5.3. In Figure 5.3, v_m, i_m are the motor's armature voltage and current, q_m, $\dot{q}_m$ are the angular position and velocity of the motor shaft and $q, \dot{q}$ are the angular position and velocity obtained at the output of the gearbox shaft indicating the joint position and the velocity. The position input received via the transceiver is denoted by q_{cmd}.

Based on the position feedback, the microcontroller in the servo derives the control using the PID controller programmed into it to move the servo to the desired joint position sensed by the transceiver [5]. The sensor data can be transmitted to the PC through the transceiver. As the block diagram indicates, the actuating command that the user can send to the servos is only the desired position value. Therefore, manipulators having such actuators in their joints can be termed as position controlled manipulators since direct torque or voltage commanding of the joints is not possible without resorting to suitable hardware modifications.

5.4 Torque to position converter

The basic principle of a servo motion system is to use feedback gain to obtain the desired output at the motor shaft. The proportional (P)-integral-(I)-derivative(D) controller is the most commonly used controller in the servo system owing to its simplicity in design. In [5] it was validated that in RX-28 and the RX-64, the proportional (P) control played the dominant part and that was followed in this work. For facilitating a simplified implementation of the torque to position conversion, the I and D gains in Dynamixel RX-28 and RX-64 were made zero, operating the motors only with P control. The output of this lower level controller is generally obtained as the motor torque required to produce the desired movement. The electrical time constant of the DC motor in RX-28 is 0.025ms and that of RX-64 is 0.032ms which is much lower than their mechanical time constants 6.25ms and 6.72ms respectively. Hence for both the motors, the mechanical dynamics are the prominent part that can be expressed as

$$\frac{J}{k_g}\ddot{q} + \frac{B}{k_g}\dot{q} = \tau - \tau_l \tag{5.1}$$

where q, $\dot{q}$, $\ddot{q}$ are respectively the angular position, speed and acceleration of the gear shaft, τ is the motor torque, τ_l is the disturbance torque and k_g is the motor gear ratio. Further, J, B are the motor's effective inertia and damping coefficients respectively. The block diagram of the motor control is shown in Figure 5.4, where ω_m is the motor shaft speed and ω is the speed output of the gear-box. The tracking error is denoted as $e = q_{cmd} - q$ where q_{cmd} is the commanded motor position and k_p is the proportional (P) gain of the controller. The servo motors in the arm have bounded positions and velocities and so the joint accelerations must also be bounded. The output of the lower level P controller can be written as

$$\begin{aligned} \tau = k_p(q_{cmd} - q) = k_p\ e \\ \Rightarrow e = k_p^{-1}\tau \end{aligned} \tag{5.2}$$

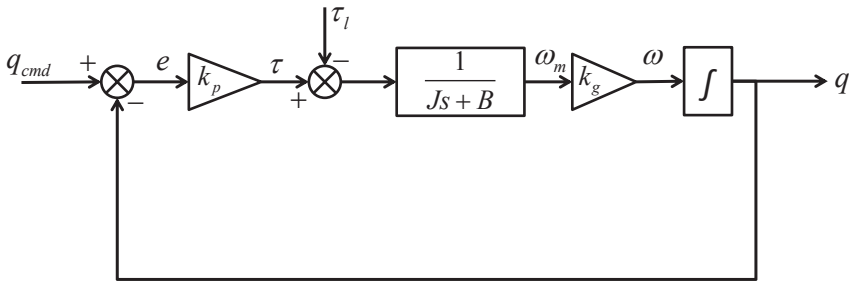

Figure 5.4: Simplified servo motor block diagram

The torque to position converter will produce a position command q_{cmd} as shown in Figure 5.5 based on the derived torque τ of the dynamic controller obtained as per the desired joint angular position q_d, desired joint angular velocity $\dot{q_d}$ and desired joint angular acceleration $\ddot{q_d}$. This law is similar to the control law suggested in [117]. The derived torque and the torque produced by the low level P-controller in the servo should be equivalent, which indicates the following relation:

$$\begin{aligned} \tau &= k_p(q_{cmd} - q) \\ q_{cmd} &= k_p^{-1}\tau + q. \end{aligned} \tag{5.3}$$

Since the implementation of the controller is software based, assuming a sampling time of T_s, (5.3) at the $k-th$ instant can be written as

$$q_{cmd}[k+1] = k_p^{-1}\tau[k] + q[k] \tag{5.4}$$

which shows that the position command to be sent to the motor in the $(k+1)-th$ instant is based on the torque derived and the actual motor position at the $k-th$ instant. This conversion can be used to implement an external dynamic control loop to the robot arm as shown in Figure 5.5.

5.5 Experimental results with ABSMC-PID

The proposed ABSMC-PID given by (3.28), (3.29) and (3.30) is experimentally investigated for joint trajectory tracking the Coordinated Links (COOL) robot arm shown in Figure 2.12 using the laboratory set-up shown in Fig. 5.2. The robot is operated as a 3DoF manipulator by taking the joints 1, 4 and 7 as the first, second and the third joint respectively, while the rest of the joints are fixed in the zero positions. The description of the robot arm parameters can be found in Table 2.8 and the details of the 3DoF manipulator model are elaborated in Appendix A.9. The robot arm has Dynamixel servos as the joint actuators which can be controlled by position command only. In order to facilitate dynamic control in the position commanded joint actuators, the torque to position conversion (5.4) proposed in Chapter 5 is used. The controller is implemented using Python programming in an Intel(R) Core 2 Quad CPU Q6700 2.66 GHz processor desktop computer with 4GB RAM on Windows

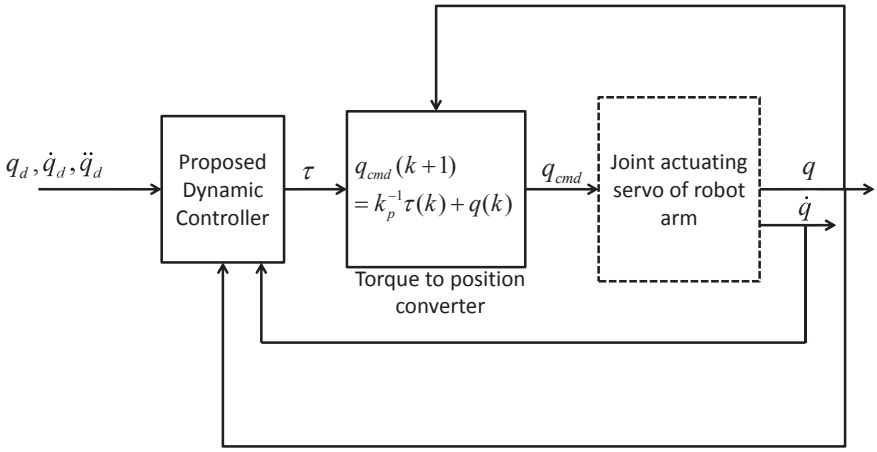

Figure 5.5: Block diagram of proposed dynamical control

7 platform. The sampling time is determined based on the communication delay between the servo and the PC, which is found to be 0.048s. The parameters of the controller used for the experiment are as follows:

$$\boldsymbol{c_1} = 15\boldsymbol{I_2}, \quad \boldsymbol{c_2} = 20\boldsymbol{I_2}, \quad \boldsymbol{W} = 10\boldsymbol{I_2}, \quad \boldsymbol{\Gamma} = 100\boldsymbol{I_2}, \quad \boldsymbol{\epsilon} = 1\boldsymbol{I_2}.$$

During experimentation it was found that replacing $\boldsymbol{c_1}$ with a tracking error dependent varying function $\boldsymbol{c_1(z_1)} = diag\{15\,(1 - exp(-100|z_{1i}|))\}$ induced a varying damping ratio which improved the controller performance and this controller variant was named as ABSMC-NPID (ABSMC with nonlinear PID surface).

The aim of the experiment is to make the joints follow the following reference trajectories:

$$q_{d1} = 1 + 0.2\sin(0.5\pi t)\ rad \tag{5.5}$$

$$q_{d2} = 1 - 0.2\cos(0.5\pi t)\ rad \tag{5.6}$$

$$q_{d3} = 1 + 0.2\sin(0.25\pi t)\ rad \tag{5.7}$$

where t is the time in seconds. The performance of the dynamic controller is compared against the case when position command in terms of the reference trajectory is directly applied to each servo which is controlled by a built-in P-type controller as explained earlier in Chapter 5. This study is conducted to test the reliability of the proposed ABSMC against the built-in P controller. A mass of 100g is attached to the manipulator gripper to introduce a structural uncertainty in the system. The trajectory tracking performances with the direct position command, ABSMC-PID and the ABSMC-NPID are compared in Figure 5.6 and the tracking performances of the all three methods are compared in Table 5.5.

It can be concluded from the experiments that the proposed conversion method is reliable as the position command reconstructed from the generated torque and sent to the actuator can drive

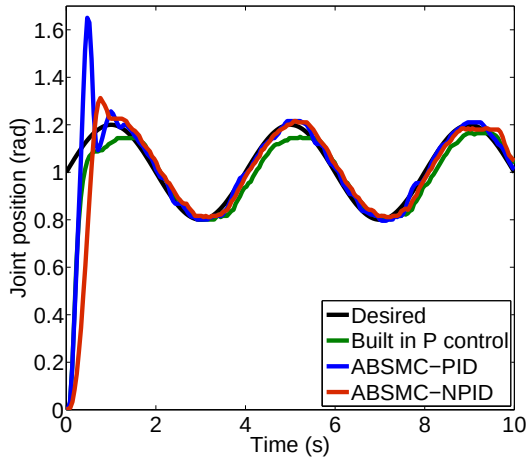

(a) Trajectory of joint 1

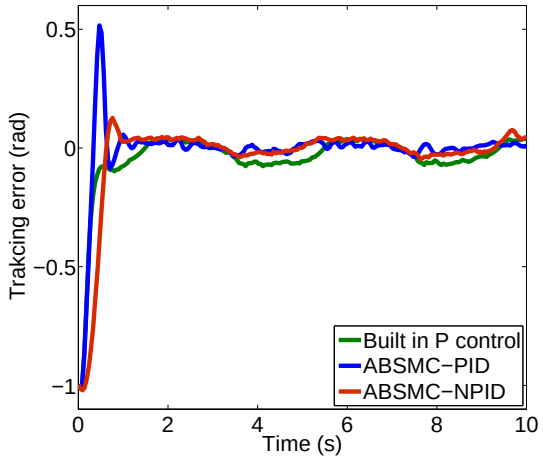

(b) Tracking error of joint 1

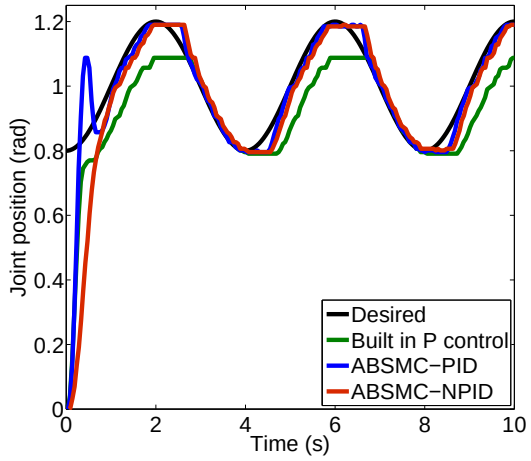

(c) Trajectory of joint 2

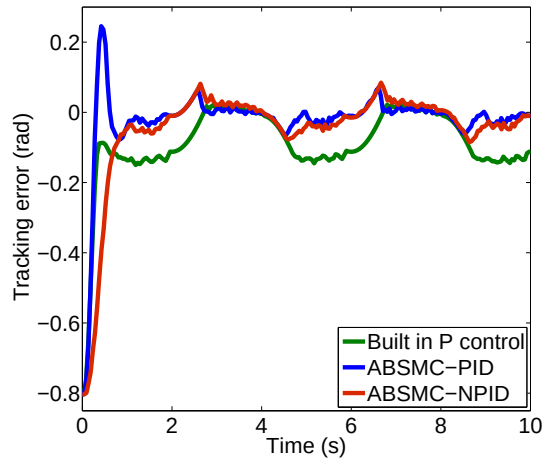

(d) Tracking error of joint 2

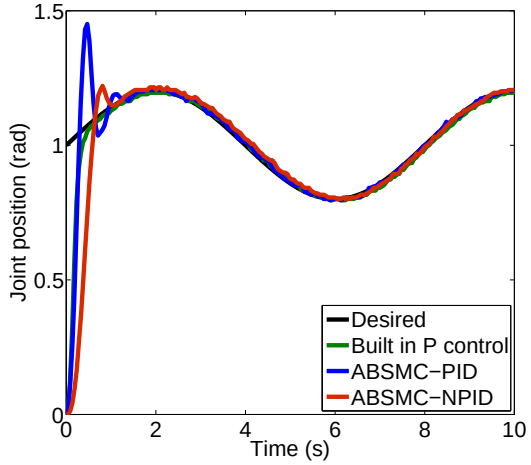

(e) Trajectory of joint 3

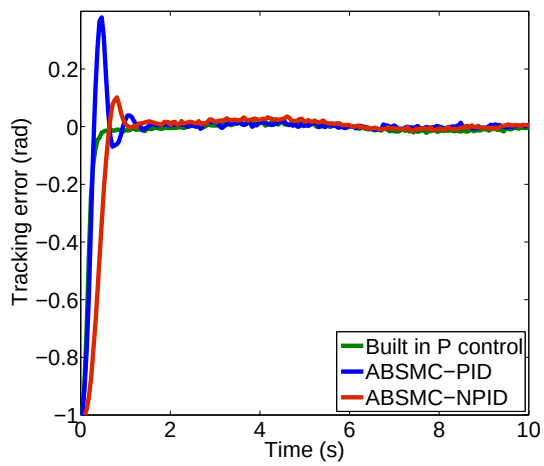

(f) Tracking error of joint 3

Figure 5.6: Experimental results with direct position command, proposed ABMSC-PID and ABSMC-NPID

the system to follow the reference trajectory correctly. Secondly, it is to be noted from the error responses in Figure 5.6 that in case of coupled motions with load, the performance of the built-in P-type controller is not consistent (observed from the tracking results of joint 2), whereas the dynamic controller maintains a consistent performance in all the three joints. The inclusion of the nonlinear PID sliding surface is able to further improve the proposed ABSMC's performance by reducing the peak overshoot as can be observed in Figure 5.6 and Table 5.5.

Table 5.5: Performance comparison for trajectory tracking of 3DoF manipulator

Joint	Controller	t_r(s)	t_s(s)	M_p(rad)	t_p(s)	MASSE
Joint 1	Built-in P control	0.42	0.85	-	-	0.04
	ABSMC-PID	0.32	0.90	0.52	0.46	0.01
	ABSMC-NPID	0.54	0.95	0.12	0.76	0.02
Joint 2	Built-in P control	0.32	0.70	-	-	0.07
	ABSMC-PID	0.27	0.66	0.24	0.421	0.02
	ABSMC-NPID	0.76	0.71	-	-	0.03
Joint 3	Built-in P control	0.47	0.80	-	-	0.008
	ABSMC-PID	0.27	1.28	0.37	0.46	0.005
	ABSMC-NPID	0.61	1.09	0.10	0.81	0.013

t_r = rise time, t_s = settling time, M_p = peak overshoot,
t_p = peak time, MASSE= mean absolute steady state error

5.6 Experimental results with ABFTSMC

The proposed adaptive backstepping based FTSMC given by (4.24) and (4.25) is applied to the position commanded 14DoF Coordinated Links (COOL) robot arm as shown in Figure 5.2. In the experiment only the joints 1, 4 and 7 of the robot arm are used as the first, second and third joints respectively, keeping the other joints locked in the zero position. The selected joints have RX-28 servo as the actuator.

In the experiment, the nominal model of the manipulator is used. The results obtained with the proposed ABFTSMC and the proposed ABSMC-NPID are compared with the the built-in P controller of the servo, where the desired position is sent directly sent. The torque is derived using (4.24) and implemented using (5.4). The parameters used for the controller (4.24) in the experiment are the following: $\boldsymbol{c_1} = 15\boldsymbol{I_3}$, $\delta = 1.1$, $\boldsymbol{W} = 2\boldsymbol{I_3}$, $\beta = 1.6$, $\boldsymbol{\Gamma} = 20\boldsymbol{I_3}$, $\boldsymbol{\epsilon} = 1\boldsymbol{I_3}$, where $\boldsymbol{I_3}$ is a 3×3 identity matrix. The sampling time L is chosen as 0.048sec which is decided by considering the communication delay between the joint servos and the PC. The reference trajectories for the three joints are considered as

$$\begin{aligned} q_{d1} &= 1 + 0.2\sin(0.5\pi t)\ rad \\ q_{d2} &= 1 - 0.2\cos(0.5\pi t)\ rad \\ q_{d3} &= 1 + 0.2\sin(0.25\pi t)\ rad. \end{aligned} \tag{5.8}$$

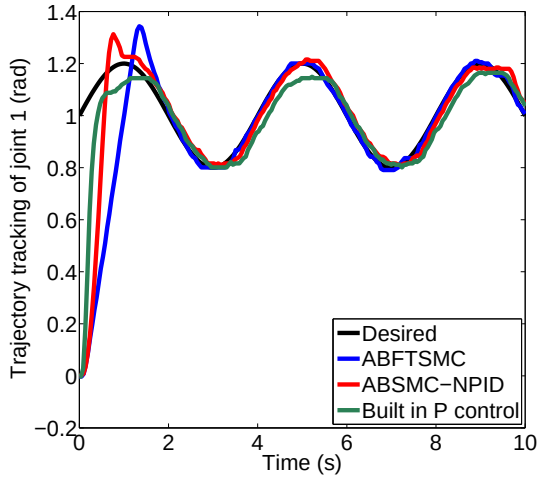

(a) Tracking of joint 1

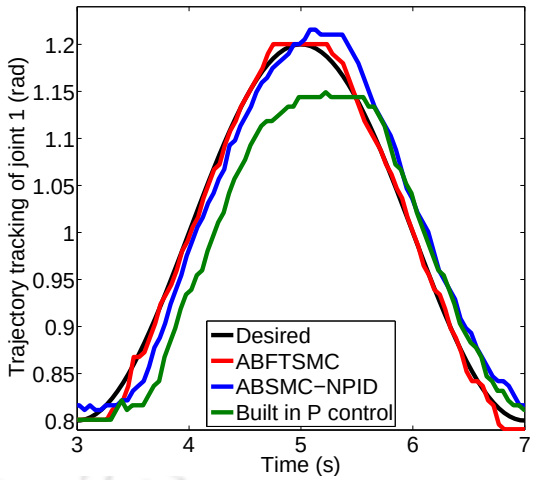

(b) Magnified view (Joint 1)

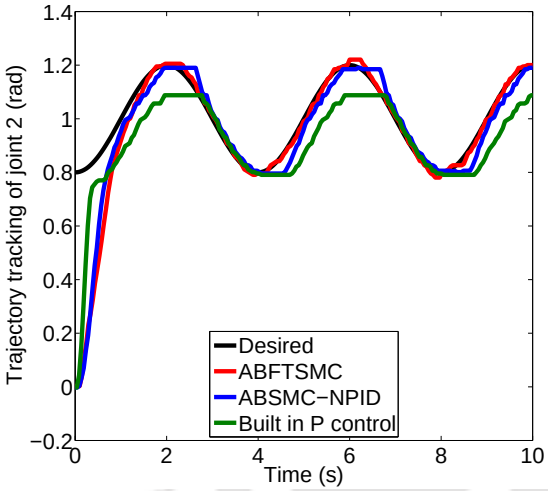

(c) Tracking of joint 2

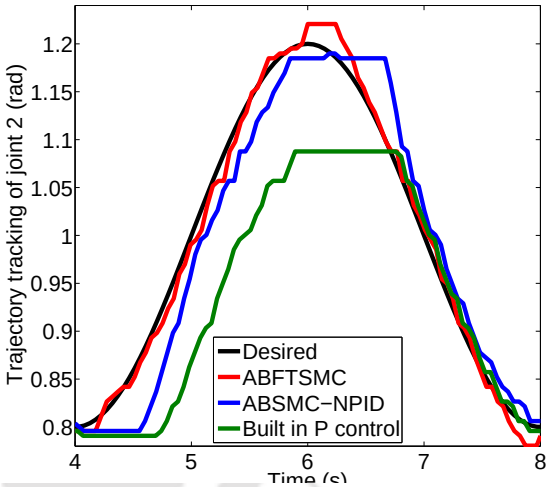

(d) Magnified view (Joint 2)

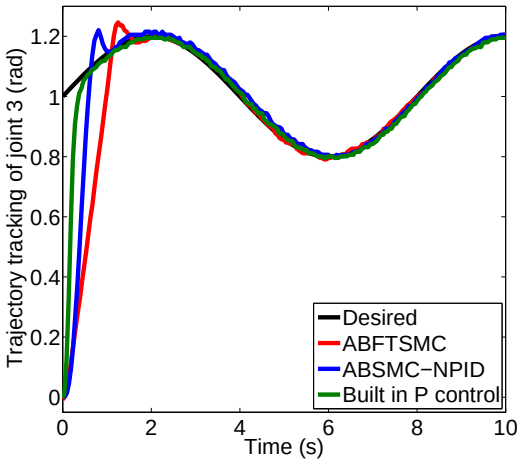

(e) Tracking of joint 3

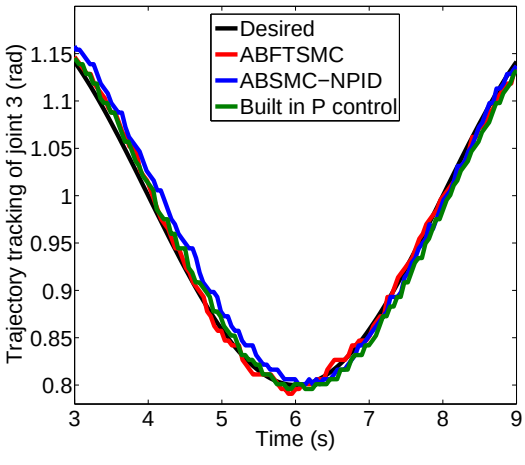

(f) Magnified view (Joint 3)

Figure 5.7: Results with direct position command, proposed ABMSC-NPID and ABFTSMC

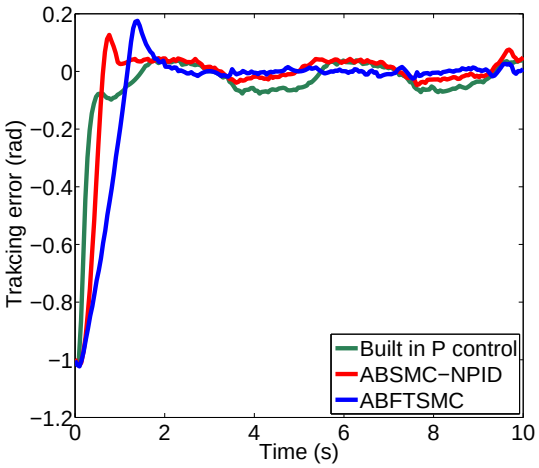

(a) Tracking error of joint 1

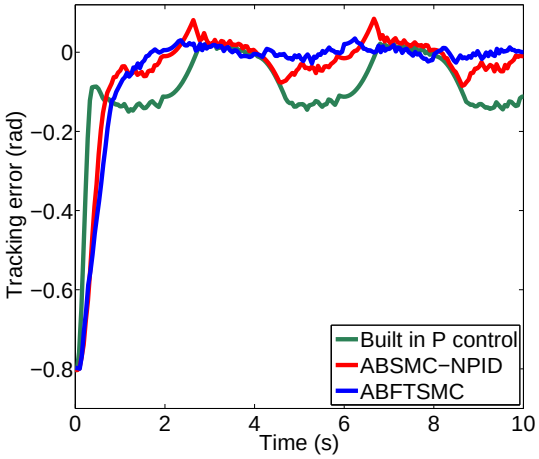

(b) Tracking error of joint 2

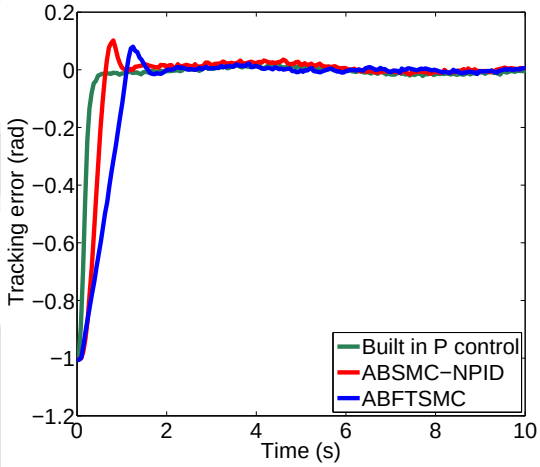

(c) Tracking error of joint 3

Figure 5.8: Results with direct position command, proposed ABMSC-NPID and ABFTSMC

Experimental results obtained by using the proposed backstepping based adaptive FTSMC for all the three joints are shown in Figure 5.7, Figure 5.8 . From Figure 5.7 and Figure 5.8, it is obvious that in the case of position commanded robots, instead of directly applying the desired trajectory as the command input to the system, if the dynamic controller is used first, better tracking results are achieved. The dynamic controller takes into account all the coupled torques, additional loads to the motors in the manipulator based on which a suitable torque profile for each motor is developed. This torque profile is then converted to an equivalent motion profile using (5.4).

The experimental results are summarized in Table 5.6, which shows that although the proposed torque control method yields a slower convergence, yet the steady state error is much lower than both the built-in P controller and the ABSMC-NPID controller. Moreover with the proposed ABFTSMC, the overshoot is also lower than with the ABSMC-NPID.

Table 5.6: Performance comparison for trajectory tracking of 3DoF manipulator

Joint	Controller	t_r(s)	t_s(s)	M_p(rad)	t_p(s)	MASSE
Joint 1	Built-in P control	0.42	0.85	-	-	0.04
	ABSMC-NPID	0.54	0.95	0.12	0.76	0.02
	ABFTSMC	1.10	1.77	0.18	1.39	0.013
Joint 2	Built-in P control	0.32	0.70	-	-	0.07
	ABSMC-NPID	0.76	0.71	-	-	0.03
	ABFTSMC	1.20	1.32	-	-	0.006
Joint 3	Built-in P control	0.47	0.80	-	-	0.008
	ABSMC-NPID	0.61	1.09	0.10	0.81	0.013
	ABFTSMC	1.05	1.63	0.08	1.20	0.006

t_r = rise time, t_s = settling time, M_p = peak overshoot,
t_p = peak time, MASSE= mean absolute steady state error

5.7 Summary

A simple torque to position conversion method is proposed in this chapter for use in position commanded servo actuators present in robot manipulators. The torque to position conversion is based on the low level controller of the servomotor. Although being highly simplified as compared to the existing methods, such simplified conversions can be successfully used for implementing the torque control methodology in the position commanded servos with proper selection of the inverse dynamics algorithm. As such, this method can be adopted for torque control of the position commanded robotic manipulators without having to perform any hardware modifications. The experimental results presented in the chapter, which have implemented the ABSMC-PID and the ABFTSMC controller proposed previously in the thesis, show that such a conversion method can be utilized to implement a dynamical controller in a position commanded manipulator. Therefore such a method can be useful when a position commanded manipulator is to be operated to obtain compliance behaviour using impedance control methods.

Although the proposed method develops a much simpler torque to position conversion law, it still has some drawbacks as mentioned below:

- The method relies on the knowledge of the internal controller of the servo and without this information it cannot be guaranteed that such a conversion will work.
- Communication delay between the motor and the PC can produce constraints in the implementation of the torque controller, especially for high speed operations. The motors being connected through daisy chaining in the experimental set-up, this delay increases with each added motor.

However, such a conversion approach is important to implement force or impedance control on robot manipulators in order to achieve compliant behavior while interacting with the environment. Therefore, further study can be dedicated into achieving such a conversion method while at the same time tackling its above mentioned drawbacks.

6

Conclusions and Scope for Future Work

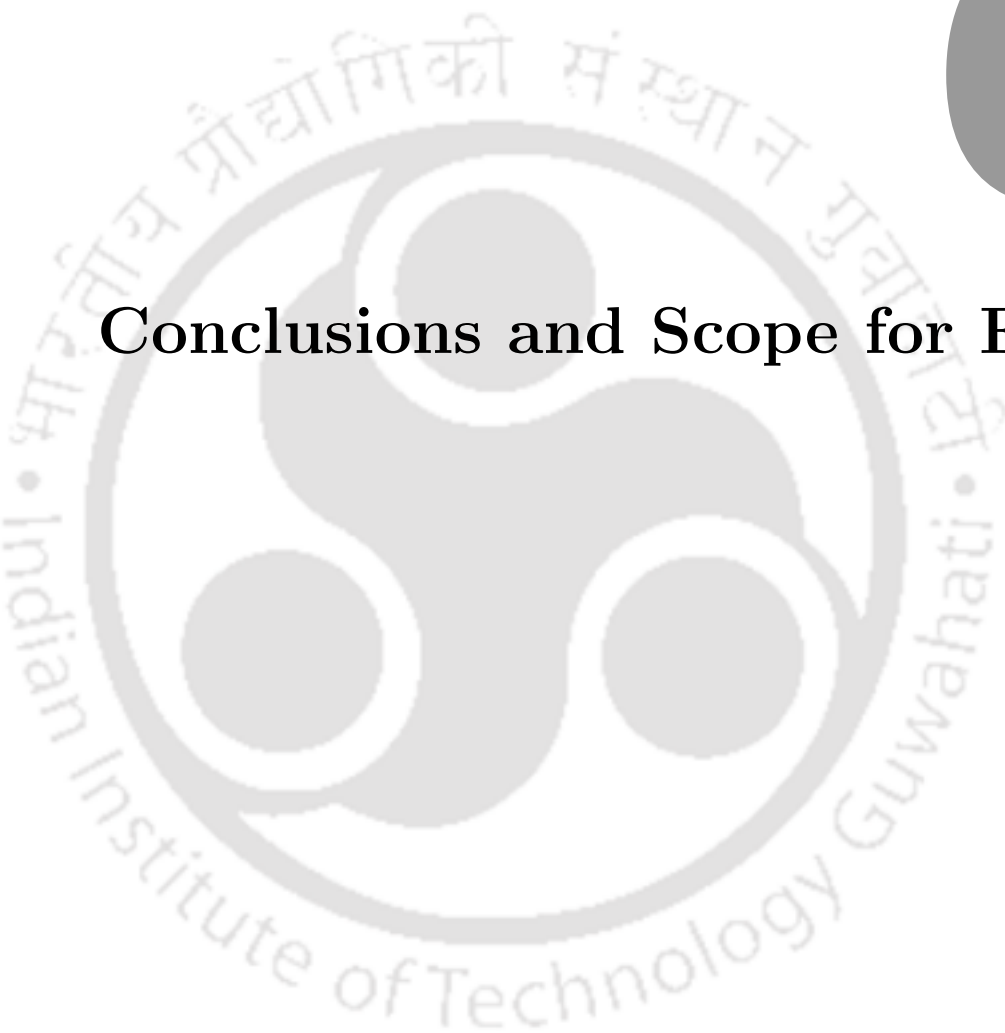

Contents

6.1 Conclusions

In practical applications such as industries and low cost commercial manipulators, the Proportional Integral Derivative (PID) controllers are still dominant owing to their simple structure, despite the availability of other robust control methods showing better performance than the PID. Keeping in focus the utility and portability of the controller offering an acceptable performance, the study presented in this thesis attempts to devise a sliding mode controller free of its inherent drawbacks while at the same time maintaining its original simple structure that can be possibly used as universally as the PID control method. The primary goal of this thesis is to design a simple structured robust dynamic controller based on the backstepping sliding mode control methodology and four variants of dynamic controllers are proposed for robust control of robot manipulators.

The first control method proposed is the integral backstepping sliding mode controller (IBSMC) which used an extra integrator block augmented with the actual system. This allowed to obtain the control input to the system as an output of the integrator block, thus providing a chattering free smooth control law. The proposed IBSMC was also used for underactuated systems by proper selection of the backstepping regulatory variables. Simulations for both the robot manipulator and the underactuated cart-pendulum system were presented showing the efficacy of the proposed IBSMC controller.

The inherent *explosion of terms* due to backstepping led to increased structural complexity in the IBSMC, which was eliminated using integral adaptive dynamic surface control (IADSC). In IADSC filtered signals were used to replace the differentiation of the nonlinear model of the manipulator. The versatility of the controller was improved by adaptively tuning the controller gain so that it could be implemented without the knowledge of the bounds of the uncertainty affecting the system.

Considering practical implementation, especially for digital realization, the IADSC was not very suitable as the filter constant required to be redesigned in case of change in sampling interval or the presence of small delays. The IADSC faced stability issues which could be attributed to the presence of the filter. Therefore the integrator block was entirely eliminated and instead a PID sliding surface was introduced to form the adaptive backstepping sliding mode controller with PID sliding surface (ABSMC-PID) that did not require the filter. The PID type sliding surface helped in improving the steady state behavior. The simulation results demonstrated applicability and the efficacy of the proposed ABSMC-PID. The ABSMC-PID was also implemented for impedance control of robot manipulators which was an important issue while interacting with the external environment.

The dynamics of a high DoF manipulator tends to have high structural complexity which ultimately affects the model based dynamic controller. Therefore a model free controller is a major need and was realized using time delay estimation of the soft nonlinearities of the manipulator model. Consequently, an adaptive backstepping based fast terminal sliding mode controller (ABFTSMC) was developed. The fast terminal sliding mode obtained using backstepping provided a finite time convergence for the closed loop system. The comparison of the simulation results with some existing robust control method showed that despite being a model free controller without having any observer, the proposed controller was able to offer good trajectory tracking performance. Moreover, the control input obtained was chattering free owing to the fast terminal sliding surface.

The thesis attempted to implement the proposed dynamic control methods in position commanded digital servo systems. A torque to position command conversion method was used to convert the generated torque profile to position command for actuating servo motors in a robot manipulator. Experimental studies demonstrated promising potential for practical applicability of the proposed method on position commanded robots.

6.2 Scope for Future Work

The thesis explores simple yet effective robust backstepping sliding mode control method for joint control of robot manipulators. This research can be further extended in the following directions:

- The adaptive backstepping sliding mode method proposed for impedance controller can be experimented for better compliance behavior for interaction tasks. The variable damping and stiffness induced using the nonlinear backstepping design parameter can be further explored to obtain improved results for the manipulator in its interaction with the external environment. The backstepping offers a much flexible design and also provides a better approach for the parameter design as any desired control parameter can be inserted in the intermediate stages of backstepping. Hence this control method can be further explored for impedance control tasks.
- Although the proposed torque to position conversion method was successfully used for the servos, the conversion relies on the availability of the information of the motor and the internal controller of the servo. A better solution to this can be explored.
- Another area where the scope of the control method proposed in the thesis can be extended is the dual arm manipulation. The proposed impedance control via ABSMC with variable backstepping parameter and time delay estimation based fast terminal sliding mode control shows promising results and can be combined for an effective controller for the dual arm manipulation tasks. The time delay estimation offers a model free robust controller design. This can be very useful for the complicated dynamics of the dual arm operation while achieving compliant motion. Moreover, the stability offered by backstepping can be utilised to design a robust impedance controller producing a better compliance along with a guaranteed stability.

A

Appendix

Contents

A.1 Dynamic modeling of rigid manipulators

The dynamics of an open chain rigid link manipulator can be derived using the Lagrangian of the manipulator [11]. The kinetic energy for each link of the manipulator ($T_i(q, \dot{q})$) can be defined as

$$T_i(\boldsymbol{q}, \dot{\boldsymbol{q}}) = \frac{1}{2}\dot{q}_i J_i^T(\boldsymbol{q})\mathcal{M}_i J_i(\boldsymbol{q})\dot{q}_i \tag{A.1}$$

where $\boldsymbol{q}, \dot{\boldsymbol{q}} \in \mathbb{R}^n$ are the position and velocity of the manipulator joints, $\mathcal{M}_i$ is the generalized inertia matrix and $J_i(\boldsymbol{q})$ is the Jacobian of the $i-th$ link of the manipulator. The total kinetic energy of the manipulator is obtained as

$$\boldsymbol{T(q, \dot{q})} = \sum_{i=1}^{n} T_i(\boldsymbol{q}, \dot{\boldsymbol{q}}) = \frac{1}{2}\dot{\boldsymbol{q}}^{\boldsymbol{T}}\boldsymbol{M(q)}\dot{\boldsymbol{q}} \tag{A.2}$$

where $M(q)$ is the manipulator inertia matrix.

The potential energy for the $i-th$ link of the manipulator is given as

$$U_i(\boldsymbol{q}) = m_i g h_i(\boldsymbol{q}) \tag{A.3}$$

where m_i is the mass and $h_i(\boldsymbol{q})$ is the height of the center of mass for the $i-th$ link and g is the gravitational constant. The total potential energy of the manipulator is found as:

$$U(\boldsymbol{q}) = \sum_{i=1}^{n} U_i(\boldsymbol{q}) = \sum_{i=1}^{n} m_i g h_i(\boldsymbol{q}). \tag{A.4}$$

The manipulator Lagrangian is defined as

$$\begin{aligned}\mathcal{L}(\boldsymbol{q}, \dot{\boldsymbol{q}}) = \sum_{i=1}^{n} (T_i(\boldsymbol{q}, \dot{\boldsymbol{q}}) - U_i(\boldsymbol{q})) =& \frac{1}{2}\dot{\boldsymbol{q}}^{\boldsymbol{T}}\boldsymbol{M(q)}\dot{\boldsymbol{q}} - U(\boldsymbol{q}) \\ =& \frac{1}{2}\sum_{i=1}^{n} m_{ij}(\boldsymbol{q}) q_i q_j - U(\boldsymbol{q}).\end{aligned} \tag{A.5}$$

The Lagrange's equation for the manipulator can be written as follows:

$$\frac{d}{dt}\frac{\partial \mathcal{L}}{\partial \dot{q}_i} - \frac{\partial \mathcal{L}}{\partial q_i} = \Upsilon_i \tag{A.6}$$

where Υ_i represents the actuator torque and other non-conservative generalized forces acting on the manipulator joint. Now, using (A.5), the following can be derived:

$$\frac{d}{dt}\frac{\partial \mathcal{L}}{\partial \dot{q}_i} = \frac{d}{dt}\left(\sum_{j=1}^{n} M_{ij}\dot{q}_j\right) = \sum_{j=1}^{n}\left(M_{ij}\ddot{q}_j + \dot{M}_{ij}\dot{q}_j\right) \tag{A.7}$$

$$\frac{\partial \mathcal{L}}{\partial q_i} = \frac{1}{2}\sum_{j,k=1}^{n} \frac{\partial M_{kj}}{\partial q_i}\dot{q}_k\dot{q}_j - \frac{\partial U}{\partial q_i}. \tag{A.8}$$

Replacing (A.7) and (A.8) in (A.6) yields

$$\sum_{j=1}^{n} M_{ij}(q)\ddot{q}_j + \sum_{j,k=1}^{n}\left(\frac{\partial M_{ij}}{\partial q_k}\dot{q}_j\dot{q}_k l - \frac{1}{2}\frac{\partial M_{kj}}{\partial q_i}\dot{q} - k\dot{q}_j\right) + \frac{\partial U(q)}{\partial q_i} = \upsilon_i, \quad i = 1\ldots n$$

$$\sum_{j=1}^{n} M_{ij}(q)\ddot{q}_j + \sum_{j,k=1}^{n}\Gamma_{ijk}\dot{q}_j\dot{q}_k + \frac{\partial U(q)}{\partial q_i} = \Upsilon_i, \quad i = 1\ldots n \tag{A.9}$$

where

$$\Gamma_{ijk} = \frac{1}{2}\left(\frac{\partial m_{ij}(q)}{\partial q_k} + \frac{\partial M_{ij}(q)}{\partial q_j} - \frac{\partial M_{kj}(q)}{\partial q_i}\right)$$

are called the *Christoffel symbols* where the terms containing $q_i q_j,\ i \neq j$ represent the Coriolis forces and the terms containing q_i^2 are the centrifugal forces on the $i-th$ joint. Now the matrix $C(q,\dot{q}) \in \mathbb{R}^{n\times n}$ called the Coriolis matrix is defined as follows:

$$\begin{aligned} C_{ij}(q,\dot{q}) =& \sum_{k=1}^{n}\Gamma_{ijk}\dot{q}_k \\ =& \frac{1}{2}\sum_{k=1}^{n}\left(\frac{\partial M_{ij}}{\partial q_k} + \frac{\partial M_{ik}}{\partial q_j} - \frac{\partial M_{kj}}{\partial q_i}\right)\dot{q}_k. \end{aligned} \tag{A.10}$$

The manipulator dynamics in the vector form can now be defined as

$$\boldsymbol{M(q)\ddot{q} + C(q,\dot{q})\dot{q} + G(q) = \tau - \tau_d} \tag{A.11}$$

where $G(q) = \sum_{i=1}^{n}\frac{\partial U(q)}{\partial q_i}$ is the force due to gravity, τ is the vector representing the joint actuating torques and τ_d is the vector denoting disturbance torques and any unmodeled torques acting on the manipulator joints.

A.2 Characteristics of symmetric positive definite block matrix using Schur's complement

As described in [135], for an $n \times n$ symmetric block matrix $\boldsymbol{M}$ of the form

$$\boldsymbol{M} = \begin{pmatrix} \boldsymbol{A} & \boldsymbol{B} \\ \boldsymbol{B^T} & \boldsymbol{C} \end{pmatrix} \tag{A.12}$$

where $\boldsymbol{A} \in \mathbb{R}^{p\times p}$ and $\boldsymbol{C} \in \mathbb{R}^{q\times q}$ are symmetric matrices and $\boldsymbol{B} \in \mathbb{R}^{p\times q}$, the positive definiteness of $\boldsymbol{M}$ can be guaranteed *iff* $\boldsymbol{C > 0}$ and $\boldsymbol{A - BC^{-1}B^T > 0}$.

A.3 Dynamics of the cart-pendulum system used in (A.13)

The cart-pendulum system is represented by the following differential equation:

$$\boldsymbol{M(q)\ddot{q} + C(q,\dot{q})\dot{q} + G(q) = F + F_d} \tag{A.13}$$

where $\boldsymbol{q}$, $\boldsymbol{\dot{q}}$ and $\boldsymbol{\ddot{q}}$ represent the position, velocity and acceleration of the system, $\boldsymbol{M(q)}$ is the inertia matrix, $\boldsymbol{C(q,\dot{q})}$ is the centripetal and Coriolis force matrix and $\boldsymbol{G(q)}$ is the gravitational force vector. Furthermore, $\boldsymbol{F}$ represents the applied force and $\boldsymbol{F_d}$ denotes the disturbance force caused by uncertainties. It is to be noted that

$$\boldsymbol{q} = \begin{bmatrix} q_1 \\ q_2 \end{bmatrix} = \begin{bmatrix} y \\ \theta \end{bmatrix}; \quad \boldsymbol{\dot{q}} = \begin{bmatrix} \dot{q}_1 \\ \dot{q}_2 \end{bmatrix} = \begin{bmatrix} \dot{y} \\ \dot{\theta} \end{bmatrix}; \quad \boldsymbol{\ddot{q}} = \begin{bmatrix} \ddot{q}_1 \\ \ddot{q}_2 \end{bmatrix} = \begin{bmatrix} \ddot{y} \\ \ddot{\theta} \end{bmatrix};$$

$$\boldsymbol{M(q)} = \begin{bmatrix} lm_c + m_p & m_p l\cos q_2 \\ m_p l\cos q_2 & J + m_p l^2 \end{bmatrix};$$

$$\boldsymbol{C(q,\dot{q})} = \begin{bmatrix} 0 & m_p l\dot{q}_2 \sin q_2 \\ 0 & 0 \end{bmatrix};$$

$$\boldsymbol{G(q)} = \begin{bmatrix} 0 \\ -m_p g l\sin q_2 \end{bmatrix};$$

$$\boldsymbol{F} = \begin{bmatrix} f_1 \\ 0 \end{bmatrix}; \quad \boldsymbol{F_d} = \begin{bmatrix} f_{d_1} \\ f_{d_2} \end{bmatrix}$$

where m_c is the mass of the cart, m_p is the mass of the pendulum, l is the length of the pendulum and J is the moment of inertia of the pendulum. The cart-pendulum system has two equilibrium points, one being the stable vertically downward position where $\theta = \pi$ and the other being the unstable vertically upward position where $\theta = 0$. Furthermore, f_1 is the control force applied to the cart and f_{d_1}, f_{d_2} are the disturbance forces due to matched and mismatched uncertainties present in the system whose upper bounds are considered to be known. As observed from the above mathematical model, the cart-pendulum is an underactuated system and the objective is to apply a control force f_1 to the cart in such a way that the pendulum will swing up to the vertically upward position, where $q_1 = 0, q_2 = 0, \dot{q}_1 = 0, \dot{q}_2 = 0$ from the initial vertically downward position where $q_1 = y, q_2 = \pi, \dot{q}_1 = 0, \dot{q}_2 = 0$. The system parameters are: $m_c = 1.12kg.$ $m_p = 0.11kg,$ $l = 0.1407m,$ $J = 0.0038kg - m^2$.

From (A.13), the dynamics of the pendulum can be written as

$$\begin{bmatrix} m_{11} & m_{12} \\ m_{12} & m_{22} \end{bmatrix} \begin{bmatrix} \ddot{q}_1 \\ \ddot{q}_2 \end{bmatrix} + \begin{bmatrix} C_{11} & C_{12} \\ C_{21} & C_{22} \end{bmatrix} \begin{bmatrix} \dot{q}_1 \\ \dot{q}_2 \end{bmatrix} + \begin{bmatrix} g_{11} \\ g_{21} \end{bmatrix} = \begin{bmatrix} f_1 \\ 0 \end{bmatrix} + \begin{bmatrix} f_{d_1} \\ f_{d_2} \end{bmatrix} \tag{A.14}$$

where

$m_{11} = m_c + m_p,$

$m_{12} = m_p l\cos q_2,$

$m_{22} = J + m_p l^2,$

$C_{11} = C_{21} = C_{22} = 0,$

$C_{12} = m_p l \dot{q}_2 \sin q_2,$
$g_{11} = 0,$
$g_{21} = -m_p g l \sin q_2.$

From (A.14), the following are derived,

$$\begin{aligned}\ddot{q}_1 =& \frac{1}{d}[m_{22}f_1 - m_{22}C_{12}\dot{q}_2 + m_{12}g_{21} + m_{22}f_{d_1} - m_{12}f_{d_2}] \\ \ddot{q}_2 =& \frac{1}{d}[-m_{12}f_1 + m_{12}C_{12}\dot{q}_2 - m_{11}g_{21} - m_{12}f_{d_1} - m_{11}f_{d_2}]\end{aligned} \tag{A.15}$$

where $d = m_{11}m_{22} - m_{12}^2$.

A.4 Derivation of IBSMC for cart-pendulum system

As suggested in literature, an underactuated system can be partially linearized for reducing design complexity of the controller as complete linearization may generally fail. Such a partial linearization may be collocated, meaning linearization of the actuated joint variables or noncollocated, meaning linearization of the unactuated joint variables [198]. After such linearization, the underactuated system is controlled using the dynamic coupling between the system variables. In order to perform such linearization, Man and Lin's approach [199] is followed where a new control input v is chosen in terms of the cart acceleration. To achieve this, the applied control input f_1 is chosen as follows,

$$\begin{aligned}f_1 =& \beta(v) \\ =& \frac{d}{m_{22}}v + \dot{q}_2 C_{12} - \frac{m_{12}g_{21}}{m_{22}}.\end{aligned} \tag{A.16}$$

The above control law (A.16) transforms (A.15) into the following form:

$$\ddot{q}_1 = v + h_1 \tag{A.17a}$$

$$\ddot{q}_2 = \frac{m_{12}^2 g_{21}}{d m_{22}} - \frac{m_{12}}{m_{22}}v - \frac{m_{11}g_{21}}{d} + h_2 \tag{A.17b}$$

where $h_1 = \frac{m_{22}}{d}f_{d_1} + \varphi_1,$
$\varphi_1 = -\frac{m_{12}}{d}f_{d_2},$
$h_2 = -\frac{m_{12}}{d}f_{d_1} + \varphi_2,$
$\varphi_2 = -\frac{m_{11}}{d}f_{d_2}.$

Now an integral backstepping sliding mode controller will be designed for the system (A.17). The aim is to design a sliding surface using which the system can be stabilized at the vertically upward position and develop a controller to bring the system states from the vertical downward position to this sliding surface and keep them there.

A.4.1 The Backstepping Algorithm design for cart-pendulum system

Step 1:

(i) As defined in [200], the cart-pendulum is a Class-III type of unactuated system which has a nontriangular structure and backstepping cannot be directly applied to it. Also, this system has the underactuated coordinate q_2 as the shape variable (the variable present in the inertia matrix $\boldsymbol{M(q)}$) and it possesses kinetic symmetry with respect to the external variable q_1 (the variable not present in the inertia matrix $M(q)$) which establishes the following identity,

$$\frac{\partial K(q,\dot{q})}{\partial \dot{q}_1} = 0 \tag{A.18}$$

where $K(q,\dot{q}) = \frac{1}{2}\boldsymbol{\dot{q}^T M(q)\dot{q}}$ is the kinetic energy of the system.
Now the *generalized momentum* p_s [200] is defined as

$$\begin{aligned} p_s =& \frac{\partial L(q,\dot{q})}{\partial \dot{q}_2} \\ or\ p_s =& 2(m_{12}\dot{q}_1 + m_{22}\dot{q}_2). \end{aligned} \tag{A.19}$$

Here $L(q,\dot{q})$ is the Lagrangian of the system and $L(q,\dot{q}) = \frac{1}{2}\boldsymbol{\dot{q}^T M(q)\dot{q}} - U$, where $U = m_p g l cos(q_2)$ is the potential energy of the system.

The *normalized momentum* of the system π_s is defined as

$$\begin{aligned} \pi_s =& m_{12}^{-1}\frac{\partial L(q,\dot{q})}{\partial \dot{q}_2} \\ \Rightarrow \pi_s =& \dot{q}_1 + \frac{m_{22}}{m_{12}}\dot{q}_2. \end{aligned} \tag{A.20}$$

By the definition of Class-III type of underactuated system given in [200], the normalized momentum is integrable and hence $\psi_s = \int \pi_s dt = q_1 + kq_2$ (considering $\frac{m_{22}}{m_{12}} = k$ to be almost constant near the equilibrium point). Now, the term $\frac{m_{12}}{m_{22}} = \frac{m_p l \cos q_2}{J + m_p l^2}$ is an integrable term and hence the product of the two integrable terms π_s and $\frac{m_{12}}{m_{22}}$, which will also be integrable, is defined as follows,

$$\begin{aligned} \psi &= \int \frac{m_{12}}{m_{22}}\pi_s dt \\ &= \int (\dot{q}_2 + \frac{m_{12}}{m_{22}}\dot{q}_1)dt \\ &= q_2 + k'q_1 \end{aligned}$$

where $k' = 1/k$.

Combining the generalized momentum and ψ as obtained above, the first regulatory variable z_1 for the backstepping algorithm is defined as follows:

$$z_1 = q_2 + k_1 q_1 + k_2(m_{12}\dot{q}_1 + m_{22}\dot{q}_2) \tag{A.21}$$

where k_1, k_2 are design constants derived based on the momentum equations.

The Lyapunov function is now defined in terms of the regulatory variable z_1 as

$$V_1 = \frac{1}{2} z_1^2 \tag{A.22}$$

which is positive definite by definition.

(ii) The time derivative of z_1 is obtained as,

$$\dot{z}_1 = \dot{q}_2 + k_1 \dot{q}_1 + k_2(m_{12}\ddot{q}_1 + m_{22}\ddot{q}_2) + k_2 \dot{m}_{12}\dot{q}_1.$$

From (A.14) and (A.15) $\dot{z}_1$ can be found as

$$\begin{aligned} \dot{z}_1 =& (1 - k_2 m_p l \dot{q}_1 \sin q_2)\dot{q}_2 + k_1 \dot{q}_1 + k_2 m_p g l \sin q_2 + h_3 \\ =& \zeta(q, \dot{q})\dot{q}_2 + k_1 \dot{q}_1 + k_2 m_p g l \sin q_2 + h_3 \end{aligned} \tag{A.23}$$

where $\zeta(q, \dot{q}) = (1 - k_2 m_p l \dot{q}_1 \sin q_2)$ and h_3 includes the uncertainty terms with the known upper bound $|h_{3_m}|$.

The derivative of V_1 is found as

$$\begin{aligned} \dot{V}_1 &= z_1 \dot{z}_1 \\ &= z_1[\zeta(q, \dot{q})\dot{q}_2 + k_1 \dot{q}_1 + k_2 m_p g l \sin q_2 + h_3]. \end{aligned} \tag{A.24}$$

The term $\zeta(q, \dot{q})\dot{q}_2$ is now considered as a virtual control input which will be used to bring the system (A.23) to the equilibrium point zero. Hence a stabilizing function α_1 is now used which is assumed to be equal to the virtual control input $\zeta(q, \dot{q})\dot{q}_2$ and will linearize as well as stabilize (A.23) at zero. This stabilizing function is defined as

$$\alpha_1 = -k_1 \dot{q}_1 - k_2 m_p g l \sin q_2 - c_1 z_1 - z_1 \bar{h}_3 \tag{A.25}$$

where $c_1 > 0$ is a design constant. Considering the uncertainty to be known, the upper bound of h_3 can be calculated. Let this upper bound be h_{3m} and then the term $\bar{h}_3$ is so chosen that $\bar{h}_3 > |h_{3m}|$.

(iii) It is only an assumption that the virtual control law, when equal to the stabilizing function, will stabilize the z_1 subsystem and this is not yet true. Hence the error between the chosen virtual control input $\zeta(q, \dot{q})\dot{q}_2$ and the derived stabilizing function α_1 is defined as the new regulatory variable z_2 to be used in the next step:

$$z_2 = \zeta(q, \dot{q})\dot{q}_2 - \alpha_1 \tag{A.26}$$

or,

$$\zeta(q,\dot{q})\dot{q}_2 = z_2 + \alpha_1. \tag{A.27}$$

Equations (A.23), (A.25) and (A.27) yield

$$\dot{z}_1 = -c_1 z_1 + z_2 - (z_1\bar{h}_3 - h_3) \tag{A.28}$$

which is an almost linear form. From (A.24) and (A.28) the derivative of V_1 is obtained as

$$\dot{V}_1 = -c_1 z_1^2 + z_1 z_2 - (z_1^2\bar{h}_3 - z_1 h_3). \tag{A.29}$$

It can be observed from above that solution z_1 will still not be driven to the equilibrium point i.e., the origin. Hence succeeding steps are now followed.

Step 2:

(i) The time derivative of the new regulatory variable z_2 is now derived as given below:

$$\dot{z}_2 = \dot{\zeta}(q,\dot{q})\dot{q}_2 + \zeta(q,\dot{q})\ddot{q}_2 + k_1\ddot{q}_1 + k_2 m_p g l \dot{q}_2 \cos q_2 + c_1\dot{z}_1 + \dot{z}_1\bar{h}_3$$

Replacing the expressions for $\ddot{q}_1$ and $\ddot{q}_2$ from (A.17) and simplifying the above expression, $\dot{z}_2$ can be written as

$$\dot{z}_2 = \eta_1(q,\dot{q}) + \eta_2(q,\dot{q})v + c_1\dot{z}_1 + \dot{z}_1\bar{h}_3 + h_4 \tag{A.30}$$

where

$$\eta_1(q,\dot{q}) = -k_2 m_p l \dot{q}_1 \dot{q}_2^2 \cos q_2 + k_2 m_p g l \dot{q}_2 \cos q_2 + \zeta(q,\dot{q})\frac{m_{12}^2 g_{21}}{d m_{22}} - \zeta(q,\dot{q})\frac{m_{11} g_{21}}{d}$$
$$\eta_2(q,\dot{q}) = -\zeta(q,\dot{q})\frac{m_{12}}{m_{22}} - k_2 m_p l \dot{q}_2 \sin q_2 + k_1$$

and h_4 includes the uncertainty.

A new Lyapunov function is now defined in terms of the two regulatory variables z_1 and z_2 as

$$V_2 = V_1 + \frac{1}{2}z_2^2 \tag{A.31}$$

and the derivative of V_2 is found as

$$\begin{aligned}\dot{V}_2 &= z_1\dot{z}_1 + z_2\dot{z}_2 \\ &= -c_1 z_1^2 + z_1 z_2 - (z_1^2\bar{h}_3 - z_1 h_3) + z_2[\eta_1 + \eta_2 v + c_1\dot{z}_1 + \dot{z}_1\bar{h}_3 + h_4].\end{aligned} \tag{A.32}$$

A new virtual control input for the system (A.30) is chosen as $\eta_2 v$. Using nonlinear feedback,

the stabilizing function α_v is obtained from (A.30) as

$$\alpha_v = -[\eta_1 + c_1\dot{z}_1 + \dot{z}_1\bar{h}_3 + c_2 z_2 + z_2\bar{h}_4] \tag{A.33}$$

where c_2 is the design constant. As the upper bound of the uncertainty is assumed to be known, the upper bound of h_4 i.e., h_{4m} can be calculated and the value of $\bar{h}_4$ is set so that $\bar{h}_4 > |h_{4m}|$.

(ii) When the virtual control input will be equal to the stabilizing function α_v, this error variable z_2 will be brought to zero and stabilized.

(iii) Similar to the previous step (Step 1(iii)), the error between the virtual control $\eta_2 v$ and the stabilizing function α_v is defined as the next regulatory variable z_3,

$$\begin{aligned} z_3 &= \eta_2 v - \alpha_v \\ &= \eta_2 v + \eta_1 + c_1\dot{z}_1 + \dot{z}_1\bar{h}_3 + c_2 z_2 + z_2\bar{h}_4. \end{aligned} \tag{A.34}$$

The virtual control law $\eta_2 v$ can now be written as

$$\eta_2 v = z_3 + \alpha_v. \tag{A.35}$$

Using (A.35) and (A.33) in (A.30), the following linear like form is obtained,

$$\dot{z}_2 = -c_2 z_2 + z_3 - (z_2\bar{h}_4 - h_4). \tag{A.36}$$

The derivative of the Lyapunov function V_2 will have the following expression with $\eta_2 v$ as the control input,

$$\dot{V}_2 = -c_1 z_1^2 - c_2 z_2^2 + z_1 z_2 + z_2 z_3 - (z_1^2\bar{h}_3 - z_1 h_3) - (z_2^2\bar{h}_4 - z_2 h_4). \tag{A.37}$$

Taking derivative of the latest regulatory variable z_3 in (A.34), an equation containing $\dot{v} = \xi$ is obtained as follows:

$$\begin{aligned} \dot{z}_3 &= \dot{\eta}_2 v + \eta_2\dot{v} - \dot{\alpha}_v \\ &= \dot{\eta}_2 v + \eta_2\xi + \dot{\eta}_1 + c_1\ddot{z}_1 + \ddot{z}_3\bar{h}_3 + c_2\dot{z}_2 + \dot{z}_2\bar{h}_4 + h_5 \end{aligned} \tag{A.38}$$

where h_5 includes the uncertainty term whose upper bound is $|h_{5_m}|$.

A.4.2 Sliding Mode Algorithm design for cart-pendulum system

In order to design the sliding surface, the system equations obtained in terms of the transformed coordinates given by (A.28), (A.36) and (A.38) are considered again. If the uncertainty terms are not

considered, the nominal system described by (A.28), (A.36) and (A.38) will take the following form:

$$\dot{z}_1 = -c_1 z_1 + z_2 \tag{A.39a}$$
$$\dot{z}_2 = -c_2 z_2 + z_3 \tag{A.39b}$$
$$\dot{z}_3 = \dot{\eta}_2 v + \eta_2 \xi + \dot{\eta}_1 + c_1 \ddot{z}_1 + c_2 \dot{z}_2. \tag{A.39c}$$

The above representation has the structure of a *regular form* with (A.39a) and (A.39b) being the *null space dynamics* and (A.39c) being the *range space dynamics* having ξ as the control input. Now, following the conventional linear sliding surface design method the surface is defined as

$$s = \boldsymbol{\sigma} z = 0 \tag{A.40}$$

where $\sigma = [\sigma_1 \ \sigma_2 \ 1]$ and $z = [z_1 \ z_2 \ z_3]^T$. The terms σ_1 and σ_2 are the sliding surface parameters and should be so chosen that the sliding surface is Hurwitz stable. Now, the sliding variable s can be described as,

$$s = \sigma_1 z_1 + \sigma_2 z_2 + z_3. \tag{A.41}$$

The time derivative of s is obtained as

$$\begin{aligned} \dot{s} &= \sigma_1 \dot{z}_1 + \sigma_2 \dot{z}_2 + \dot{z}_3 \\ &= \sigma_1 \dot{z}_1 + \sigma_2 \dot{z}_2 + \dot{\eta}_2 v + \eta_2 \xi + \dot{\eta}_1 + c_1 \ddot{z}_1 + \ddot{z}_3 \bar{h}_3 + c_2 \dot{z}_2 + \dot{z}_2 \bar{h}_4 + h_5 \end{aligned} \tag{A.42}$$

where $\dot{z}_1$, $\dot{z}_2$ are given by (A.28) and (A.36) respectively.

The Lyapunov function defined in (A.31) is redefined by augmenting a term containing the sliding variable to it and the new Lyapunov function V_3 is obtained as follows:

$$V_3 = \frac{1}{2}(z_1^2 + z_2^2 + s^2) \tag{A.43}$$

which too is a positive definite function by definition. The derivative of V_3 is given by

$$\begin{aligned} \dot{V}_3 &= z_1 \dot{z}_1 + z_2 \dot{z}_2 + s\dot{s} \\ &= -c_1 z_1^2 - c_2 z_2^2 + z_1 z_2 + z_2 z_3 - (z_1^2 \bar{h}_3 - z_1 h_3) - (z_2^2 \bar{h}_4 - z_2 h_4) + s[\sigma_1 \dot{z}_1 + \sigma_2 \dot{z}_2 \\ &\quad + \dot{\eta}_2 v + \eta_2 \xi + \dot{\eta}_1 + c_1 \ddot{z}_1 + \ddot{z}_3 \bar{h}_3 + c_2 \dot{z}_2 + \dot{z}_2 \bar{h}_4 + h_5] \end{aligned} \tag{A.44}$$

The system dynamics in terms of the regulatory variables has the following form:

$$\begin{aligned} \dot{z}_1 &= -c_1 z_1 + z_2 - (z_1 \bar{h}_3 - h_3) \\ \dot{z}_2 &= -c_2 z_2 + z_3 - (z_2 \bar{h}_4 - h_4) \\ \dot{z}_3 &= \dot{\eta}_2 v + \eta_2 \xi + \dot{\eta}_1 + c_1 \ddot{z}_1 + \ddot{z}_3 \bar{h}_3 + c_2 \dot{z}_2 + \dot{z}_2 \bar{h}_4 + h_5. \end{aligned} \tag{A.45}$$

As can be observed from the above equation, the whole nonlinear cart-pendulum system dynamics has

now been reduced to an almost linear form which can be further linearized and eventually stabilized by using a nonlinear feedback control law ξ.

Following the conventional sliding mode controller design technique, the equivalent control law (ξ_{eq}) is obtained by making $\dot{s} = 0$ as,

$$\xi_{eq} = -\frac{1}{\eta_2}[\sigma_1\dot{z}_1 + \sigma_2\dot{z}_2 + \dot{\eta}_2 v + \dot{\eta}_1 + c_1\ddot{z}_1 + \ddot{z}_3\bar{h}_3 + c_2\dot{z}_2 + \dot{z}_2\bar{h}_4] \tag{A.46}$$

and the switching part of the control law is given as

$$\xi_{sw} = -\frac{1}{\eta_2}(Wsign(s) + \kappa s) \tag{A.47}$$

where κ and W are positive design constants.

Now, combining both the controls ξ_{eq} and ξ_{sw}, the control ξ is defined as

$$\begin{aligned}\xi &= \xi_{eq} + \xi_{sw} \\ &= -\frac{1}{\eta_2}[\sigma_1\dot{z}_1 + \sigma_2\dot{z}_2 + \dot{\eta}_2 v + \dot{\eta}_1 + c_1\ddot{z}_1 + \ddot{z}_3\bar{h}_3 + c_2\dot{z}_2 + \dot{z}_2\bar{h}_4 + Wsign(s) + \kappa s].\end{aligned} \tag{A.48}$$

To avoid any kind of singularity occurring in the expression of ξ, the value of η_2 is replaced by $\bar{\eta}_2$ by defining a very small constant ϵ such that,

$$\bar{\eta}_2 = \begin{cases} \epsilon, & 0 \leq \eta_2(q,\dot{q}) \leq \epsilon \\ -\epsilon, & -\epsilon \leq \eta_2(q,\dot{q}) < 0 \\ \eta_2, & otherwise \end{cases}$$

A.4.3 Addition of the Integral Block

The discontinuous signal ξ is now obtained, which will act as the control law for the system (A.45). However, for the cart-pendulum system (A.17), the control input is v. In order to obtain v, an integral block is added to the controller so that ξ will pass through the integrator block to yield v as

$$v = \int_0^t \xi(\lambda)d\lambda \tag{A.49}$$

A.4.4 Derivation of the Force Control Law for cart-pendulum system

Now following equation (A.16), the actual control force applied to the cart-pendulum is obtained as

$$f_1 = \frac{d}{m_{22}}v + \dot{q}_2 C_{12} - \frac{m_{12}g_{21}}{m_{22}}. \tag{A.50}$$

From (A.17), the zero dynamics of the cart-pendulum system can be written as

$$\ddot{q}_2 + \frac{m_{12}}{m_{22}}v + \frac{g_{21}}{m_{22}} = 0$$

$$or,\ \ddot{q}_2 + \frac{m_p l \cos q_2}{J + m_p l^2} v + g \tan q_2 = 0$$
$$\Rightarrow v = (J + m_p l^2)(\frac{\ddot{q}_2 - g \tan q_2}{m_p l \cos q_2}). \tag{A.51}$$

From the above equation it can be observed that on the horizontal plane i.e., when $q_2 = \frac{\pi}{2}$, the system has a singularity in its zero dynamics. So, when the pendulum crosses the horizontal plane, it may lead to unbounded control input. To overcome such a situation, a saturation function [1] is incorporated to the actuator control which will prevent the control law from becoming unbounded. However, while doing so, it should also be noted that the control law is able to pump enough energy to the system so that it can cross the horizontal plane.

Therefore, the control force f_1 is further modified to f_{1new} by adding a saturation function to obtain a bounded value of the control input [1] as given below:

$$f_{1new} = \bar{f}_1\ sat\left(f_1/\bar{f}_1\right) \tag{A.52}$$

where the saturation function $sat(.)$ is defined as

$$b\ sat(\frac{a}{b}) = \begin{cases} b, & when\, a > b \\ -b, & when\, a < b \\ a, & otherwise \end{cases}$$

and $\bar{f}_1$ is the least amount of force required by the pendulum to cross the horizontal plane.

A.5 Coupled SMC proposed by Park and Chwa [1] for stabilization control of cart-pendulum system

The coupled sliding mode controller [1] is of the following form,

$$u_c = u_{eq} + u_{sw} \tag{A.53}$$
$$u_{eq} = (\lambda_u g_x u_x^{eq} + g_\theta u_\theta^{eq})/(\lambda_u g_x + g_\theta)$$
$$u_{sw} = -\ (k\ sign(s_{smc}))/(\lambda_u g_x + g_\theta) \tag{A.54}$$

where

$g_x = m_{22}/(m_{11}m_{22} - m_{12}^2)$
$g_\theta = -m_{12}/(m_{11}m_{22} - m_{12}^2)$
$u_x^{eq} = g_x^{-1}(-f_x - c_x\dot{q}_1)$
$u_\theta^{eq} = g_\theta^{-1}(-f_\theta - c_\theta\dot{q}_2)$
$f_x = -(C_{12}m_{22}\dot{q}_2 - m_{12}g_{21})/(m_{11}m_{22} - m_{12}^2)$
$f_\theta = -(-C_{12}m_{12}\dot{q}_2 + m_{11}g_{21})/(m_{11}m_{22} - m_{12}^2)$
$s_{smc} = \lambda s_a + s_u$

$s_a = \dot{q}_1 + c_x q_1$
$s_u = \dot{q}_2 + c_\theta q_2$
$c_x = 0.3, \quad , c_\theta = 3.1077, \quad \lambda = 0.1, \quad k = 20.$

A.6 Proof of Lemma 4

From the relation $\tilde{\boldsymbol{k}} = \hat{\boldsymbol{k}} - \boldsymbol{k_d}$, where $\hat{\boldsymbol{k}}$, $\boldsymbol{k_d}$ are $n \times 1$ vectors, for an $n \times n$ positive definite diagonal matrix $\boldsymbol{\epsilon}$, the following can be written:

$$
\begin{aligned}
\tilde{\boldsymbol{k}} =& \hat{\boldsymbol{k}} - \boldsymbol{k_d} \Rightarrow \boldsymbol{\epsilon k_d} = \boldsymbol{\epsilon}(\hat{\boldsymbol{k}} - \tilde{\boldsymbol{k}}) \\
\boldsymbol{k_d^T \epsilon k_d} =& (\hat{\boldsymbol{k}} - \tilde{\boldsymbol{k}})^{\boldsymbol{T}} \boldsymbol{\epsilon}(\hat{\boldsymbol{k}} - \tilde{\boldsymbol{k}}) \\
& \sum_{i=1}^{n} k_{di}\epsilon_i k_{di} = \sum_{i=1}^{n} (\hat{k}_i - \tilde{k}_i)\epsilon_i(\hat{k}_i - \tilde{k}_i) \\
\Rightarrow & \sum_{i=1}^{n} k_{di}^2 \epsilon_i = \sum_{i=1}^{n} (\hat{k}_i^2 + \tilde{k}_i^2 - 2\hat{k}_i\tilde{k}_i)\epsilon_i \\
\Rightarrow & \sum_{i=1}^{n} 2\hat{k}_i\tilde{k}_i\epsilon_i = \sum_{i=1}^{n} (\hat{k}_1^2 + \tilde{k}_i^2 - k_{di}^2)\epsilon_i \\
\Rightarrow & \sum_{i=1}^{n} 2\hat{k}_i\tilde{k}_i\epsilon_i \geq \sum_{i=1}^{n} (\tilde{k}_i^2 - k_{di}^2)\epsilon_i \\
\Rightarrow & \sum_{i=1}^{n} 2\tilde{k}_i\epsilon_i\hat{k}_i \geq \sum_{i=1}^{n} (\tilde{k}_i\epsilon_i\tilde{k}_i) - \sum_{i=1}^{n} (k_{di}\epsilon_i k_{di}) \\
\Rightarrow & \boldsymbol{\tilde{k}^T \epsilon \hat{k}} \geq \frac{\mathbf{1}}{\mathbf{2}} (\boldsymbol{\tilde{k}^T \epsilon \tilde{k} - k_d^T \epsilon k_d}).
\end{aligned}
\tag{A.55}
$$

A.7 Model of 2DoF manipulator used in Yang *et al.* [2]

The mathematical model of the 2DoF robot manipulator (Fig. A.1) used by Yang *et al.* [2] is given by

$$
\begin{bmatrix} m_{11}(q) & m_{12}(q) \\ m_{21}(q) & m_{22}(q) \end{bmatrix} \begin{bmatrix} \ddot{q}_1 \\ \ddot{q}_2 \end{bmatrix} + \begin{bmatrix} h_1(q,\dot{q}) \\ h_2(q,\dot{q}) \end{bmatrix} + \begin{bmatrix} g_1(q) \\ g_2(q) \end{bmatrix} + \begin{bmatrix} f_1 \\ f_2 \end{bmatrix} = \begin{bmatrix} u_1 \\ u_2 \end{bmatrix} \tag{A.56}
$$

where

$$
\begin{aligned}
m_{11}(q) =& m_1 l_{c1}^2 + m_2(l_1^2 + l_{c1}^2) + J_1 + J_2 + 2m_2 l_1 l_{c2}\cos(q2), \\
m_{12}(q) =& m_2 l_{c2}^2 + J_2 + m_2 l_1 l_{c2}\cos(q_2), \\
m_{21} =& m_{12}, \; m_{22} = m_1 l_{c2}^2 + J_2, \\
h_1(q,\dot{q}) =& -m_2 l_1 l_{c2}(2\dot{q}_1\dot{q}_2 + \dot{q}_2^2)\sin(q_2), \; h_2(q,\dot{q}) = m_2 l_1 l_{c2}\dot{q}_1^2\sin(q_2),
\end{aligned}
$$

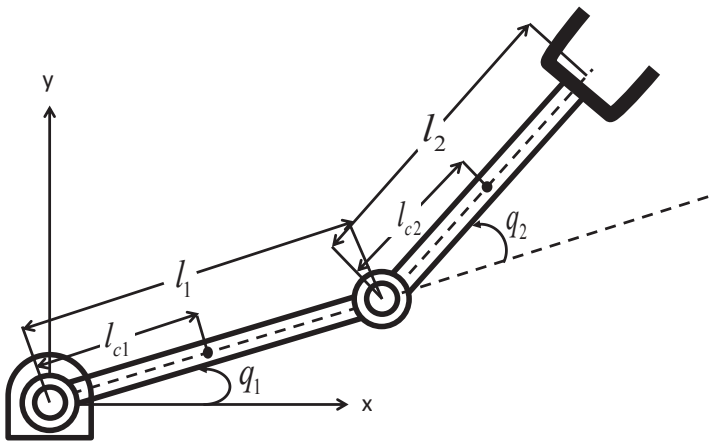

Figure A.1: 2DoF manipulator schematics used for simulation

$$g_1(q) = g(m_1 l_{c1} + m_2 l_1)\cos(q_1) + m_2 g l_{c2}\cos(q_1 + q_2),\ g_2(q) = m_2 g l_{c2}\cos(q_1 + q_2),$$
$$f_1 = 5.0q_1 + 3.0sign(\dot{q}_1),\ f_2 = 4.0q_1 + 2.0sign(q_2).$$

The physical parameters of the manipulator (A.56) are given in Table (A.1).

Table A.1: Physical parameters of the robot manipulator (A.56)

Joint No. i	Link mass m_i (kg)	Link length l_i (m)	Center of Mass l_{ci} (m)	Inertia J_i (kg·m^2)
1	4.0	0.50	0.25	1.0
2	2.0	0.25	0.15	0.8

In the simulations it is assumed that only the position feedback is available and it has an added uniform noise with the bounds ±0.00001 rad. The angular velocity is derived from the position feedback using pseudo-differentiation [2] with $\frac{a}{0.001a+1}$. The input torque amplitude is limited in [-200,200]Nm. A 150% increment in manipulator parameters is also added after t=40s in order to induce structural uncertainty to the systems. Accordingly, in Table A.1 m_1 changes from 4kg to 6 kg, m_2 changes from 2kg to 3kg, J_1 changes from 1kg·m^2 to 1.5kg·m^2 and J_2 changes from 0.8kg·m^2 to 1.2kg·m^2.

A.8 Disturbance observer based adaptive robust controller proposed by Yang *et al.* [2]

Yang *et al.* proposed a controller using the local information available for each joint subsystem in order to ensure the boundedness of the control system and to achieve a satisfactory performance. For

the $i-th$ joint of the manipulator they proposed the following controller:

$$u_i = -k_i r_i - \rho_i r_i^3 - \sigma_i |\hat{w}_i| r_i - \hat{w}_i - \frac{\eta_{it}^2}{\hat{\eta}_{it}|r_i| + \delta_i} r_i \tag{A.57}$$

where $k_i, \rho_i, \sigma_i, \delta_i > 0$ are the controller gains and $\hat{\eta}_{it}$ is the adaptive gain of the sliding mode controller tuned using the following law

$$\dot{\hat{\eta}}_{it} = \gamma_i(|r_i| - \epsilon_i \hat{\eta}_{it}) \tag{A.58}$$

where $\gamma_i \geq 0$ is the adaptive gain and $\epsilon_i \geq 0$ is the leakage parameter that prevents $\hat{\eta}_{it}$ from growing unbounded. For each local system $\hat{w}_i$ is the compensation term used by the disturbance observer for the disturbance terms w_i, where

$$\hat{w}_i = \begin{cases} \bar{\hat{w}}_i, & \text{for } Q_i(s) w_i \geq \bar{\hat{w}}_i \\ Q_i(s)(m_{oi} s r_i - u_i), & \text{for} |Q_i(s)(m_{oi} s r_i - u_i)| < \bar{\hat{w}}_i \\ -\bar{\hat{w}}_i, & \text{for} Q_i(s) w_i \leq -\bar{\hat{w}}_i \end{cases} \tag{A.59}$$

where $Q_i(s) = (\frac{1}{1+\lambda_i s})^2, \quad \lambda_i > 0$, is a second order filter, $\bar{\hat{w}}_i > 0$ is a selected upperbound for $|w_i|$, s is the complex number frequency parameter of Laplace transform and m_{oi} is the element of the positive definite diagonal inertia matrix estimated for the manipulator. Also, $r_i \in r = \dot{e} + \phi e$ where $e = q - q_d$ is the position tracking error and $\phi = diag\{\phi_1, \ldots \phi_n\} > 0$ is a constant matrix.

The parameters used by Yang *et al.* [2] are given as follows:

$$\phi_1 = \phi_2 = 10, \quad k_1 = k_2 = 20, \quad \rho_1 = \rho_2 = 5, \quad \lambda_1 = \lambda_2 = 0.02$$
$$\sigma_1 = \sigma_2 = 5, \quad \delta_1 = \delta_2 = 0.05, \quad \gamma_1 = \gamma_2 = 50, \quad \epsilon_1 = \epsilon_2 = 0.001, \quad m_{o1} = m_{o2} = 1.$$

A.9 Dynamics of the 3DoF manipulator simulated in the Coordinated Links (COOL) robot arm

Dynamics of the 3DoF manipulator in the Coordinated Links (COOL) robot arm is given by

$$\begin{bmatrix} m_{11} & m_{12} & m_{13} \\ m_{21} & m_{22} & m_{23} \\ m_{31} & m_{32} & m_{33} \end{bmatrix} \begin{bmatrix} \ddot{q}_1 \\ \ddot{q}_2 \end{bmatrix} + \begin{bmatrix} h_1 \\ h_2 \\ h_3 \end{bmatrix} \begin{bmatrix} \dot{q}_1 \\ \dot{q}_2 \end{bmatrix} + \begin{bmatrix} g_1 \\ g_2 \end{bmatrix} + \begin{bmatrix} f_1 \\ f_2 \end{bmatrix} = \begin{bmatrix} \tau_1 \\ \tau_2 \end{bmatrix} \tag{A.60}$$

where

$$\begin{aligned} m_{11} =& I_{z1} + m_3 \left[r_2 \cos(q_2 + q_3) + l_1 \cos(q_2)\right]^2 + I_{z3} \cos(q_2 + q_3)^2 + I_{y3} \sin(q_2 + q_3)^2 + I_{z2} \cos(q_2)^2 \\ & + I_{y2} \sin(q_2)^2 + m_2 r_1^2 \cos(q_2)^2 \\ m_{12} =& m_{21} = m_{13} = m_{31} = 0 \end{aligned}$$

$$
\begin{aligned}
m_{22} =& I_{x2} + I_{x3} + m_2 r_1^2 + m_3 \left[r_2 + l_1 \cos(q_3)\right]^2 + l_1^2 m_3 \sin(q_3)^2 \\
m_{23} =& m_{32} = I_{x3} + m_3 r_2 \left[r_2 + l_1 \cos(q_3)\right] \\
m_{33} =& m_3 r_2^2 + I_{x3} \\
h_1 =& -\dot{q}_1 \big[I_{z2}\dot{q}_2 \sin(2q_2) - I_{y2}\dot{q}_2 \sin(2q_2) - I_{y3}\dot{q}_2 \sin(2q_2 + 2q_3) - I_{y3}\dot{q}_3 \sin(2q_2 + 2q_3) \\
& + I_{z3}\dot{q}_2 \sin(2q_2 + 2q_3) + I_{z3}\dot{q}_3 \sin(2q_2 + 2q_3) + l_1^2 m_3 \dot{q}_2 \sin(2q_2) + m_2 r_1^2 \dot{q}_2 \sin(2q_2) \\
& + m_3 r_2^2 \dot{q}_2 \sin(2q_2 + 2q_3) + m_3 r_2^2 \dot{q}_3 \sin(2q_2 + 2q_3) + l_1 m_3 r_2 \dot{q}_3 \sin(q_3) \\
& + 2 l_1 m_3 r_2 \dot{q}_2 \sin(2q_2 + q_3) + l_1 m_3 r_2 \dot{q}_3 \sin(2q_2 + q_3)\big] \\
h_2 =& \big[I_{z2}\dot{q}_1^2 \sin(2q_2) - I_{y2}\dot{q}_1^2 \sin(2q_2) - I_{y3}\dot{q}_1^2 \sin(2q_2 + 2q_3) + I_{z3}\dot{q}_1^2 \sin(2q_2 + 2q_3) + l_1^2 m_3 \dot{q}_1^2 \sin(2q_2) \\
& + m_2 r_1^2 \dot{q}_1^2 \sin(2q_2) + m_3 r_2^2 \dot{q}_1^2 \sin(2q_2 + 2q_3)\big]/2 - l_1 m_3 r_2 \dot{q}_3^2 \sin(q_3) + l_1 m_3 r_2 \dot{q}_1^2 \sin(2q_2 + q_3) \\
& - 2 l_1 m_3 r_2 \dot{q}_2 \dot{q}_3 \sin(q_3) \\
h_3 =& \sin(q_2 + q_3)\big[m_3 \cos(q_2 + q_3) r_2^2 + l_1 m_3 \cos(q_2) r_2 - I_{y3} \cos(q_2 + q_3) + I_{z3} \cos(q_2 + q_3)\big]\dot{q}_1^2 \\
& + l_1 m_3 r_2 \sin(q_3)\dot{q}_2^2 \\
G_1 =& 0, \;\; G_2 = -g m_3 \left[r_2 \cos(q_2 + q_3) + l_1 \cos(q_2)\right] - g m_2 r_1 \cos(q_2) \\
G_3 =& -g m_3 r_2 \cos(q_2 + q_3), \;\; f = [f_1, \;\; f_2]^T = 0.04\dot{q} + 0.007 sign(\dot{q}).
\end{aligned}
$$

A.10 Proof of Theorem 6

Considering the Lyapunov function

$$V = \frac{1}{2}\dot{\boldsymbol{z}}_{\boldsymbol{2}}^{\boldsymbol{T}} \boldsymbol{M_d} \dot{\boldsymbol{z}}_{\boldsymbol{2}} + \frac{1}{2}\boldsymbol{e_x^T \zeta(t) e_x} \tag{A.61}$$

where $\boldsymbol{\zeta(t)}$ is a function of the variable damping and the stiffness coefficients of the desired impedance and is a symmetric, positive definite matrix with continuously differentiable elements. Differentiating V and using (3.56) and (3.57), the following is obtained:

$$
\begin{aligned}
\dot{V} =& \dot{\boldsymbol{z}}_{\boldsymbol{2}}^{\boldsymbol{T}} \boldsymbol{M_d} \ddot{\boldsymbol{z}}_{\boldsymbol{2}} + \boldsymbol{e_x^T \zeta(t) \dot{e}_x} + \frac{1}{2}\boldsymbol{e_x^T \dot{\zeta}(t) e_x} \\
\dot{V} =& \boldsymbol{(\dot{e}_x + c_1 e_x)^T M_d (\ddot{e}_x + c_1 \dot{e}_x) + e_x^T \zeta(t) \dot{e}_x} + \frac{1}{2}\boldsymbol{e_x^T \dot{\zeta}(t) e_x}
\end{aligned} \tag{A.62}
$$

Now, from (3.48), considering $\boldsymbol{F_e = 0}$ the following can be derived

$$\boldsymbol{M_d \ddot{e}_x = -B_d(t)\dot{e}_x - K_d(t) e_x} \tag{A.63}$$

Using (A.63) in (A.62), $\dot{V}$ can be derived as follows

$$
\begin{aligned}
\dot{V} =& \boldsymbol{(\dot{e}_x + c_1 e_x)^T (-B_d(t)\dot{e}_x - K_d(t) e_x + M_d c_1 \dot{e}_x) + e_x^T \zeta(t) \dot{e}_x} + \frac{1}{2}\boldsymbol{e_x^T \dot{\zeta}(t) e_x} \\
=& -\boldsymbol{e_x^T} \left(\boldsymbol{c_1 k_d(t)} - \frac{\boldsymbol{1}}{\boldsymbol{2}}\boldsymbol{\dot{\zeta}(t)}\right) \boldsymbol{e_x} - \boldsymbol{\dot{e}_x^T \left(B_d(t) - M_d c_1\right) \dot{e}_x} \\
& - \boldsymbol{\dot{e}_x^T \left(K_d(t) + c_1 B_d(t) - c_1 M_d c_1 - \zeta(t)\right) e_x}
\end{aligned} \tag{A.64}
$$

In order to ascertain negative definiteness of $\dot{V}$, the variable matrix $\boldsymbol{\zeta(t)}$ is chosen as

$$\boldsymbol{\zeta(t)} = \boldsymbol{K_d(t)} + \boldsymbol{c_1 B_d(t)} - \boldsymbol{c_1 M_d c_1} \tag{A.65}$$

$$\Rightarrow \dot{\boldsymbol{\zeta}}\boldsymbol{(t)} = \dot{\boldsymbol{K}}_{\boldsymbol{d}}\boldsymbol{(t)} + \boldsymbol{c_1}\dot{\boldsymbol{B}}_{\boldsymbol{d}}\boldsymbol{(t)}. \tag{A.66}$$

Now, replacing $\boldsymbol{\zeta(t)}$ and $\dot{\boldsymbol{\zeta}}\boldsymbol{(t)}$ in (A.64), the following is obtained

$$\dot{V} = -\boldsymbol{e_x^T}\left(\boldsymbol{c_1 K_d(t)} - \frac{\mathbf{1}}{\mathbf{2}}\dot{\boldsymbol{K}}_{\boldsymbol{d}}\boldsymbol{(t)} - \frac{\mathbf{1}}{\mathbf{2}}\boldsymbol{c_1}\dot{\boldsymbol{B}}_{\boldsymbol{d}}\boldsymbol{(t)}\right) - \dot{\boldsymbol{e}}_{\boldsymbol{x}}^{\boldsymbol{T}}\left(\boldsymbol{B_d(t)} - \boldsymbol{c_1 M_d}\right)\dot{\boldsymbol{e}}_{\boldsymbol{x}}. \tag{A.67}$$

Therefore, to ensure stability of the chosen impedance characteristics, the following conditions should be satisfied:

(i) $\boldsymbol{B_d(t)} - \boldsymbol{c_1 M_d}$ should be a positive definite matrix,

(ii) $\boldsymbol{c_1 K_d(t)} - \frac{\mathbf{1}}{\mathbf{2}}\dot{\boldsymbol{K}}_{\boldsymbol{d}}\boldsymbol{(t)} - \frac{\mathbf{1}}{\mathbf{2}}\boldsymbol{c_1}\dot{\boldsymbol{B}}_{\boldsymbol{d}}\boldsymbol{(t)}$ must be positive definite.

A.11 Time derivative of the sliding manifold used in Chapter 4

The fast terminal sliding manifold (4.9) can be rewritten as

$$s = \begin{cases} z_1 + \beta z_2^{\lambda}, & z_2 > 0 \\ z_1, & z_2 = 0 \\ z_1 - \beta(-z_2)^{\lambda}, & z_2 < 0 \end{cases} \tag{A.68}$$

The sliding variable is continuous for both $z_2 > 0$, $z_2 < 0$ and also at $z_2 = 0$ as shown in the following:

$$s(z_1, 0) = \lim_{z_2 \to 0+} s(z_1, z_2) = \lim_{z_2 \to 0-} s(z_1, z_2) = z_1. \tag{A.69}$$

Since the partial derivatives of s at right and left hand sides of z_2 exist as shown below, hence $s(z_1, z_2)$ is differentiable at $z_2 = 0$.

$$\left.\frac{\partial s(z_1, z_2)}{\partial z_2}\right|_{z_2=0_-} = \lim_{h \to 0-} \frac{\beta(-z_2)^{\lambda}}{-h} = \lim_{h \to 0-} \beta(-h)^{\lambda-1} = 0 \tag{A.70}$$

and

$$\left.\frac{\partial s(z_1, z_2)}{\partial z_2}\right|_{z_2=0_+} = \lim_{h \to 0+} \frac{\beta(z_2)^{\lambda}}{h} = \lim_{h \to 0+} \beta(h)^{\lambda-1} = 0. \tag{A.71}$$

Therefore

$$\frac{\partial s(z_1, z_2)}{\partial z_2} = \begin{cases} \beta\lambda z_2^{\lambda-1}, & z_2 > 0 \\ 0, & z_2 = 0 \\ \beta\lambda(-z_2)^{\lambda-1}, & z_2 < 0 \end{cases}$$

which can be equivalently written as

$$\frac{\partial s(z_1, z_2)}{\partial z_2} = \beta\lambda|z_2|^{\lambda-1}.$$

Hence, the time derivative of the sliding variable will be,

$$\begin{aligned}\dot{s}(z_1, z_2) =& \frac{\partial s(z_1, z_2)}{\partial z_1}\dot{z}_1 + \frac{\partial s(z_1, z_2)}{\partial z_2}\dot{z}_2 \\ =& \dot{z}_1 + \beta\lambda|z_2|^{\lambda-1}\dot{z}_2.\end{aligned} \tag{A.72}$$

A.12 Derivation of $\dot{s}$ in (4.16)

From (4.9) and (4.11), the time derivative of $\boldsymbol{s}$ for $\boldsymbol{z_2 > 0, z_2 = 0}$ and $\boldsymbol{z_2 < 0}$ can be obtained as

$$\dot{\boldsymbol{s}} = \begin{cases} \dot{\boldsymbol{z}}_{\boldsymbol{1}} + \beta\delta|\boldsymbol{z_2}|^{\delta-2} \circ \boldsymbol{z_2} \circ \dot{\boldsymbol{z}}_{\boldsymbol{2}}, & \boldsymbol{z_2 > 0} \\ \dot{\boldsymbol{z}}_{\boldsymbol{1}}, & \boldsymbol{z_2 = 0} \\ \dot{\boldsymbol{z}}_{\boldsymbol{1}} - \beta\delta|\boldsymbol{z_2}|^{\delta-2} \circ \boldsymbol{z_2} \circ \dot{\boldsymbol{z}}_{\boldsymbol{2}}, & \boldsymbol{z_2 < 0} \end{cases} \tag{A.73}$$

Now, (A.73) can be written as the following generalized form giving the derivative $\dot{\boldsymbol{s}}$

$$\begin{aligned}\dot{\boldsymbol{s}} =& \dot{\boldsymbol{z}}_{\boldsymbol{1}} + \beta\delta|\boldsymbol{z_2}|^{\delta-2} \circ \boldsymbol{z_2} \circ sign(\boldsymbol{z_2}) \circ \dot{\boldsymbol{z}}_{\boldsymbol{2}} \\ =& \dot{\boldsymbol{z}}_{\boldsymbol{1}} + \beta\delta|\boldsymbol{z_2}|^{\delta-2} \circ |\boldsymbol{z_2}| \circ \dot{\boldsymbol{z}}_{\boldsymbol{2}} \\ =& \dot{\boldsymbol{z}}_{\boldsymbol{1}} + \beta\delta|\boldsymbol{z_2}|^{\delta-1} \circ \dot{\boldsymbol{z}}_{\boldsymbol{2}} \\ =& \dot{\boldsymbol{z}}_{\boldsymbol{1}} + \beta\delta|\boldsymbol{z_2}|^{\delta-1} \circ \left(\boldsymbol{M_h^{-1}}(\boldsymbol{\tau_m} - \boldsymbol{C_h}\dot{\boldsymbol{q}} - \boldsymbol{G_h}) - \ddot{\boldsymbol{q}}_{\boldsymbol{d}} + \boldsymbol{c_1}\dot{\boldsymbol{z}}_{\boldsymbol{1}}\right).\end{aligned} \tag{A.74}$$

A.13 2 DoF manipulator model used in Simulation 4.3

The model of the 2 DoF robot arm is given by

$$\begin{bmatrix} m_{11}(q_2) & m_{12}(q_2) \\ m_{12}(q_2) & m_{22} \end{bmatrix} \begin{bmatrix} \ddot{q}_1 \\ \ddot{q}_2 \end{bmatrix} + \begin{bmatrix} -c_{12}(q_2)\dot{q}_1^2 - 2c_{12}(q_2)\dot{q}_1\dot{q}_2 \\ c_{12}\dot{q}_2^2 \end{bmatrix} + \begin{bmatrix} G_1(q_1, q_2) \\ G_2(q_1, q_2) \end{bmatrix} = \begin{bmatrix} \tau_1 \\ \tau_2 \end{bmatrix} + \begin{bmatrix} \tau_{d1} \\ \tau_{d2} \end{bmatrix} \tag{A.75}$$

where

$$\begin{aligned} m_{11}(q_2) =& (m_1 + m_2)l_1^2 + m_2 l_2^2 + 2m_2 l_1 l_2 \cos(q_2) + J_1 \\ m_{12}(q) =& m_1 l_2^2 + m_2 l_1 l_2 \cos(q_2) \\ m_{22} =& m_2 l_2^2 + J_2 \\ c_{12}(q_2) =& m_2 l_1 l_2 \sin(q_2) \\ G_1(q_1, q_2) =& (m_1 + m_2)l_1 g \cos(q_2) + m_2 l_2 g \cos(q_1 + q_2) \\ G_2(q_1, q_2) =& m_2 l_2 g \cos(q_1 + q_2) \end{aligned}$$

and $g = 9.81\text{m/s}^2$ is the acceleration due to gravity.

A.14 RFTSM controller by Zhao *et al.* [3] used in Chapter 4

The RFTSC based controller proposed in [3] has the following structure:

$$\begin{aligned}
\tau_Z =& \tau_0 + \tau_1 \\
\tau_0 =& C_0(x_1 + q_d, x_2)x_2 + G_0(x_1 + q_d) \\
&+ M_0(x + q_d)(\dot{\phi}(x_1) - x_1 - k_2 z) \\
\tau_1 =& \begin{cases} \frac{-(z^T M_0^{-1}(x_1+q_d))^T}{||z_0^T M_0^{-1}(x_1+q_d)||}\big(b_0 + b_1||x_1 + q_d|| & \\ +b_2||x_2||^2\big), & ||z|| \neq 0 \\ 0, & ||z|| = 0 \end{cases}
\end{aligned} \tag{A.76}$$

where

$$\begin{aligned}
\phi(x_1) &= -k_1 sig(x_1)^p \\
z &= x_2 - \phi(x_1) \\
x_1 = q - q_d;\ x_2 &= \dot{q} - \dot{q}_d
\end{aligned}$$

and τ_Z is the applied control law obtained using Zhao *et al.* 's algorithm [3]. The terms M_0, C_0 and G_0 are the manipulator parameter matrices under nominal conditions. The parameters used for the controller τ_Z are $k_1 = k_2 = diag(1.8, 1.8)$, $p = 3/5$, $b_0 = 0.9$, $b_1 = 0.1$, $b_2 = 0.1$. The notation $sig(x_1)^p$, $x_1 \in \mathbb{R}^n$, $0 < p < 1$ defines the following:
$sig(x_1)^p = \big[|x_{11}|^p sign(x_{11}), \ldots, |x_{1n}|^p sign(x_{1n})\big]^T$.

References

[1] M.-S. Park and D. Chwa, "Swing-up and stabilization control of inverted-pendulum systems via coupled sliding-mode control method," *IEEE Transactions on Industrial Electronics*, vol. 56, no. 9, pp. 3541 –3555, Sept. 2009.

[2] Z. J. Yang, Y. Fukushima, and P. Qin, "Decentralized adaptive robust control of robot manipulators using disturbance observers," *IEEE Transactions on Control Systems Technology*, vol. 20, no. 5, pp. 1357–1365, Sept 2012.

[3] D. Zhao, S. Li, Q. Zhu, and F. Gao, "Robust finite-time control approach for robotic manipulators," *IET Control Theory Applications*, vol. 4, no. 1, pp. 1–15, Jan 2010.

[4] "Robotis Co. Ltd." 2017. [Online]. Available: http://www.robotis.com/

[5] J. Wojtusch, "Development of Electronics and Control for Servo Actuators in Robotic Applications," Diploma thesis, Department of Computer Science, Technische Universitt Darmstadt, Darmstadt, Germany, January 2011.

[6] "Robotis Co. Ltd." [Online]. Available: http://support.robotis.com/en/product/actuator/dynamixel/rx_series/rx-28.htm

[7] "Robotis Co. Ltd." [Online]. Available: http://support.robotis.com/en/product/actuator/dynamixel/rx_series/rx-64.htm

[8] "www.maxonmotor.com." [Online]. Available: http://www.maxonmotor.com/medias/sys_master/root/8813529792542/14-151-EN.pdf

[9] "www.maxonmotor.com." [Online]. Available: http://www.maxonmotor.com/medias/sys_master/root/8821063024670/16-225-EN.pdf

[10] M. W. Spong, S. Hutchinson, and M. Vidyasagar, *Robot modeling and control*. Wiley New York, 2006, vol. 3.

[11] R. M. Murray, Z. Li, S. S. Sastry, and S. S. Sastry, *A mathematical introduction to robotic manipulation*. CRC press, 1994.

[12] W. R. Ferrell and T. B. Sheridan, "Supervisory control of remote manipulation," *IEEE Spectrum*, vol. 4, no. 10, pp. 81–88, Oct 1967.

[13] H. A. Ernst, "Mh-1, a computer-operated mechanical hand," in *Proceedings of the May 1-3, 1962, Spring Joint Computer Conference*, ser. AIEE-IRE '62 (Spring). New York, NY, USA: ACM, 1962, pp. 39–51. [Online]. Available: http://doi.acm.org/10.1145/1460833.1460839

[14] I. Morishita and M. Sakurai, "Automatic manipulation using a binocular sensory system," *IEEE Transactions on Automatic Control*, vol. 13, no. 6, pp. 694–697, Dec 1968.

[15] A. Freedy, F. C. Hull, L. F. Lucaccini, and J. Lyman, "A computer-based learning system for remote manipulator control," *IEEE Transactions on Systems, Man, and Cybernetics*, vol. SMC-1, no. 4, pp. 356–363, Oct 1971.

[16] A. K. Bejczy, "Robot arm dynamics and control," Jet Propulsion Lab., California Inst. of Tech., Pasadena, CA, United States, Tech. Rep., Feb 1974.

[17] S. J. Merhav and O. B. Ya'Acov, "Control augmentation and work load reduction by kinesthetic information from the manipulator," *IEEE Transactions on Systems, Man, and Cybernetics*, vol. SMC-6, no. 12, pp. 825–835, Dec 1976.

[18] B. Markiewicz, "Analysis of the computed torque drive method and comparison with conventional position servo for a computer-controlled manipulator," Jet Propulsion Lab., California Inst. of Tech., Pasadena, CA, United States, Tech. Rep., Mar 1973.

[19] M. Raibert, "Manipulator control using the configuration space method," *Industrial Robot: An International Journal*, vol. 5, no. 2, pp. 69–73, 1978.

[20] J. Yuan, "Dynamic decoupling of a remote manipulator system," *IEEE Transactions on Automatic Control*, vol. 23, no. 4, pp. 713–717, Aug 1978.

[21] H. Sage, M. De Mathelin, and E. Ostertag, "Robust control of robot manipulators: a survey," *International Journal of Control*, vol. 72, no. 16, pp. 1498–1522, 1999.

[22] D. Katić and M. Vukobratović, "Survey of intelligent control techniques for humanoid robots," *Journal of Intelligent Robotic Systems*, vol. 37, no. 2, pp. 117–141, Jun 2003. [Online]. Available: http://dx.doi.org/10.1023/A:1024172417914

[23] C. Abdallah, D. M. Dawson, P. Dorato, and M. Jamshidi, "Survey of robust control for rigid robots," *IEEE Control Sysems*, vol. 11, no. 2, pp. 24–30, Feb 1991.

[24] X. Yu and M. Zhihong, "Fast terminal sliding-mode control design for nonlinear dynamical systems," *IEEE Transactions on Circuits and Systems I, Fundamemtal Theory and Applications*, vol. 49, no. 2, pp. 261–264, Feb 2002.

[25] K. Youcef-Toumi and O. Ito, "A time delay controller for systems with unknown dynamics," *Journal of Dynamic Systems, Measurement and Control*, vol. 112, no. 1, pp. 133–142, 1990.

[26] S. Kawamura, F. Miyazaki, and S. Arimoto, "Is a local linear PD feedback control law effective for trajectory tracking of robot motion?" vol. 3, pp. 1335–1340, Apr 1988.

[27] P. Tomei, "Adaptive pd controller for robot manipulators," *IEEE Transactions on Robotics and Automation*, vol. 7, no. 4, pp. 565–570, Aug 1991.

[28] Y. Su, P. C. Muller, and C. Zheng, "Global asymptotic saturated pid control for robot manipulators," *IEEE Transactions on Control Systems Technology*, vol. 18, no. 6, pp. 1280–1288, Nov 2010.

[29] I. Cervantes and J. Alvarez-Ramirez, "On the PID tracking control of robot manipulators," *Systems & Control Letters*, vol. 42, no. 1, pp. 37 – 46, Jan 2001. [Online]. Available: http://www.sciencedirect.com/science/article/pii/S0167691100000773

[30] V. Parra-Vega, S. Arimoto, Y.-H. Liu, G. Hirzinger, and P. Akella, "Dynamic sliding PID control for tracking of robot manipulators: theory and experiments," *IEEE Transactions on Robotics and Automation*, vol. 19, no. 6, pp. 967–976, Dec 2003.

[31] Y. X. Su, B. Y. Duan, and C. H. Zheng, "Nonlinear PID control of a six-DOF parallel manipulator," *IEEE Proceedings - Control Theory and Applications*, vol. 151, no. 1, pp. 95–102, Jan 2004.

[32] Y. Su, D. Sun, and B. Duan, "Design of an enhanced nonlinear PID controller," *Mechatronics*, vol. 15, no. 8, pp. 1005 – 1024, Oct 2005. [Online]. Available: http://www.sciencedirect.com/science/article/pii/S0957415805000590

[33] J. L. Meza, V. Santibanez, R. Soto, and M. A. Llama, "Fuzzy self-tuning PID semiglobal regulator for robot manipulators," *IEEE Transactions on Industrial Electronics*, vol. 59, no. 6, pp. 2709–2717, June 2012.

[34] A. Dumlu and K. Erenturk, "Trajectory tracking control for a 3-DOF parallel manipulator using fractional-order $PI^{\lambda}D^{\mu}$ control," *IEEE Transactions on Industrial Electronics*, vol. 61, no. 7, pp. 3417–3426, July 2014.

[35] W. L. Stout and M. E. Sawan, "Application of H∞ theory to robot manipulator control," in *in Proceedings of The First IEEE Conference on Control Applications*, vol. 1, Sep 1992, pp. 148–153.

[36] H. G. Sage, M. F. de Mathelin, G. Abba, J. A. Gangloff, and E. Ostertag, "Performance optimized H_{∞} control of industrial robot manipulators," in *1997 European Control Conference (ECC)*, July 1997, pp. 2395–2400.

[37] S. Arimoto and M. Takegaki, "A new feedback method for dynamic control of manipulators," *Journal of Dynamic Systems, Measurement Control*, vol. 102, pp. 119–125, 1981.

[38] R. Ortega and M. W. Spong, "Adaptive motion control of rigid robots: a tutorial," in *Proceedings of the 27th IEEE Conference on Decision and Control*, Dec 1988, pp. 1575–1584 vol.2.

[39] R. L. Leal and C. C. DeWit, "Passivity based adaptive control for mechanical manipulators using LS-type estimation," *IEEE Transactions on Automatic Control*, vol. 35, no. 12, pp. 1363–1365, Dec 1990.

[40] Y. Tang and M. A. Arteaga, "Adaptive control of robot manipulators based on passivity," in *Proceedings of 32nd IEEE Conference on Decision and Control*, Dec 1993, pp. 148–152 vol.1.

[41] L. Villani, C. C. D. Wit, and B. Brogliato, "An exponentially stable adaptive control for force and position tracking of robot manipulators," *IEEE Transactions on Automatic Control*, vol. 44, no. 4, pp. 798–802, Apr 1999.

[42] L. Hsu, R. R. Costa, and F. Lizarralde, "Lyapunov/passivity-based adaptive control of relative degree two MIMO systems with an application to visual servoing," *IEEE Transactions on Automatic Control*, vol. 52, no. 2, pp. 364–371, Feb 2007.

[43] H. Berghuis and H. Nijmeijer, "A passivity approach to controller-observer design for robots," *IEEE Transactions on Robotics and Automation*, vol. 9, no. 6, pp. 740–754, Dec 1993.

[44] J. Kasac, B. Novakovic, D. Majetic, and D. Brezak, "Passive finite-dimensional repetitive control of robot manipulators," *IEEE Transactions on Control Systems Technology*, vol. 16, no. 3, pp. 570–576, May 2008.

[45] B. Siciliano and L. Villani, "A passivity-based approach to force regulation and motion control of robot manipulators," *Automatica*, vol. 32, no. 3, pp. 443 – 447, 1996.

[46] J.-H. Ryu, D.-S. Kwon, and B. Hannaford, "Stability guaranteed control: time domain passivity approach," *IEEE Transactions on Control Systems Technology*, vol. 12, no. 6, pp. 860–868, Nov 2004.

[47] G. Leitmann, "On the efficacy of nonlinear control in uncertain linear systems," *ASME, Transactions, Journal of Dynamic Systems, Measurement and Control*, vol. 103, pp. 95–102, 1981.

[48] M. Corless and G. Leitmann, "Continuous state feedback guaranteeing uniform ultimate boundedness for uncertain dynamic systems," *IEEE Transactions on Automatic Control*, vol. 26, no. 5, pp. 1139–1144, Oct 1981.

[49] M. W. Spong, J. S. Thorp, and J. M. Kleinwaks, "The control of robot manipulators with bounded input: Part II: Robustness and disturbance rejection," in *The 23rd IEEE Conference on Decision and Control*, Dec 1984, pp. 1047–1052.

[50] R. Shoureshi, M. E. Momot, and M. Roesler, "Robust control for manipulators with uncertain dynamics," *Automatica*, vol. 26, no. 2, pp. 353 – 359, 1990.

[51] M. W. Spong, "On the robust control of robot manipulators," *IEEE Transactions on Automatic Control*, vol. 37, no. 11, pp. 1782–1786, Nov 1992.

[52] J.-J. E. Slotine and W. Li, "On the adaptive control of robot manipulators," *The International Journal of Robotics Research*, vol. 6, no. 3, pp. 49–59, 1987.

[53] R. Johansson, "Adaptive control of robot manipulator motion," *IEEE Transactions on Robotics and Automation*, vol. 6, no. 4, pp. 483–490, Aug 1990.

[54] M. Krstic, I. Kanellakopoulos, and P. V. Kokotovic, *Nonlinear and adaptive control design*. Wiley, 1995.

[55] P. V. Kokotovic, M. Krstic, and I. Kanellakopoulos, "Backstepping to passivity: recursive design of adaptive systems," in *Proceedings of the 31st IEEE Conference on Decision and Control*, 1992, pp. 3276–3280 vol.4.

[56] D. M. Dawson, J. J. Carroll, and M. Schneider, "Integrator backstepping control of a brush DC motor turning a robotic load," *IEEE Transactions on Control Systems Technology*, vol. 2, no. 3, pp. 233–244, Sep 1994.

[57] C.-Y. Su, Y. Stepanenko, and S. Dost, "Hybrid integrator backstepping control of robotic manipulators driven by brushless DC motors," *IEEE/ASME Transactions on Mechatronics*, vol. 1, no. 4, pp. 266–277, Dec 1996.

[58] Y. Yang, G. Feng, and J. Ren, "A combined backstepping and small-gain approach to robust adaptive fuzzy control for strict-feedback nonlinear systems," *IEEE Transactions on Systems, Man, and Cybernetics - Part A: Systems and Humans*, vol. 34, no. 3, pp. 406–420, May 2004.

[59] M. R. Soltanpour and S. E. Shafiei, "Robust backstepping control of robot manipulator in task space with uncertainties in kinematics and dynamics." *Electronics & Electrical Engineering*, no. 96, pp. 75 – 80, 2009. [Online]. Available: http://search.ebscohost.com/login.aspx?direct=true&db=egs&AN=47055138&site=eds-live

[60] Q. Hu, L. Xu, and A. Zhang, "Adaptive backstepping trajectory tracking control of robot manipulator," *Journal of the Franklin Institute*, vol. 349, no. 3, pp. 1087 – 1105, 2012. [Online]. Available: http://www.sciencedirect.com/science/article/pii/S0016003212000026

[61] N. Chen, F. Song, G. Li, X. Sun, and C. Ai, "An adaptive sliding mode backstepping control for the mobile manipulator with nonholonomic constraints," *Communications in Nonlinear Science and Numerical Simulation*, vol. 18, no. 10, pp. 2885 – 2899, 2013. [Online]. Available: http://www.sciencedirect.com/science/article/pii/S1007570413000658

[62] N. Nikdel, M. Badamchizadeh, V. Azimirad, and M. Nazari, "Adaptive backstepping control for an n-degree of freedom robotic manipulator based on combined state augmentation," *Robotics and Computer-Integrated Manufacturing*, vol. 44, pp. 129 – 143, 2017. [Online]. Available: http://www.sciencedirect.com/science/article/pii/S0736584515300430

[63] V. Utkin, "Variable structure systems with sliding modes," *IEEE Transactions on Automatic Control*, vol. 22, no. 2, pp. 212–222, Apr 1977.

[64] C. Edwards and S. Spurgeon, *Sliding mode control: theory and applications*. CRC Press, 1998.

[65] K. K. D. Young, "Controller design for a manipulator using theory of variable structure systems," *IEEE Transactions on Systems, Man, and Cybernetics*, vol. 8, no. 2, pp. 101–109, Feb 1978.

[66] R. Morgan and U. Ozguner, "A decentralized variable structure control algorithm for robotic manipulators," *IEEE Journal on Robotics and Automation*, vol. 1, no. 1, pp. 57–65, Mar 1985.

[67] F. Harashima, J. X. Xu, and H. Hashimoto, "Tracking control of robot manipulators using sliding mode," *IEEE Transactions on Power Electronics*, vol. PE-2, no. 2, pp. 169–176, April 1987.

[68] J. X. Xu, H. Hashimoto, J. J. E. Slotine, Y. Arai, and F. Harashima, "Implementation of VSS control to robotic manipulators-smoothing modification," *IEEE Transactions on Industrial Electronics*, vol. 36, no. 3, pp. 321–329, Aug 1989.

[69] A. Bellini, G. Figalli, P. Pinello, and G. Ulivi, "Realization of a control device for a robotic manipulator based on nonlinear decoupling and sliding mode control," *IEEE Transactions on Industry Applications*, vol. 25, no. 5, pp. 790–799, Sep 1989.

[70] G. Ambrosino, G. Celektano, and F. Garofalo, "Variable structure model reference adaptive control systems," *International Journal of Control*, vol. 39, no. 6, pp. 1339–1349, 1984.

[71] F. Harashima, H. Hashimoto, and K. Maruyama, "Practical robust control of robot arm using variable structure system," in *Proceedings. 1986 IEEE International Conference on Robotics and Automation*, vol. 3, Apr 1986, pp. 532–539.

[72] J.-J. Slotine and S. S. Sastry, "Tracking control of non-linear systems using sliding surfaces, with application to robot manipulators," *International journal of control*, vol. 38, no. 2, pp. 465–492, 1983.

[73] P. Kachroo and M. Tomizuka, "Chattering reduction and error convergence in the sliding-mode control of a class of nonlinear systems," *IEEE Transactions on Automatic Control*, vol. 41, no. 7, pp. 1063–1068, Jul 1996.

[74] V. Utkin and J. Shi, "Integral sliding mode in systems operating under uncertainty conditions," in *Proceedings of 35th IEEE Conference on Decision and Control*, vol. 4, Dec 1996, pp. 4591–4596 vol.4.

[75] H. Sira-Ramirez, "On the dynamical sliding mode control of nonlinear systems," *International journal of control*, vol. 57, no. 5, pp. 1039–1061, 1993.

[76] M. Rios-Bolivar, A. Zinober, and H. Sira-Ramirez, "Dynamical adaptive sliding mode output tracking control, of a class of nonlinear," *International Journal of Robust and Nonlinear Control*, vol. 7, pp. 387–405, 1997.

[77] M. Zak, "Terminal attractors for addressable memory in neural networks," *Physics Letters A*, vol. 133, no. 1, pp. 18–22, 1988. [Online]. Available: http://www.sciencedirect.com/science/article/pii/0375960188907281

[78] M. Zhihong, A. P. Paplinski, and H. R. Wu, "A robust MIMO terminal sliding mode control scheme for rigid robotic manipulators," *IEEE Transactions on Automatic Control*, vol. 39, no. 12, pp. 2464–2469, Dec 1994.

[79] Y. Wu, X. Yu, and Z. Man, "Terminal sliding mode control design for uncertain dynamic systems," *Systems & Control Letters*, vol. 34, no. 5, pp. 281 – 287, 1998. [Online]. Available: http://www.sciencedirect.com/science/article/pii/S016769119800036X

[80] Y. Feng, X. Yu, and Z. Man, "Non-singular terminal sliding mode control of rigid manipulators," *Automatica*, vol. 38, no. 12, pp. 2159–2167, 2002. [Online]. Available: http://www.sciencedirect.com/science/article/pii/S0005109802001474

[81] A. Levant, "Sliding order and sliding accuracy in sliding mode control."

[82] L. M. Capisani, A. Ferrara, and L. Magnani, "Design and experimental validation of a second-order sliding-mode motion controller for robot manipulators," *International Journal of Control*, vol. 82, no. 2, pp. 365–377, 2009. [Online]. Available: http://www.tandfonline.com/doi/abs/10.1080/00207170802112591

[83] S. Mondal and C. Mahanta, "Adaptive second order terminal sliding mode controller for robotic manipulators," *Journal of the Franklin Institute*, vol. 351, no. 4, pp. 2356 – 2377, 2014, special Issue on 2010-2012 Advances in Variable Structure Systems and Sliding Mode Algorithms. [Online]. Available: http://www.sciencedirect.com/science/article/pii/S0016003213003189

[84] A. Ferrara and G. P. Incremona, "Design of an integral suboptimal second-order sliding mode controller for the robust motion control of robot manipulators," *IEEE Transactions on Control Systems Technology*, vol. 23, no. 6, pp. 2316–2325, Nov 2015.

[85] G. Bartolini, A. Levant, A. Pisano, and E. Usai, "Adaptive second-order sliding mode control with uncertainty compensation," *International Journal of Control*, vol. 89, no. 9, pp. 1747–1758, 2016.

[86] C.-I. Huang, K.-Y. Lian, C.-S. Chiu, and L.-C. Fu, "Smooth sliding mode control for constrained manipulator with joint flexibility," *IFAC Proceedings Volumes*, vol. 38, no. 1, pp. 91 – 96, 2005, 16th IFAC World Congress.

[87] L. M. Capisani, A. Ferrara, and A. Pisano, "Second-order sliding mode control with adaptive control authority for the tracking control of robotic manipulators," *IFAC Proceedings Volumes*, vol. 44, no. 1, pp. 10 319 – 10 324, 2011, 18th IFAC World Congress. [Online]. Available: http://www.sciencedirect.com/science/article/pii/S1474667016452705

[88] J. Yim and J. H. Park, "Nonlinear H_∞ control of robotic manipulator," in *Conference Proceedings of IEEE International Conference on Systems, Man, and Cybernetics (IEEE SMC '99)*, vol. 2, Oct 1999, pp. 866–871 vol.2.

[89] M. J. Kim, Y. Choi, and W. K. Chung, "Bringing nonlinear $\mathcal{H}_\infty$ optimality to robot controllers," *IEEE Transactions on Robotics*, vol. 31, no. 3, pp. 682–698, June 2015.

[90] G. Rigatos, P. Siano, and G. Raffo, "An H-infinity nonlinear control approach for multi-DOF robotic manipulators," *IFAC-PapersOnLine*, vol. 49, no. 12, pp. 1406 – 1411, June 2016. [Online]. Available: http://www.sciencedirect.com/science/article/pii/S2405896316310473

[91] J.-J. E. Slotine and W. Li, "On the adaptive control of robot manipulators," *The International Journal of Robotics Research*, vol. 6, no. 3, pp. 49–59, 1987. [Online]. Available: http://dx.doi.org/10.1177/027836498700600303

[92] M. W. Spong, "Adaptive control of flexible joint manipulators," *Systems & Control Letters*, vol. 13, no. 1, pp. 15 – 21, 1989. [Online]. Available: http://www.sciencedirect.com/science/article/pii/0167691189900169

[93] S. Singh, "Adaptive model following control of nonlinear robotic systems," *IEEE Transactions on Automatic Control*, vol. 30, no. 11, pp. 1099–1100, Nov 1985.

[94] J.-J. E. Slotine and W. Li, "Composite adaptive control of robot manipulators," *Automatica*, vol. 25, no. 4, pp. 509 – 519, 1989. [Online]. Available: http://www.sciencedirect.com/science/article/pii/0005109889900940

[95] L. L. Whitcomb, A. A. Rizzi, and D. E. Koditschek, "Comparative experiments with a new adaptive controller for robot arms," *IEEE Transactions on Robotics and Automation*, vol. 9, no. 1, pp. 59–70, Feb 1993.

[96] P. Ioannou and K. Tsakalis, "A robust direct adaptive controller," *IEEE Transactions on Automatic Control*, vol. 31, no. 11, pp. 1033–1043, Nov 1986.

[97] G. Tao, "On robust adaptive control of robot manipulators," *Automatica*, vol. 28, no. 4, pp. 803 – 807, 1992. [Online]. Available: http://www.sciencedirect.com/science/article/pii/000510989290040M

[98] J. Peng, J. Yu, and J. Wang, "Robust adaptive tracking control for nonholonomic mobile manipulator with uncertainties," {*ISA*} *Transactions*, vol. 53, no. 4, pp. 1035 – 1043, 2014, disturbance Estimation and Mitigation. [Online]. Available: http://www.sciencedirect.com/science/article/pii/S0019057814001013

[99] J. S. Reed and P. A. Ioannou, "Instability analysis and robust adaptive control of robotic manipulators," *IEEE Transactions on Robotics and Automation*, vol. 5, no. 3, pp. 381–386, Jun 1989.

[100] P. Tomei, "Robust adaptive control of robots with arbitrary transient performance and disturbance attenuation," *IEEE Transactions on Automatic Control*, vol. 44, no. 3, pp. 654–658, Mar 1999.

[101] L. C. Fu, "Robust adaptive decentralized control of robot manipulators," *IEEE Transactions on Automatic Control*, vol. 37, no. 1, pp. 106–110, Jan 1992.

[102] H. Berghuis, R. Ortega, and H. Nijmeijer, "A robust adaptive robot controller," *IEEE Transactions on Robotics and Automation*, vol. 9, no. 6, pp. 825–830, Dec 1993.

[103] R. H. Middletone and G. C. Goodwin, "Adaptive computed torque control for rigid link manipulators," in *1986 25th IEEE Conference on Decision and Control*, Dec 1986, pp. 68–73.

[104] P. Hsu, M. Bodson, S. Sastry, and B. Paden, "Adaptive identification and control for manipulators without using joint accelerations," in *Proceedings. 1987 IEEE International Conference on Robotics and Automation*, vol. 4, Mar 1987, pp. 1210–1215.

[105] S. Mohammad-Hoseini, M. Farrokhi, and A. Koshkouei, "Robust adaptive control of uncertain non-linear systems using neural networks," *International Journal of Control*, vol. 81, no. 8, pp. 1319–1330, 2008. [Online]. Available: http://dx.doi.org/10.1080/00207170701771885

[106] V. E. Oscar Barambones, "Robust adaptive control for robot manipulators with unmodelled dynamics," *Cybernetics and Systems*, vol. 31, no. 1, pp. 67–86, 2000. [Online]. Available: http://dx.doi.org/10.1080/019697200124928

[107] G. FENG and R. L. REN, "Robust adaptive control for robot manipulators," *International Journal of Systems Science*, vol. 26, no. 5, pp. 1017–1028, 1995. [Online]. Available: http://dx.doi.org/10.1080/00207729508929085

[108] C. S. Chen, "Dynamic structure neural-fuzzy networks for robust adaptive control of robot manipulators," *IEEE Transactions on Industrial Electronics*, vol. 55, no. 9, pp. 3402–3414, Sept 2008.

[109] Z. J. Yang, Y. Fukushima, and P. Qin, "Decentralized adaptive robust control of robot manipulators using disturbance observers," *IEEE Transactions on Control Systems Technology*, vol. 20, no. 5, pp. 1357–1365, Sept 2012.

[110] S. Islam and P. X. Liu, "Robust adaptive fuzzy output feedback control system for robot manipulators," *IEEE/ASME Transactions on Mechatronics*, vol. 16, no. 2, pp. 288–296, April 2011.

[111] A. A. Pyrkin, A. A. Bobtsov, S. A. Kolyubin, M. V. Faronov, O. I. Borisov, V. S. Gromov, S. M. Vlasov, and N. A. Nikolaev, "Simple robust and adaptive tracking control for mobile robots," *IFAC-PapersOnLine*, vol. 48, no. 11, pp. 143 – 149, 2015. [Online]. Available: http://www.sciencedirect.com/science/article/pii/S2405896315012550

[112] M. Vijay and D. Jena, "Optimal backstepping sliding mode control for robot manipulator," in *2015 IEEE International Conference on Signal Processing, Informatics, Communication and Energy Systems (SPICES)*, Feb 2015, pp. 1–5.

[113] Q. Chen, L. Shi, L. Tao, and F. Dong, "Adaptive tracking control of robotic manipulators with unknown input saturation using backstepping sliding mode technique," in *2016 Chinese Control and Decision Conference (CCDC)*, May 2016, pp. 26–31.

[114] Y. Jin, P. H. Chang, M. Jin, and D. G. Gweon, "Stability guaranteed time-delay control of manipulators using nonlinear damping and terminal sliding mode," *IEEE Transactions on Industrial Electronics*, vol. 60, no. 8, pp. 3304–3317, Aug 2013.

[115] A.-C. Huang and Y.-C. Chen, "Adaptive sliding control for single-link flexible-joint robot with mismatched uncertainties," *IEEE Transactions on Control Systems Technology*, vol. 12, no. 5, pp. 770–775, Sept 2004.

[116] O. Khatib, P. Thaulad, T. Yoshikawa, and J. Park, "Torque-position transformer for task control of position controlled robots," in *IEEE International Conference on Robotics and Automation, ICRA*. IEEE, 2008, pp. 1729–1734.

[117] A. D. Prete, N. Mansard, O. E. Ramos, O. Stasse, and F. Nori, "Implementing torque control with high-ratio gear boxes and without joint-torque sensors," *International Journal of Humanoid Robotics*, p. 1550044, 2015.

[118] V. Utkin, J. Guldner, and J. Shi, *Sliding mode control in electro-mechanical systems*. CRC press, 2009, vol. 34.

[119] H. Sira-Ramirez and O. Llanes-Santiago, "Adaptive dynamical sliding mode control via backstepping," in *Proceedings of the 32nd IEEE Conference on Decision and Control*, Dec 1993, pp. 1422–1427 vol.2.

[120] M. Rios-Bolivar, H. Sira-Ramirez, and A. S. I. Zinober, "Output tracking control via adaptive input-output linearization: a backstepping approach," in *Proceedings of the 34th IEEE Conference on Decision and Control*, vol. 2, Dec 1995, pp. 1579–1584 vol.2.

[121] P. Liu and A. S. I. Zinober, "Robust control of nonlinear uncertain systems via sliding-mode with recursive-interlacing design," in *IEEE International Workshop on Variable Structure Systems,*, Dec 1996, pp. 26–30.

[122] J. Qing-xuan, Z. Xiao-dong, and S. Han-xu, "Integral backstepping sliding-mode control for space manipulator modular joint using RBFN observer," in *2007 International Conference on Information Acquisition*, July 2007, pp. 385–390.

[123] D. Swaroop, J. C. Gerdes, P. P. Yip, and J. K. Hedrick, "Dynamic surface control of nonlinear systems," in *Proceedings of the American Control Conference*, vol. 5, Jun 1997, pp. 3028–3034 vol.5.

[124] D. Swaroop, J. K. Hedrick, P. P. Yip, and J. C. Gerdes, "Dynamic surface control for a class of nonlinear systems," *IEEE Transactions on Automatic Control*, vol. 45, no. 10, pp. 1893–1899, Oct 2000.

[125] P. V. Kokotovic, M. Krstic, and I. Kanellakopoulos, "Backstepping to passivity: recursive design of adaptive systems," in *Proceedings of the 31st IEEE Conference on Decision and Control*, 1992, pp. 3276–3280 vol.4.

[126] C.-H. Lu, Y.-R. Hwang, and Y.-T. Shen, "Backstepping sliding mode tracking control of a vane-type air motor table motion system," *ISA Transactions*, vol. 50, no. 2, pp. 278 – 286, 2011.

[127] A. Zinober and P. Liu, "Robust control of nonlinear uncertain systems via sliding mode with backstepping design," in *UKACC International Conference on (Conf. Publ. No. 427) Control*, vol. 1, 1996, pp. 281 – 286 vol.1.

[128] T. Zhang, S. Ge, and C. Hang, "Adaptive neural network control for strict-feedback nonlinear systems using backstepping design," in *Proceedings of the 1999 American Control Conference*, vol. 2, 1999, pp. 1062 –1066.

[129] N. Adhikary and C. Mahanta, "Integral backstepping sliding mode control for underactuated systems: Swing-up and stabilization of the cart-pendulum system," *ISA Transactions*, vol. 52, no. 6, pp. 870–880, 2013. [Online]. Available: http://www.sciencedirect.com/science/article/pii/S0019057813001080

[130] B. Yao and M. Tomizuka, "Adaptive robust control of MIMO nonlinear systems in semi-strict feedback forms," *Automatica*, vol. 37, no. 9, pp. 1305 – 1321, 2001. [Online]. Available: http://www.sciencedirect.com/science/article/pii/S0005109801000826

[131] L. Ma, K. Schilling, and C. Schmid, "Adaptive backstepping sliding-mode control with application to a flexible-joint manipulator," *IFAC Proceedings Volumes*, vol. 39, no. 16, pp. 55 – 60, 2006, 4th IFAC Symposium on Mechatronic Systems. [Online]. Available: http://www.sciencedirect.com/science/article/pii/S1474667015341410

[132] N. Chen, F. Song, G. Li, X. Sun, and C. Ai, "An adaptive sliding mode backstepping control for the mobile manipulator with nonholonomic constraints," *Communications in Nonlinear Science and Numerical Simulation*, vol. 18, no. 10, pp. 2885 – 2899, 2013. [Online]. Available: http://www.sciencedirect.com/science/article/pii/S1007570413000658

[133] P. A. Ioannou and J. Sun, *Robust adaptive control*. Courier Corporation, 2012.

[134] W. Gao and J. C. Hung, "Variable structure control of nonlinear systems: a new approach," *IEEE Transactions on Industrial Electronics*, vol. 40, no. 1, pp. 45–55, Feb 1993.

[135] J. Gallier, "The Schur complement and symmetric positive semidefinite (and definite) matrices," *Penn Engineering*, 2010.

[136] S. Skogestad, "Simple analytic rules for model reduction and PID controller tuning," *Journal of Process Control*, vol. 13, no. 4, pp. 291 – 309, 2003. [Online]. Available: http://www.sciencedirect.com/science/article/pii/S0959152402000628

[137] C.-Y. Li, W.-X. Jing, and C.-S. Gao, "Adaptive backstepping-based flight control system using integral filters," *Aerospace Science and Technology*, vol. 13, no. 2, pp. 105 – 113, 2009. [Online]. Available: http://www.sciencedirect.com/science/article/pii/S1270963808000618

[138] W. Dong, J. A. Farrell, M. M. Polycarpou, V. Djapic, and M. Sharma, "Command filtered adaptive backstepping," *IEEE Transactions on Control Systems Technology*, vol. 20, no. 3, pp. 566–580, May 2012.

[139] H. Li, L. Dou, and Z. Su, "Adaptive dynamic surface based nonsingular fast terminal sliding mode control for semistrict feedback system," *Journal of Dynamic Systems, Measurement, and Control*, vol. 134, no. 2, p. 021011, 2012.

[140] Q. Zong, F. Wang, B. Tian, and J. Wang, "Robust adaptive approximate backstepping control design for a flexible air-breathing hypersonic vehicle," *Journal of Aerospace Engineering*, vol. 28, no. 4, p. 04014107, 2015. [Online]. Available: http://dx.doi.org/10.1061/(ASCE)AS.1943-5525.0000438

[141] F. Wang, Q. Zong, and B. Tian, "Adaptive backstepping finite time attitude control of reentry RLV with input constraint," *Mathematical Problems in Engineering*, vol. 2014, 2014.

[142] H. Lee and V. I. Utkin, "Chattering suppression methods in sliding mode control systems," *Annual Reviews in Control*, vol. 31, no. 2, pp. 179 – 188, 2007. [Online]. Available: http://www.sciencedirect.com/science/article/pii/S1367578807000363

[143] Y.-J. Huang, T.-C. Kuo, and S.-H. Chang, "Adaptive sliding-mode control for nonlinear systems with uncertain parameters," *IEEE Transactions on Systems, Man, and Cybernetics, Part B: Cybernetics*, vol. 38, no. 2, pp. 534–539, 2008.

[144] F. Plestan, Y. Shtessel, V. Brgeault, and A. Poznyak, "Sliding mode control with gain adaptation–application to an electropneumatic actuator," *Control Engineering Practice*, vol. 21, no. 5, pp. 679 – 688, 2013. [Online]. Available: http://www.sciencedirect.com/science/article/pii/S0967066112001037

[145] M. B. R. Neila and D. Tarak, "Adaptive terminal sliding mode control for rigid robotic manipulators," *International Journal of Automation and Computing*, vol. 8, no. 2, pp. 215–220, 2011. [Online]. Available: http://dx.doi.org/10.1007/s11633-011-0576-2

[146] P. Ioannou and J. Sun, *Robust Adaptive Control*, ser. Control theory. PTR Prentice-Hall, 1996.

[147] F.-J. Lin, P.-H. Shen, and S.-P. Hsu, "Adaptive backstepping sliding mode control for linear induction motor drive," *IEEE Proceedings-Electric Power Applications*, vol. 149, no. 3, pp. 184–194, 2002.

[148] V. I. Utkin and A. S. Poznyak, "Adaptive sliding mode control with application to super-twist algorithm: Equivalent control method," *Automatica*, vol. 49, no. 1, pp. 39 – 47, 2013. [Online]. Available: http://www.sciencedirect.com/science/article/pii/S0005109812004694

[149] T. Gonzalez, J. A. Moreno, and L. Fridman, "Variable gain super-twisting sliding mode control," *IEEE Transactions on Automatic Control*, vol. 57, no. 8, pp. 2100–2105, Aug 2012.

[150] A. Polyakov and A. Poznyak, "Reaching time estimation for super-twisting second order sliding mode controller via lyapunov function designing," *IEEE Transactions on Automatic Control*, vol. 54, no. 8, pp. 1951–1955, Aug 2009.

[151] J. Zhang and W. X. Zheng, "Design of adaptive sliding mode controllers for linear systems via output feedback," *IEEE Transactions on Industrial Electronics*, vol. 61, no. 7, pp. 3553–3562, July 2014.

[152] D. Fulwani, B. Bandyopadhyay, and L. Fridman, "Non-linear sliding surface: towards high performance robust control," *IET Control Theory and Applications*, vol. 6, no. 2, pp. 235–242, January 2012.

[153] Y. Li and Q. Xu, "Adaptive sliding mode control with perturbation estimation and PID sliding surface for motion tracking of a piezo-driven micromanipulator," *IEEE Transactions on Control Systems and Technology*, vol. 18, no. 4, pp. 798–810, July 2010.

[154] Y. Stepanenko, Y. Cao, and C.-Y. Su, "Variable structure control of robotic manipulator with PID sliding surfaces," *International Journal of Robust and Nonlinear Control*, vol. 8, no. 1, pp. 79–90, 1998.

[155] L. Wang, T. Chai, and L. Zhai, "Neural-network-based terminal sliding-mode control of robotic manipulators including actuator dynamics," *IEEE Transactions on Industrial Electronics*, vol. 56, no. 9, pp. 3296–3304, Sept 2009.

[156] N. Adhikary and C. Mahanta, "Backstepping sliding mode controller for a co-ordinated links COOL robot arm," in *13th International Workshop Variable Structure Systems (VSS)*, June 2014, pp. 1–5.

[157] I. Eker, "Sliding mode control with PID sliding surface and experimental application to an electromechanical plant," *ISA Transactions*, vol. 45, no. 1, pp. 109 – 118, 2006. [Online]. Available: http://www.sciencedirect.com/science/article/pii/S0019057807600706

[158] W. Gao and J. C. Hung, "Variable structure control of nonlinear systems: a new approach," *IEEE Transactions on Industrial Electronics*, vol. 40, no. 1, pp. 45–55, Feb 1993.

[159] S. A. M. Dehghan, M. Danesh, and F. Sheikholeslam, "Adaptive hybrid force/position control of robot manipulators using an adaptive force estimator in the presence of parametric uncertainty," *Advanced Robotics*, vol. 29, no. 4, pp. 209–223, 2015. [Online]. Available: http://dx.doi.org/10.1080/01691864.2014.985609

[160] G. Xia, C. Li, Q. Zhu, and X. Xie, "Hybrid force/position control of industrial robotic manipulator based on kalman filter," in *IEEE International Conference on Mechatronics and Automation*, Aug 2016, pp. 2070–2075.

[161] W. He, Y. Dong, and C. Sun, "Adaptive neural impedance control of a robotic manipulator with input saturation," *IEEE Transactions on Systems, Man, and Cybernetics: Systems*, vol. 46, no. 3, pp. 334–344, March 2016.

[162] Z. Li, C. Yang, C. Y. Su, S. Deng, F. Sun, and W. Zhang, "Decentralized fuzzy control of multiple cooperating robotic manipulators with impedance interaction," *IEEE Transactions on Fuzzy Systems*, vol. 23, no. 4, pp. 1044–1056, Aug 2015.

[163] F. Ficuciello, L. Villani, and B. Siciliano, "Variable impedance control of redundant manipulators for intuitive human-robot physical interaction," *IEEE Transactions on Robotics*, vol. 31, no. 4, pp. 850–863, Aug 2015.

[164] R. Ikeura and H. Inooka, "Variable impedance control of a robot for cooperation with a human," in *Proceedings of 1995 IEEE International Conference on Robotics and Automation*, vol. 3, May 1995, pp. 3097–3102 vol.3.

[165] R. Ikeura, T. Moriguchi, and K. Mizutani, "Optimal variable impedance control for a robot and its application to lifting an object with a human," in *Proceedings of the 11th IEEE International Workshop on Robot and Human Interactive Communication*, 2002, pp. 500–505.

[166] R. V. Dubey, T. F. Chan, and S. E. Everett, "Variable damping impedance control of a bilateral telerobotic system," *IEEE Control Systems*, vol. 17, no. 1, pp. 37–45, Feb 1997.

[167] T. Tsumugiwa, R. Yokogawa, and K. Hara, "Variable impedance control based on estimation of human arm stiffness for human-robot cooperative calligraphic task," in *Proceedings of the 2002 IEEE International Conference on Robotics and Automation (Cat. No.02CH37292)*, vol. 1, 2002, pp. 644–650.

[168] C. Yang, G. Ganesh, S. Haddadin, S. Parusel, A. Albu-Schaeffer, and E. Burdet, "Human-like adaptation of force and impedance in stable and unstable interactions," *IEEE Transactions on Robotics*, vol. 27, no. 5, pp. 918–930, Oct 2011.

[169] M. Howard, D. J. Braun, and S. Vijayakumar, "Transferring human impedance behavior to heterogeneous variable impedance actuators," *IEEE Transactions on Robotics*, vol. 29, no. 4, pp. 847–862, Aug 2013.

[170] J. Buchli, F. Stulp, E. Theodorou, and S. Schaal, "Learning variable impedance control," *The International Journal of Robotics Research*, vol. 30, no. 7, pp. 820–833, 2011. [Online]. Available: http://dx.doi.org/10.1177/0278364911402527

[171] K. Kronander and A. Billard, "Online learning of varying stiffness through physical human-robot interaction," in *IEEE International Conference on Robotics and Automation*, May 2012, pp. 1842–1849.

[172] J. Bae, J. Ko, and D. Hong, "Variable impedance control with stiffness for human-robot cooperation system," in *15th International Conference on Control, Automation and Systems (ICCAS)*, Oct 2015, pp. 1231–1233.

[173] K. Kronander and A. Billard, "Stability considerations for variable impedance control," *IEEE Transactions on Robotics*, vol. 32, no. 5, pp. 1298–1305, Oct 2016.

[174] B. Yao, S. Chan, and D. Wang, "Variable structure adaptive motion and force control of robot manipulators," *Automatica*, vol. 30, no. 9, pp. 1473 – 1477, 1994. [Online]. Available: http://www.sciencedirect.com/science/article/pii/0005109894900140

[175] Q. Xu, "Robust impedance control of a compliant microgripper for high-speed position/force regulation," *IEEE Transactions on Industrial Electronics*, vol. 62, no. 2, pp. 1201–1209, Feb 2015.

[176] M. B. Fard and S. Khorashadizadeh, "Model free robust impedance control of robot manipulators using fourier series expansion," in *AI Robotics (IRANOPEN)*, April 2015, pp. 1–7.

[177] L. Sciavicco and B. Siciliano, *Modeling and control of robot manipulators*. McGraw Hill Inc., 1996.

[178] Y. Jin, P. H. Chang, M. Jin, and D. G. Gweon, "Stability guaranteed time-delay control of manipulators using nonlinear damping and terminal sliding mode," *IEEE Transactions on Industrial Electronics*, vol. 60, no. 8, pp. 3304–3317, Aug 2013.

[179] M. Jin, J. Lee, and K. K. Ahn, "Continuous nonsingular terminal sliding-mode control of shape memory alloy actuators using time delay estimation," *IEEE/ASME Transactions on Mechatronics*, vol. 20, no. 2, pp. 899–909, April 2015.

[180] M. Jin, S. H. Kang, and P. H. Chang, "Robust compliant motion control of robot with nonlinear friction using time-delay estimation," *IEEE Transactions on Industrial Electronics*, vol. 55, no. 1, pp. 258–269, Jan 2008.

[181] G. R. Cho, P. H. Chang, S. H. Park, and M. Jin, "Robust tracking under nonlinear friction using time-delay control with internal model," *IEEE Transactions on Control Systems Technology*, vol. 17, no. 6, pp. 1406–1414, Nov 2009.

[182] A. Levant, "Robust exact differentiation via sliding mode technique*," *Automatica*, vol. 34, no. 3, pp. 379 – 384, 1998. [Online]. Available: http://www.sciencedirect.com/science/article/pii/S0005109897002094

[183] T. C. Hsia and L. S. Gao, "Robot manipulator control using decentralized linear time-invariant time-delayed joint controllers," in *IEEE International Conference on Robotics and Automation*, vol. 3, May 1990, pp. 2070–2075.

[184] H. Li, L. Dou, and Z. Su, "Adaptive nonsingular fast terminal sliding mode control for electromechanical actuator," *International Journal of Systems Science*, vol. 44, no. 3, pp. 401–415, 2013. [Online]. Available: http://dx.doi.org/10.1080/00207721.2011.601348

[185] Z. Hou, Y. Wang, and L. Liu, "Improved nonsingular fast terminal sliding mode controller for nonlinear systems," in *International Conference on Mechatronics and Control (ICMC)*, July 2014, pp. 678–683.

[186] M. Jin, J. Lee, P. H. Chang, and C. Choi, "Practical nonsingular terminal sliding-mode control of robot manipulators for high-accuracy tracking control," *IEEE Transactions on Industrial Electronics*, vol. 56, no. 9, pp. 3593–3601, Sept 2009.

[187] S. Yu, X. Yu, B. Shirinzadeh, and Z. Man, "Continuous finite-time control for robotic manipulators with terminal sliding mode," *Automatica*, vol. 41, no. 11, pp. 1957–1964, 2005. [Online]. Available: http://www.sciencedirect.com/science/article/pii/S000510980500227X

[188] S. Blažič, D. Matko, and I. Škrjanc, "A new leakage term in the adaptive law," *IFAC Proceedings Volumes*, vol. 41, no. 2, pp. 8913–8918, 2008, 17th IFAC World Congress. [Online]. Available: http://www.sciencedirect.com/science/article/pii/S147466701640385X

[189] S. Mobayen, "An adaptive fast terminal sliding mode control combined with global sliding mode scheme for tracking control of uncertain nonlinear third-order systems," *Nonlinear Dynamics*, vol. 82, no. 1-2, pp. 599–610, 2015.

[190] M. J. Beelen, G. J. Naus, M. R. J. van de Molengraft, and M. Steinbuch, "Force feedback control design for nonideal teleoperators," *Control Engineering Practice*, vol. 21, no. 12, pp. 1694 – 1705, 2013.

[191] A. Joubair, L. F. Zhao, P. Bigras, and I. Bonev, "Absolute accuracy analysis and improvement of a hybrid 6-DOF medical robot," *Industrial Robot: An International Journal*, vol. 42, no. 1, pp. 44–53, 2015.

[192] W. Xu, B. Chu, and E. Rogers, "Iterative learning control for robotic-assisted upper limb stroke rehabilitation in the presence of muscle fatigue," *Control Engineering Practice*, vol. 31, pp. 63 – 72, 2014.

[193] A. Tapus, M. J. Mataric, and B. Scasselati, "Socially assistive robotics [grand challenges of robotics]," *IEEE Robotics and Automation Magazine*, vol. 14, no. 1, pp. 35–42, 2007.

[194] L. Sentis, J. Park, and O. Khatib, "Compliant control of multicontact and center-of-mass behaviors in humanoid robots," *IEEE Transactions on Robotics*, vol. 26, no. 3, pp. 483–501, 2010.

[195] Z. Shao, G. Zheng, D. Efimov, and W. Perruquetti, "Modelling and control for position-controlled modular robot manipulators," in *IEEE/RSJ International Conference on Intelligent Robots and Systems (IROS)*, Sept 2015, pp. 3290–3295.

[196] F. Flacco and A. D. Luca, "Discrete-time velocity control of redundant robots with acceleration/torque optimization properties," in *2014 IEEE International Conference on Robotics and Automation (ICRA)*, May 2014, pp. 5139–5144.

[197] "Robotis Co. Ltd." 2017. [Online]. Available: http://support.robotis.com/en/product/auxdevice/interface/usb2dxl_manual.htm

[198] M. W. Spong, "Underactuated mechanical systems," in *Control Problems in Robotics and Automation*. Springer-Verlag, 1998.

[199] W.-S. Man and J.-S. Lin, "Nonlinear control design for a class of underactuated systems," in *IEEE International Conference on Control Applications (CCA)*, 2010, pp. 1439 –1444.

[200] R. Olfati-Saber, "Nonlinear control of underactuated mechanical systems with application to robotics and aerospace vehicles," Ph.D. dissertation, 2001.